MODELING TECHNIQUES FOR MULTICONDUCTOR CABLES: THEORY AND PRACTICE

Robert C. Keyser
Gulf Radiation Technology

TECHNICAL REPORT NO. AFWL-TR-72-89

FOREWORD

This report was prepared by Gulf Radiation Technology, San Diego, California, under Contract F29601-70-C-0029. The research was performed under Program Element 11213F, Project 133B, and was funded by the Space and Missile Systems Organization (SAMSO).

Inclusive dates or research were 1 June 1971 through 30 June 1972. The report was submitted 20 December 1972 by the Air Force Weapons Laboratory Project Officer, Mr. James M. Baca (ELE).

Messrs. D. B. Breuner, R. J. Butcher, and W. R. Stone were contributors to the theoretical developments. In particular, Mr. Breuner developed the open-impedance method and Mr. Stone developed the shorted-impedance method. The modeling of actual cables was accomplished by Mr. Breuner and Mr. Butcher, with the assistance of Mr. R. G. Zaller, who developed computer codes to manipulate the voluminous measured data. The experimental transfer functions were taken by Messrs. J. L. Oberg and J. A. Young, with frequent assistance from Messrs. Breuner and Butcher.

This technical report has been reviewed and is approved.

James M. Baca
JAMES M. BACA
Project Officer

John P. Portasik
JOHN P. PORTASIK
Colonel, USAF
Chief, Electromagnetic Pulse Branch

Carl F. Davis
CARL F. DAVIS
Colonel, USAF
Chief, Electronics Division

ABSTRACT

An approach to modeling of complex multiconductor cables is developed, based on measuring a set of parameters for the cable to be modeled, and then manipulating these to obtain the required model parameters. The theoretical foundation for the approach is based on the assumption of pure TEM-mode propagation on the cable, and this is shown not to impose any significant limitation for practical cables. The approach is then applied to a series of actual cables of varying complexity up to 15 wires and five internal shields within an overall shield. The results for 85 transfer functions taken on these cables show that ~70% of them exhibit agreement of ~6 dB between analysis and experiment. Also included is an analysis of the errors to be expected from the use of a lumped approximation as a function of the section length.

(Distribution Limitation Statement B)

CONTENTS

List of Tables

List of Figures

1. INTRODUCTION

This report will present the theoretical foundation for an approach to the analytical modeling of multiconductor cables and document the problems and results of a program of practical application of the technique to real cables.

The requirement for modeling of such cables arises because they form one link in the coupling chain between the electromagnetic pulse resulting from a nuclear detonation and the noise signals which finally reach the critical circuits. The complete coupling chain may be broken down as follows.

1. Field generation by detonation
2. Interaction of field with structure
3. Energy penetration through points of entry
4. Excitation of cables by points of entry
5. Coupling of signals to critical circuits
6. Critical circuit response

In order to accomplish an analytical assessment program, each of these links must be modeled analytically, and this report addresses the modeling of link No. 5.

In addition to its application to detailed modeling of this link in a given coupling chain, the technique has an application of even greater potential usefulness. This is in contributing to the understanding of how signals distribute on complex cables, what parameters are important in determining this distribution, how these parameters vary with cable construction, etc. Any program directed at studying this problem will require the modeling of complex real cables, and the techniques described in this report are applicable for such modeling.

Three methods of determining the L and C parameters for cables will be presented. The first of the methods developed is based on making capacitance measurements on the cable to be modeled and then manipulating these to obtain actual model L and C parameters. This method is straightforward in application and yields good results, but unfortunately is not capable of handling branched cables. This limitation prompted the development of two additional methods based on the measurement of characteristic impedances on the cable rather than capacitances. The advantage of these methods is that the impedance measurements can be made using high-resolution time-domain reflectometry (TDR) techniques, allowing one branch to be distinguished from the others.

The development of the technique will proceed in the following manner. First, the general transmission line equations and solutions for an N+1 conductor cable will be developed, based on the assumption of pure TEM-mode propagation, which will be shown to impose no serious limitation for practical cables. Second, the worst-case errors resulting from the use of a lumped approximation to the distributed line will be calculated. Finally, the three methods of determining the distributed L and C parameters and one method for determining distributed R will be developed, based on the transmission line solutions.

The various methods will then be applied to modeling of real cables of varying complexity (3 to 20 conductors). The problems of applying the methods and the results obtained will be discussed in detail. Finally, a number of miscellaneous topics will be discussed.

The analytical results for the cable models were obtained by use of the TRAFFIC (TRAnsfer Functions For Internal Coupling) computer code developed by the Boeing Company. This code was especially developed for frequency-domain analysis of very large, passive, reciprocal, linear networks, of which lumped-parameter cable models are a good example. The code is presently operational on the AFWL CDC-6600 computers.

2. DERIVATION OF TRANSMISSION LINE EQUATIONS

In this section, the transmission line equations for an N+1 conductor transmission line will be derived, preceded by derivation of the same equations for a two-conductor line to illustrate the method. Assuming TEM-mode propagation, these equations can be derived either from a circuit theory approach or by use of Maxwell's electromagnetic field equations. Examples of the application of both methods to the two-wire case appear in many texts on the subject.[1-4] Until recently, however, the case of more than two conductors in a transmission system has been almost completely neglected, particularly the derivation of the transmission line equations. A derivation of these equations for multiconductor transmission lines (MTL) based on Maxwell's equations has recently appeared in a paper by Kajfez,[5] and the reader is referred to that paper for the field theory approach. The derivations which follow will be based on circuit theory.

Before proceeding to the derivations, a word should be said about the assumption of pure TEM wave propagation and the limitations such an assumption imposes on the results. As is well known, several modes of signal propagation are possible for perfectly conducting transmission lines, depending on the conductor geometry. These modes are, of course, transverse electric (TE), transverse magnetic (TM), and transverse electromagnetic (TEM), where the word transverse refers to the direction of the field(s) with respect to the direction of propagation. TEM waves are sustained along open-wire or coaxial transmission lines only[1] and are, therefore, sometimes called "transmission line" or "principal" waves. The term "principal" arises from the fact that, while TEM waves are the principal mode of signal propagation on open-wire or coaxial lines, they are not the only mode. But

even though TE and/or TM modes will be sustained on these lines, for practical dimensions these modes will be subject to severe attenuation at frequencies below about 10^{10} Hz. For example, the lowest cutoff frequency for a complementary mode in a coax is for a TE mode, and is given by[1]

$$f \simeq \frac{3 \times 10^{10}\ \text{Hz}}{\pi(r_i + r_o)} .$$

For even a relatively large coax cable such as RG-213, $r_i + r_o = 0.97$ cm, and then $f \simeq 10^{10}$ Hz. As the dimensions of the coax decrease, the cutoff frequency becomes even higher.

Another characteristic of real transmission lines which differs from the ideal and which affects the validity of the pure TEM assumption is finite conductivity of the conductors. Due to the resistance of the conductors and the current which must flow in them to propagate a wave, there will be a finite voltage drop and resulting electric field along the axial dimension of the conductors. Since this drop is in the same direction as the propagation of the wave, and since by definition the electric field must be always transverse to the direction of propagation for TEM waves, it is clear that the resulting waves are not pure TEM. But again, for practical cables the variation from perfect conductivity is not great enough for this to be a serious problem. For example, assume a piece of RG-8 coax is terminated in its 50-ohm characteristic impedance and is driven by a 50-volt, 10^8-Hz source. The resulting current flow is 1 amp neglecting losses, and for the nominal ac resistance of 0.8 ohm/m at 10^8 Hz, the axial drop is then ~0.8 V/m. But the radial drop across the ~0.1-in. thickness of dielectric between the center conductor and shield is greater than 20 kV/m, which is so much larger than the axial drop that it is perfectly reasonable to ignore the axial component of field and assume pure TEM propagation.

The preceding discussion shows clearly that the assumption of pure TEM-mode propagation is not a significant limitation for practical transmission lines so long as (1) the geometry and maximum applied signal

frequency are such that complementary modes (TE and TM) cannot be efficiently transmitted and (2) the lines are relatively low-loss. The example for the first condition showed that for even a large coax cable, frequencies up to 10^8 Hz are still a factor of ~100 below the TE-mode cutoff frequency, and so the complementary modes will indeed not be efficiently transmitted. (A frequency of 10^8 Hz is considered an acceptable upper limit on the useful frequency range of the models to be developed in this report.) The example for the second condition suggests that for cables as much as 100 times as lossy as an RG-8 coax (2 dB/100 ft nominal attenuation at 10^8 Hz), the deviation from pure TEM mode is acceptably small, being on the order of 1%.

With the assurance that the assumption of pure TEM-mode propagation on the transmission lines of interest is not a limitation of any significance, we are ready to proceed to the derivation of the transmission line equations.

2.1 TWO-CONDUCTOR TRANSMISSION LINE EQUATIONS

A "transmission line" formed by two conductors of completely arbitrary geometry is shown in Fig. 2.1. This transmission line can be represented schematically as shown in Fig. 2.2, which also defines the direction of x, the measure of distance along the line from a reference point — i. e., the receiving end. The properties of this line can be described in terms of the distributed parameters of series resistance R, inductance L, shunt conductance G, and capacitance C, with units of ohms, henrys, mhos, and farads per unit length, respectively, An incremental section of this line may then be drawn as shown in the equivalent circuit of Fig. 2.3, where the per-unit-length parameters have been multiplied by the increment length Δx. (A "T" section has been used here, but the derivations that follow could be just as easily accomplished for other configurations, e. g., "π" or "L" sections.)[2] Now, it is clear from the arbitrary shape of the line shown in Fig. 2.1 that the distributed parameters will not be uniform over the full length of the

RT-00358

Fig. 2.1. General two-conductor transmission line

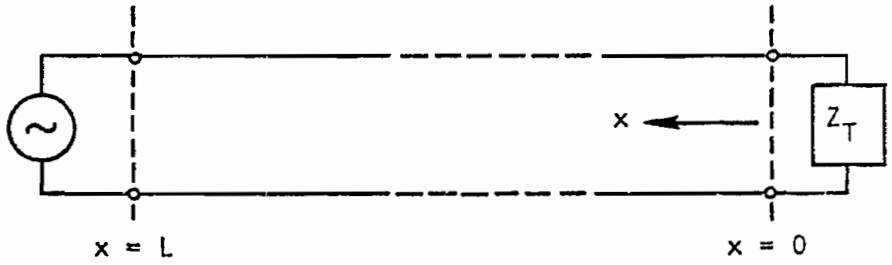

RT-00359

Fig. 2.2. Schematic representation of transmission line

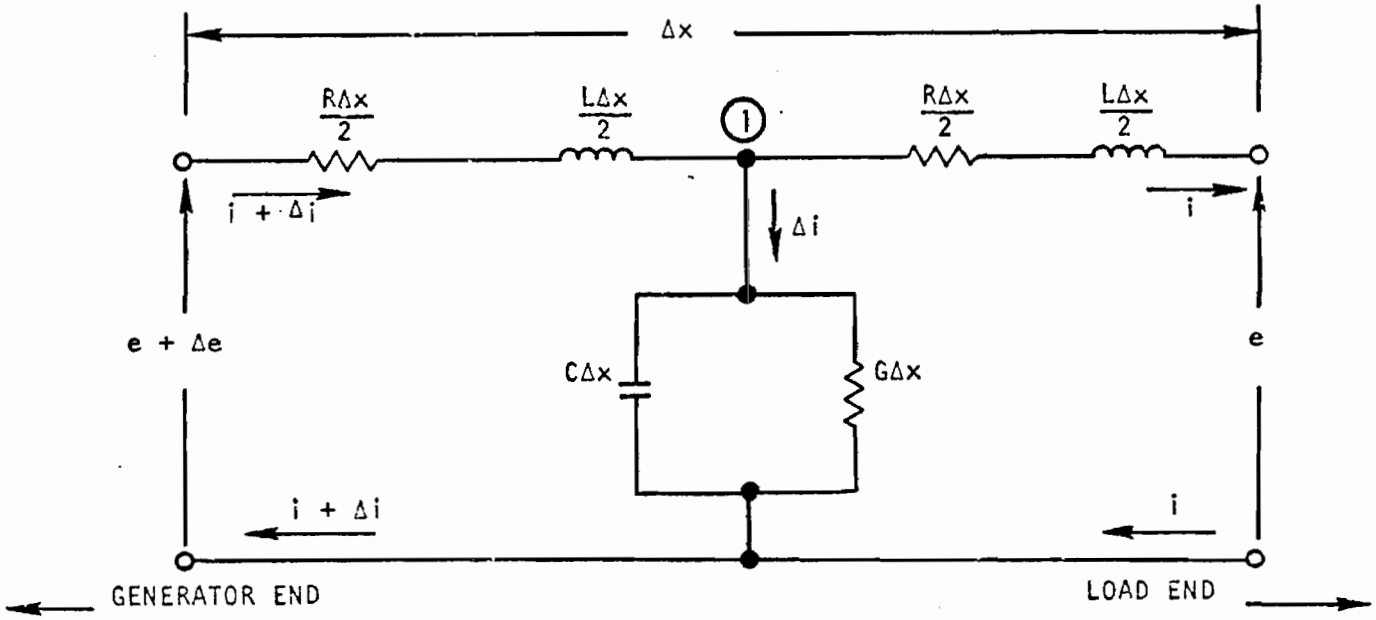

RT-00360

Fig. 2.3. Equivalent circuit for incremental section of two-conductor transmission line

line, but rather will be functions of x. For these derivations, the parameters are, of course, constrained to be uniform over the increment Δx. But then, as $\Delta x \to 0$, this constraint vanishes and, as a result, there are no limitations on the variation of the parameters with x.

Proceeding now to the derivation of the equations, let us write a Kirchoff's Voltage Law equation around the outer loop of the incremental section. This results in

$$(e + \Delta e) - (i + \Delta i)\frac{R\Delta x}{2} - \frac{L\Delta x}{2}\frac{\partial(i + \Delta i)}{\partial t}$$

$$- i\frac{R\Delta x}{2} - \frac{L\Delta x}{2}\frac{\partial i}{\partial t} - e = 0 .$$

Collecting terms and dividing through by Δx gives

$$\frac{\Delta e}{\Delta x} = (2i + \Delta i)\frac{R}{2} + \frac{L}{2}\left(\frac{\partial i}{\partial t} + \frac{\partial(i + \Delta i)}{\partial t}\right) .$$

Then, as $\Delta x \to 0$, $\Delta i \to 0$ also, and we have

$$\frac{\partial e}{\partial x} = Ri + L\frac{\partial i}{\partial t} . \qquad (1)$$

In a similar fashion, applying Kirchoff's Current Law to node (1) results in

$$(i + \Delta i) = i + \left[(e + \Delta e) - (i + \Delta i)\frac{R\Delta x}{2} - \frac{L\Delta x}{2}\frac{\partial(i + \Delta i)}{\partial t}\right] G\Delta x$$

$$+ \frac{\partial}{\partial t}\left[(e + \Delta e) - (i + \Delta i)\frac{R\Delta x}{2} - \frac{L\Delta x}{2}\frac{\partial(i + \Delta i)}{\partial t}\right] C\Delta x .$$

Collecting terms and dividing through by Δx as before results in

$$\frac{\Delta i}{\Delta x} = \left[(e + \Delta e) - (i + \Delta i)\frac{R\Delta x}{2} - \frac{L\Delta x}{2}\frac{\partial(i + \Delta i)}{\partial t}\right] G$$

$$+ \frac{\partial}{\partial t}\left[(e + \Delta e) - (i + \Delta i)\frac{R\Delta x}{2} - \frac{L\Delta x}{2}\frac{\partial(i + \Delta i)}{\partial t}\right] C .$$

And once again, as $\Delta x \to 0$, $\Delta e \to 0$ also, and we have

$$\frac{\partial i}{\partial x} = G e + C \frac{\partial e}{\partial t} \quad . \tag{2}$$

For sinusoidal excitation, the instantaneous values of e and i as functions of distance and time can be written as

$$e(x, t) = E(x) \exp(j\omega t) \tag{3}$$

and

$$i(x, t) = I(x) \exp(j\omega t) \quad , \tag{4}$$

where E(x) and I(x) are functions only of distance. Substituting Eqs. 3 and 4 into Eqs. 1 and 2 and differentiating as required gives

$$\frac{dE}{dx} = RI + j\omega LI = (R + j\omega L)I = zI \tag{5}$$

and

$$\frac{dI}{dx} = GE + j\omega CE = (G + j\omega C)E = yE \quad . \tag{6}$$

Note that in Eqs. 5 and 6, the notation f(x) has been dropped, but remember that each quantity in these equations is still a function of x, including the transmission line distributed parameters R, L, G, and C. Note also that the signs of both sides of these equations are positive, whereas they frequently appear in other literature with the right-hand side of the equation negative. This seeming discrepancy results merely from different choices of x = 0, and simple physical reasoning shows that for x = 0 at the receiving or load end, the signs of Eqs. 5 and 6 are correct.

Taking the derivative of Eqs. 5 and 6 with respect to x yields

$$\frac{d^2E}{dx^2} = \frac{dz}{dx} I + z \frac{dI}{dx} \tag{7}$$

and

$$\frac{d^2I}{dx^2} = \frac{dy}{dx} E + y \frac{dE}{dx} \quad . \tag{8}$$

Substituting Eqs. 5 and 6 into Eqs. 7 and 8 gives

$$\frac{d^2E}{dx^2} = \frac{dz}{dx}\left(\frac{1}{z}\frac{dE}{dx}\right) + z(yE)$$

and

$$\frac{d^2I}{dx^2} = \frac{dy}{dx}\left(\frac{1}{y}\frac{dI}{dx}\right) + y(zI) \ .$$

If the transmission line is assumed to be uniform, then

$$\frac{dz}{dx} = \frac{dy}{dx} = 0 \ ,$$

and we have

$$\frac{d^2E}{dx^2} = zyE \tag{9}$$

and

$$\frac{d^2I}{dx^2} = zyI \ , \tag{10}$$

where we have taken advantage of the fact that the scalar products zy and yz are equal. These are second-order, linear, homogeneous differential equations, and their solutions will be of the form

$$E = A \exp(\gamma_1 x) + B \exp(\gamma_2 x)$$

and

$$I = C \exp(\gamma_1 x) + D \exp(\gamma_2 x) \ ,$$

where γ_1 and γ_2 are roots of the auxiliary equation

$$\gamma^2 - zy = 0 \ .$$

These roots are found to be

$$\gamma = \pm\sqrt{zy} \ ,$$

and the solutions for E and I are then

$$E = A \exp(\sqrt{zy}\, x) + B \exp(-\sqrt{zy}\, x) \tag{11}$$

and

$$I = C \exp(\sqrt{zy}\, x) + D \exp(-\sqrt{zy}\, x) \ . \qquad (12)$$

To facilitate evaluation of the constants, we can express C and D in terms of A and B, respectively, by first differentiating Eq. 11, which then becomes equal to zI according to Eq. 5, then multiplying both sides of Eq. 12 by z, and finally equating coefficients of like powers of the exponential. The results are

$$C = A\sqrt{y/z}$$

and

$$D = -B\sqrt{y/z} \ .$$

Substituting these back into Eq. 12 and using the boundary conditions $E(0) = E_L$ and $I(0) = I_L$ at $x = 0$, we have

$$E_L = A + B$$

and

$$I_L = A\sqrt{y/z} - B\sqrt{y/z} \ .$$

Solving for A, B, C, and D, and substituting these constants into Eqs. 11 and 12, the equations for E and I are

$$E = \frac{1}{2}\left[(E_L + I_L\sqrt{z/y}) \exp(\sqrt{zy}\, x) + (E_L - I_L\sqrt{z/y}) \exp(-\sqrt{zy}\, x)\right] \qquad (13)$$

and

$$I = \frac{1}{2}\left[(E_L\sqrt{y/z} + I_L) \exp(\sqrt{zy}\, x) - (E_L\sqrt{y/z} - I_L) \exp(-\sqrt{zy}\, x)\right] \ . \qquad (14)$$

The dimensionless quantity $\sqrt{zy}$ is defined as the propagation constant (γ), and the term $\sqrt{z/y}$ which has dimensions of impedance is defined as the characteristic impedance (Z_0).

With the propagation constant defined as $\gamma = \sqrt{zy}$ and since z and y are complex numbers, it is clear that γ is a complex number also. That is,

$$\gamma = \sqrt{zy} = \alpha + j\beta \ ,$$

where α is defined as the attenuation constant and β is the phase constant. For a lossless transmission line, $R = G = \alpha = 0$; then,

$$\gamma^2 = (j\omega L)(j\omega C) = (j\beta)^2$$

or

$$\omega^2 LC = \beta^2 \ .$$

But the velocity of propagation of waves on the transmission line, also known as phase velocity, is defined as[1]

$$v_p = \frac{\omega(\text{radians/unit time})}{\beta(\text{radians/unit length})} \ ;$$

therefore,

$$LC = \frac{\beta^2}{\omega^2} = \frac{1}{v_p^2} \ . \qquad (15)$$

If we know any two of the transmission line parameters, L, C, or v_p, we know the third also.

At this point, it is important to review the conditions we have imposed on the various equations we have developed. The equations and corresponding conditions are summarized as follows.

$$\left.\begin{aligned} \frac{dE}{dx} &= zI \\ \frac{dI}{dx} &= yE \end{aligned}\right\} \quad \text{Pure TEM-mode propagation and sinusoidal excitation}$$

$$\left.\begin{aligned} \frac{d^2E}{dx^2} - zyE &= 0 \\ \frac{d^2I}{dx^2} - zyI &= 0 \end{aligned}\right\} \quad \text{Pure TEM-mode propagation, sinusoidal excitation, and uniform parameters}$$

$$E = \frac{1}{2}\left[(E_L + I_L Z_0)\exp(\gamma x) + (E_L - I_L Z_0)\exp(-\gamma x)\right]$$

$$I = \frac{1}{2}\left[\left(\frac{E_L}{Z_0} + I_L\right)\exp(\gamma x) - \left(\frac{E_L}{Z_0} - I_L\right)\exp(-\gamma x)\right]$$

} Pure TEM-mode, sinusoidal excitation, uniform parameters

$$LC = \frac{1}{v_p^2}$$

} Pure TEM-mode, sinusoidal excitation, uniform parameters, lossless

We will now proceed to the derivations for multiconductor transmission lines.

2.2 N+1 CONDUCTOR TRANSMISSION LINE EQUATIONS

In the same fashion as for the two-conductor line, the equivalent circuit for an incremental section of an N+1 conductor transmission line can be drawn, as shown in Fig. 2.4. The N conductors are designated 1 through N (including k), and the "+1" conductor is the return. (The use of N+1 conductors to describe the complete transmission line system, including return, is for later convenience in indexing summations. It would have been just as correct, of course, to include the return in the N conductors and then run the indices to only N-1.) Although not shown for clarity, each of the other conductors consists of complete "T" sections, the same as shown for the k^{th} wire. And, of course, each of the other N conductors has a shunt admittance and mutual inductance to every other conductor (except the return), which are also omitted for clarity. Again, we are making no assumptions regarding uniformity of R, L, G, and C on this line, except that they be uniform over Δx, a constraint which vanishes as $\Delta x \to 0$.

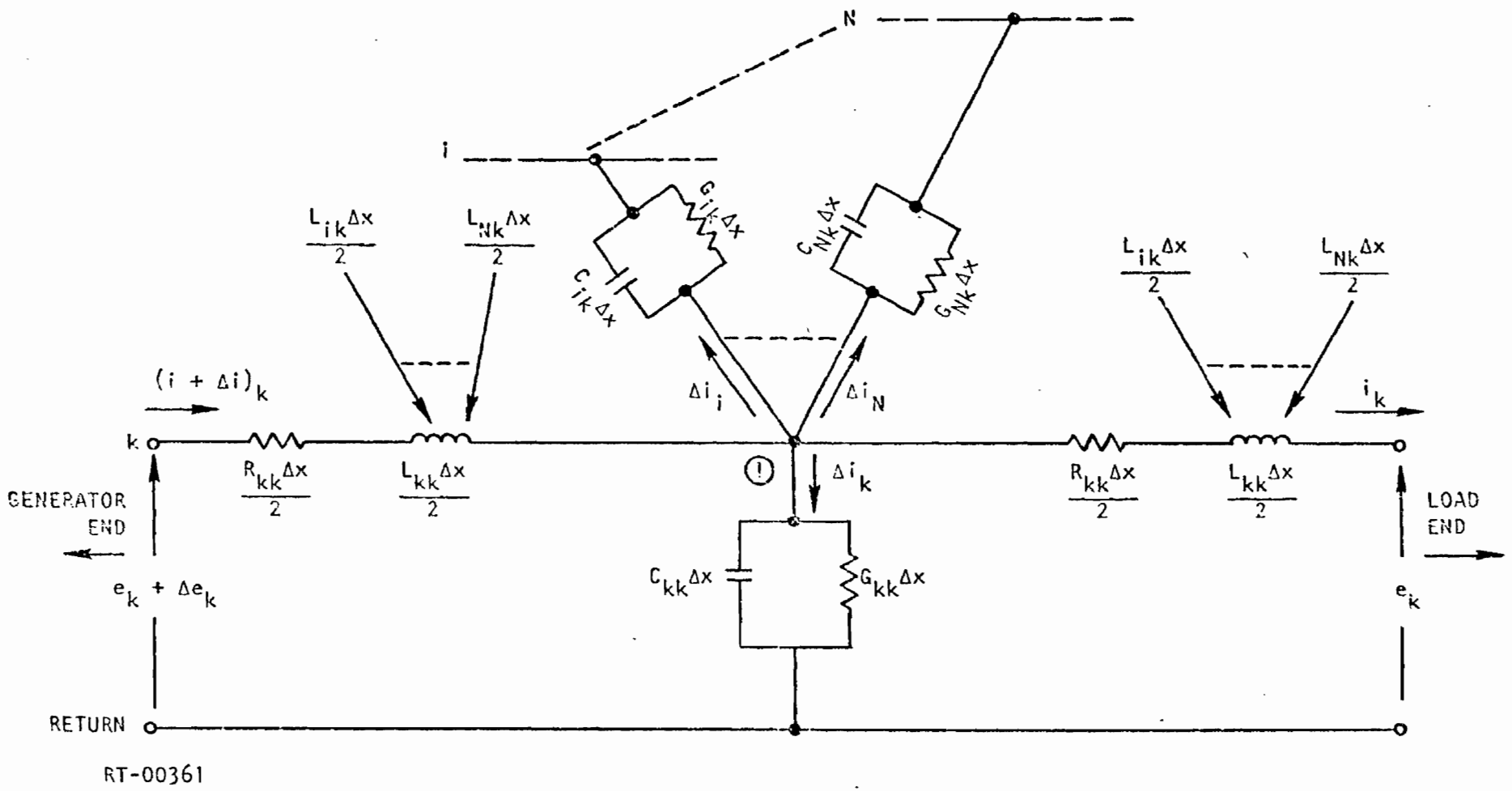

Fig. 2.4. Incremental section of N+1 conductor transmission line

First, writing a KVL equation around the outer loop of the k^{th} wire section shown in Fig. 2.4 gives

$$(e + \Delta e)_k - (i + \Delta i)_k \frac{R_{kk}\,\Delta x}{2} - \frac{L_{kk}\,\Delta x}{2} \frac{\partial (i + \Delta i)_k}{\partial t}$$

$$- \sum_{\substack{i=1 \\ i \neq k}}^{N} \frac{L_{ik}\,\Delta x}{2} \frac{\partial (i + \Delta i)_i}{\partial t} - \frac{R_{kk}\,\Delta x}{2} i_k$$

$$- \frac{L_{kk}\,\Delta x}{2} \frac{\partial i_k}{\partial t} - \sum_{\substack{i=1 \\ i \neq k}}^{N} \frac{L_{ik}\,\Delta x}{2} \frac{\partial i_i}{\partial t} - e_k = 0 \,.$$

This is the same equation as was previously written for the two-conductor transmission line, except for the addition of the two voltage drops due to mutual inductance between the k^{th} wire and all other wires. These two terms are the two summations, of course. Note that the term immediately preceding each summation could have been conveniently included in the summations merely by allowing the index i to pass through k. But that would obscure the fact that these drops result from different causes — i. e., circuit inductance of the k^{th} wire versus mutual inductances; and in any case, they will have to be separated later on. Combining terms and dividing through by Δx gives

$$\frac{\Delta e_k}{\Delta x} = (2i + \Delta i)_k \frac{R_{kk}}{2} + \frac{L_{kk}}{2} \frac{\partial (2i + \Delta i)_k}{\partial t}$$

$$+ \sum_{\substack{i=1 \\ i \neq k}}^{N} \frac{L_{ik}}{2} \frac{\partial (2i + \Delta i)_i}{\partial t} \,.$$

Then, as $\Delta x \to 0$, $\Delta i \to 0$ also, and we have

$$\frac{\partial e_k}{\partial x} = R_{kk}\, i_k + L_{kk} \frac{\partial i_k}{\partial t} + \sum_{\substack{i=1 \\ i \neq k}}^{N} L_{ik} \frac{\partial i_i}{\partial t} \,.$$

For sinusoidal excitation, this equation becomes

$$\frac{dE_k}{dx} = (R_{kk} + j\omega L_{kk})\, I_k + \sum_{\substack{i=1 \\ i\neq k}}^{N} j\omega L_{ik}\, I_i \ .$$

For the system of N+1 conductors, there are N of these equations since k varies from 1 to N, and the final result is

$$\frac{d}{dx}\begin{bmatrix} E_1 \\ E_2 \\ \vdots \\ E_N \end{bmatrix} = \begin{bmatrix} (R_{11} + j\omega L_{11}) & (j\omega L_{12}) \cdots (j\omega L_{1N}) \\ (j\omega L_{21}) & (R_{22} + j\omega L_{22}) \cdots (j\omega L_{2N}) \\ \vdots & \vdots \\ (j\omega L_{N1}) & (j\omega L_{N2}) \cdots (R_{NN} + j\omega L_{NN}) \end{bmatrix} \begin{bmatrix} I_1 \\ I_2 \\ \\ I_N \end{bmatrix}$$

This result, of course, can be written more conveniently as

$$\frac{d}{dx}\,\vec{E} = \underline{Z}\,\vec{I} \ . \qquad (16)$$

Now, writing a KCL equation at node 1 of Fig. 2.3 results in

$$(i + \Delta i)_k = i_k + \sum_{i=1}^{N} \Delta i_i = i_k + \Delta i_k + \sum_{\substack{i=1 \\ i\neq k}}^{N} \Delta i_i$$

$$= i_k + e_{kk}\, G_{kk}\, \Delta x + C_{kk}\, \Delta x\, \frac{\partial e_{kk}}{\partial t}$$

$$+ \sum_{\substack{i=1 \\ i\neq k}}^{N} (e_{kk} - e_{ii})\, G_{ik}\, \Delta x + \sum_{\substack{i=1 \\ i\neq k}}^{N} C_{ik}\, \Delta x\, \frac{\partial (e_{kk} - e_{ii})}{\partial t} \ ,$$

where

e_{ii} = the voltage with respect to return of the center node of the incremental section of the k^{th} wire (i = 1 to N, excluding k)

$$= \left[(e + \Delta e)_i - (i + \Delta i)_i \frac{R_{ii} \Delta x}{2} - \frac{L_{ii} \Delta x}{2} \frac{\partial (i + \Delta i)_i}{\partial t} - \sum_{\substack{j=1 \\ j \neq k}}^{N} \frac{L_{ij} \Delta x}{2} \frac{\partial (i + \Delta i)_j}{\partial t} \right]$$

and

e_{kk} = the voltage with respect to return of the center node of the incremental section of the k^{th} wire

$$= \left[(e + \Delta e)_k - (i + \Delta i)_k \frac{R_{kk} \Delta x}{2} - \frac{L_{kk} \Delta x}{2} \frac{\partial (i + \Delta i)_k}{\partial t} - \sum_{\substack{i=1 \\ i \neq k}}^{N} \frac{L_{ik} \Delta x}{2} \frac{\partial (i + \Delta i)_i}{\partial t} \right] .$$

Combining terms and dividing through by Δx results in

$$\frac{\Delta i_k}{\Delta x} = e_{kk} G_{kk} + C_{kk} \frac{\partial e_{kk}}{\partial t} + \sum_{\substack{i=1 \\ i \neq k}}^{N} (e_{kk} - e_{ii}) G_{ik} + \sum_{\substack{i=1 \\ i \neq k}}^{N} C_{ik} \frac{\partial (e_{kk} - e_{ii})}{\partial t} .$$

Then, letting $\Delta x \rightarrow 0$, $\Delta e \rightarrow 0$ also, and we have

$$e_{kk} = e_k$$

and

$$e_{ii} = e_i ,$$

which results in

$$\frac{\partial i_k}{\partial x} = e_k G_{kk} + C_{kk} \frac{\partial e_i}{\partial t} + \sum_{\substack{i=1 \\ i\neq k}}^{N} (e_k - e_i) G_{ik}$$

$$+\sum_{\substack{i=1 \\ i\neq k}}^{N} C_{ik} \frac{\partial (e_k - e_i)}{\partial t} .$$

For sinusoidal excitation, this becomes

$$\frac{dI_k}{dx} = E_k G_{kk} + E_k j\omega C_{kk} + \sum_{\substack{i=1 \\ i\neq k}}^{N} (E_k - E_i) G_{ik}$$

$$+ \sum_{\substack{i=1 \\ i\neq k}}^{N} j\omega C_{ik} (E_k - E_i) .$$

Rearranging and combining some terms gives*

$$\frac{dI_k}{dx} = \sum_{i=1}^{N} E_k (G_{ki} + j\omega C_{ki}) - \sum_{\substack{i=1 \\ i\neq k}}^{N} E_i (G_{ki} + j\omega C_{ki}) .$$

Once again, there are N of these equations as k varies from 1 to N, and these N equations can be written in matrix form as

$$\frac{d}{dx} \begin{bmatrix} I_1 \\ I_2 \\ \vdots \\ I_N \end{bmatrix} = \begin{bmatrix} \sum_{i=1}^{N} (G_{1i} + j\omega C_{1i}) & -(G_{12} + j\omega C_{12}) \cdots -(G_{1N} + j\omega C_{1N}) \\ -(G_{21} + j\omega C_{21}) & \sum_{i=1}^{N} (G_{2i} + j\omega C_{2i}) \cdots -(G_{2N} + j\omega C_{2N}) \\ \vdots & \ddots \\ -(G_{N1} + j\omega C_{N1}) & -(G_{N2} + j\omega C_{N2}) \cdots \sum_{i=1}^{N} (G_{Ni} + j\omega C_{Ni}) \end{bmatrix} \begin{bmatrix} E_1 \\ E_2 \\ \\ E_N \end{bmatrix}$$

*Note that the order of the subscripts has been reversed also. This does not alter the basic equations, but is necessary to make the matrix equation correct.

or more conveniently as

$$\frac{d}{dx}\vec{I} = \underline{Y}\,\vec{E} \ . \tag{17}$$

Reiterating these results, we have developed the transmission line equations for an N+1 conductor transmission line which can be written in matrix form as

$$\frac{d}{dx}\vec{E} = \underline{Z}\,\vec{I} \tag{16}$$

and

$$\frac{d}{dx}\vec{I} = \underline{Y}\,\vec{E} \tag{17}$$

so long as the matrices $\underline{Z}$ and $\underline{Y}$ are defined as shown above in their fully expanded form. As we did for the two-conductor line, we can take the derivatives of Eqs. 16 and 17 with respect to x and then substitute Eqs. 16 and 17 into the derivative equations to obtain

$$\frac{d^2}{dx^2}\vec{E} = \frac{d\underline{Z}}{dx}\left(\underline{Z}^{-1}\frac{d\vec{E}}{dx}\right) + \underline{Z}\,\underline{Y}\,\vec{E}$$

and

$$\frac{d^2}{dx^2}\vec{I} = \frac{d\underline{Y}}{dx}\left(\underline{Y}^{-1}\frac{d\vec{I}}{dx}\right) + \underline{Y}\,\underline{Z}\,\vec{I} \ .$$

Then, if the transmission line is assumed to be uniform,

$$\frac{d\underline{Z}}{dx} = \frac{d\underline{Y}}{dx} = 0 \ ,$$

and we have

$$\frac{d^2}{dx^2}\vec{E} = \underline{Z}\,\underline{Y}\,\vec{E} \tag{18}$$

and

$$\frac{d^2}{dx^2}\vec{I} = \underline{Y}\,\underline{Z}\,\vec{I} \ . \tag{19}$$

These equations are quite similar, of course, to the equivalent equations for the two-conductor line, i.e., Eqs. 9 and 10, but the manner of obtaining solutions will be different.

By analogy to the two-conductor case, it might be anticipated that the solutions will be of the form

$$\vec{E} = \exp(\underline{\gamma} x)\ \vec{E}_+ + \exp(-\underline{\gamma} x)\ \vec{E}_- \tag{20}$$

and

$$\vec{I} = \exp(\underline{\gamma}' x)\ \vec{I}_+ + \exp(-\underline{\gamma}' x)\ \vec{I}_- \ , \tag{21}$$

and, indeed, many authors simply assume this form of solution without proof. Also by this analogy we have

$$\underline{\gamma} = \sqrt{\underline{Z}\underline{Y}}$$

and

$$\underline{\gamma}' = \sqrt{\underline{Y}\underline{Z}} \ .$$

It is clear that $\underline{\gamma}$ and $\underline{\gamma}'$ are the propagation constant matrices for voltage and current waves, respectively. These will be general NxN matrices, with no special properties, and are not even necessarily equal to each other since, in general $\underline{Z}\underline{Y} \neq \underline{Y}\underline{Z}$. Under these conditions, we do not know how to define the elements of $\underline{\gamma}$.

One approach to obtaining more useful solutions to Eqs. 18 and 19 is to introduce a change of coordinates so as to diagonalize $\underline{Z}\underline{Y}$ and $\underline{Y}\underline{Z}$. To do this for Eq. 18, for example, we find the eigenvalues and eigenvectors of $\underline{Z}\underline{Y} = \underline{A}$ and let

$$\vec{E}' = \underline{Q}^{-1}\ \vec{E}$$

or

$$\vec{E} = \underline{Q}\ \vec{E}' ,$$

where $\underline{Q}$ is the square matrix made up of the N eigenvectors of $\underline{Z}\underline{Y}$ placed side by side, and $\vec{E}'$ is a new variable. We then have

$$\frac{d^2}{dx^2}\underline{Q}\vec{E}' = \underline{A}\vec{E} = \underline{A}\underline{Q}\vec{E}' . \tag{22}$$

The diagonalized or canonical form of $\underline{A}$ is given by

$$\underline{\Lambda} = \underline{Q}^{-1}\,\underline{A}\underline{Q} ,$$

from which we have

$$\underline{A} = \underline{Q}\,\underline{\Lambda}\,\underline{Q}^{-1}$$

and then

$$\frac{d^2}{dx^2} = \underline{Q}\,\vec{E}' = \underline{Q}\,\underline{\Lambda}\,\underline{Q}^{-1}\underline{Q}\,\vec{E}' = \underline{Q}\,\underline{\Lambda}\,\vec{E}' ,$$

or finally,

$$\frac{d^2}{dx^2}\vec{E}' = \underline{\Lambda}\,\vec{E}' . \tag{23}$$

Since $\underline{\Lambda}$ is a diagonal matrix, this can be written as N independent equations; i. e.,

$$\frac{d^2}{dx^2}E_i' = \lambda_i\,E_i' \quad (i = 1 \text{ to } N) \tag{24}$$

and each of these will have a solution of the form

$$E_i' = \exp(\gamma_i x)\,E_{i+}' + \exp(-\gamma_i x)\,E_{i-}' \quad (i = 1 \text{ to } N)$$

where $\gamma_i = \sqrt{\lambda_i}$. The N solutions can be written more compactly as

$$\vec{E}' = \exp(\underline{\gamma}x)\,\vec{E}_+' + \exp(-\underline{\gamma}x)\,\vec{E}_-' \tag{25}$$

where now $\underline{\gamma}$ is also a diagonal matrix. In general, however, each E_i' will now be a linear combination of some or all of the original E_is as determined by the eigenvectors of $\underline{Z}\underline{Y}$. Thus, we have simplified $\underline{\gamma}$ at the expense of complicating $\vec{E}$.

The N waves described by Eq. 25 may have N distinct propagation constants γ_i. Consider the special case, however, of all propagation constants equal; i. e.,

$$\lambda_1 = \lambda_2 = \cdots = \lambda_N = \lambda_E = \gamma_E^2 \, .$$

We then have

$$\underline{\Lambda} = \lambda_E \, \overline{I} \, . \tag{26}$$

Substituting into

$$\underline{A} = \underline{Q} \, \underline{\Lambda} \, \underline{Q}^{-1} \, , \tag{27}$$

we obtain

$$\underline{A} = \underline{Q} \, \lambda_E \, \overline{I} \underline{Q}^{-1}$$

$$= \lambda_E \, \overline{I} \, (\underline{Q}\underline{Q}^{-1}) = \lambda_E \, \overline{I} \tag{28}$$

or

$$\underline{Z}\underline{Y} = \gamma_E^2 \, \overline{I} \, . \tag{29}$$

One form of the eigenvector matrix $\underline{Q}$ which will satisfy Eq. 27 for this case is $\underline{Q} = \overline{I}$ from which we have $E_i' = E_i$ for i = 1 to N, or $\vec{E}' = \vec{E}$. Thus, we have not only simplified $\underline{\gamma}$ to the very simple form of a scalar times the unit matrix, but have also not complicated $\vec{E}$ as before. For Eq. 19, we have a similar solution:

$$\underline{Y}\underline{Z} = \gamma_I^2 \, \overline{I} \, . \tag{30}$$

Finally, since for this case $\underline{Z}\underline{Y}$ and $\underline{Y}\underline{Z}$ are diagonal matrices, it is apparent from the fundamental theorem

$$(\underline{A}\underline{B})^T = \underline{B}^T \, \underline{A}^T \, ,$$

and the fact that $\underline{Z} = \underline{Z}^T$ and $\underline{Y} = \underline{Y}^T$, that $\underline{Z}\underline{Y} = \underline{Y}\underline{Z}$. Therefore,

$$\gamma_I = \gamma_E = \gamma \, .$$

Reiterating these results, we have the solutions to Eqs. 18 and 19 as shown by Eqs. 20 and 21, where $\underline{\gamma} = \underline{\gamma}'$ and

$$\underline{\gamma}^2 = \underline{Z}\underline{Y} = \gamma^2 \, \overline{I} \, . \tag{31}$$

If the line is assumed lossless, $R = G = \alpha = 0$, and then

$$\underline{Z} = j\omega\underline{L} ,$$

$$\underline{Y} = j\omega\underline{K} ,$$

$$\gamma = j\beta ,$$

and

$$(j\omega)^2 \underline{L}\underline{K} = (j\beta)^2 \overline{I}$$

or

$$\underline{L}\underline{K} = \frac{\beta^2}{\omega^2} \overline{I} = \frac{\overline{I}}{v_p^2} . \tag{32}$$

Equation 32 is analogous to Eq. 15 for the two-conductor line and shows again that if we know any two quantities, we know the third also. The $\underline{Y}$ matrix has been replaced here by a matrix designated $\underline{K}$ to emphasize the fact that the imaginary parts of $\underline{Y}$ are not truly capacitances.

In the foregoing solution, we had to assume equal propagation constants for all conductor pairs to be able to treat the system as a set of independent equations. An interesting solution results if, rather than forcing the independence, we simply assume it; i. e., we neglect the interaction between wires. The solution is then of the form

$$\underline{Z}\underline{Y} = \underline{\gamma}^2 , \tag{33}$$

where $\underline{\gamma}$ is a diagonal matrix with N distinct propagation constants γ_i (i = 1 to N) along the diagonal. Again, for the lossless case, this becomes

$$\underline{L}\underline{K} = (\underline{v}_p^{\,2})^{-1} \tag{34}$$

where now $\underline{v}_p$ is made up of N different phase velocities v_{p_i} (i = 1 to N) on the diagonal. This form of solution is more representative of practical multiconductor transmission lines since it accounts at least partially for

the variation in phase velocity which will always occur on such lines. It is not completely representative, however, since it still requires all off-diagonal terms to be zero. So long as the individual phase velocities do not vary significantly from the mean value on a practical line, either Eq. 32 or Eq. 34 may be expected to give acceptable results.

Summarizing the developments for the multiconductor transmission line, we have the following results subject to the stated assumptions.

$$\frac{d}{dx}\vec{E} = \underline{Z}\,\vec{I}$$

$$\frac{d}{dx}\vec{I} = \underline{Y}\,\vec{E}$$

} Pure TEM-mode propagation and sinusoidal excitation

$$\frac{d^2}{dx^2}\vec{E} = \underline{Z}\,\underline{Y}\,\vec{E}$$

$$\frac{d^2}{dx^2}\vec{I} = \underline{Y}\,\underline{Z}\,\vec{I}$$

$$\vec{E} = \exp(\underline{\gamma}\,x)\,\vec{E}_+ + \exp(-\underline{\gamma}\,x)\,\vec{E}_-$$

$$\vec{I} = \exp(\underline{\gamma}\,x)\,\vec{I}_+ + \exp(-\underline{\gamma}\,x)\,\vec{I}_-$$

} All of the above and uniform parameters

$$\underline{L}\,\underline{K} = \left(\underline{v}_p^{\,2}\right)^{-1}$$

} All of the above and a lossless line

$$\underline{L}\,\underline{K} = \frac{\overline{I}}{v_p^{\,2}}$$

} All of the above and uniform phase velocity

These results are essentially the same as those listed previously for the two-conductor line, except that the constants, $\vec{E}_+$, $\vec{E}_-$, $\vec{I}_+$, and $\vec{I}_-$ have not been determined. However, for the work which follows, these constants will not be required.

One final point which should be mentioned is the conclusion that $\gamma = \underline{\gamma}'$. For a lossless line, the propagation constants are determined by the phase velocities. Equal propagation constants for the voltage and current waves then simply imply that they travel with equal velocity. This is a reasonable conclusion from physical considerations and tends to verify the mathematical results.

3. COMPARISON OF THE DISTRIBUTED AND LUMPED SECTION MODEL SOLUTIONS FOR THE TRANSMISSION LINE EQUATIONS

The transmission line equations developed in Section 2 are for a distributed parameter model of the line, such as that shown in Fig. 3.1. For such a line, the transmission line equations can be solved directly for the exact solution. However, direct solutions may not always be possible.

A solution can also be obtained by representing the line as a series of sections made up of lumped circuit elements, and then applying circuit analysis techniques. Such a solution will be approximate, with the accuracy increasing as the number of sections used to represent a given length of line increases. This portion of the report will calculate the worst-case error of the lumped approximation as a function of the line length represented by each section.

3.1 DISTRIBUTED PARAMETER MODEL

Figure 3.1 shows the distributed model of a single-wire transmission line over a ground plane; the line is modeled by an admittance to ground per unit length, y, and by an impedance per unit length of the conductor, z. This configuration is solved by writing the partial differential equations that describe the propagation of currents and voltages along the line. The solution is shown in detail in Section 2 and in standard texts on transmission lines. The solution is in the form of forward- and backward-traveling waves that satisfy the boundary or terminal values of impedances and sources.

Figure 3.2 shows a unit section of transmission line to be solved for the ratio of output to input voltage. This could be any section of the

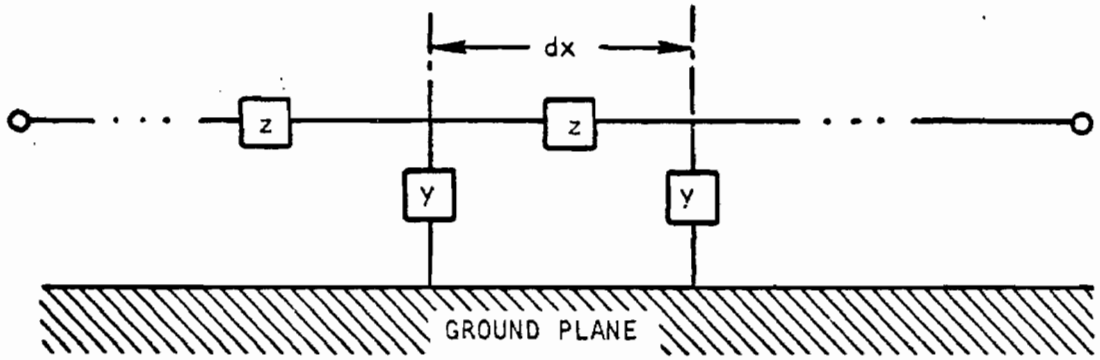

Fig. 3.1. Distributed model of transmission line

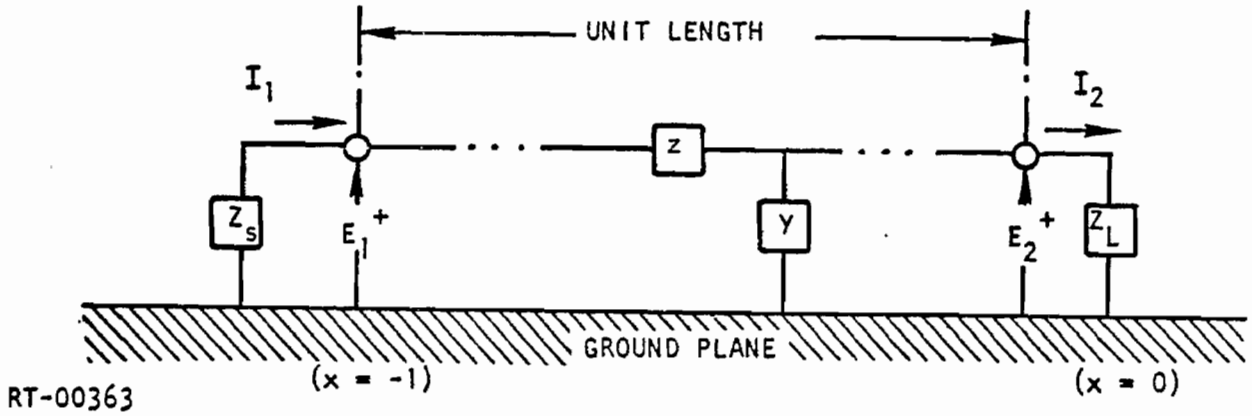

Fig. 3.2. Unit length section of transmission line

cable; i. e., Z_s could represent the impedance of the cable to the left and Z_L the impedance of the cable looking to the right. It could also represent the entire length of the cable where Z_s is a source impedance and Z_L is a termination impedance.

For the distributed model, the transmission line equations must be solved. Call the position of E_1, $x = -1$; call the position of E_2, $x = 0$. Then following the solution given by Ramo et al.,[11]

$$E_1 = E^+ \exp(+\gamma\ell) + E^- \exp(-\gamma\ell)$$

$$E_2 = E^+ + E^-$$

$$I_1 = I^+ \exp(+\gamma\ell) - I^- \exp(-\gamma\ell)$$

$$I_2 = I^+ - I^-$$

$$\gamma = \sqrt{zy} \qquad [\exp(+j\omega t) \text{ understood}]$$

where E^+ and E^- refer to forward- (towards the load) and reverse-traveling voltage waves and I^+ and I^- refer to forward- and reverse-traveling current waves.

At the load end, the terminal condition exists that $E_2/I_2 = Z_L$, and from the characteristic impedance of the line, $E^+/I^+ = E^-/I^- = Z_0$.* Combining these gives

$$\frac{E_2}{I_2} = Z_L = \frac{E^+ + E^-}{(E^+/Z_0) - (E^-/Z_0)} ,$$

$$\frac{E^-}{E^+} = \frac{Z_L - Z_0}{Z_L + Z_0} .$$

Then the transfer function between E_2 and E_1 is

*This can be verified readily using the constants E^+, E^-, I^+, and I^- from Eqs. 13 and 14 in Section 2.

$$\frac{E_2}{E_1} = \frac{E^+ + \left(\frac{Z_L - Z_0}{Z_L + Z_0}\right) E^+}{E^+ \exp(\gamma\ell) + \left(E^+ \frac{Z_L - Z_0}{Z_L + Z_0}\right) \exp(-\gamma\ell)}$$

$$= \frac{2 Z_L}{Z_L [\exp(+\gamma\ell) + \exp(-\gamma\ell)] + Z_0 [\exp(\gamma\ell) - \exp(-\gamma\ell)]} \quad (35)$$

for the distributed parameter model.

3.2 LUMPED ELEMENT MODEL

Figure 3.3 shows the lumped element model for modeling this section of cable by only one lump; the distributed parameters, z and y, per meter have been multiplied by the length of the cable section, ℓ, to give the lumped element values. This is solved by ac circuit theory as follows.

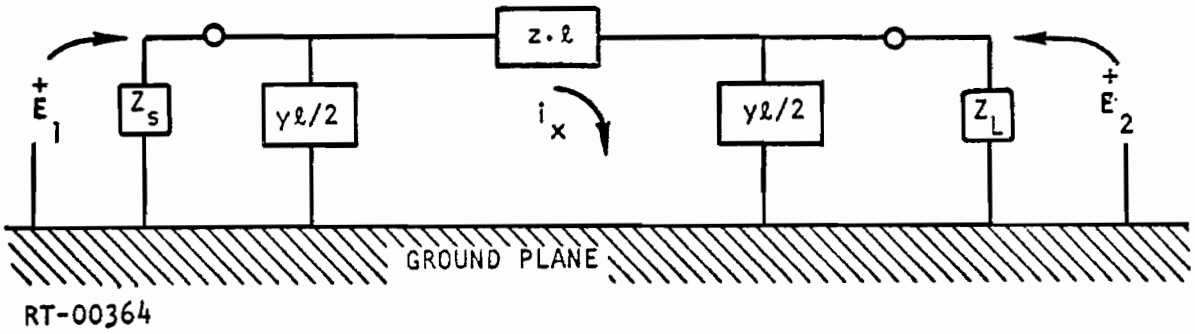

Fig. 3.3. Lumped element model of transmission line

Using the loop current, i_x, gives

$$E_1 = \left(z\ell + \frac{\left(\frac{1}{y\ell/2}\right) Z_L}{\left(\frac{1}{y\ell/2}\right) + Z_L}\right) i_x$$

$$E_2 = \left(\frac{\frac{1}{y\ell/2} \; Z_L}{\frac{1}{y\ell/2} + Z_L} \right) i_x$$

$$\frac{E_2}{E_1} = \frac{Z_L}{Z_L \left(1 + \frac{yz\ell^2}{2}\right) + z\ell} \tag{36}$$

for the lumped element model.

3.3 COMPARISON OF MODELS

It is now desired to show that Eqs. 35 and 36 are the same within some error bound for a lumped section that is sufficiently short; that is, it is necessary to show that:

1. For a lumped section that is sufficiently short, the error in the transfer function E_2/E_1 will be less than some desired number, e.g., ±10%.
2. As the lumped sections get smaller, Eqs. 35 and 36 approach each other; i.e., the lumped section becomes a distributed section.

Substituting into Eq. 35 with the relations $Z_0 = \sqrt{z/y}$ and $\gamma = \sqrt{zy}$ gives

$$\frac{E_2}{E_1} = \frac{2 \, Z_L}{Z_L \left[\exp(+\sqrt{yz}\,\ell) + \exp(-\sqrt{yz}\,\ell)\right] + \sqrt{z/y} \left[\exp(+\sqrt{yz}\,\ell) - \exp(-\sqrt{yz}\,\ell)\right]} \tag{37}$$

Using the trig identities

$$\exp(x) = 1 + x + \frac{x^2}{2!} + \frac{x^3}{3!} + \cdots$$

$$\exp(x) + \exp(-x) = 2 \left(1 + \frac{x^2}{2!} + \frac{x^4}{4!} + \cdots\right)$$

$$\exp(x) - \exp(-x) = 2 \left(x + \frac{x^3}{3!} + \frac{x^5}{5!} + \cdots\right)$$

in Eq. 35 gives

$$\frac{E_2}{E_1} = \frac{Z_L}{Z_L\left[1 + \frac{yz\ell^2}{2!} + \frac{(yz\ell^2)^2}{4!} + \cdots\right] + z\ell\left[1 + \frac{yz\ell^2}{3!} + \frac{(yz\ell^2)^2}{5!} + \cdots\right]}$$

This is the power series expansion of Eq. 35, the solution to the transmission line equations for the distributed parameter model.

The expansion is in terms of $yz\ell^2$ or in terms of $(\gamma\ell)^2$. The quantity z is usually of the form $z = r + j\omega\ell_i$, where r is the resistance per unit length of the transmission line and ℓ_i is the self-inductance per unit length of the transmission line. The quantity y is usually of the form $y = g + j\omega c$, where g is the conductance per unit length between the transmission line and ground and c is the capacitance per unit length between the transmission line and ground. These are finite quantities, and for a finite frequency, ω is finite, which in turn makes both y and z finite.

For convenience, Eq. 35 can be rewritten as a series expansion in x where $x = yz\ell^2 = (\gamma\ell)^2$. Then

DISTRIBUTED MODEL

$$\frac{E_2}{E_1} = \frac{Z_L}{Z_L\left(1 + \frac{x}{2!} + \frac{x^2}{4!} + \cdots\right) + z\ell\left(1 + \frac{x}{3!} + \frac{x^2}{5!} + \cdots\right)} \quad . \tag{38}$$

Equation 36 can be written in this form also to show the comparison.

LUMPED MODEL

$$\frac{E_2}{E_1} = \frac{Z_L}{Z_L\left(1 + \frac{x}{2}\right) + z\ell(1)} \tag{39}$$

If the lumped section length, ℓ, approaches 0, $(\gamma\ell)^2$ also approaches 0, and then Eq. 38 equals Eq. 39; that is, as the section length approaches zero, the lumped and distributed solutions become the same. This is expected since both describe the same model as $\ell \to 0$.

It can be seen also that if x is small compared to 1, the lumped approximation will give good results per section; that is, the extra terms

in the denominator of Eq. 38 (e.g., $x^2/4! + \ldots$ and $x/3! + x^2/5! + \ldots$) will be negligibly small compared to 1.

3.4 ERROR ANALYSIS

The quantity γ, the propagation constant, is in general complex; it can be written as

$$\gamma = \alpha + j\beta$$

where

α = attenuation constant, a real number, and

β = phase velocity, a real number.

In terms of the distributed element values, $\gamma = \alpha + j\beta = \sqrt{zy}$, and $z = r + j\omega\ell$, $y = g + j\omega c$; for parameters such that $r/\omega\ell \ll 1$, $g/\omega c \ll 1$, it can be shown that

$$\alpha \cong \frac{r}{2\sqrt{\ell/c}} + \frac{g\sqrt{\ell/c}}{2} ,$$

$$\beta \cong \omega\sqrt{\ell c}\left(1 - \frac{rg}{4\omega^2\ell c} + \frac{g^2}{8\omega^2 c} + \frac{r^2}{8\omega^2\ell}\right) ,$$

$$Z_0 \cong \sqrt{\ell/c}\left[\left(1 + \frac{r^2}{8\omega^2\ell^2} - \frac{3g^2}{8\omega^2 c^2} + \frac{rg}{4\omega^2\ell c}\right) + j\left(\frac{g}{2\omega c} - \frac{r}{2\omega\ell}\right)\right] .$$

For most real cables and frequencies up to 30 MHz, $|\alpha| \ll |\beta|$, and $\beta = 2\pi/\lambda$. Then the quantity $x = (\gamma\ell)^2$ can be written as $x = (\gamma\omega)^2 = (\alpha + j\beta)^2 \cdot \ell^2$ and, since $\alpha \ll \beta$, this can be expressed as

$$x \cong (j\beta\ell)^2 = -\beta^2\ell^2 = -4\pi^2(\ell/\lambda)^2 .$$

Suppose $\ell = \lambda/10$; i.e., each lumped section of cable is 1/10 of a wavelength long. Then,

$$x = -0.3947841760 ,$$

$$1 + \frac{x}{2} = 0.80261$$

$$1 + \frac{x}{2} + \frac{x^2}{4!} + \cdots = 0.80919$$

$$1 = 1.0$$

$$1 + \frac{x}{3!} + \frac{x^2}{5!} + \cdots = 0.93289$$

This shows an error of 0.81% in the coefficient of Z_L and an error of 6.7% in the coefficient of $z\ell$ for Eq. 39 compared to Eq. 38.

This calculation has been done for several values of ℓ in units of fractions of a wavelength. The results are shown in Table 3.1.

Table 3.1

ERROR IN COEFFICIENTS OF Z_L and $z\ell$

ℓ/λ	Error in Coefficient of Z_L	Error in Coefficient of $z\ell$
1/40	0.002%	0.4%
1/20	0.04%	1.6%
1/10	0.81%	6.7%
1/8	2.2%	11.0%

The effect of the error in the coefficients of Z_L and $z\ell$ of Eq. 39 as compared to Eq. 38 can be evaluated as follows.

From Table 3.1, it can be seen that the error in the coefficient of $z\ell$ is always greater than the error in the coefficient of Z_L; therefore, a worst-case error in the magnitude of E_2/E_1 would occur if $|z\ell|$ is much greater than $|Z_L|$; then the error in the magnitude of E_2/E_1 will be just the error in the coefficient of $z\ell$. It should be noted that this is a theoretical worst-case analysis and represents a greater error than expected in real cables where Z_L is equal or greater than $z\ell$.

The effect of the error in the coefficients of $z\ell$ and Z_L upon the phase angle of E_2/E_1 can be considered by rewriting Eq. 35 as:

$$\frac{E_2}{E_1} = \frac{Z_L}{Z_L \alpha (1 + \epsilon_A) + z\ell\beta (1 + \epsilon_B)} \tag{40}$$

where

α = coefficient of Z_L ,

β = coefficient of $z\ell$,

ϵ_A = error in the coefficient of Z_L , and

ϵ_B = error in the coefficient of $z\ell$.

A worst-case phase angle error occurs when the complex numbers $Z_L \alpha$ and $z\ell\beta$ are of equal magnitude and differ in angle by 90°; i. e., they are perpendicular. Considering only an error in the coefficient of β (i. e., $\epsilon_A = 0$), Table 3.2 can be constructed to show the effect upon the phase angle of E_2/E_1 for an error in the coefficient of $z\ell$.

Table 3. 2

ERROR IN PHASE ANGLE OF E_2/E_1

Error in Coefficient of $z\ell$ (ϵ_B)	Error in Phase Angle of E_2/E_1 (ϵ_φ)
0. 1%	0. 0286°
0. 2%	0. 057°
0. 5%	0. 143°
1%	0. 295°
2%	0. 567°
5%	1. 40°
10%	2. 73°
20%	5. 20°
50%	11. 3°

Using Tables 3.1 and 3.2, it is possible to determine the maximum amplitude and phase angle error per lumped section; this is shown in Table 3.3.

Table 3.3

MAXIMUM AMPLITUDE AND PHASE ERROR PER SECTION

Length of Lumped Sections in Fractions of a Wavelength	Maximum Magnitude Error in $\lvert E_2/E_1 \rvert$	Maximum Phase Error in E_2/E_1
1/40	≤ 0.4% (0.035 dB)	≤ 0.11°
1/20	≤ 1.6% (0.138 dB)	≤ 0.45°
1/10	≤ 1.6% (0.563 dB)	≤ 1.86°
1/8	≤ 11.0% (0.906 dB)	≤ 2.98°

3.5 MULTIPLE-SECTION MODELING

In general, a cable of interest is modeled by more than one lumped section. For example, consider the error analysis applied to a 10-m-long cable; suppose the velocity of propagation for the cable is 2.0×10^8 m/sec; suppose also the highest frequency of interest is 20 MHz. Then,

$$\lambda = \frac{v_p}{f} = \frac{2 \times 10^8 \text{ m/sec}}{20 \times 10^6 \text{ Hz}} = 10 \text{ m} . \qquad (41)$$

This cable is one wavelength long; it can be modeled by ten 1/10-wavelength-long sections. As a worst-case error analysis, the phase error will add for each section and the amplitude error will multiply. (Multiplying amplitude errors per section is the same as adding dB errors.)

The total magnitude error for ten 1/10-wavelength-long sections can be determined from Table 3.3 as follows.

Magnitude error = $(1.067)^{10}$ = 10 x 0.563 dB = 5.63 dB

Phase error = 10 x 1.86° = 18.6°

Then the total error for the cable will be 5.63 dB error in the magnitude of E_2/E_1 and 18.6° in the phase of E_2/E_1. This analysis has been performed on sections of 1/8, 1/10, 1/20, and 1/40 of a wavelength and is summarized in Table 3.4.

Table 3.4

TOTAL AMPLITUDE AND PHASE ERROR

Length of Section (ℓ/λ)	Maximum Total Amplitude Error $\lvert E_2/E_1 \rvert$	Maximum Total Phase Error (°)
1/40	≤ 18% (1.40 dB)	≤ 4.4°
1/20	≤ 36% (2.76 dB)	≤ 9.0°
1/10	≤ 92% (5.63 dB)	≤ 18.6°
1/8	≤ 232% (7.25 dB)	≤ 23.8°

The improvement by using more sections that are smaller fractions of a wavelength can be seen in Table 3.4; i.e., 40 sections of 1/40 wavelength give an amplitude error of 1.4 dB and phase error of 4.4° compared to 8 sections of 1/8 wavelength which gives an amplitude error of 7.25 dB and a phase error of 23.8°.

It can be seen that Table 3.3 can be used to bound the error caused by the lumped model approximation. It should also be noted that these are worst-case estimates of the error.

4. METHODS FOR DETERMINING PARAMETER VALUES

The previously developed transmission line equations and solutions for an N+1 conductor line will now be used to develop methods for determining a line's distributed parameters from those parameters that can be measured in the laboratory. The distributed parameters for an MTL cannot be measured directly because of the numerous interactions between conductors, thus necessitating this indirect approach.

The question may be asked, of course, "Why not calculate the required parameters directly from the conductor geometry?" An example of such a calculation and the results will be presented in the section on miscellaneous topics, Section 6. This direct approach can, in fact, be used quite effectively if the conductor configuration is very simple. Unfortunately, this will seldom be the case for practical control and communication cables, with the possible exception of simple coaxial cables used for rf transmission. And in large installations, even these cables may be bundled together so that their interactions must be considered. Examination of the equations for determining the various parameters for a configuration no more complex than four unshielded wires in an overall shield[9] reveal the extreme complexity of the required calculations. Further, these equations still assume a certain degree of wire symmetry which simply will not occur in randomly configured cables. Thus, an approach based on laboratory measurements of actual cable parameters is required.

The direct calculation technique does have application to the problem of modeling the cable to structure interactions. Separate modeling of the cable proper and the cable-structure pair will be the subject of a later section.

We have previously mentioned four parameters which are required for the cable characterization, namely, R, L, G, and C. The parameters R and G will be those which account for losses or attenuation. In particular, the attenuation constant in dB/100 ft of a two-conductor line at ultra-high frequencies is given by[6]

$$\alpha = \underbrace{\frac{4.34\, R_t}{Z_0}}_{\text{R CONTRIBUTION}} + \underbrace{2.78\, \epsilon\, f\, F_p}_{\text{G CONTRIBUTION}}$$

where

$R_t = 0.1 \left(\frac{1}{d} + \frac{1}{D}\right) f^{\frac{1}{2}}$ (for copper coaxial conductors),

$R_t = 0.2 \left(\frac{1}{d}\right) f^{\frac{1}{2}}$ (for parallel copper wires),

D = inside diameter of outer coaxial conductor (inches),

d = diameter of parallel wires or center coaxial conductor (inches),

f = frequency in MHz,

ϵ = relative dielectric constant at f,

F_p = power factor of dielectric at f.

Calculation of several numerical examples for typical conductor dimensions and dielectric materials shows that, at frequencies of 10^8 Hz or less, the attenuation due to R is a factor of 10 or more greater than that due to G. Therefore, little error will be introduced by neglecting the shunt conductance G, leaving only R, L, and C to be determined.*

Methods of determining L and C will be presented first, assuming a lossless line; then a method for determining R will be presented.

*This will be true for the MTL also since, in the limit, a wire surrounded by a number of other wires merely becomes the coaxial case discussed above.

4.1 CAPACITANCE-BASED L AND C PARAMETERS

This section presents a method for determining the L and C parameters of an MTL based on capacitance measurements made on the cable to be modeled. This method is based on the assumption of pure TEM-mode waves on the MTL despite the obvious imperfections of real cables which prevent this from being true. However, as pointed out earlier, the assumption of pure TEM propagation is a reasonable approximation for most practical cases, and the simplifications which result from the assumption make it well worthwhile.

With the assumption of TEM propagation, the coefficients of potential, induction, and capacitance for a set of conductors can be determined from static fields.[5] The relationship between potentials and charges on a system of N straight conductors of arbitrary shape over a ground plane can be found in many textbooks on field theory. Using Kajfez's notation, the charges are related to potentials by

$$q_i = K_{i1} E_1 + K_{i2} E_2 + \cdots + K_{ii} E_i + \cdots + K_{iN} E_N \qquad \text{for } i = 1, 2, \cdots N \tag{42}$$

where

q_i = line charge on the i^{th} conductor (C/m),

E_i = potential of the i^{th} conductor with respect to ground (V).

The coefficients of K_{ij} are coefficients of proportionality between voltage and charge and have units of coulombs/volt-meter or farads/meter, the units of capacitance. However, Maxwell calls only the diagonal terms K_{ii} of the $\underline{K}$ matrix coefficients of capacitance, and the off-diagonal terms K_{ij} he calls coefficients of electrostatic induction.[4]

In Section 2, we derived the transmission line equations of the MTL, based on the previously stated conditions of single-velocity pure-TEM waves

on the MTL. The important result for the purposes of this development is Eq. 32 of that section, namely,

$$\underline{L}\,\underline{K} = \frac{1}{v_p^2}\,\bar{I} \ .$$

In this equation, the terms of the $\underline{L}$ matrix represent actual inductances of the MTL; i. e., the L_{ii} terms are the actual inductances of the closed circuit formed by the i^{th} conductor and ground, and the L_{ij} terms are the mutual inductances between the i^{th} and j^{th} conductors. Solving for $\underline{L}$ in Eq. 34 gives

$$\underline{L} = \frac{1}{v_p^2}\,\bar{I}\,\underline{K}^{-1} \ . \tag{43}$$

Thus, if we can determine $\underline{K}$ for the cable, we can determine the cable inductance parameters. The next consideration, then, is how we can determine $\underline{K}$, and whether we can then also calculate the cable capacitance parameters.

In a system of conductors, there will be a capacitance from each conductor to all other conductors which we may call the partial capacitance, denoted C^p, and it is these that we must determine for the cable model. * The manner in which the coefficients K_{ij} are related to these partial capacitances C^p_{ij} is determined as follows.

Consider the partial capacitances of the i^{th} conductor, shown in Fig. 4.1. The total charge on this conductor is the sum of the charges on its partial capacitances, given by

$$q_i = \sum_{j=1}^{N} C^p_{ij}\,E_{ij} \ , \tag{44}$$

where

$$E_{ij} = E_i - E_j \ ,$$

*These are the same capacitances as shown in Section 2. The superscript p is used merely to prevent confusing these capacitances with the measured capacitances (superscript m) to be introduced later.

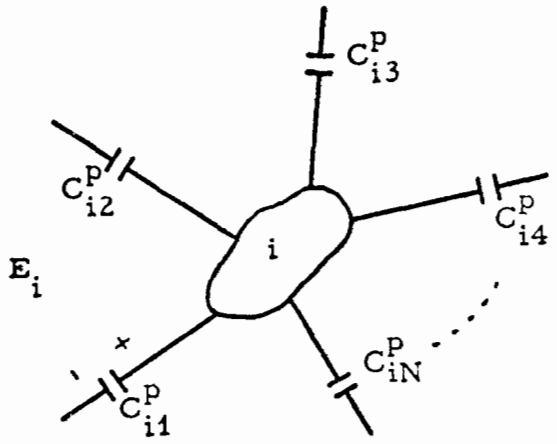

Fig. 4.1. Partial capacitances of the i^{th} conductor

C^p_{ij} = capacitance from wire i to wire j ,

and

C^p_{ii} = capacitance from wire i to ground .

Expanding this expression gives

$$q_i = C^p_{i1}(E_i - E_1) + C^p_{i2}(E_i - E_2) + \cdots + C^p_{ii} E_i + \cdots + C^p_{iN}(E_i - E_N) . \quad (45)$$

Grouping the E_i terms yields

$$q_i = -C^p_{i1} E_1 - C^p_{i2} E_2 - \cdots + \sum_{j=1}^{N} C^p_{ij} E_i - \cdots - C^p_{iN} E_N . \quad (46)$$

Comparing Eqs. 42 and 46, we see that*

$$K_{ij} = -C^p_{ij} \quad (47)$$

*Note that, since the K_{ij} terms are the negative of real capacitances which will always be positive, the K_{ij} will always be negative. Thus, the K_{ij} cannot be legitimately called capacitances as indicated by Maxwell.

and

$$K_{ii} = \sum_{j=1}^{N} C_{ij}^{P} \, . \tag{48}$$

Comparison of Eqs. 47 and 48 to the expanded form of Eq. 17 in Section 2 shows that, with G no longer considered, Eq. 48 gives the diagonal terms of Eq. 17 and Eq. 47 gives the off-diagonal terms. Thus, the $\underline{K}$ matrix has been derived by an alternate method.

Now the K_{ii} or diagonal terms will be simple to measure on a cable since they are the sum of all partial capacitances to wire i from the other wires. That is, by merely shorting all but the i^{th} wire to the ground and then measuring the capacitance C_{ii}^{m} (using an impedance bridge) from i to ground, K_{ii} is determined directly since all of the appropriate partial capacitances are then in parallel. Thus, we have the diagonal terms of the $\underline{K}$ matrix as determined by N measurements of C_{ii}^{m} $(i = 1, 2, \cdots N)$.

Some manipulation is necessary to obtain the off-diagonal terms, K_{ij}. Consider the partial capacitances of the i^{th} and j^{th} conductors, as shown in Fig. 4.2. If we try to measure C_{ij} directly with an impedance bridge as we previously measured K_{ii}, we would actually get the parallel combination of C_{ij} and a complex series-parallel combination of other

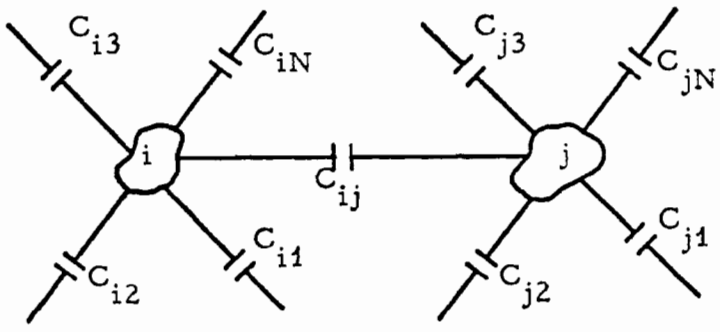

RT-00370

Fig. 4.2. Partial capacitances of the i^{th} and j^{th} conductors

partial capacitances. In measuring C_{ii}^m and C_{jj}^m, however, observe that we can take C_{ij}^p out of the summation and have

$$C_{ii}^m = C_{ij}^p + \sum_{\substack{k=1 \\ k\neq j}}^{N} C_{ik}^p \tag{49}$$

and

$$C_{jj}^m = C_{ji}^p + \sum_{\substack{k=1 \\ k\neq i}}^{N} C_{jk}^p \ . \tag{50}$$

Solving for C_{ij}^p by making use of $C_{ij}^p = C_{ji}^p$ gives the result

$$C_{ij}^p = \frac{1}{2}\left(C_{ii}^m - \sum_{\substack{k=1 \\ k\neq j}}^{N} C_{ik}^p + C_{jj}^m - \sum_{\substack{k=1 \\ k\neq i}}^{N} C_{jk}^p\right) \ . \tag{51}$$

This is still not quite the desired result due to the presence of the two partial capacitance summations. However, these summations can be very conveniently disposed of by the following.

If we short conductors i and j together and also short all other conductors to ground and then measure the capacitance between these two conductor sets, which we designate C_{ij}^m, we find that

$$C_{ij}^m = \sum_{\substack{k=1 \\ k\neq j}}^{N} C_{ik}^p + \sum_{\substack{k=1 \\ l\neq i}}^{N} C_{jk}^p \ . \tag{52}$$

The C_{ij}^p and C_{ji}^p terms drop out of these summations, of course, because C_{ij}^p is shorted. Combining Eqs. 51 and 52 gives the result

$$C_{ij}^p = \frac{1}{2}\left(C_{ii}^m + C_{jj}^m - C_{ij}^m\right) \ , \tag{53}$$

and by merely changing sign we have the off-diagonal terms K_{ij} of the $\underline{K}$ matrix,

$$K_{ij} = \frac{1}{2}\left(C_{ij}^{m} - C_{ii}^{m} - C_{jj}^{m}\right) . \tag{54}$$

We can now fill the $\underline{K}$ matrix based on a series of capacitance measurements on the cable whose parameters we wish to determine. With the $\underline{K}$ matrix available, we can solve for the inductance parameters. All that is left to complete the model then is to determine the elements of the partial capacitance matrix $\underline{C^{p}}$ from $\underline{K}$.

The off-diagonal terms of the $\underline{C^{p}}$ matrix have already been determined above in Eq. 53. The diagonal terms can be found from

$$K_{ii} = C_{ii}^{m} = \sum_{k=1}^{N} C_{ik}^{p} . \tag{55}$$

By removing C_{ii}^{p} from the summation,

$$C_{ii}^{m} = C_{ii}^{p} + \sum_{\substack{k=1 \\ k\neq i}}^{N} C_{ik}^{p} , \tag{56}$$

which when rearranged gives

$$C_{ii}^{p} = C_{ii}^{m} - \sum_{\substack{k=1 \\ k\neq i}}^{N} C_{ik}^{p} . \tag{57}$$

Unfortunately, there is no clever way of grouping conductors and making capacitance measurements which will dispose of the summation in Eq. 56, as we were able to do previously with Eq. 51. However, the C_{ik} will all be available for making the summation; therefore, the C_{ii}^{p} can be calculated from Eq. 57.

In summary, we have developed a technique for determining the capacitance and inductance parameters for a cable model, based on capacitance measurements on the cable to be modeled. To reiterate the procedure, the steps are as follows.

First, a matrix of measured capacitances $\underline{C}^m$ is created by making the following measurements.

C_{ii}^m = measured capacitance from the i^{th} wire to all other wires shorted to ground,

C_{ij}^m = measured capacitance from the i^{th} and j^{th} wires shorted together to all other wires shorted to ground ($i \neq j$).

This amounts to somewhat more than $1/2\ N^2$ measurements* on an N+1 conductor cable (including ground). The elements of the $\underline{K}$ matrix are determined from

$$K_{ii} = C_{ii}^m$$

and

$$K_{ij} = \frac{1}{2}\left(C_{ij}^m - C_{ii}^m - C_{jj}^m\right) (i \neq j) .$$

Remember that the K_{ij} terms will always be negative. The inductance matrix $\underline{L}$ can then be determined from $\underline{K}$ and v_p by use of Eq. 32.

Note that on practical cables, v_p will not be uniform but will have different values for each conductor pair. An average value of v_p will have to be used for the calculation. Of course, this will introduce some error in the parameters for wires whose v_p is different from this average. If improved accuracy is necessary, the solution shown in Eq. 34 may give better results.

The elements of the $\underline{L}$ matrix are the actual inductance parameters for the cable, as has been mentioned before. That is,

L_{ii} = the inductance of closed circuit formed by the i^{th} wire and ground,

L_{ij} = mutual inductance between i^{th} and j^{th} wires ($i \neq j$).

*In fact, exactly 1/2 N(N+1) measurements.

The final parameters to be determined are the partial capacitances from each wire to all other wires and from each wire to ground. These are given by

$$C_{ij}^{p} = -K_{ij} \quad (i \neq j)$$

and

$$C_{ii}^{p} = C_{ii}^{m} - \sum_{\substack{j=1 \\ j\neq i}}^{N} C_{ij}^{p} = K_{ii} + \sum_{\substack{j=1 \\ j\neq i}}^{N} K_{ij} \ .$$

The elements of the $\underline{L}$ and $\underline{C^{p}}$ matrices then are the final inductance and capacitance parameters for the MTL. These can be used to create a lumped-parameter equivalent circuit model of the cable for which they have been determined.

4.2 OPEN-CIRCUIT IMPEDANCE-BASED L AND C PARAMETERS

In Section 2, we developed the differential equation for an MTL (Eq. 16) and solved the equation for the case of arbitrary velocities of propagation for each wire-reference pair (Eq. 20). For a lossless line, Eq. 16 becomes

$$\frac{d}{dx} \vec{E} = j\omega \underline{L} \vec{I} \ . \tag{58}$$

Equation 20 is

$$\vec{E} = \exp(\underline{\gamma} x) \vec{E}_{+} + \exp(-\underline{\gamma} x) \vec{E}_{-} \ .$$

By substituting Eq. 20 into Eq. 58, we obtain

$$\underline{\gamma} \exp(\underline{\gamma} x) \vec{E}_{+} - \underline{\gamma} \exp(-\gamma x) E^{-} = j \omega \underline{L} \vec{I}$$

or

$$\vec{I} = \underline{Z_0}^{-1} [\exp(\underline{\gamma} x) \vec{E}_{+} - \exp(-\underline{\gamma} x) \vec{E}_{-}] \ , \tag{59}$$

where $\underline{Z_0}$ is defined as the characteristic impedance matrix and is equal to $(1/\underline{v_p})\ \underline{K}^{-1}$.

It is observed that the matrix $\underline{Z_0}$ is a function of MTL parameters only and is not affected by terminations at either end of the cable. Let us rewrite Eq. 59 into the following form.

$$\exp(\underline{\gamma} x)\, \vec{E}_+ - \exp(-\underline{\gamma} x)\, \vec{E}_- = \underline{Z_0}\, \vec{I} \,. \tag{60}$$

Since we know that $\underline{Z_0}$ is not a function of external loading, let us terminate the i^{th} conductor into its characteristic impedance Z_{0_i} with all other conductors left open. By making such a termination, the left-traveling wave in the i^{th} conductor will be zero, and Eq. 60 becomes

$$\exp(\gamma_i x)\, E_i^+ = Z_{i1}\, I_1 + Z_{i2}\, I_2 + \cdots + Z_{ii}\, I_i + \cdots + Z_{iN}\, I_N \,, \tag{61}$$

and for $x = 0$,

$$E_i^+ = Z_{i1}\, I_1 + Z_{i2}\, I_2 + \cdots + Z_{ii}\, I_i + \cdots + Z_{iN}\, I_N \,. \tag{62}$$

If we are exciting the i^{th} conductor with a voltage E, then $E_i^+ = E$, and

$$E = Z_{i1}\, I_1 + Z_{i2}\, I_2 + \cdots + Z_{ii}\, I_i + \cdots + Z_{iN}\, I_N \,. \tag{63}$$

It is known that if a lossless transmission line is excited by an ideal voltage source at one end and terminated in its characteristic impedance at the other, the source voltage and current are related by

$$E_s = Z_0\, I_s \,. \tag{64}$$

Assuming that $I_1, I_2, \ldots$ are much smaller than I_i at $x = 0$, Eq. 63 can be reduced to

$$E \cong Z_{ii}\, I_i \,. \tag{65}$$

On comparison of Eqs. 64 and 65, we see that

$$Z_{ii} \cong Z_{0_i} \,. \tag{66}$$

Therefore, we conclude that the diagonal terms of the $\underline{Z_0}$ matrix approximately represent the characteristic impedance of an individual conductor with respect to the reference node.

Now let us terminate both the i^{th} and j^{th} conductors in their characteristic impedances Z_{0_i} and Z_{0_j}, respectively, with all other conductors open. As before, the magnitude of the left-traveling wave in each conductor will be zero. Then from Eq. 60 we have, at x = 0,

$$E_i^+ = Z_{i1} I_1 + Z_{i2} I_2 + \cdots + Z_{ii} I_i + \cdots + Z_{ij} I_j + \cdots + Z_{iN} I_N \tag{67}$$

and

$$E_j^+ = Z_{j1} I_1 + Z_{j2} I_2 + \cdots + Z_{ji} I_i + \cdots + Z_{jj} I_j + \cdots + Z_{jN} I_N \, . \tag{68}$$

If the magnitude and phase relationships of the excitation voltages for the i^{th} and j^{th} conductors are chosen such that $I_i = -I_j$, then

$$\begin{aligned} E_{i-j} &= E_i - E_j \\ &= Z_{i1} I_1 + Z_{i2} I_2 + \cdots + Z_{ii} I_i + \cdots + Z_{ij} I_j + \cdots \\ &\quad + Z_{iN} I_N - \left(Z_{j1} I_1 + Z_{j2} I_2 + \cdots + Z_{ji} I_i + \cdots \right. \\ &\quad \left. + Z_{jj} I_j + \cdots + Z_{jN} I_N\right) \\ &= (Z_{i1} - Z_{j1}) I_1 + (Z_{i2} - Z_{j2}) I_2 + \cdots + (Z_{ii} - Z_{ji}) I_i \\ &\quad + \cdots + (Z_{ij} - Z_{jj}) I_j + \cdots + (Zi_N - Z_{jN}) I_N \, . \end{aligned} \tag{69}$$

Again, if all other wire currents are small compared to I_i and I_j,

$$E_{i-j} \cong (Z_{ii} - Z_{ji}) I_i + (Z_{ij} - Z_{jj}) I_j \, . \tag{70}$$

But since we required that $I_i = -I_j$,

$$E_{i-j} \cong (Z_{ii} - Z_{ji})\, I_i + (Z_{ij} - Z_{jj})(-I_i)$$

$$\cong (Z_{ii} + Z_{jj} - Z_{ij} - Z_{ji})\, I_i \,. \tag{71}$$

Since for a linear network $Z_{ij} = Z_{ji}$, the relationship between differential voltage applied to a conductor pair and the current is approximately

$$E_{i-j} \cong (Z_{ii} + Z_{jj} - 2Z_{ij})\, I_i \,. \tag{72}$$

Comparison once again with Eq. 64 leads us to conclude that the characteristic impedance between any wire pair is given by

$$Z_{0_{ij}} = Z_{ii} + Z_{jj} - 2Z_{ij} \,. \tag{73}$$

From the relationships in Eqs. 66 and 73, it should now be possible to generate the $\underline{Z_0}$ matrix from measured characteristic impedances. The terms of the $\underline{Z_0}$ matrix are given by

$$Z_{ii} \cong Z_{ii}^{m} \tag{74}$$

and

$$Z_{ij} = \frac{Z_{ii}^{m} + Z_{jj}^{m} - Z_{ij}^{m}}{2} \,, \tag{75}$$

where superscript m indicates measured impedances. Z_{ii}^{m} is the measured characteristic impedance of the i^{th} conductor and reference node. Z_{jj}^{m} is the measured characteristic impedance of the j^{th} conductor and reference node. Z_{ij}^{m} is the measured characteristic impedance of the i^{th} and j^{th} conductor pair.

It is interesting to note the results for a symmetrical* cable. In a symmetrical configuration, the characteristic impedance matrix is of the form

*This refers to mathematical rather than physical symmetry, and is also called "the completely transposed" line in Dr. L. A. Pipes's paper, "Matrix Theory of Multiconductor Transmission Lines," Philosophical Magazine, July 1937.

$$\underline{Z_0} = \begin{bmatrix} Z_d & & Z_m \\ & \ddots & \\ Z_m & & Z_d \end{bmatrix},$$

where all diagonal terms equal Z_d and the off-diagonal terms equal Z_m. Looking now at Eq. 69, we see that all terms are exactly zero except those related to I_i and I_j. Therefore,

$$E_{i-j} = (Z_{ii} + Z_{jj} - 2Z_{ij}) I_i .$$

But since $Z_{ii} = Z_{jj} = Z_d$ and $Z_{ij} = Z_m$, we obtain

$$E_{ij} = 2(Z_d - Z_m) I_i ,$$

and the characteristic impedance of a wire pair in a symmetrical cable is given by

$$Z_{0_{ij}} = 2(Z_d - Z_m) .$$

This agrees with the results presented in Hiroshi Kogo's paper entitled "A Study of Multielement Transmission Lines."[7]

We have thus far developed a method for determining the elements of the characteristic impedance matrix $\underline{Z_0}$ of an MTL based on impedance measurements. These measurements can be made using a time-domain reflectometer. Note that, although the derivation called for terminating the pair being measured in its characteristic impedance to eliminate reflections, with a TDR that is not necessary since the characteristic impedance can be determined before any reflection occurs. The characteristic impedance matrix is related to the previously mentioned $\underline{K}$ matrix by

$$\underline{K} = \frac{1}{v_p} \underline{Z_0}^{-1} .$$

Once the $\underline{K}$ matrix is available, the $\underline{L}$ and $\underline{C^p}$ matrices can be determined as before. The only change is that another technique has been used to

determine the elements of $\underline{K}$. If the individual phase velocities are assumed equal, then

$$\underline{K} = \frac{\bar{I}}{v_p} Z_0^{-1}$$

can be used.

In summary, then, we have developed a technique for determining $\underline{K}$ for cable branches based on TDR measurements of characteristic impedance. To reiterate, the procedure is to fill out the $\underline{Z_0}$ matrix by the expressions

$$Z_{ii} = Z_{ii}^m$$

and

$$Z_{ij} = \frac{1}{2}\left(Z_{ii}^m + Z_{jj}^m - Z_{ij}^m\right),$$

where

Z_{ii}^m = the characteristic impedance of the i^{th} wire to ground with all other wires open at both ends,

and

Z_{ij}^m = the characteristic impedance of the i^{th} wire to the j^{th} wire with all other wires open at both ends.

Then the $\underline{K}$ matrix is determined from

$$\underline{K} = \frac{1}{v_p} \underline{Z_0}^{-1} .$$

The $\underline{C^p}$ matrix is determined from the elements of $\underline{K}$, i. e.,

$$C_{ij}^p = -K_{ij}$$

and

$$C_{ii}^p = K_{ii}^m + \sum_{\substack{j=1 \\ j\neq i}}^{N} K_{ij} .$$

The $\underline{L}$ matrix is determined from

$$\underline{L} = \frac{\underline{Z_0}}{\underline{v_p}}$$

or

$$\underline{L} = \frac{\bar{I}}{v_p}\,\underline{Z_0}$$

for uniform phase velocity, v_p.

4.3 SHORT-CIRCUIT IMPEDANCE-BASED L AND C PARAMETERS

Reiterating the results of Section 2, we derived one differential equation for a lossless multiconductor transmission line to be Eq. 58, which is

$$\frac{d}{dx}\vec{E} = j\omega\underline{L}\,\vec{I}\ ,$$

and the solution is Eq. 20, i. e.,

$$\vec{E} = \exp(\underline{\gamma}x)\,\vec{E}_+ + \exp(-\underline{\gamma}x)\,\vec{E}_-\ .$$

Substituting Eq. 20 into Eq. 58, we have

$$\underline{\gamma}\exp(\underline{\gamma}x)\,\vec{E}_+ - \underline{\gamma}\exp(-\underline{\gamma}x)\,\vec{E}_- = j\omega\underline{L}\,\vec{I}\ . \tag{76}$$

Let the i^{th} conductor be driven and all other conductors be grounded at both ends. Then, at $x = 0$, $E_k = 0$ for $k \neq i$. Furthermore, let the i^{th} conductor be terminated with its characteristic impedance to ground. Then $E^- = 0$ and $E_i^+ = E_0$, the driving voltage, and at $x = 0$ Eq. 76 becomes

$$E_0 = \frac{\omega}{\gamma_i}\sum_{k=1}^{N} L_{ik}\,I_k \tag{77}$$

$$= \frac{\omega}{\gamma_i}\left(L_{ii}\,I_i + \sum_{k\neq i}^{N} L_{ik}\,I_k\right)\ . \tag{77}$$

By definition,

$$Z_{ii}^{m} = \frac{E_0}{I_i} , \tag{78}$$

where Z_{ii}^{m} is the measured characteristic impedance between the i^{th} conductor and all other conductors tied to ground.

Thus, from Eq. 77,

$$Z_{ii}^{m} = \frac{\omega}{\gamma_i} \left(L_{ii} + \sum_{k \neq i}^{N} L_{ik} \frac{I_k}{I_i} \right) . \tag{79}$$

If it is assumed that the return current splits equally in the N-1 return conductors plus ground (shield), then

$$I_k = -\frac{I_i}{N} , \tag{80}$$

and Eq. 79 becomes

$$Z_{ii}^{m} = \frac{\omega}{\gamma_i} \left(L_{ii} - \frac{1}{N} \sum_{k \neq i}^{N} L_{ik} \right) . \tag{81}$$

Solving Eq. 81 for L_{ii} gives

$$L_{ii} = \frac{Z_{ii}^{m}}{v_i} + \frac{1}{N} \sum_{k \neq i}^{N} L_{ik} , \tag{82}$$

where

$$v_i = \frac{\omega}{\gamma_i} .$$

Now let i and j be shorted together, let all other conductors be shorted to ground, and let the line formed by (i + j) as one conductor and ground as the other be terminated in its characteristic impedance. Then, with driving voltage E_0, at x = 0,

$$\frac{\gamma_{ij}}{\omega} E_0 = \sum_{k \neq j}^{N} L_{ik} I_k + \sum_{k \neq i}^{N} L_{jk} I_k . \tag{83}$$

Dividing Eq. 83 by I_{ij} yields

$$\frac{\gamma_{ij}}{\omega}\frac{E_0}{I_{ij}} = \sum_{k\neq i}^{N} L_{jk}\left(\frac{I_k}{I_{ij}}\right) + \sum_{k\neq j}^{N} L_{ik}\left(\frac{I_k}{I_{ij}}\right) . \tag{84}$$

Once again, by definition,

$$Z_{ij}^{m} = \frac{E_0}{I_{ij}} , \tag{85}$$

where Z_{ij}^{m} is the measured characteristic impedance between the i^{th} and j^{th} conductors tied together, with all other conductors shorted to ground. Equation 84 now becomes

$$\frac{\gamma_{ij}}{\omega} Z_{ij}^{m} = \sum_{k\neq i}^{N} L_{jk}\left(\frac{I_k}{I_{ij}}\right) + \sum_{k\neq j}^{N} L_{ik}\left(\frac{I_k}{I_{ij}}\right) . \tag{86}$$

If it is assumed that currents split equally in the i^{th} and j^{th} conductors, then $I_i = I_j = I_{ij}/2$, and Eq. 86 can be written as

$$\frac{\gamma_{ij}}{\omega} Z_{ij}^{m} = \sum_{k\neq i,j}^{N} L_{jk}\left(\frac{I_k}{I_{ij}}\right) + \sum_{k\neq i,j}^{N} L_{ik}\left(\frac{I_k}{I_{ij}}\right) + \frac{1}{2} L_{ii} + \frac{1}{2} L_{jj} . \tag{87}$$

From Eq. 79, we know that

$$L_{ii} = \frac{\gamma_i}{\omega} Z_{ii}^{m} - \sum_{k\neq i}^{N} L_{ik}\left(\frac{I_k}{I_i}\right)$$

$$= \frac{\gamma_i}{\omega} Z_{ii}^{m} - 2\sum_{k\neq i}^{N} L_{ik}\left(\frac{I_k}{I_{ij}}\right) . \tag{88}$$

Substituting Eq. 88 into Eq. 87 gives

$$\frac{\gamma_{ij}}{\omega} Z_{ij}^{m} = \sum_{k\neq i,j}^{N} L_{jk}\left(\frac{I_k}{I_{ij}}\right) + \sum_{k\neq i,j}^{N} L_{ik}\left(\frac{I_k}{I_{ij}}\right)$$

$$+ \frac{1}{2}\left[\frac{\gamma_i}{\omega} Z_{ii}^{m} - 2\sum_{k\neq i}^{N} L_{ik}\left(\frac{I_k}{I_{ij}}\right)\right]$$

$$+ \frac{1}{2}\left[\frac{\gamma_j}{\omega} Z_{jj}^{m} - 2\sum_{k\neq j}^{N} L_{jk}\left(\frac{I_k}{I_{ij}}\right)\right] . \qquad (89)$$

Equation 89 reduces to

$$\frac{\gamma_{ij}}{\omega} Z_{ij}^{m} = -L_{ij}\left(\frac{I_i}{I_{ij}}\right) - L_{ji}\left(\frac{I_j}{I_{ij}}\right) + \frac{\gamma_i}{2\omega} Z_{ii}^{m}$$

$$+ \frac{\gamma_i}{2\omega} Z_{jj}^{m} , \qquad (90)$$

but since it was assumed that $I_i = I_j = I_{ij}/2$, Eq. 90 becomes

$$\frac{\gamma_{ij}}{\omega} Z_{ij}^{m} = -\frac{L_{ij}}{2} - \frac{L_{ji}}{2} + \frac{\gamma_i}{2\omega} Z_{ii}^{m} + \frac{\gamma_j}{2\omega} Z_{jj}^{m} . \qquad (91)$$

For a linear network, $L_{ij} = L_{ji}$, and so

$$\frac{\gamma_{ij}}{\omega} Z_{ij}^{m} = -L_{ij} + \frac{\gamma_i}{2\omega} Z_{ii}^{m} + \frac{\gamma_j}{2\omega} Z_{jj}^{m} . \qquad (92)$$

Solving for L_{ij} yields

$$L_{ij} = \frac{Z_{ii}^{m}}{2v_i} + \frac{Z_{jj}^{m}}{2v_j} - \frac{Z_{ij}^{m}}{v_{ij}} , \qquad (93)$$

where v_i, v_j, and v_{ij} are velocities of propagation.

The other differential equation for a lossless line is

$$\frac{\partial}{\partial x}\vec{I} = j\omega\underline{K}\,\vec{E} , \qquad (94)$$

and its solution is Eq. 21, i.e.,

$$\vec{I} = \exp(\underline{\gamma}x)\,\vec{I}_{+} + \exp(-\underline{\gamma}x)\,\vec{I}_{-} \ .$$

Substituting Eq. 21 into Eq. 94 gives

$$\underline{\gamma}\exp(\underline{\gamma}x)\,\vec{I}_{+} - \underline{\gamma}\exp(-\underline{\gamma}x)\,\vec{I}_{-} = -\omega\,\underline{K}\,\vec{E} \ . \tag{95}$$

Let the i^{th} conductor be driven and all other conductors be shorted to ground. Also let the i^{th} conductor be terminated in its characteristic impedance. From Eq. 95, at $x = 0$, we obtain

$$\gamma_i I_i = \omega \sum_{k=1}^{N} K_{ik} E_k \ , \tag{96}$$

but since $E_i = 0$ for the $i \neq k$, Eq. 96 reduces to

$$\gamma_i I_i = \omega K_{ii} E_i \tag{97}$$

or

$$\frac{E_i}{I_i} = \frac{\omega K_{ii}}{\gamma_i} \ . \tag{98}$$

By definition,

$$Z_{ii}^{m} = \frac{E_i}{I_i} = \frac{\gamma_i}{\omega K_{ii}} \tag{99}$$

or

$$K_{ii} = \frac{1}{v_i\, Z_{ii}^{m}} \ , \tag{100}$$

where

$$v_i = \frac{\omega}{\gamma_i} \ .$$

From the definition of K_{ii}, we have

$$K_{ii} = C_{ii} + \sum_{k\neq i}^{N} C_{ik} = \frac{1}{v_i\, Z_{ii}^{m}} \ . \tag{101}$$

Solving for C_{ii} yields

$$C_{ii} = \frac{1}{v_i Z_{ii}^m} - \sum_{k \neq i}^{N} C_{ik} \quad . \tag{102}$$

Now short together the i^{th} and j^{th} conductors, and let all other conductors be shorted to ground. Also let the line formed by (i + j) and ground be terminated in its characteristic impedance. For the case of (i + j) being driven against all other conductors shorted to ground, Eq. 95 at x = 0 reduces to

$$\gamma_{ij} I_{ij} = \omega (K_{ii} + K_{jj} + 2K_{ij}) E_i \tag{103}$$

or

$$\frac{E_i}{I_{ij}} = \frac{\gamma_{ij}}{\omega} \left(\frac{1}{K_{ii} + K_{jj} + 2K_{ij}} \right) \quad . \tag{104}$$

Since by definition

$$Z_{ij}^m = \frac{E_i}{I_{ij}} \quad , \tag{105}$$

$$Z_{ij}^m = \frac{1}{v_{ij}} \left(\frac{1}{K_{ii} + K_{jj} + 2K_{ij}} \right) \quad , \tag{106}$$

where

$$v_{ij} = \frac{\omega}{\gamma_{ij}} \quad .$$

Solving for K_{ij} in Eq. 106 gives

$$K_{ij} = \frac{1}{2} \left(\frac{1}{v_{ij} Z_{ij}^m} - K_{ii} - K_{jj} \right) \quad . \tag{107}$$

From Eq. 100, we know that

$$K_{ii} = \frac{1}{v_i Z_{ii}^m} ;$$

therefore,

$$K_{ij} = \frac{1}{2}\left(\frac{1}{v_{ij} Z_{ij}^m} - \frac{1}{v_i Z_{ii}^m} - \frac{1}{v_j Z_{jj}^m}\right) . \tag{108}$$

Since K_{ij} is defined as $-C_{ij}$,

$$C_{ij} = \frac{1}{2}\left(\frac{1}{v_i Z_{ii}^m} + \frac{1}{v_j Z_{jj}^m} - \frac{1}{v_{ij} Z_{ij}^m}\right) . \tag{109}$$

In summary, we have shown that model L and C values can be obtained directly from measured values of characteristic impedance and velocities of propagation. The equations relating model values to measured values are

$$L_{ii} = \frac{Z_{ii}^m}{v_i} + \frac{1}{N}\sum_{k\neq i}^{N} L_{ik} ,$$

$$L_{ij} = \frac{Z_{ii}^m}{2v_i} + \frac{Z_{jj}^m}{2v_j} - \frac{Z_{ij}^m}{v_{ij}} ,$$

$$C_{ii} = \frac{1}{v_i Z_{ii}^m} - \sum_{k\neq i}^{N} C_{ik} ,$$

and

$$C_{ij} = \frac{1}{2}\left(\frac{1}{v_i Z_{ii}^m} + \frac{1}{v_j Z_{jj}^m} - \frac{1}{v_{ij} Z_{ij}^m}\right) .$$

4.4 DETERMINATION OF R

This section describes a method for determining the resistance R for pairs of conductors. The method is based on measurement of transfer

function E_0/E_{IN} for a pair of conductors at the quarter-wavelength resonant point with the receiving end "open-circuited," i. e., $Z_L = \infty$. The theoretical basis for determining R_{ac}* in this manner is as follows.

Solving the differential equations for a transmission line with TEM propagation resulted in the following equation for the voltage at a distance x back toward the generator from the load end (Section 2, Eq. 13).

$$E(x) = \frac{1}{2}\left[\left(E_L + I_L\sqrt{z/y}\right)\exp(\sqrt{zy}\,x + \left(E_L - I_L\sqrt{z/y}\right)\exp(-\sqrt{zy}\,x\right] ,$$

where

E_L = load end voltage,

I_L = load end current,

$E(x)$ = voltage at distance x from load end,

z = series impedance/unit length,

y = shunt admittance/unit length.

For $Z_L = \infty$, $I_L = 0$, and Eq. 13 reduces to

$$E(x) = \frac{1}{2}\left[E_L \exp(\gamma x) + E_L \exp(-\gamma x)\right] , \qquad (110)$$

where $\sqrt{zy} = \gamma$ (the propagation constant) has also be used. This can be expressed in hyperbolic form as

$$E(x) = E_L \cosh \gamma x . \qquad (111)$$

At $x = \ell$, $E(x) = E_{IN}$, and solving for E_L/E_{IN} gives

$$\frac{E_L}{E_{IN}} = \frac{1}{\cosh \gamma \ell} . \qquad (112)$$

*Since the measurements are made at high frequency, the calculated resistance will necessarily be an ac resistance.

Of course, $\gamma = \alpha + j\beta$; therefore,

$$\frac{E_L}{E_{IN}} = \frac{1}{\cosh(\alpha + j\beta)\ell}, \tag{113}$$

which can be written as

$$\frac{E_L}{E_{IN}} = \frac{1}{(\cosh \alpha\ell)(\cos \beta\ell) + (j \sinh \alpha\ell)(\sin \beta\ell)} \tag{114}$$

by use of fundamental identities. At the $\lambda/4$ resonant point, $\beta\ell = \pi/2$; then $\cos \beta\ell = 0$ and $\sin \beta\ell = 1$, and the equation reduces to

$$\left.\frac{E_L}{E_{IN}}\right|_{\ell=\lambda/4} = \frac{1}{0 + j(\sinh \alpha\ell)(1)}$$

$$= \frac{1}{j \sinh \alpha\ell} . \tag{115}$$

For small values of the argument ($\alpha\ell \leq 0.8$),

$$\sinh \alpha\ell \simeq \alpha\ell \tag{116}$$

to within 10% accuracy. Then,

$$\left.\frac{E_L}{E_{IN}}\right|_{\ell=\lambda/4} \simeq \frac{1}{j\alpha\ell} . \tag{117}$$

The attenuation constant α is given exactly by[8]

$$\alpha = \left(\frac{1}{2} R\sqrt{C/L} + \frac{1}{2} G\sqrt{L/C}\right)\left[1 - \frac{1}{2}\left(\frac{R}{2\omega L} - \frac{G}{2\omega C}\right)^2\right] . \tag{118}$$

In most practical transmission lines, the major contributor to α is R rather than G, as noted before; therefore, we assume $G \simeq 0$. Then,

$$\alpha = \left(\frac{1}{2} R\sqrt{C/L}\right)\left(1 - \frac{1}{2}\frac{R^2}{4\omega^2 L^2}\right) . \tag{119}$$

If the transmission line is assumed to have low losses, then

$$\omega L >> R$$

and

$$\frac{R^2}{8\omega^2 L^2} \to 0 ;$$

therefore,*

$$\alpha \simeq \frac{1}{2} R\sqrt{C/L} = \frac{1}{2} R \frac{1}{Z_0} . \tag{120}$$

Now, substituting Eq. 120 into Eq. 117 and dropping the j gives the result

$$\left.\frac{E_L}{E_{IN}}\right|_{\ell=\lambda/4} \simeq \frac{1}{\alpha \ell} = \frac{1}{\frac{R}{2Z_0}\ell} = \frac{2Z_0}{R\ell} . \tag{121}$$

Solving for R,

$$R \simeq \frac{2Z_0}{\ell}\left(\left.\frac{E_{IN}}{E_L}\right|_{\ell=\lambda/4}\right). \tag{122}$$

Thus, from Eq. 122, the ac resistance can be determined from four laboratory-measured parameters.

The voltages E_{IN} and E_L can be measured with any appropriate instrument, but care must be exercized in using an instrument with acceptably high input impedance for the E_L measurement, to avoid nullifying the approximation $Z_L \simeq \infty$. Equation 13 can be rewritten as

$$E(x) = \frac{1}{2}\left[E_L\left(1 + \frac{Z_0}{Z_L}\right)\exp(\sqrt{zy}\, x)\right.$$

$$\left. + E_L\left(1 - \frac{Z_0}{Z_L}\right)\exp(-\sqrt{zy}\, x)\right] .$$

Typical values of Z_0 for wire pairs are in the range of 100 ±50 ohms, and for acceptable accuracy, Z_L should then be at least 10 times and preferably

*Chipman[8] indicates that this expression is valid above a few hundred kHz for coaxial lines. Actually, the error is less than 1% for $\omega L/R > 5$.

100 times this value. At the high frequencies at which short cables resonate, few instruments will have even moderately high input impedance. The characteristic impedance Z_0 can be conveniently measured with a TDR.

As noted, this procedure results in a value of R_{ac} at one frequency which is generally quite high (a few MHz). Now it is well known that R_{ac} is a function of frequency for frequencies high enough that skin depth (δ) is comparable to conductor radius (r), and for all higher frequencies. At very high frequencies where δ is very small compared to radius (say, δ = 0.1 r), then R_{ac} varies simply as $\sqrt{f}$. However, Chipman[8] states that there is a frequency interval of three or four decades below this $R_{ac} = K\sqrt{f}$ region where R_{ac} variation obeys a very complicated law. For a No. 22 copper wire, the frequency at which δ = 0.1 r is 4.2 MHz. Thus, for practical cable conductors, it is considered reasonable to assume that R_{ac} varies as $\sqrt{f}$ for frequencies of the order of 1 MHz and above. Below about 1 MHz, it must be recognized that the variation may be more complex.

This procedure determines the R_{ac} for a pair of wires. The question then arises as to how to apportion the measured R_{ac} between the two wires of the pair, since in general the loss per wire will not be equal. One possible technique is to introduce a third conductor. The three possible conductor pairings can then be measured individually and the three resulting simultaneous equations solved to obtain the individual wire resistances. Since this technique can be applied to N conductors, and since the cables to be modeled will usually have three or more conductors already, this is a generally applicable technique. However, as N becomes large, the solutions become difficult.

A simpler approach is to introduce a third conductor in the form of a low-loss ground plane. A pair or pairs* of conductors can be selected

*The use of several pairs to help determine R_{ac} of the ground plane will give a more accurate value.

at random from the cable to be modeled and the ground plane R_{ac} determined by the approach outlined above for three conductors. Then all the remaining wires can be paired one at a time with the ground plane, and the wire resistance is then simply the pair resistance less the calculated ground plane resistance.

4.5 SUMMARY OF STEP-BY-STEP PROCEDURES

The various methods for determining cable parameters are summarized in the step-by-step procedures shown in Tables 4.1 through 4.4. Note that the three methods for determining $\underline{L}$ and $\underline{C^P}$ give these parameters for the total length of cable upon which the measurements are made. To obtain the parameters on a per-meter basis, simply divide by the cable physical length in meters. The R_{ac} parameter is already given in terms of ohms/meter. The measured phase velocities must be expressed in meters/second to ensure consistency of units.

Table 4.1

CAPACITANCE METHOD FOR DETERMINING L AND C

Step	Determine	By Measuring or Calculating
1	$\underline{C}^m$	C_{ii}^m = measured capacitance from the i^{th} wire to all others shorted to ground C_{ij}^m = measured capacitance from the i^{th} and j^{th} wires shorted together to all other wires shorted to ground
2	$\underline{K}$	$K_{ii} = C_{ii}^m$ $K_{ij} = \frac{1}{2}\left(C_{ij}^m - C_{ii}^m - C_{jj}^m\right) \quad (i \neq j)$
3	$\left[\frac{1}{v_p^2}\right]$	$\left(\frac{1}{v_p^2}\right)_{ii}$ = reciprocal of square of measured phase velocity of i^{th} wire to ground (nonuniform v_p) $\left(\frac{1}{v_p^2}\right)_{ij} = 0 \quad \text{for } i \neq j$
4	$\underline{L}$	$\underline{L} = \left[\frac{1}{v_p^2}\right] \underline{K}^{-1}$ (nonuniform v_p) or $\underline{L} = \left(\frac{\bar{1}}{v_p^2}\right) \underline{K}^{-1}$ (uniform v_p)
5	$\underline{C}^p$	$C_{ij}^p = -K_{ij} \quad (i \neq j)$ $C_{ii}^p = K_{ii} + \sum_{\substack{j=1 \\ j \neq i}}^{N} K_{ij}$

Table 4.2

OPEN-Z METHOD FOR DETERMINING L AND C

Step	Determine	By Measuring or Calculating
1	$\underline{Z}^m$	Z_{ii}^m = measured impedance of the i^{th} wire to ground with all other wires open at both ends Z_{ij}^m = measured impedance of the i^{th} wire to the j^{th} wire with all others open at both ends
2	$\underline{Z}_0$	$Z_{ii} = Z_{ii}^m$ $Z_{ij} = \frac{1}{2}\left(Z_{ii}^m + Z_{jj}^m - Z_{ij}^m\right) \quad (i \neq j)$
3	$\left[\frac{1}{v_p}\right]$	$\left(\frac{1}{v_p}\right)_{ii}$ = reciprocal of measured phase velocity of i^{th} wire to ground $\left(\frac{1}{v_p}\right)_{ij} = 0 \quad \text{for } i \neq j$
4	$\underline{K}$	$\underline{K} = \left[\frac{1}{v_p}\right]\underline{Z_0}^{-1} \quad$ (nonuniform v_p) or $\underline{K} = \left(\frac{\bar{I}}{v_p}\right)\underline{Z_0}^{-1} \quad$ (uniform v_p)
5	$\underline{C}^p$	$C_{ij}^p = -K_{ij} \quad (i \neq j)$ $C_{ii}^p = K_{ii} + \sum_{\substack{j=1 \\ j\neq i}}^{N} K_{ij}$
6	$\underline{L}$	$\underline{L} = \left[\frac{1}{v_p}\right]\underline{Z_0} \quad$ (nonuniform v_p) $\underline{L} = \left(\frac{\bar{I}}{v_p}\right)\underline{Z_0} \quad$ (uniform v_p)

Table 4.3

SHORTED-Z METHOD FOR DETERMINING L AND C

Step	Determine	By Measuring or Calculating
1	$\underline{Z^m}$	Z^m_{ii} = measured impedance of the i^{th} wire to ground with all other wires connected to ground at both ends Z^m_{ij} = measured impedance of the i^{th} and j^{th} wires connected together at both ends to ground with all other wires connected to ground at both ends
2	$v_{p_{ii}}$ $v_{p_{ij}}$	$v_{p_{ii}}$ = measured phase velocity of the i^{th} wire to ground with all other wires connected to ground at both ends $v_{p_{ij}} = \sqrt{v_{p_i} v_{p_j}}$
3	$\underline{L}$	$L_{ij} = \frac{Z^m_{ii}}{2v_{p_i}} + \frac{Z^m_{jj}}{2v_{p_j}} - \frac{Z^m_{ij}}{v_{p_{ij}}} \qquad (i \neq j)$ $L_{ii} = \frac{Z^m_{ii}}{v_{p_i}} + \frac{1}{N} \sum_{\substack{j=1 \\ j \neq i}}^{N} L_{ij}$
4	$\underline{C^p}$	$C^p_{ij} = \frac{1}{2}\left(\frac{1}{v_{p_i} Z^m_{ii}} + \frac{1}{v_{p_j} Z^m_{jj}} - \frac{1}{v_{p_{ij}} Z^m_{ij}}\right)$ $C^p_{ii} = \frac{1}{v_{p_i} Z^m_{ii}} - \sum_{\substack{j=1 \\ j \neq i}}^{N} C^p_{ij}$

Table 4.4

METHOD FOR DETERMINING R_{ac} FOR WIRE PAIR

Step	Determine	By Measuring or Calculating
1	E_L and E_{IN}	Monitor E_L and E_{IN} with appropriate instruments, while exciting the wire pair of interest with a variable frequency generator. Sweep frequency from low end of generator to point of first E_L peak and E_{IN} null. Record values of E_L and E_{IN}.
2	ℓ	Measure physical length in meters
3	Z_0	Measure pair characteristic impedance with a time-domain reflectometer
4	R_{ac} at $f_{\lambda/4}$	$R_{ac} = \frac{2Z_0}{\ell}\left(\frac{E_{IN}}{E_N} \text{ at } \ell = \lambda/4\right)$

5. MODELING OF SOME EXAMPLE CABLES

5.1 INTRODUCTION

The methods presented in Section 4 were used to determine the parameters for a number of actual cables of varying complexity, from three unshielded wires in an overall shield to a combination of 15 wires and five internal shields within an overall shield. Lumped-element models of these cables were then created and analytical solutions obtained. Experimental transfer functions were also measured on the actual cables for the same* drive and termination schemes, and these were compared to the analytically determined transfer functions. The resulting agreement between analysis and experiment then serves as a measure of the accuracy and usefulness of this modeling technique.

Five cables in six configurations were treated in this manner, and they were constructed as described in Table 5.1 and as shown in Fig. 5.1. The cross-section views of the random cables are approximate only, of course, since no effort was made to control the conductor lay. The sixth configuration shown in Fig. 5.1 is a modification of Cable 2 where the groups designated A, B, and C were treated as single conductors for the modeling effort. The rationale for selecting these six configurations is as follows.

Cable 1: This cable was selected because its simplicity and uniformity make it easy to model and test, yet it is complex enough to test the three methods.

*Same in the sense that the load and source resistor values were the same. However, the stray couplings and instrumentation loadings which will always occur in practical experiments were not included in the analytical model. Omission of these effects is one source of disagreement between analytical and experimental results.

Table 5.1

PHYSICAL DESCRIPTION OF TEST CABLES

Cable	Length (m)	Internal Conductors*	Conductor Lay	Uniform with X	Construction
No. 1 (Belden 8771)	2.48	3 W	Controlled, twisted	Yes	3 AWG-22 (7x30) wires Foil overall shield, vinyl jacket
No. 2	3.10	20 W	Controlled (3 layers), straight	Yes	20 AWG-16 (26x30) Belden 8521 Braid overall shield, no jacket
No. 3	3.10	15 W 5 S	Random	No	4 AWG-20 (10x30) Belden 8523 2 AWG-14 (41x30) Belden 8520 2 RG-174 coax, Belden 8216 2 twisted shielded pairs, Belden 8737 1 twisted shielded trio, Belden 8771 Braid overall shield, no jacket
No. 4	7.0	8 W 3 S	Random	Yes	2 AWG-20 (10x30) Belden 8523 1 RG-174 coax, Belden 8216 1 twisted shielded pair, Belden 8761 1 twisted shielded trio, Belden 8771 Braid overall shield, polyolefin jacket
No. 5	1.52 each branch	6 W 4 W 2 W	Random Random Random	No No No	Branch A, 6 AWG-16, Belden 8521 Branch B, 4 AWG-16, Belden 8521 Branch C, 2 AWG-16, Belden 8521 Braid overall shield, no jacket

*W = Wire, S = Shield

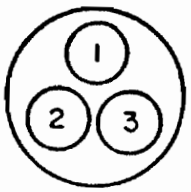

a. CABLE NO. 1
TWISTED TRIO

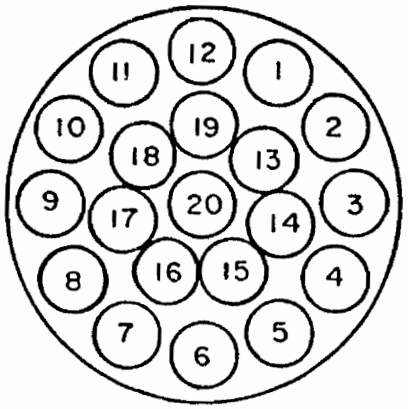

b. CABLE NO. 2
20-CONDUCTOR,
CONTROLLED LAY,
UNIFORM CABLE

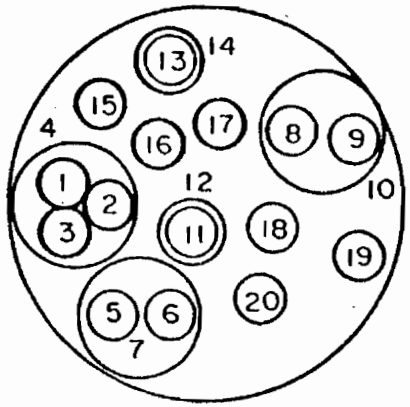

c. CABLE NO. 3
20-CONDUCTOR,
RANDOM LAY.
NON-UNIFORM CABLE

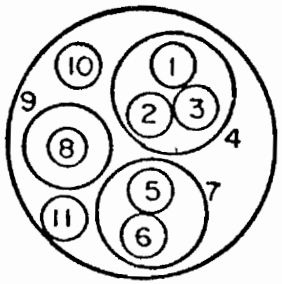

d. CABLE NO. 4
11-CONDUCTOR,
RANDOM LAY,
UNIFORM CABLE

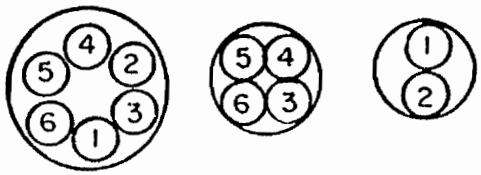

BRANCH A BRANCH B BRANCH C

e. CABLE NO. 5
6-CONDUCTOR, 3-BRANCH
RANDOM LAY,
NON-UNIFORM CABLE

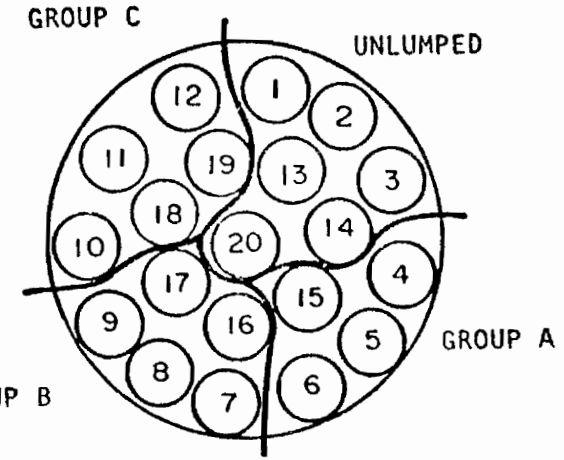

f. CABLE NO. 2
9-CONDUCTOR,
GROUPED, CONTROLLED LAY,
UNIFORM CABLE

RT-00402

Fig. 5.1. Cross-section drawings of the test cables

Cable 2: A cable with at least three layers was desired in order to verify that the technique can handle the shielding effect of intermediate layers, and 20 conductors is the minimum required to produce three layers. Uniformity was maintained in order to simplify the modeling effort.

Cable 3: This cable was designed to be most nearly representative of real system cables and is, in fact, of the same order of complexity as many branches of a typical missile raceway cable. It has a combination of unshielded and shielded wires, three different types of internal shields (wire braid, spiral wire wrap, and foil), nonuniform phase velocity, and random nonuniform conductor lay.

Cable 4: This longer cable was designed to test the ability of the technique to handle longer cables with their lower-frequency resonances.

Cable 5: This 3-branch cable was designed to test the ability of the two characteristic impedance methods to distinguish between branches, i.e., to verify that the branches can actually be modeled without having to cut up the cable.

Cable 2, Special Grouped Configuration: This configuration was designed to provide a quick test of the concept of grouping, for purposes of analysis, "uninteresting" conductors. By "uninteresting" is meant conductors for which the actual signals are not of interest, but whose effect on other conductors is important from a modeling standpoint. If this is a valid technique, it has the potential to greatly simplify many analytical problems.

5.2 SUMMARY OF RESULTS

The results of the analytical modeling efforts are compared to the experimental results in Table 5.2. The designations "Good," "Fair," and "Poor" in this table are necessarily somewhat subjective, especially for the more complex cables where rigid rules for making judgments were

Table 5.2

AGREEMENT BETWEEN ANALYTICAL AND EXPERIMENTAL RESULTS FOR SIX EXAMPLE CABLES

Cable		Results by Method*		
		C	Open-Z	Shorted-Z
No. 1	Shielded Trio	G	F	F
No. 2	20-Conductor, Controlled	F-G		
No. 3	20-Conductor, Random			
	5-Section Model	F-G		
	15-Section Model	F-G		
No. 4	11-Conductor, Controlled	F	F-P	F-P
No. 5	3-Branch Cable		G	G
No. 6	9-Conductor, Grouped	G	G	

G = Good F = Fair P = Poor

*These results are for the initial set of parameters determined by each method; i.e., no attempt was made to improve the agreement by altering parameter values.

impossible to establish. In general, "Good" means agreement within 3 dB or better over a significant portion (a decade or more) of the frequency band examined, but with occasional divergence at the ends of the band. In particular, slight shifts in resonances at the high-frequency end sometimes resulted in large errors at selected frequencies. "Fair" implies agreement within 6 to 14 dB, frequently including a general shift of the analytical result with respect to the experimental result. "Poor" means the analytical and experimental results were 14 dB or more apart over most of the frequency range examined. The comparisons summarized in Table 5.2 were made over the frequency range 0.3 MHz to the frequency at which the maximum error due to the lumped approximation was 1 dB. This upper-frequency limit was ~20 MHz for all but Cable 4, which was 12 MHz, and the 15-section model of Cable 3, which was 29 MHz.

It is important to note that the analytical results were obtained from initial sets of model parameters only; i.e., the parameters derived from the measurements were in no way altered to improve the agreement between analysis and experiment. Since nearly all of the results were "Fair" or better, it can be concluded that measured but unverified model parameters will generally give results within at worst 14 dB (factor of 5), which in many cases will be adequate. If better accuracy is required, the model parameters should be verified and then altered as necessary to provide the required agreement.

5.3 DETAILED RESULTS FOR INDIVIDUAL CABLES

The actual analytical versus experimental data plots will now be presented for all of the cables. Examination of these will provide a better picture of the results than the summary in Table 5.2. A detailed example of the modeling methods will also be presented for the shielded trio, in order to fully illustrate the approach. Problems encountered with the various methods will be discussed as they occurred.

Cable 1, Shielded Trio, Capacitance Method

This cable is a 2.48-m length of a commercial twisted, shielded, 3-wire cable (i.e., Belden 8771). It has a very uniform phase velocity of 1.98×10^8 m/sec for all conductor pairings, as measured with a TDR. The detailed steps in determining the model parameters using the capacitance method proceed as follows.

The measured capacitances for the full cable length are

$$C_{11}^m = 340 \text{ pF}$$
$$C_{12}^m = 627 \text{ pF}$$
$$C_{13}^m = 614 \text{ pF}$$
$$C_{22}^m = 350 \text{ pF}$$
$$C_{23}^m = 637 \text{ pF}$$
$$C_{33}^m = 339 \text{ pF}$$

where the measurements were made as specified in Table 4.1 using an ESI 251-C1 impedance bridge with a 1-kHz generator frequency. The shield was taken as reference or ground. On a per-meter length basis, then,

$$\underline{C^m} = \begin{bmatrix} 137.1 & 252.8 & 247.6 \\ 252.8 & 141.1 & 256.9 \\ 247.6 & 256.9 & 136.7 \end{bmatrix} \text{ pF/m} .$$

The elements of $\underline{K}$ are determined as shown in the following example calculations.

$$K_{ii} = C_{ii}^m ,$$

$$K_{11} = C_{11}^m = 137.1 \text{ pF/m} ,$$

$$K_{ij} = \frac{1}{2}(C_{ij}^m - C_{ii}^m - C_{jj}^m) ,$$

$$K_{12} = \frac{1}{2}(C_{12}^m - C_{11}^m - C_{22}^m)$$

$$= \frac{1}{2}(252.8 - 137.1 - 141.1)$$

$$= -12.7 \text{ pF/m} ;$$

then $\underline{K}$ is

$$\underline{K} = \begin{bmatrix} 137.1 & -12.7 & -13.1 \\ -12.7 & 141.1 & -10.5 \\ -13.1 & -10.5 & 136.7 \end{bmatrix} \text{ pF/m} .$$

The partial capacitance matrix elements are determined from

$$C_{ij}^p = -K_{ij} ,$$

$$C_{12}^p = -K_{12} = -(-12.7 \text{ pF/m}) = 12.7 \text{ pF/m} ,$$

$$C_{ii}^p = K_{ii} + \sum_{\substack{j=1 \\ j \neq i}}^{N} K_{ij} ,$$

$$C_{11}^p = K_{11} + K_{12} + K_{13}$$

$$= 137.1 + (-12.7) + (-13.1)$$

$$= 111.3 \text{ pF/m} ;$$

and $\underline{C^p}$ is

$$\underline{C^p} = \begin{bmatrix} 111.3 & 12.7 & 13.1 \\ 12.7 & 117.9 & 10.5 \\ 13.1 & 10.5 & 113.1 \end{bmatrix} \text{ pF/m} .$$

The $\underline{K}$ matrix can be inverted by ordinary methods to give

$$\underline{K^{-1}} = \begin{bmatrix} 7.435 & 0.726 & 0.768 \\ 0.726 & 7.199 & 0.623 \\ 0.768 & 0.623 & 7.437 \end{bmatrix} \times 10^{-3} \text{ m/pF} .$$

Then from $\underline{K}^{-1}$ and the measured phase velocity, we can determine $\underline{L}$ to be

$$\underline{L} = \frac{1}{v_p^2}\underline{K}^{-1} = \frac{1}{(1.98 \times 10^8)^2}\underline{K}^{-1} ;$$

$$\underline{L} = \begin{bmatrix} 0.1889 & 0.0184 & 0.0195 \\ 0.0184 & 0.1829 & 0.0158 \\ 0.0195 & 0.0158 & 0.1889 \end{bmatrix} \mu H/m .$$

The elements of $\underline{C}^P$ and $\underline{L}$ are the distributed cable parameters for the conductor pairs indicated by their subscripts.

The distributed ac resistance, R_{ac}, is determined as follows. The measured data, taken as specified in Table 4.4, are

Pair	Z_0 (Ω)	$f_{\lambda/4}$ (MHz)	E_{IN} (mV)	E_0 (V)	ℓ (m)
1-2	61.3	18.9	88	1.032	2.48
1-3	61.8	19.0	92	1.018	2.48
2-3	61.5	19.1	88	1.046	2.48
1-s	38.5	17.8	46	0.566	2.48

The R_{ac} of pair 1-2 is calculated to be

$$R_{ac} = \frac{2Z_0}{\ell}\frac{E_{IN}}{E_0}\bigg|_{f=\lambda/4} ,$$

$$R_{ac(1-2)} = \frac{2(61.3)}{2.48}\left(\frac{0.088}{1.032}\right) \Omega/m \text{ at } 18.9 \text{ MHz}$$

$$= 4.22\ \Omega/m \text{ at } 18.9 \text{ MHz} .$$

In a similar fashion, the remaining pair R_{ac} values are calculated to be

$$R_{ac(1-3)} = 4.50\ \Omega/m \text{ at } 19.0 \text{ MHz} ,$$

$$R_{ac(2-3)} = 4.17\ \Omega/m \text{ at } 19.1\ MHz\ ,$$

$$R_{ac(1-s)} = 2.52\ \Omega/m \text{ at } 17.8\ MHz\ .$$

In order to apportion the resistances for the most general case, the calculated values must be normalized to a common frequency using the assumption of $\sqrt{f}$ variation. In fact, it is convenient to extrapolate to dc and define

$$K = \frac{R_{ac} \text{ at } f_{\lambda/4}}{\sqrt{f_{\lambda/4}}}\ ,$$

$$K_{12} = \frac{4.22\ \Omega/m}{\sqrt{18.9\ MHz}} = 0.971 \times 10^{-3}\ \frac{\Omega\text{-Hz}^{-\frac{1}{2}}}{m}\ .$$

Then R_{ac} at any frequency is simply

$$R_{ac} \text{at } f = K\sqrt{f}\ .$$

Similarly,

$$K_{13} = 1.032 \times 10^{-3}\ \frac{\Omega\text{-Hz}^{-\frac{1}{2}}}{m}\ ,$$

$$K_{23} = 0.954 \times 10^{-3}\ \frac{\Omega\text{-Hz}^{-\frac{1}{2}}}{m}\ ,$$

$$K_{1-s} = 0.597 \times 10^{-3}\ \frac{\Omega\text{-Hz}^{-\frac{1}{2}}}{m}\ .$$

It will also be necessary, in general, to apportion the resistances between conductors by solving simultaneous equations as discussed previously. However, for this simple case, it is apparent that the three internal wires must have nearly equal resistances since the pair resistances for these wires are so nearly equal. Thus, an acceptably accurate apportionment of resistance factors can be obtained by simply taking 1/2 of the average pair resistance factor, i.e.,

$$K/\text{wire} = \frac{\text{ave } K/\text{pair}}{2} = \frac{0.986 \times 10^{-3}}{2}$$

$$= 0.493 \times 10^{-3}\ \frac{\Omega\text{-Hz}^{-\frac{1}{2}}}{m}\ .$$

The shield ac resistance factor is then given approximately by

$$K_s = K_{1-s} - K_w$$

$$= (0.597 - 0.493) \times 10^{-3}$$

$$= 0.104 \times 10^{-3} \frac{\Omega\text{-Hz}^{-\frac{1}{2}}}{\text{m}} .$$

All of the distributed parameters are now available for completing a lumped-element model.

To create the lumped-element model, we must first multiply the distributed parameters by the required section length, and then assign values to the elements according to the section configuration used. For this cable, the sections are to be 0.1 λ or less in length up to 30 MHz. The number of sections required is given by

$$N_S \geq \frac{10\, \ell\, f}{v_p}$$

$$\geq \frac{10(2.48\ \text{m})(3 \times 10^7\ \text{Hz})}{1.98 \times 10^8\ \text{m/sec}} \geq 3.75 .$$

The next highest integer is 4, and this is the number of sections which will be used. The section length will then be 0.62 m. Then $\underline{C^p}$, $\underline{L}$, and K_w, on a per-section basis, are

$$\underline{C^p} = \begin{bmatrix} 69 & 7.9 & 8.1 \\ 7.9 & 73 & 6.5 \\ 8.1 & 6.5 & 70 \end{bmatrix} \text{pF/section} ,$$

$$\underline{L} = \begin{bmatrix} 0.117 & 0.011 & 0.012 \\ 0.011 & 0.113 & 0.010 \\ 0.012 & 0.010 & 0.117 \end{bmatrix} \mu\text{H/section} ,$$

and

$$K_w = 0.3 \times 10^{-3}\ \Omega\text{-Hz}^{-\frac{1}{2}}\text{/section} .$$

The selected section configuration is a "π" section, and each inductance or series resistance will, therefore, be represented by a single discrete inductor or resistor and each capacitance by two equal-value discrete capacitors. The complete model section is shown in Fig. 5.2. Note that the resistance factor K_s has been left out of the return (shield) conductor. It is small enough compared to the value of K_w that its omission will not significantly alter the results.

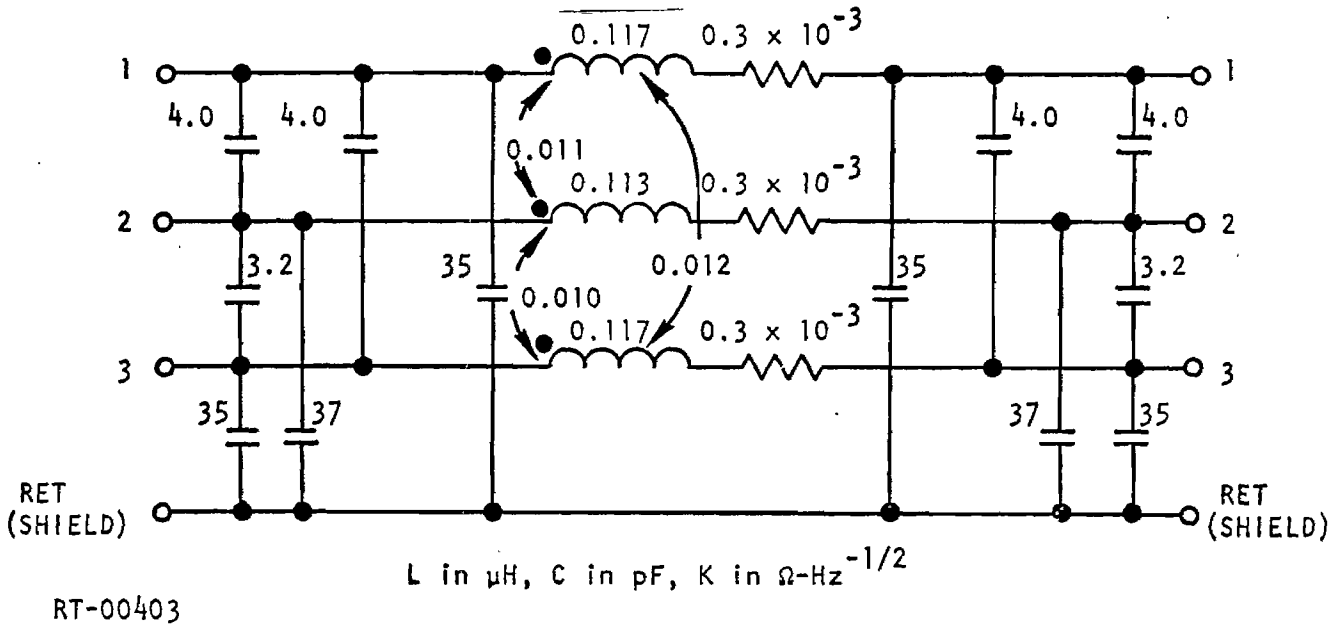

Fig. 5.2. Model section of shielded trio based on the capacitance method

The transfer functions for the 4-section model of this cable were determined analytically for the drive and termination scheme shown in Fig. 5.3. These transfer functions are plotted in Figs. 5.4a through 5.4e along with the experimentally determined transfer functions, using the same drive and termination schemes. (It should be noted that in the experimental setup, the cable was laid directly on a ground plane to which the equipment could be grounded, as necessary, to achieve minimum sensitivity to hand capacitance and other stray coupling effects.)

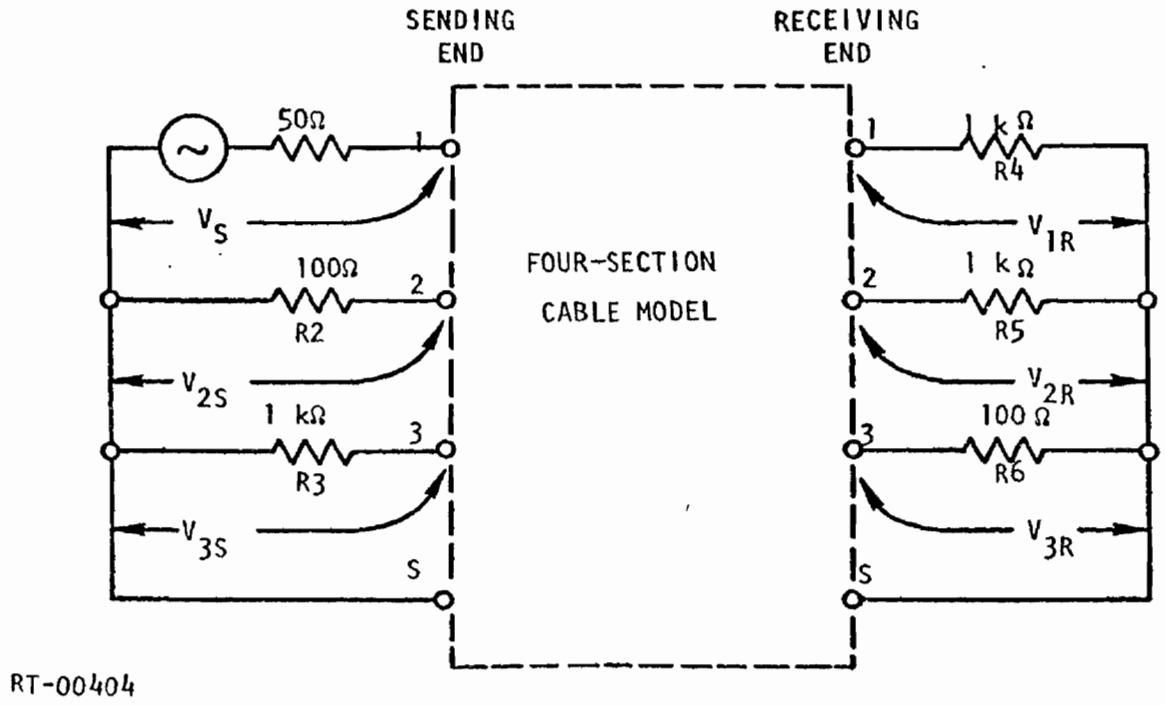

Fig. 5.3. Shielded trio model termination and drive scheme

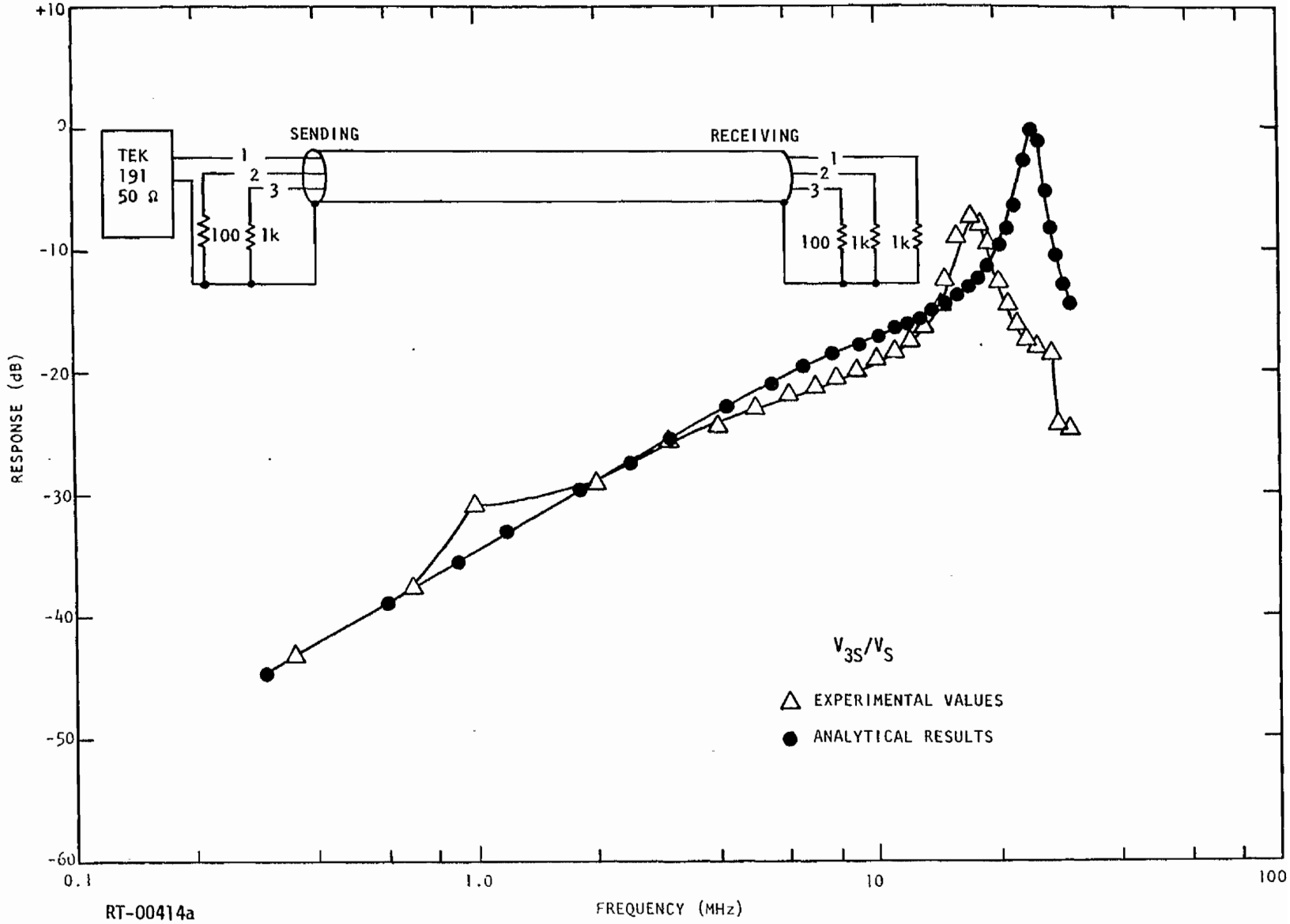

Fig. 5.4a. Transfer functions for shielded trio with driven wire terminated in 1000 ohms, capacitance method parameters

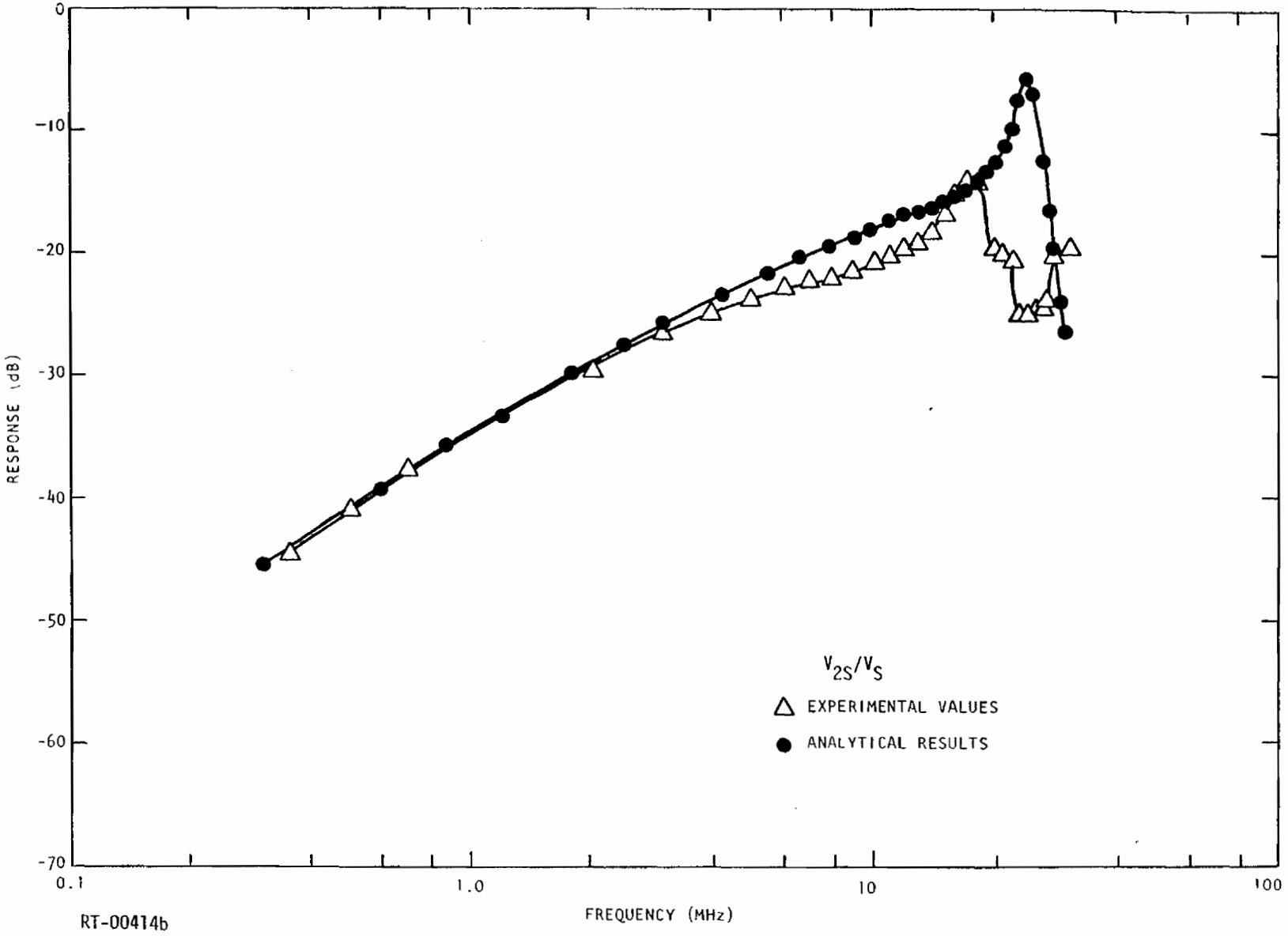
0
-10
-20
-30
-40
-50
-60
-70
RESPONSE (dB)
0.1
1.0
10
100
FREQUENCY (MHz)
V_{2S}/V_S
EXPERIMENTAL VALUES
ANALYTICAL RESULTS
RT-00414b

Fig. 5.4b

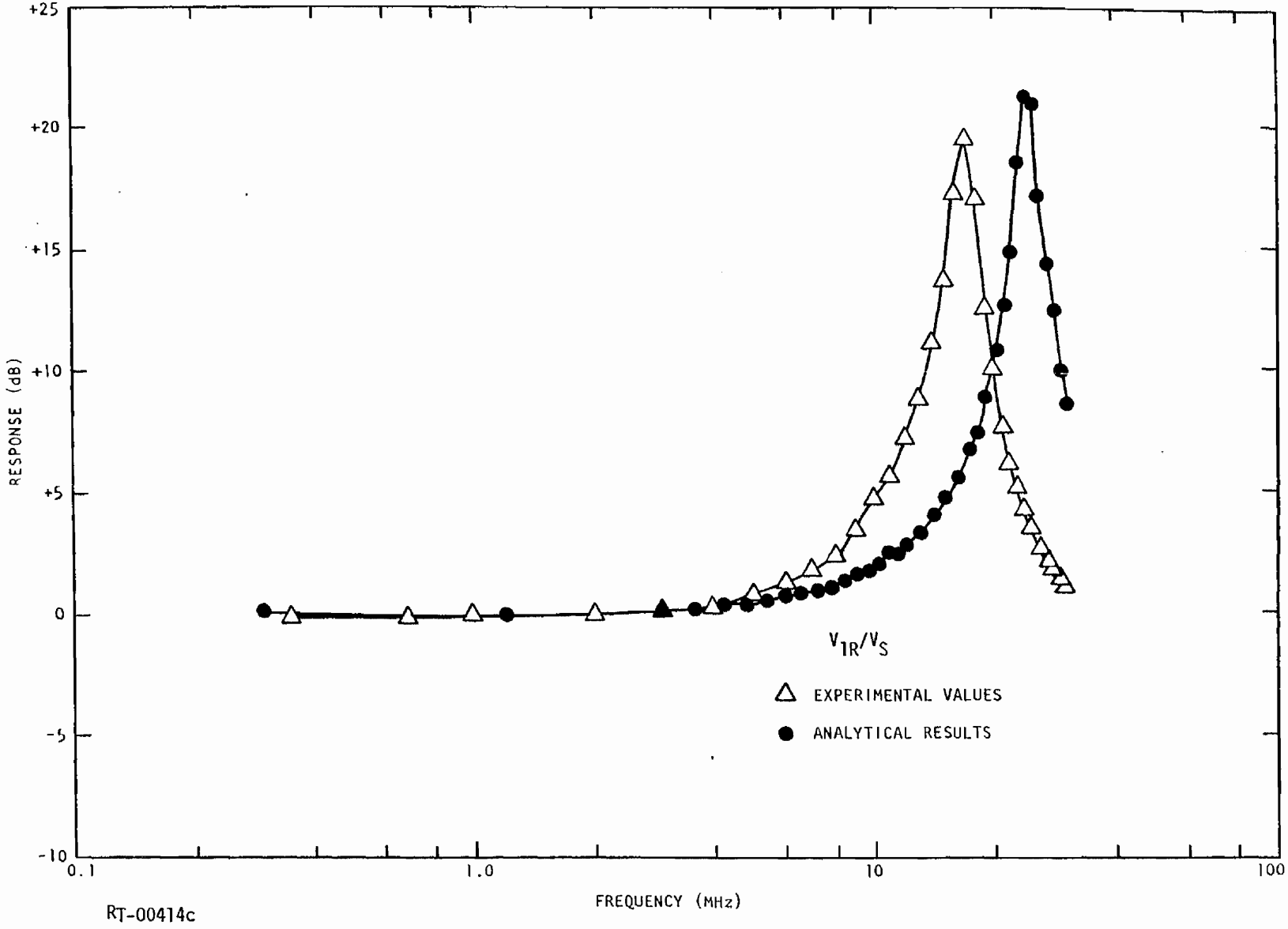
+25
+20
+15
+10
+5
0
-5
-10
RESPONSE (dB)
0.1
1.0
10
100
FREQUENCY (MHz)
V_{1R}/V_S
EXPERIMENTAL VALUES
ANALYTICAL RESULTS
RT-00414c

Fig. 5.4c

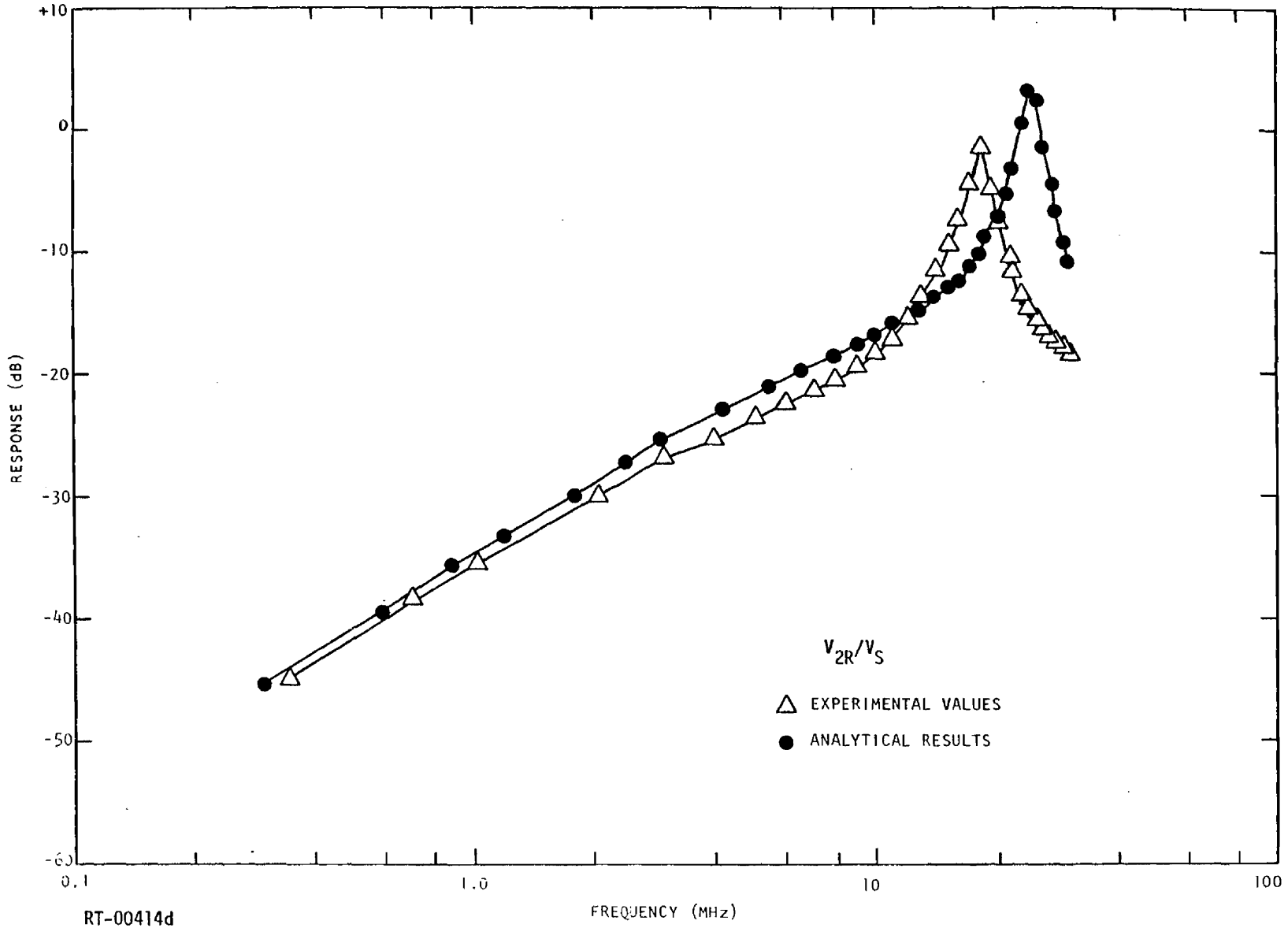
+10
0
-10
-20
-30
-40
-50
-60
RESPONSE (dB)
0.1
1.0
10
100
FREQUENCY (MHz)
V_{2R}/V_S
EXPERIMENTAL VALUES
ANALYTICAL RESULTS
RT-00414d

Fig. 5.4d

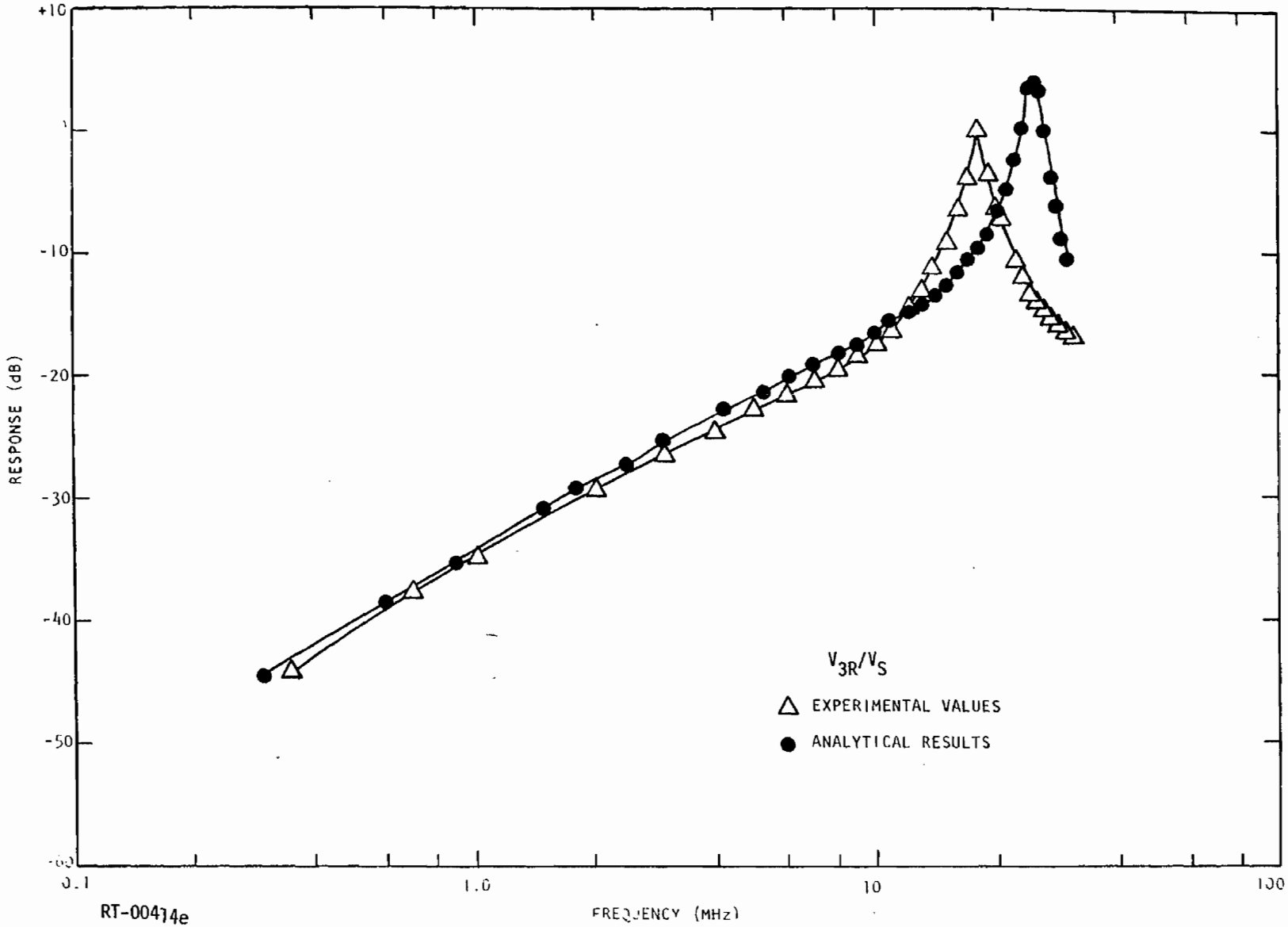
+10
-10
-20
-30
-40
-50
RESPONSE (dB)
0.1
1.0
10
100
FREQUENCY (MHz)
V_{3R}/V_S
EXPERIMENTAL VALUES
ANALYTICAL RESULTS
RT-00414e

Fig. 5.4e

The agreement between analytical and experimental results is clearly very good over the range 0.3 to 10 MHz. Between 10 and 30 MHz, considerable divergence occurs due to the shift in resonance points. This shift is believed to result from the capacitance of the oscilloscope differential input, which was not included in the analytical model.

A second set of transfer functions was determined for an altered termination scheme where the 1-kΩ terminating resistor on the driven wire (R4) was shorted out. This scheme provides a better test of the mutual inductance parameters, as will be discussed in a later section. The agreement is still good, although there is a distinct skew between the analytical and experimental results (see Figs. 5.5a through 5.5c).

Cable 1, Shielded Trio, Open-Z Method

The detailed steps for determining the model L and C parameters using the open-Z method proceed in a similar fashion as described below. The measured Z matrix is

$$\underline{Z}^m = \begin{bmatrix} 38.5 & 61.3 & 61.8 \\ 61.3 & 37.0 & 61.5 \\ 61.8 & 61.5 & 38.5 \end{bmatrix} \Omega ,$$

where the measurements were made as specified in Table 4.2 using a Hewlett-Packard 140 oscilloscope with a 1415A TDR plug-in. The cable shield was again taken as reference or ground. The elements of the characteristic impedance matrix $\underline{Z}_0$ are calculated as shown in step 2 of Table 4.2 to be

$$\underline{Z}_0 = \begin{bmatrix} 38.5 & 7.1 & 7.6 \\ 7.1 & 37.0 & 7.0 \\ 7.6 & 7.0 & 38.5 \end{bmatrix} \Omega .$$

The inverted $\underline{K}$ matrix can be determined from $\underline{Z}_0$ and the phase velocity to be

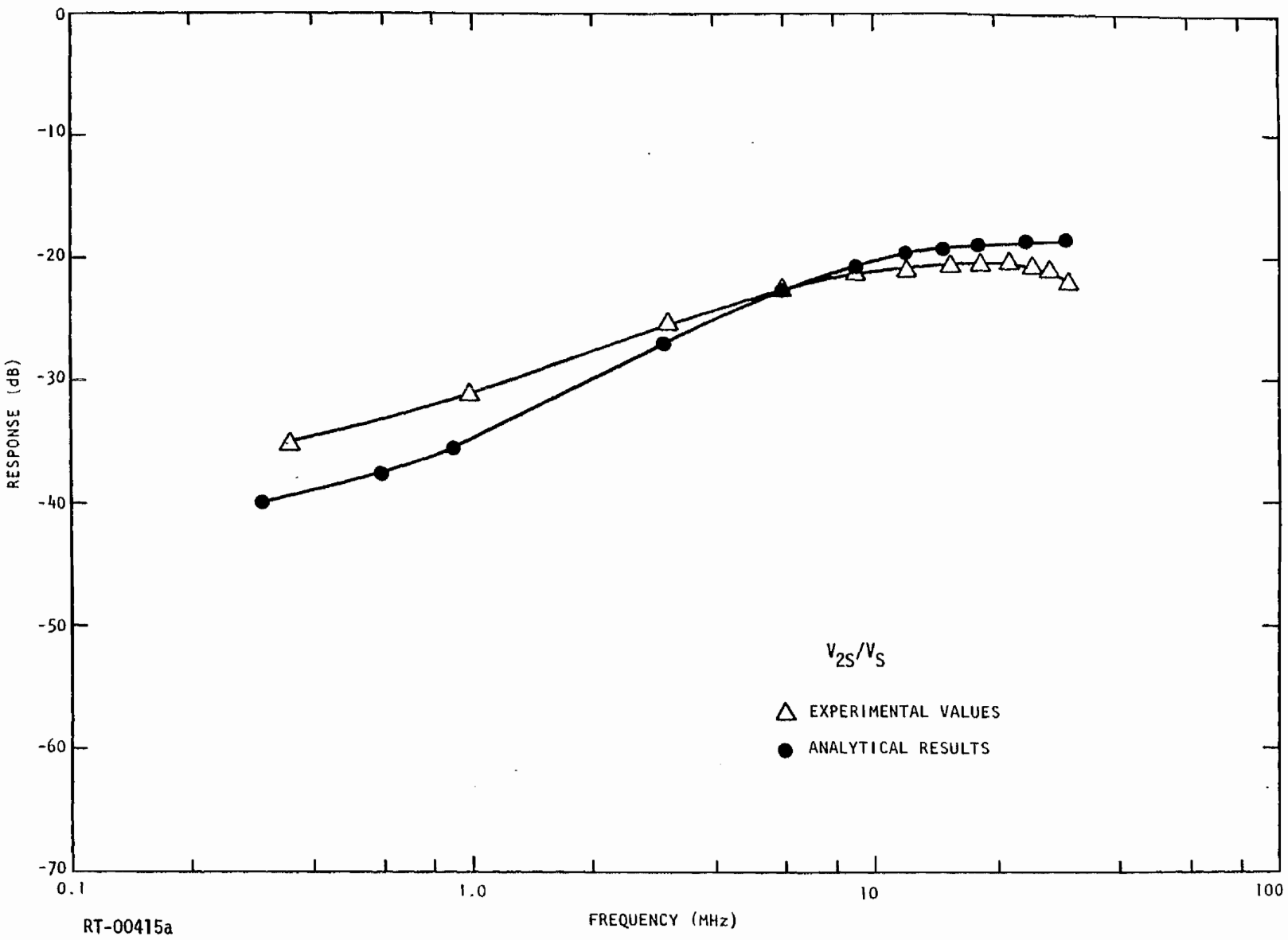

Fig. 5.5a. Transfer functions for shielded trio with driven wire terminated in a short circuit, capacitance method parameters

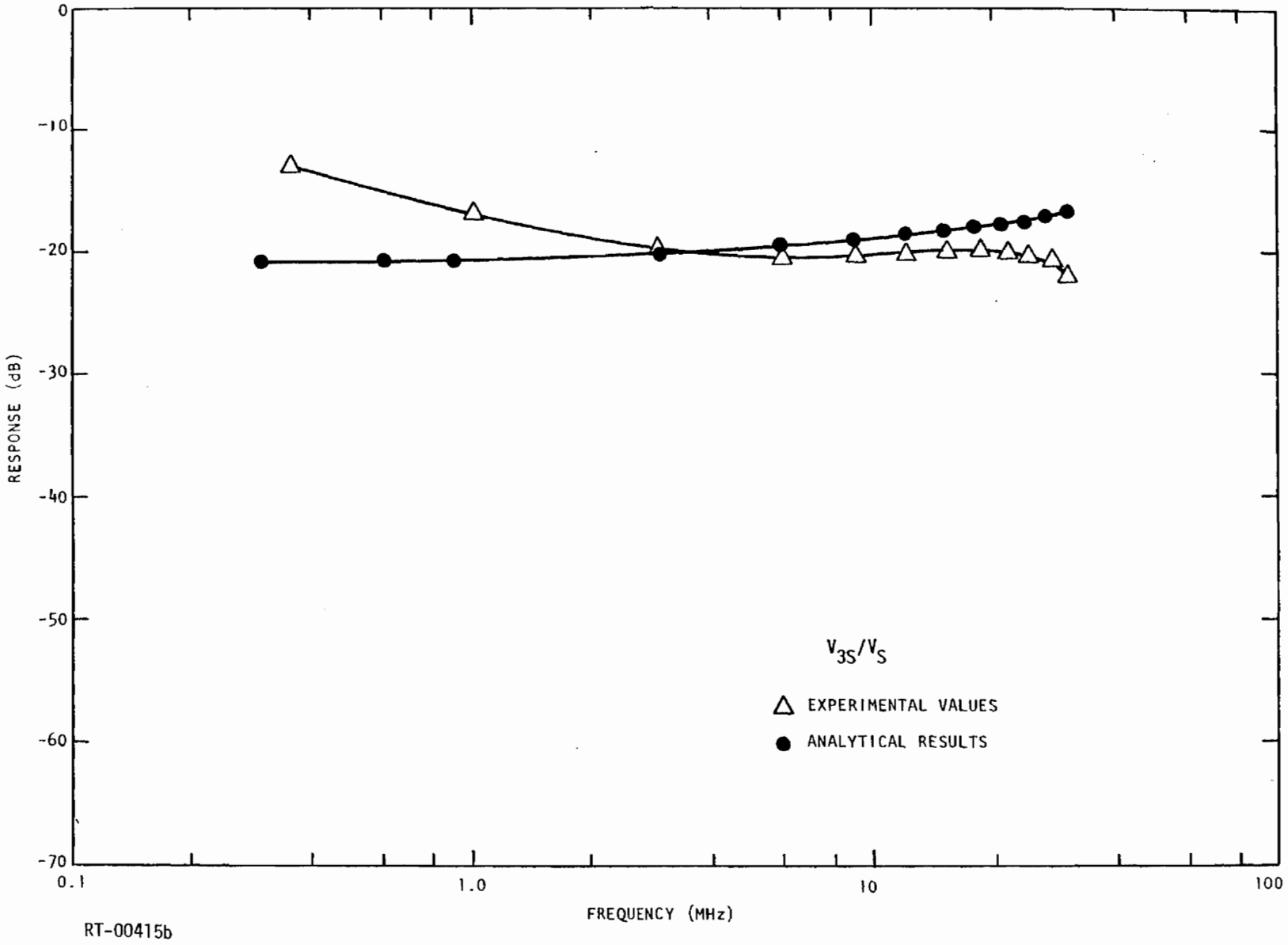
0
-10
-20
-30
-40
-50
-60
-70
RESPONSE (dB)
0.1
1.0
10
100
FREQUENCY (MHz)
V_{3S}/V_S
EXPERIMENTAL VALUES
ANALYTICAL RESULTS
RT-00415b

Fig. 5.5b

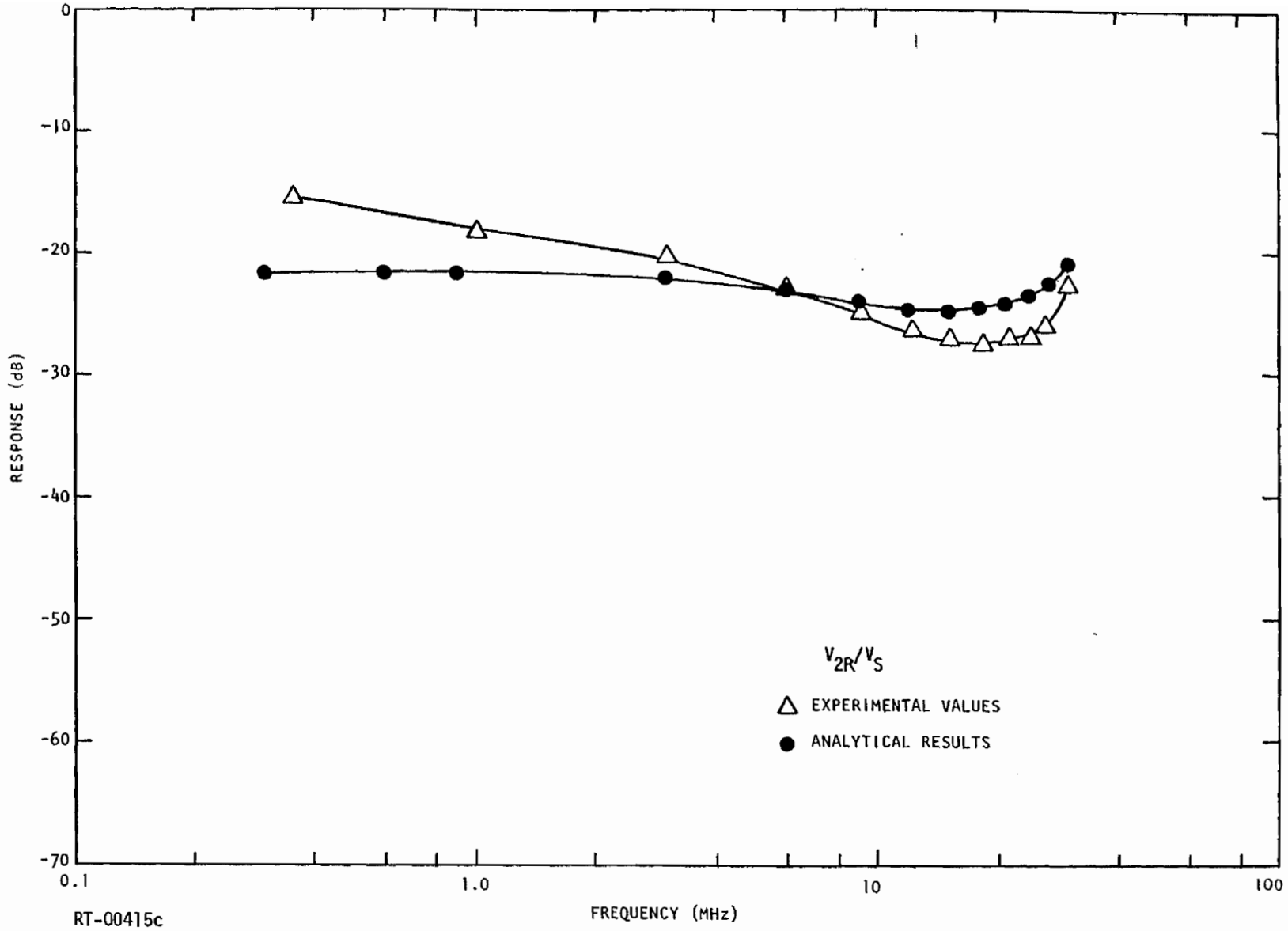
0
-10
-20
-30
-40
-50
-60
-70
RESPONSE (dB)
0.1
1.0
10
100
FREQUENCY (MHz)
V_{2R}/V_S
EXPERIMENTAL VALUES
ANALYTICAL RESULTS
RT-00415c

Fig. 5.5c

$$\underline{K}^{-1} = v_p \underline{Z}_0 = (1.98 \times 10^8 \text{ m/sec})\, \underline{Z}_0$$

$$= \begin{bmatrix} 7.638 & 1.408 & 1.508 \\ 1.408 & 7.341 & 1.389 \\ 1.508 & 1.389 & 7.638 \end{bmatrix} \times 10^9 \frac{\Omega\text{-m}}{\text{sec}} .$$

Then $\underline{K}^{-1}$ can be inverted by ordinary means to give*

$$\underline{K} = \begin{bmatrix} 139.7 & -22.3 & -23.5 \\ -22.3 & 144.6 & -21.9 \\ -23.5 & -21.9 & 139.6 \end{bmatrix} \text{ pF/m} .$$

The elements of $\underline{C}^p$ can be calculated as shown in step 5 of Table 4.2, and then

$$\underline{C}^p = \begin{bmatrix} 93.9 & 22.3 & 23.5 \\ 22.3 & 100.4 & 21.9 \\ 23.5 & 21.9 & 94.2 \end{bmatrix} \text{pF/m} .$$

From $\underline{Z}_0$ and v_p, we can calculate $\underline{L}$ as shown in step 6 of Table 4.2 and obtain

$$\underline{L} = \frac{1}{v_p} \underline{Z}_0 = \frac{1}{(1.98 \times 10^8 \text{ m/sec})} \underline{Z}_0$$

$$= \begin{bmatrix} 0.1940 & 0.0358 & 0.0383 \\ 0.0358 & 0.1865 & 0.0353 \\ 0.0383 & 0.0353 & 0.1941 \end{bmatrix} \mu\text{H/m} .$$

Using the same 0.62-m section length as used previously, the per-section parameters are

$$\underline{C}^p = \begin{bmatrix} 58.2 & 13.8 & 14.6 \\ 13.8 & 62.2 & 13.6 \\ 14.6 & 13.6 & 58.4 \end{bmatrix} \text{ pF/section}$$

*Note that the last two steps were not as specified in Table 4.2. However, this is a perfectly valid alternate approach for determining the $\underline{K}$ matrix.

and

$$\underline{L} = \begin{bmatrix} 0.1203 & 0.0222 & 0.0237 \\ 0.0222 & 0.1156 & 0.0219 \\ 0.0237 & 0.0219 & 0.1203 \end{bmatrix} \mu H/\text{section} .$$

Using these parameters and the previously determined K_w values, the π section model shown in Fig. 5.6 was created. This model was also solved analytically using the termination and drive scheme shown in Fig. 5.3. and the results as compared to experimental results are plotted in Figs. 5.7a through 5.7e.

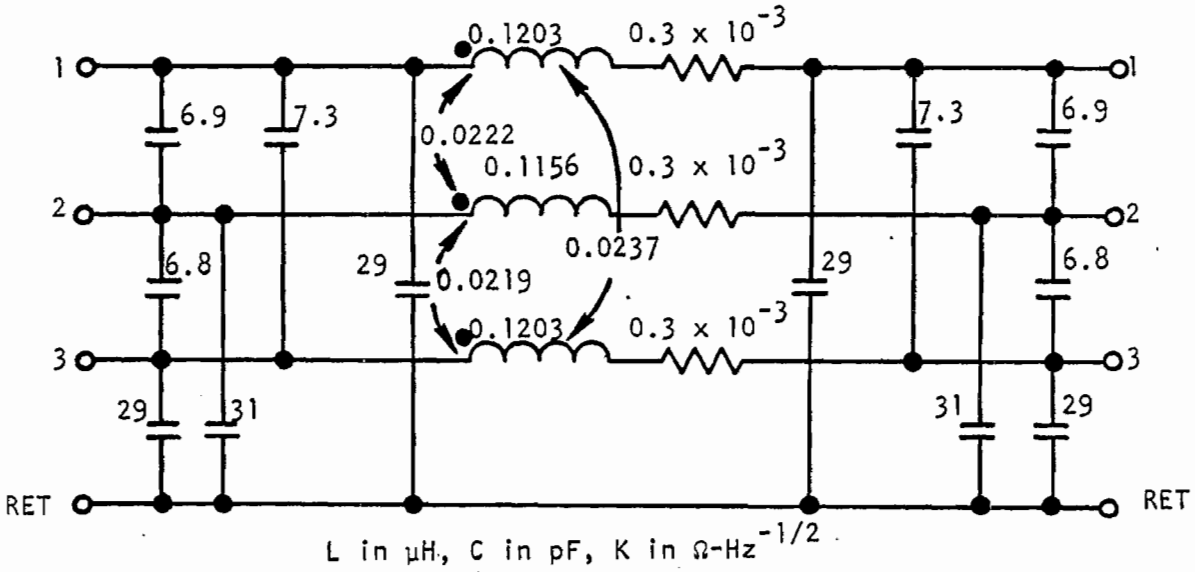

RT-00405

Fig. 5.6. Model section of shielded trio based on the open-Z method

A second set of transfer functions for the case of R4 shorted out were determined as before also. These are shown in Figs. 5.8a through 5.8c.

It is apparent that the agreement for this set of parameters is not as good as was obtained before for the capacitance parameters. By the criteria previously discussed, these results can be considered only fair, since the analytical results are consistently on the order of 6 dB above the experimental results.

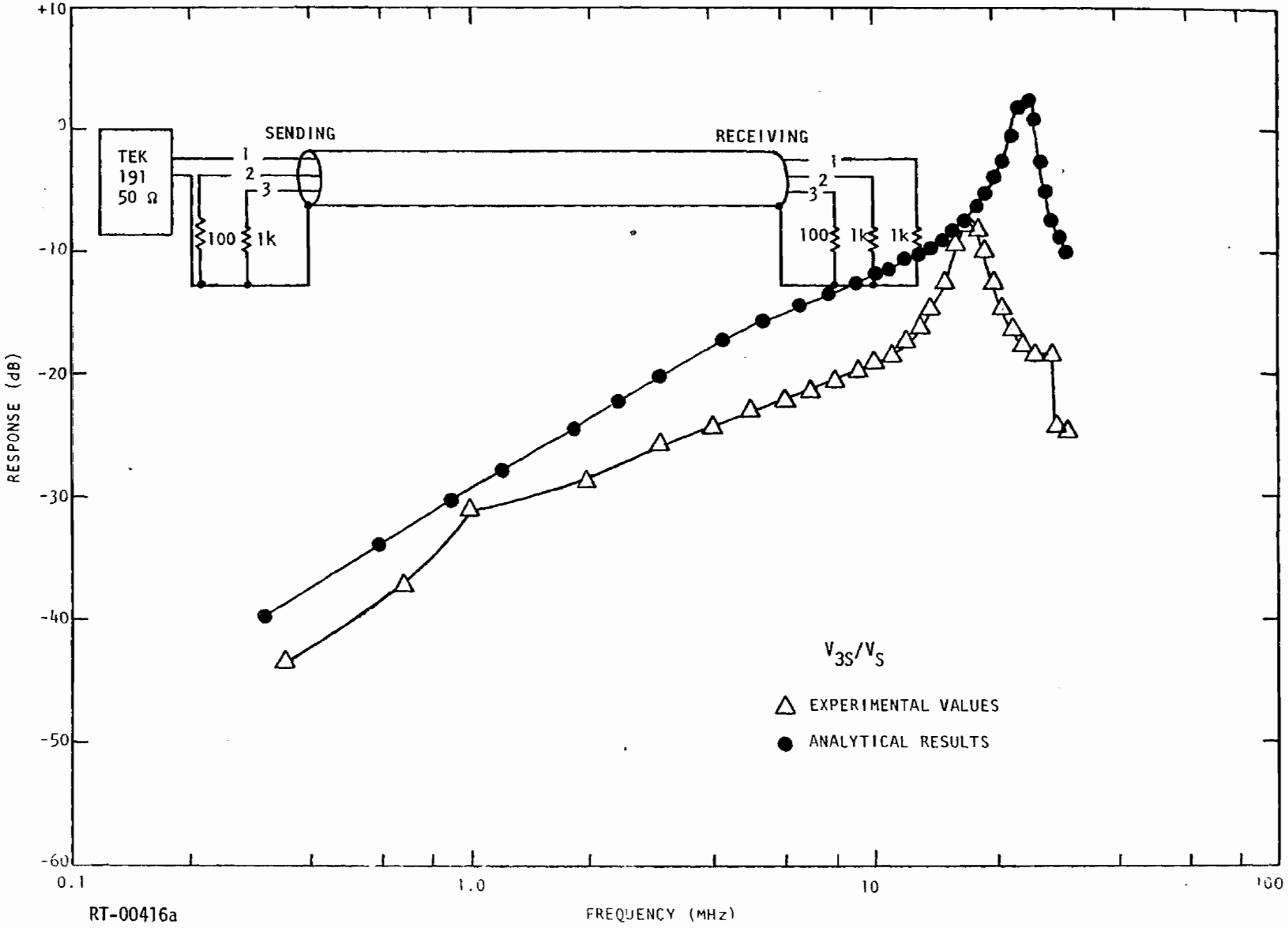

Fig. 5.7a. Transfer functions for shielded trio with driven wire terminated in 1000 ohms, open-Z method parameters

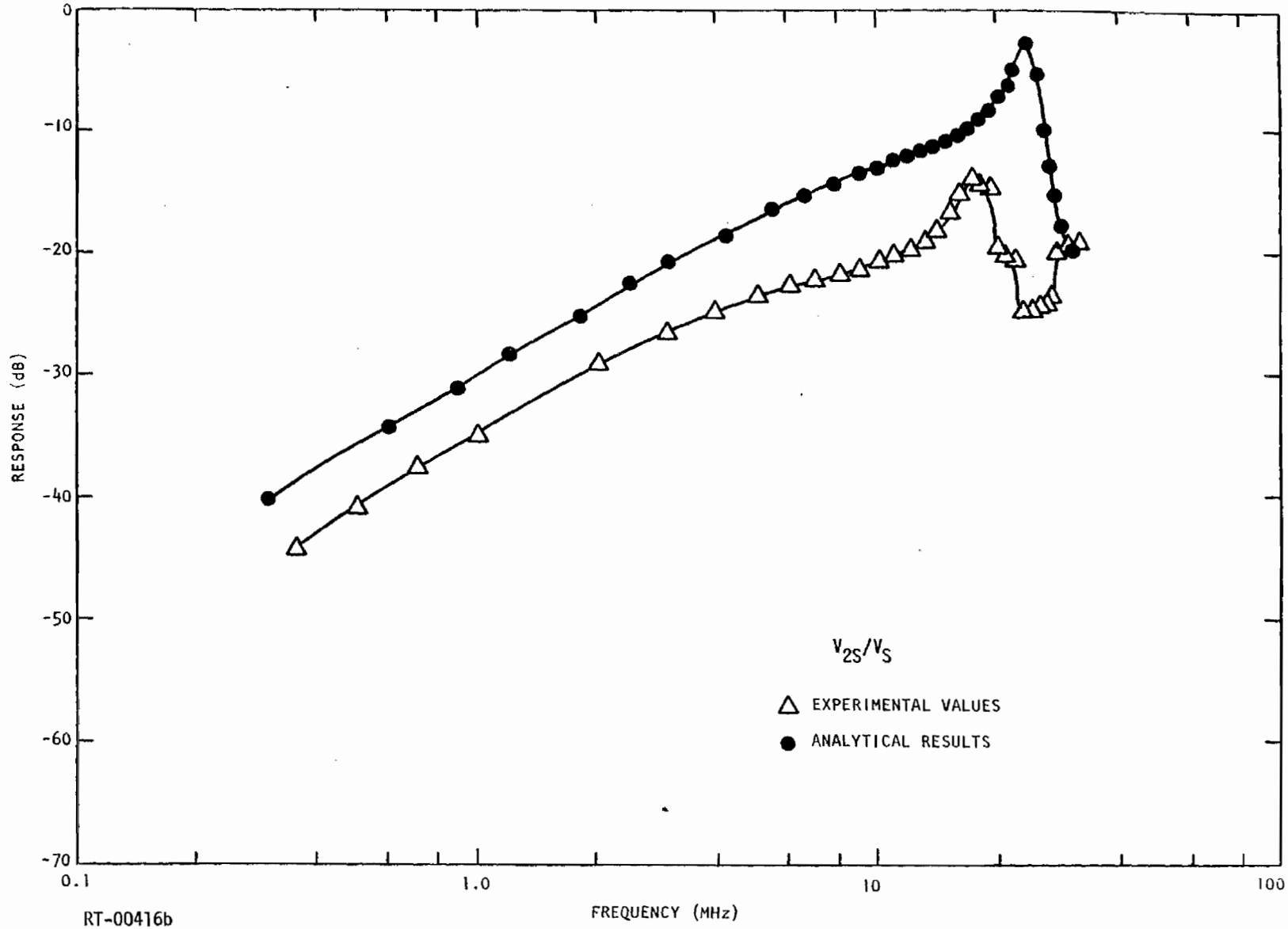
0
-10
-20
-30
-40
-50
-60
-70
RESPONSE (dB)
0.1
1.0
10
100
FREQUENCY (MHz)
V_{2S}/V_S
EXPERIMENTAL VALUES
ANALYTICAL RESULTS
RT-00416b

Fig. 5.7b

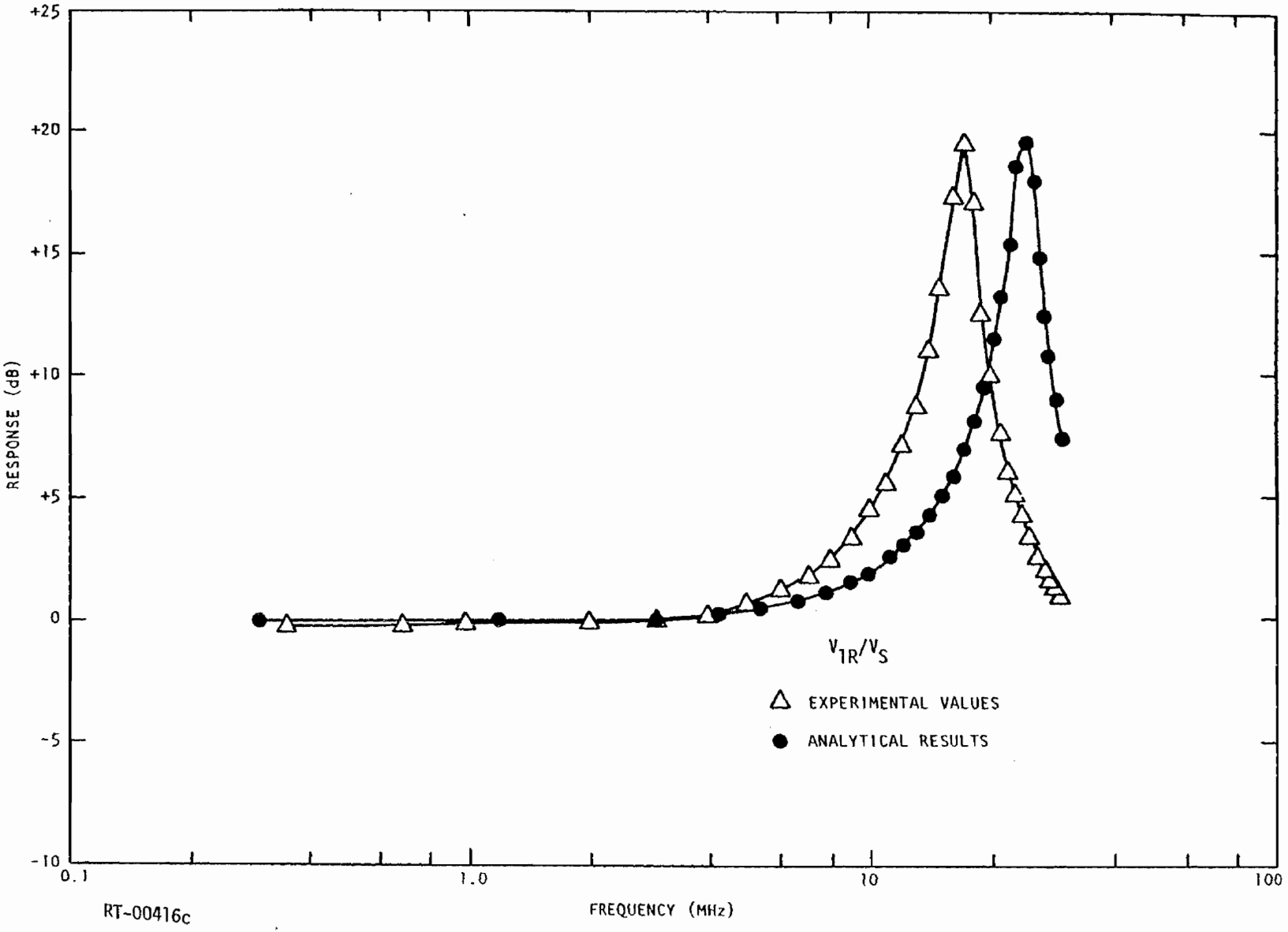
+25
+20
+15
+10
+5
0
-5
-10
RESPONSE (dB)
0.1
1.0
10
100
FREQUENCY (MHz)
V_{1R}/V_S
EXPERIMENTAL VALUES
ANALYTICAL RESULTS
RT-00416c

Fig. 5.7c

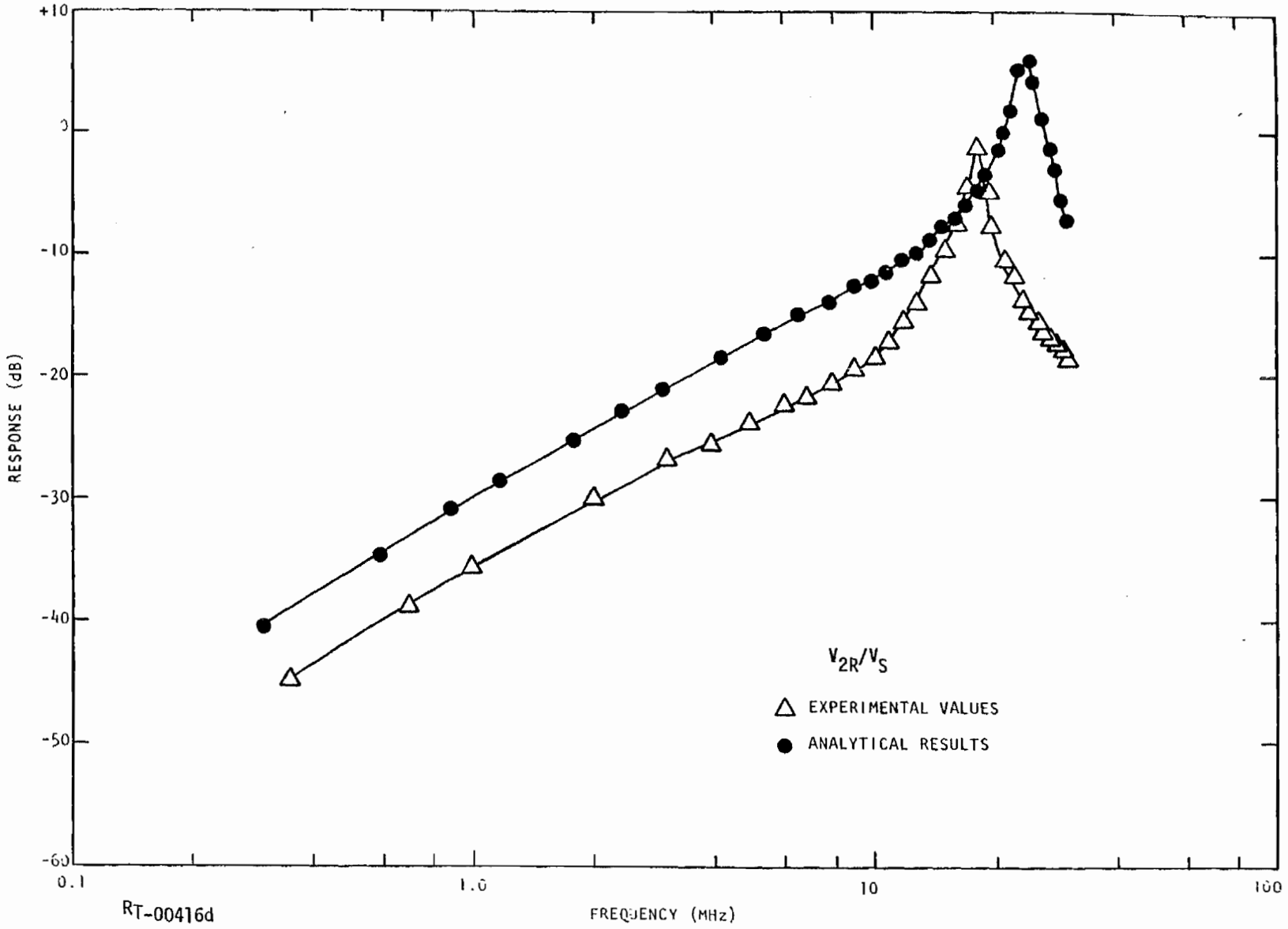
+10
0
-10
-20
-30
-40
-50
-60
RESPONSE (dB)
0.1
1.0
10
100
FREQUENCY (MHz)
V_{2R}/V_S
EXPERIMENTAL VALUES
ANALYTICAL RESULTS
RT-00416d

Fig. 5.7d

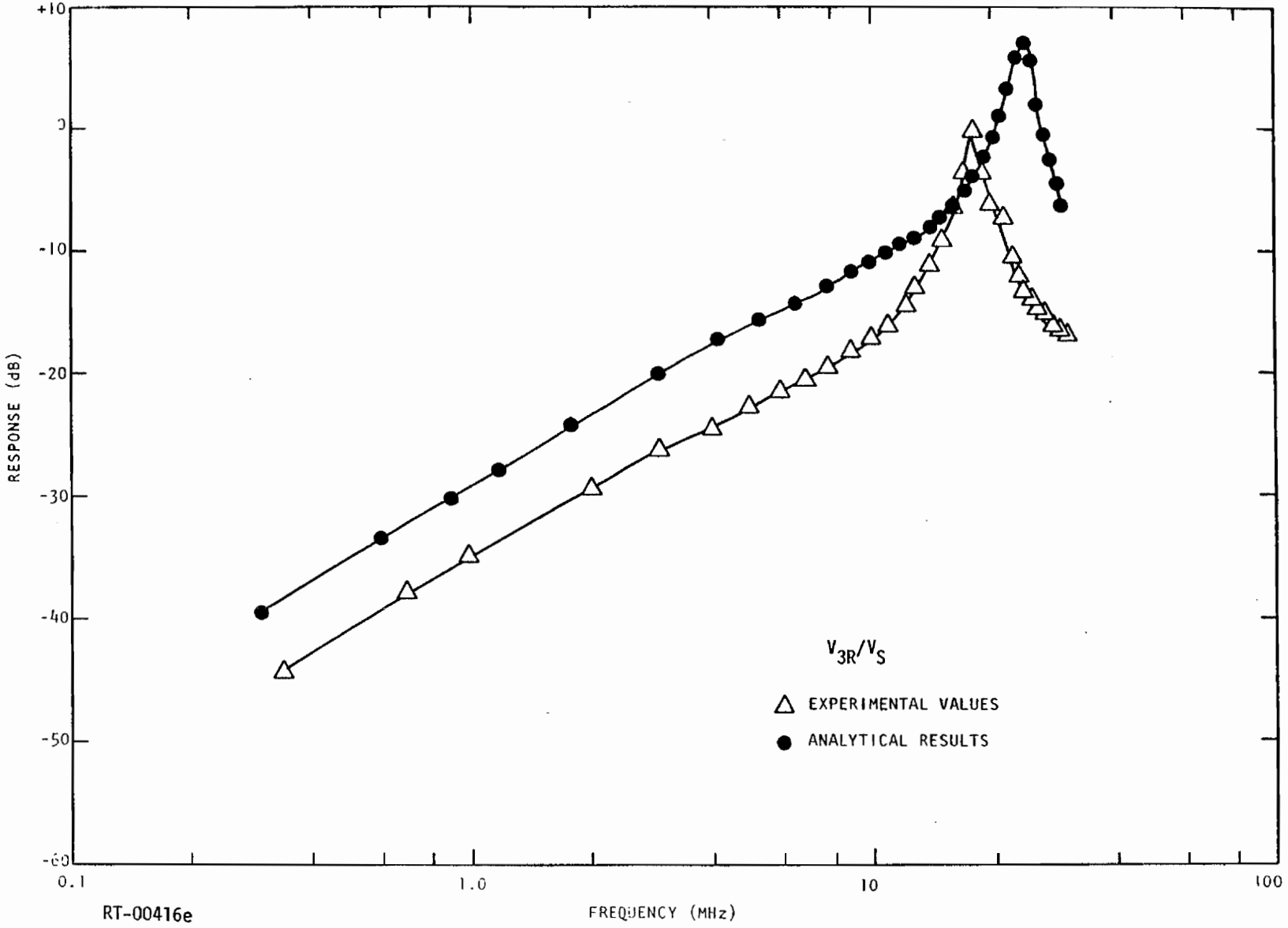
+10
0
-10
-20
-30
-40
-50
-60
RESPONSE (dB)
0.1
1.0
10
100
FREQUENCY (MHz)
V_{3R}/V_S
EXPERIMENTAL VALUES
ANALYTICAL RESULTS
RT-00416e

Fig. 5.7e

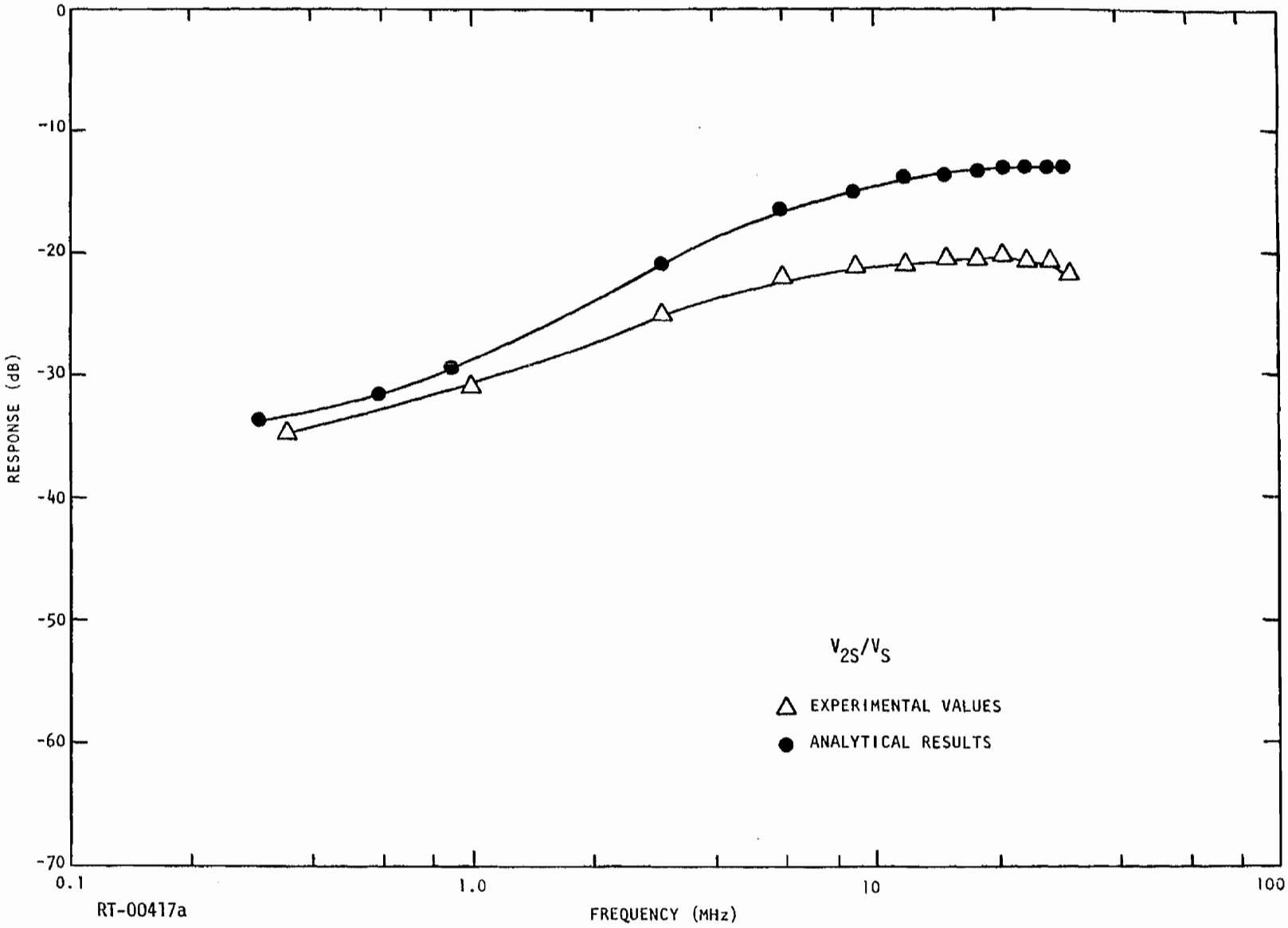

Fig. 5.8a. Transfer functions for shielded trio with driven wire terminated in a short-circuit, open-Z method parameters

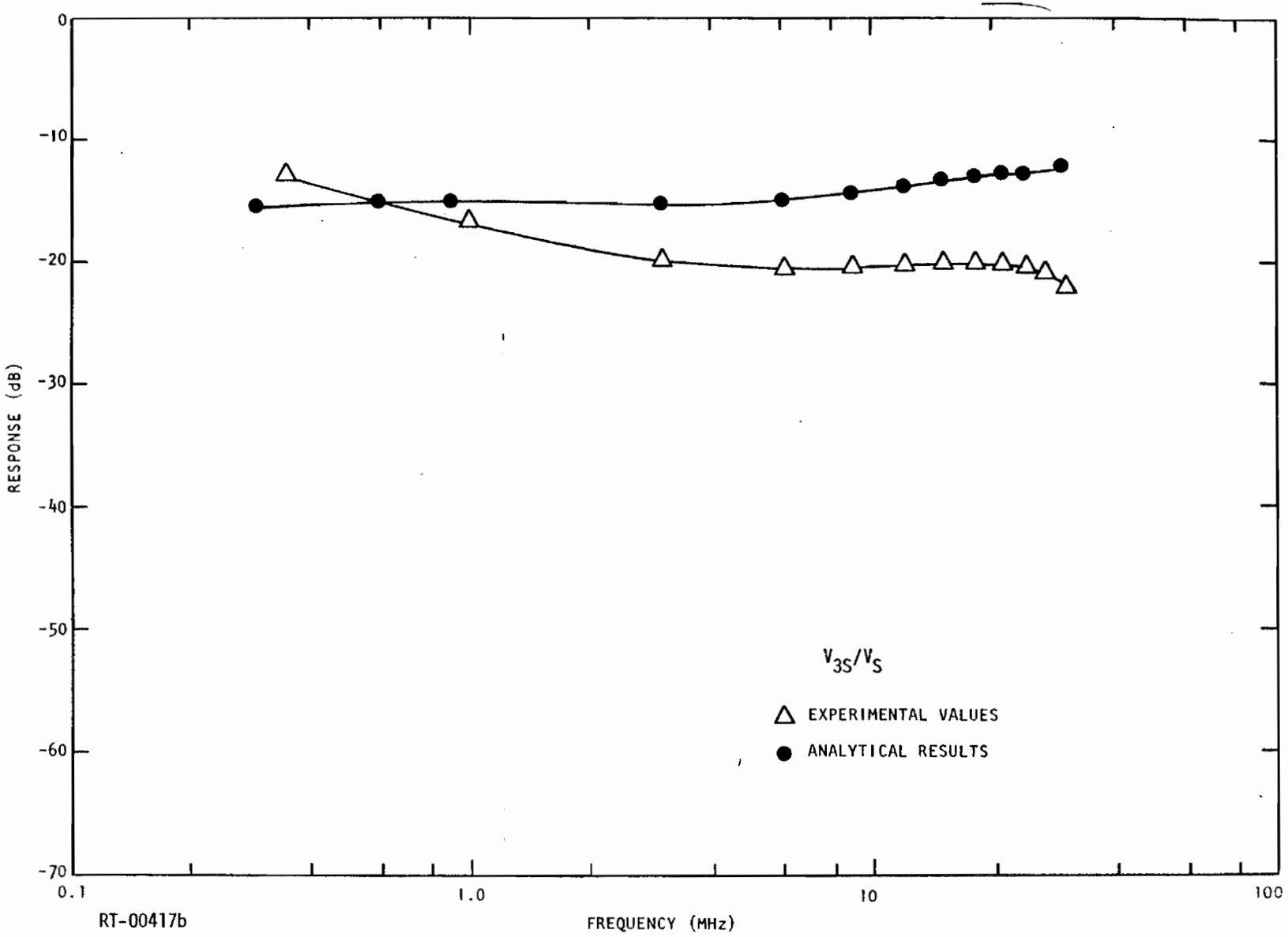
0
-10
-20
-30
-40
-50
-60
-70
RESPONSE (dB)
0.1
1.0
10
100
FREQUENCY (MHz)
RT-00417b
V_{3S}/V_S
EXPERIMENTAL VALUES
ANALYTICAL RESULTS

Fig. 5.8b

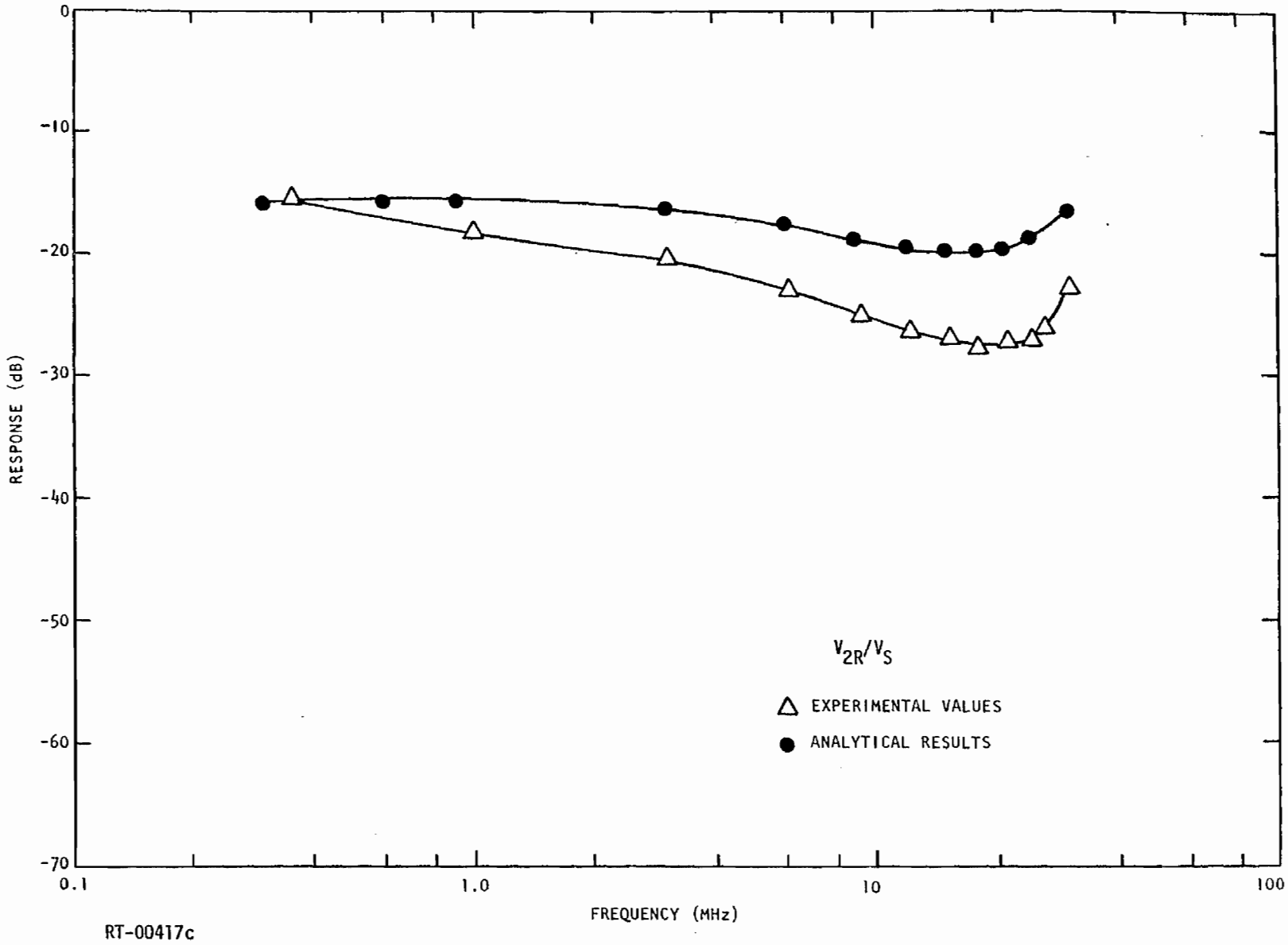
0
-10
-20
-30
-40
-50
-60
-70
RESPONSE (dB)
0.1
1.0
10
100
FREQUENCY (MHz)
V_{2R}/V_S
EXPERIMENTAL VALUES
ANALYTICAL RESULTS
RT-00417c

Fig. 5.8c

Cable 1, Shielded Trio, Shorted-Z Method

The detailed steps for determining the L and C parameters by the third (shorted-Z) method are as follows. The new set of measured impedances, taken as specified in Table 4.3, are

$$\underline{Z^m} = \begin{bmatrix} 37.0 & 19.5 & 21.5 \\ 19.5 & 37.0 & 17.5 \\ 21.5 & 17.5 & 37.8 \end{bmatrix} \Omega \ .$$

The elements of $\underline{C^p}$ are calculated directly as shown in these examples:

$$C^p_{ij} = \frac{1}{2}\left(\frac{1}{v_{p_i} Z^m_{ii}} + \frac{1}{v_{p_j} Z^m_{jj}} - \frac{1}{v_{p_{ij}} Z^m_{ij}}\right) \ ,$$

$$C^p_{12} = \frac{1}{2}\left(\frac{1}{v_{p1} Z^m_{11}} + \frac{1}{v_{p2} Z^m_{22}} - \frac{1}{v_{p12} Z^m_{12}}\right)$$

$$= \frac{1}{2}\left(\frac{1}{1.98 \times 10^8}\right)\left(\frac{1}{37} + \frac{1}{37} - \frac{1}{19.5}\right)$$

$$= 7 \text{ pF/m} \ ,$$

$$C^p_{ii} = \frac{1}{v_{p_i} Z^m_{ii}} - \sum_{\substack{j=1 \\ j \neq i}}^{N} C^p_{ij} \ ,$$

$$C^p_{11} = \frac{1}{v_{p1} Z^m_{11}} - \left(C^p_{12} + C^p_{13}\right)$$

$$= \frac{1}{(1.98 \times 10^8)(37)} - (7.0 + 17.6)$$

$$= 111.7 \text{ pF/m} \ .$$

These example calculations give quite reasonable results. However, repeating the C^p_{ij} calculation for C^p_{23} gives the result that $C^p_{23} = -9.2$ pF/m. This very interesting result illustrates the biggest disadvantage of this method, one which was observed repeatedly throughout the modeling program. The obviously incorrect negative sign results from the fact that differences of reciprocal impedances must be taken, combined with the fact that the measured impedances are inherently lower for this method and are, therefore, more difficult to measure accurately. That is, using a TDR with the universally accepted 50-ohm standard, measuring impedances as small as 20 ohms requires the use of a larger ρ scale which reduces the resolution and accuracy significantly. Then when the impedances are inverted and differences taken, small errors in Z^m become potentially very large, even to the point of giving negative results, as occurred with C^p_{23}. Thus, while based on sound theoretical background, practical considerations make this method subject to possible error.

In order to continue with the use of this method, the decision was made to simply take the absolute value of the calculated C^p_{ij} and ignore sign problems. Using this approach, we have

$$\underline{C^p} = \begin{bmatrix} 111.7 & 7.0 & 17.6 \\ 7.0 & 138.5 & 9.2 \\ 17.6 & 9.2 & 125.0 \end{bmatrix} \text{ pF/m} .$$

Calculating the elements of $\underline{L}$ from

$$L_{ij} = \frac{Z^m_{ii}}{2v_{p_i}} + \frac{Z^m_{jj}}{2v_{p_j}} - \frac{Z^m_{ij}}{v_{p_{ij}}} ,$$

Using these parameters and the previously calculated K_w values, the "π" model section shown in Fig. 5.9 results. As was done previously, two sets of analytical and experimental transfer functions were taken for the two termination schemes discussed previously. The results are shown in Figs. 5.10a through 5.11c. The results for this method are still considered only fair, since nearly all of the curves have on the order of a 6-dB general shift between analytical and experimental results.

Cable 2, 20-Conductor Controlled-Lay Cable

The next cable to be considered will be the 20-conductor controlled-lay cable which was described earlier. The following termination resistors were connected from the wire indicated to the overall shield as reference on both sending and receiving ends of the cable.

Conductor	Terminating Resistance (ohms)
1	1000
2	1000
3	1000
4	1000
5	1000
6	1000
7	100
8	100
9	100
10	100
11	100
12	100
13	1000
14	1000
15	1000
16	1000
17	1000
18	1000
19	1000

This termination scheme was used throughout all subsequent analysis and testing.

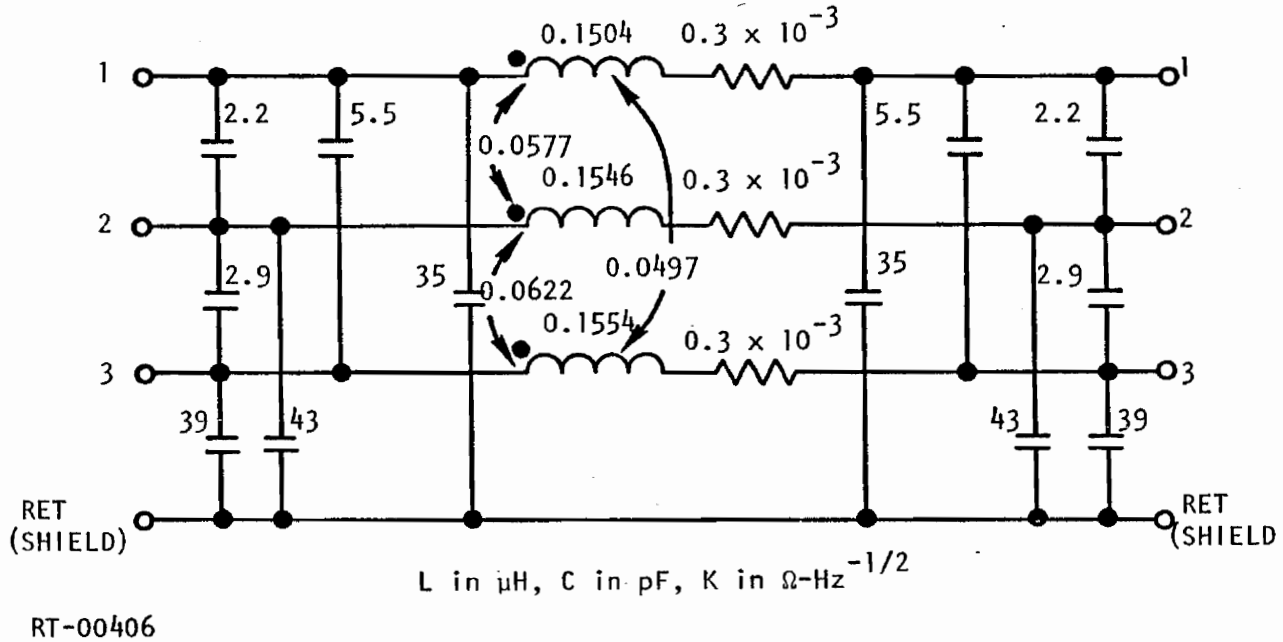

Fig. 5.9. Model section of shielded trio based on the shorted-Z method

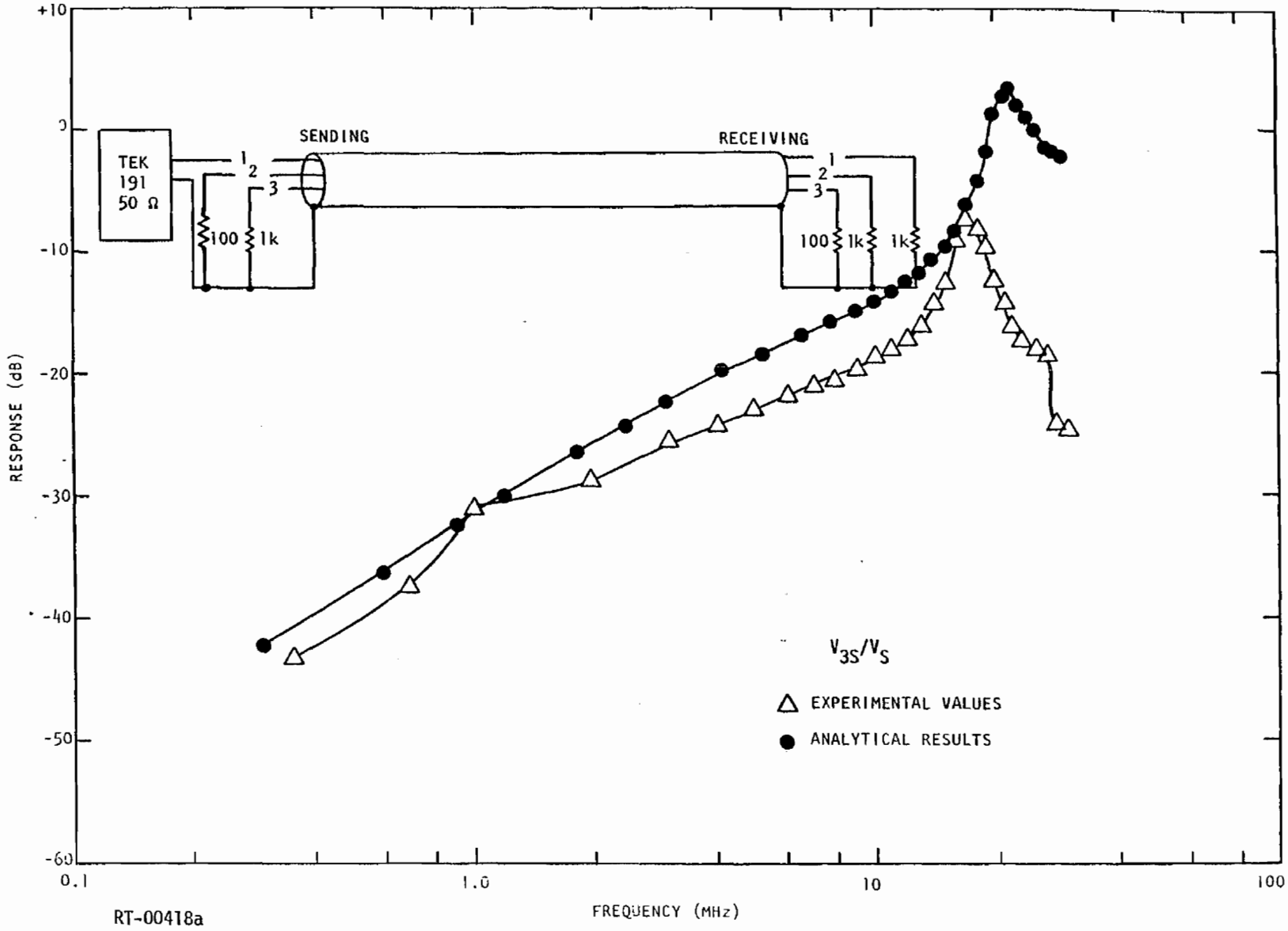

Fig. 5.10a Transfer functions for shielded trio with driven wire terminated in 1000 ohms, shorted-Z method parameters

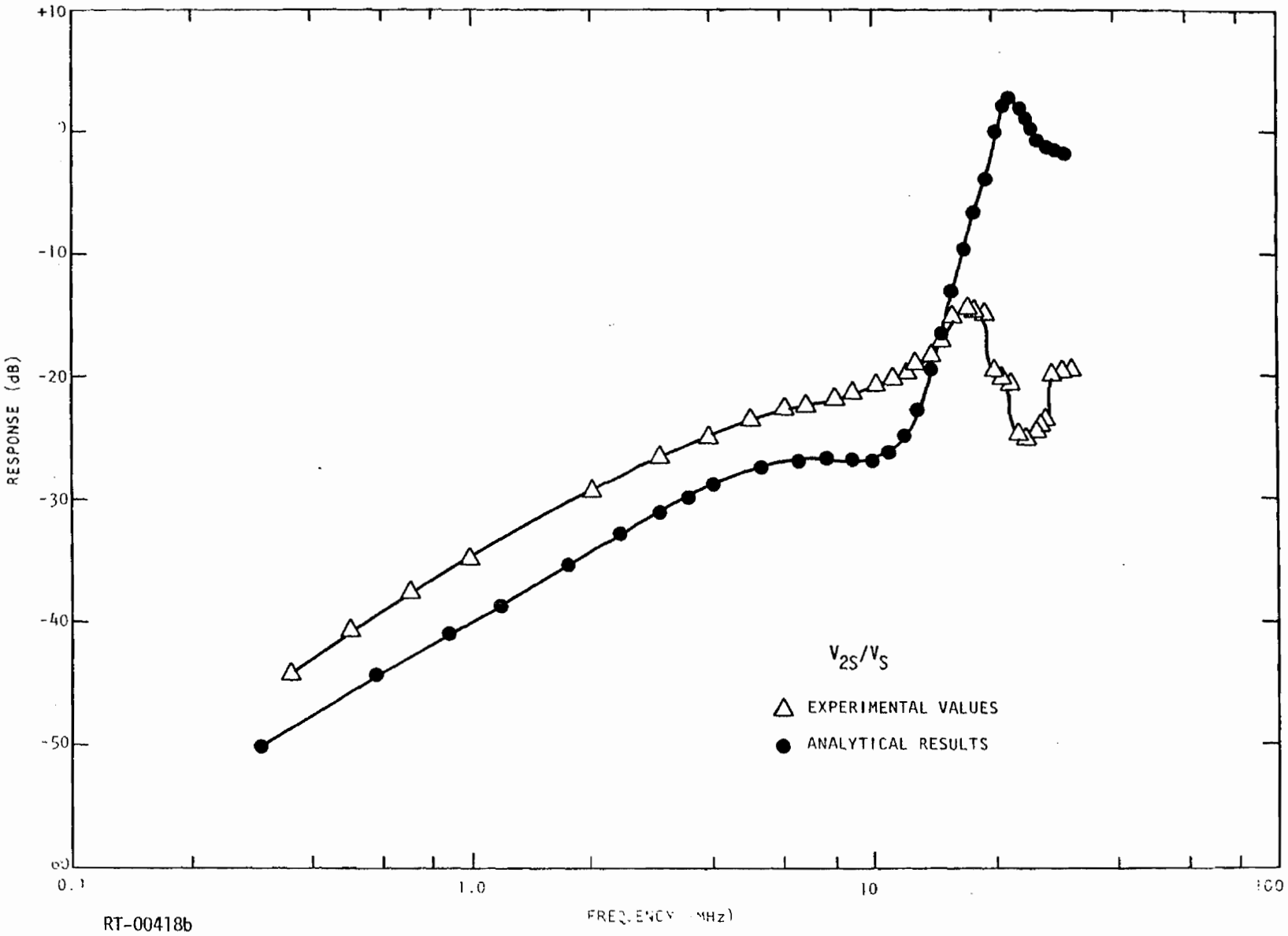
+10
0
-10
-20
-30
-40
-50
∞
RESPONSE (dB)
0.1
1.0
10
100
FREQUENCY (MHz)
V_{2S}/V_S
EXPERIMENTAL VALUES
ANALYTICAL RESULTS
RT-00418b

Fig. 5.10b

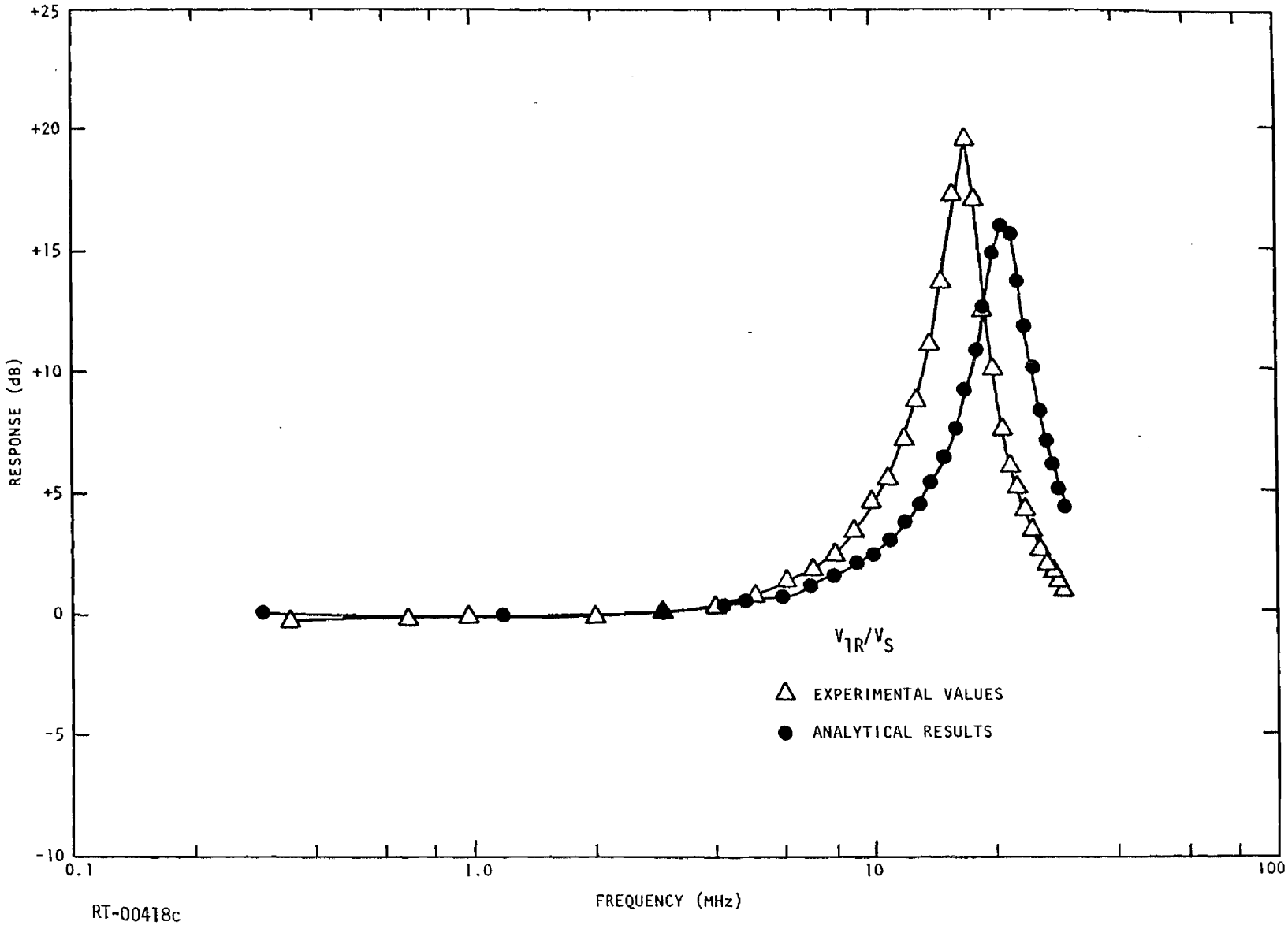
+25
+20
+15
+10
+5
0
-5
-10
RESPONSE (dB)
0.1
1.0
10
100
FREQUENCY (MHz)
V_{1R}/V_S
EXPERIMENTAL VALUES
ANALYTICAL RESULTS
RT-00418c

Fig. 5.10c

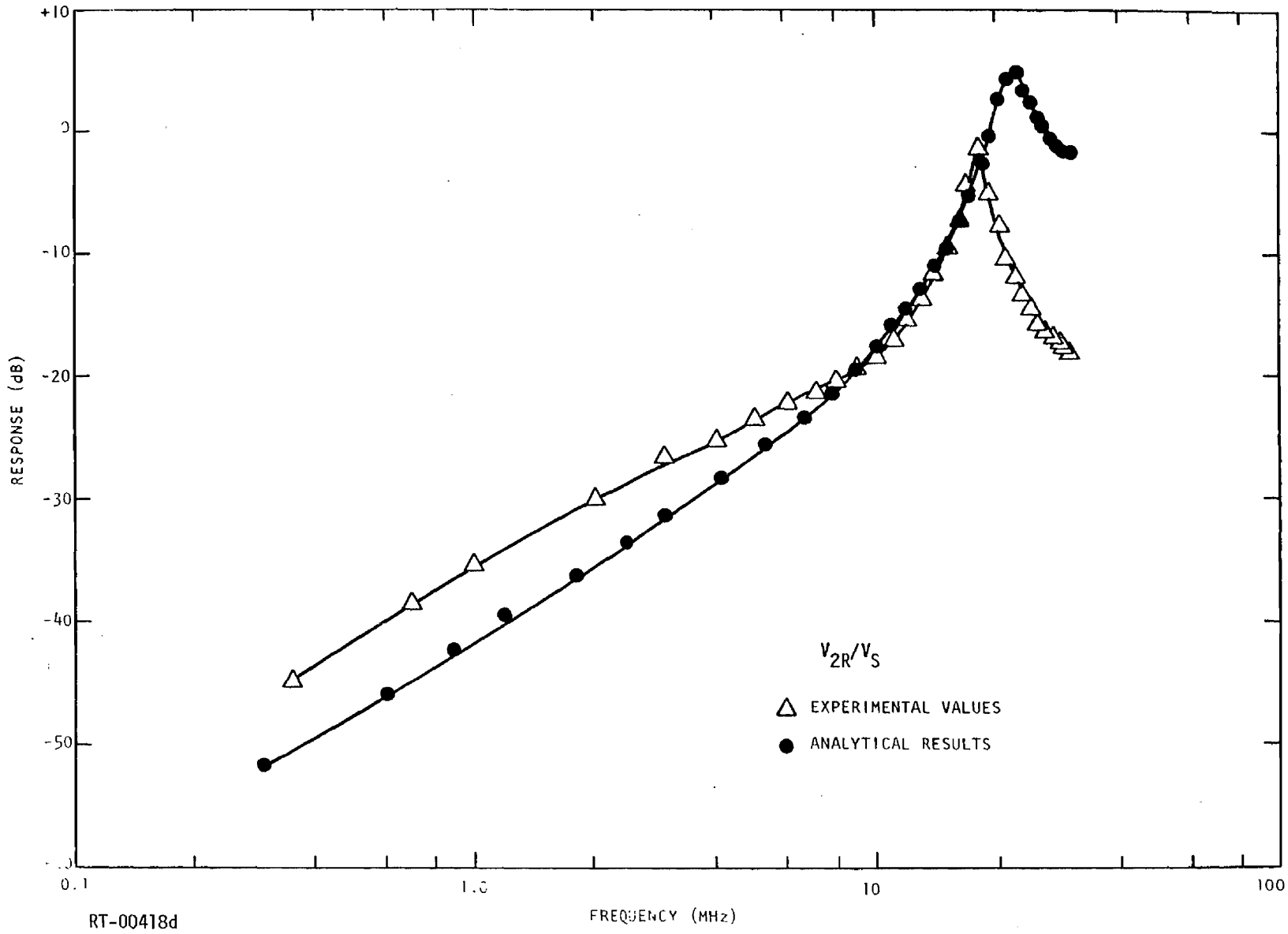
+10
0
-10
-20
-30
-40
-50
RESPONSE (dB)
0.1
1.0
10
100
FREQUENCY (MHz)
V_{2R}/V_S
EXPERIMENTAL VALUES
ANALYTICAL RESULTS
RT-00418d

Fig. 5.10d

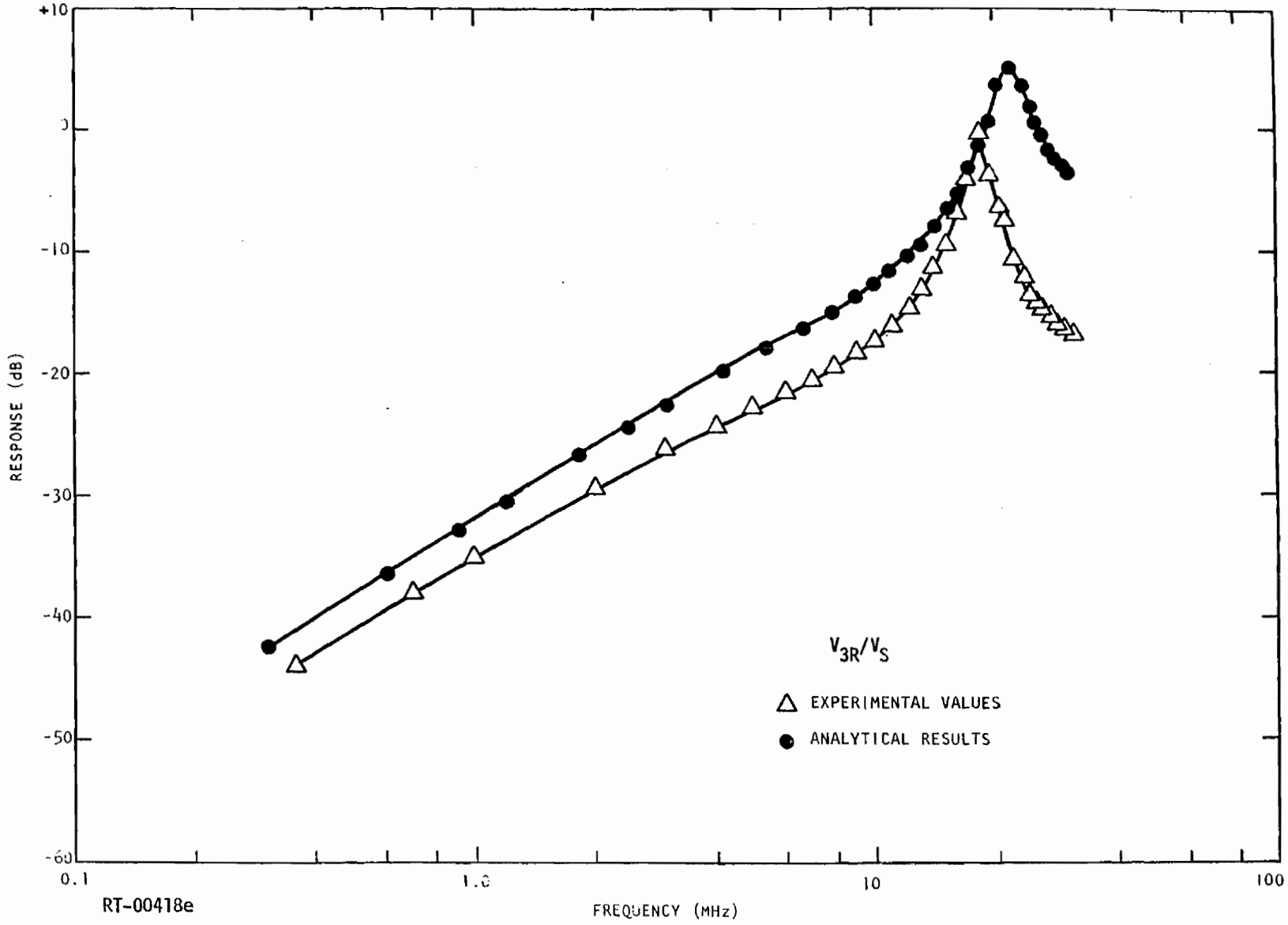
+10
0
-10
-20
-30
-40
-50
-60
RESPONSE (dB)
0.1
1.0
10
100
FREQUENCY (MHz)
V_{3R}/V_S
EXPERIMENTAL VALUES
ANALYTICAL RESULTS
RT-00418e

Fig. 5.10e

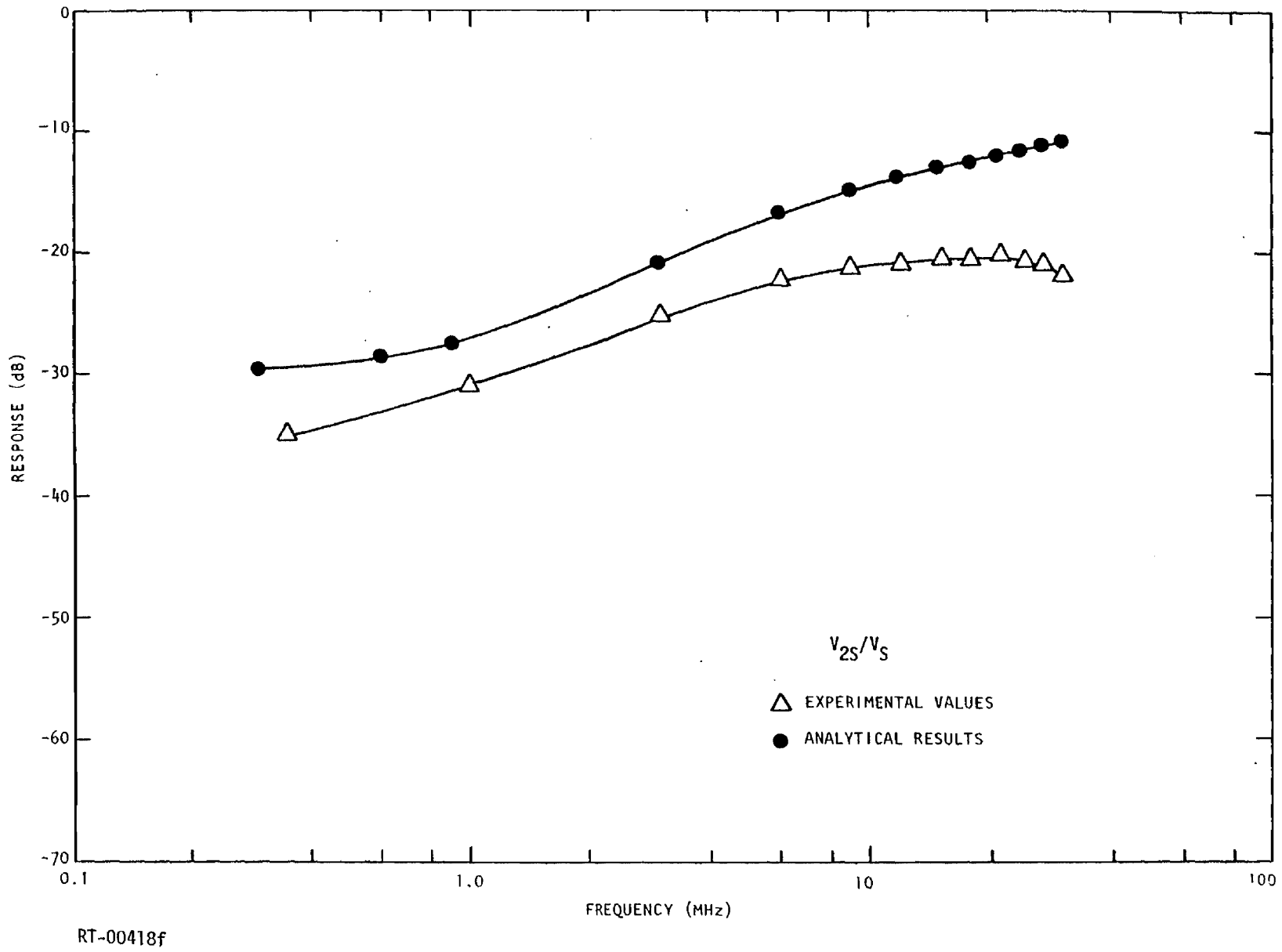

Fig. 5.11a Transfer functions for shielded trio with driven wire terminated in a short circuit, shorted-Z method parameters

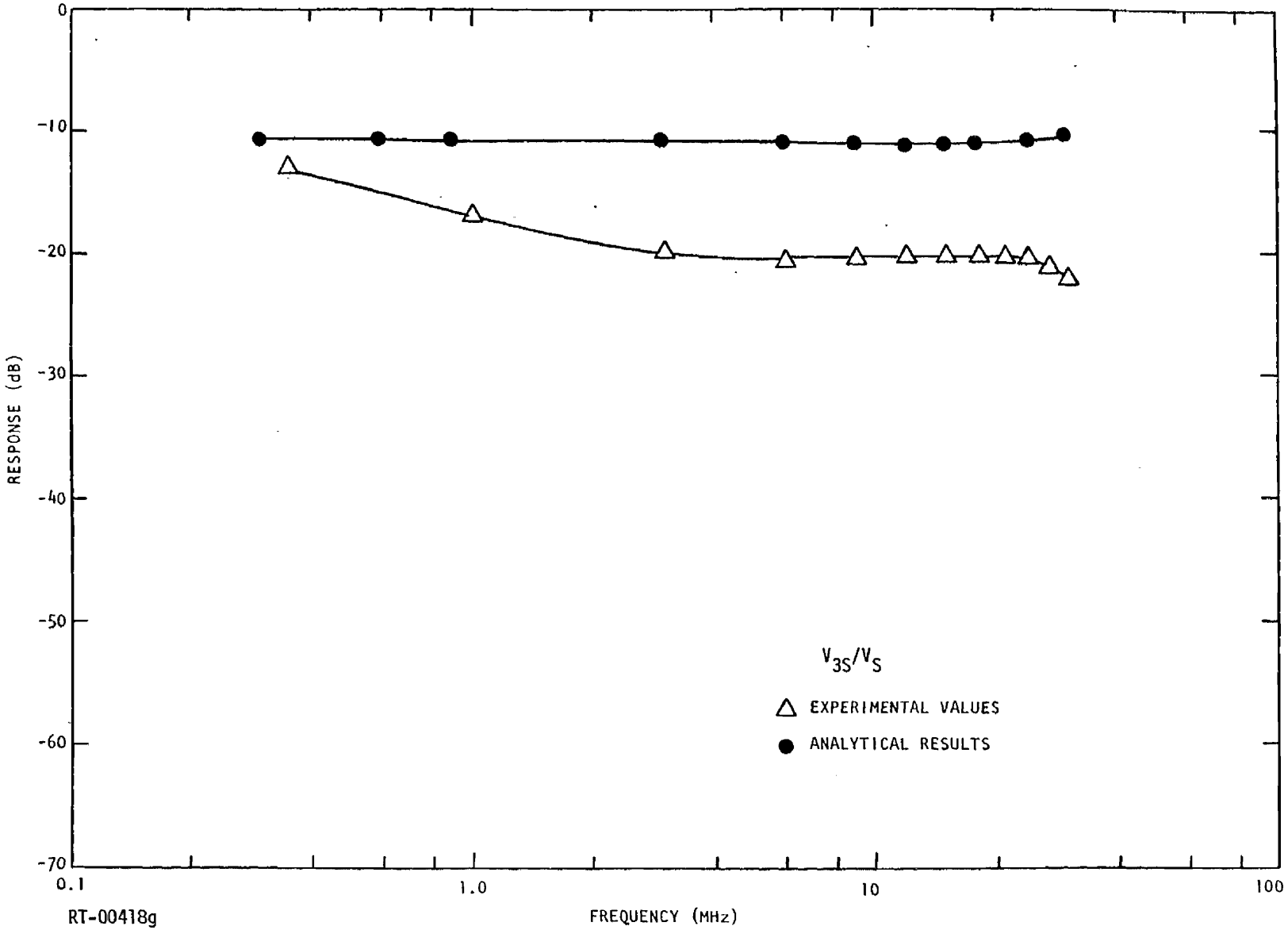
0
-10
-20
-30
-40
-50
-60
-70
RESPONSE (dB)
0.1
1.0
10
100
FREQUENCY (MHz)
RT-00418g
V_{3S}/V_S
EXPERIMENTAL VALUES
ANALYTICAL RESULTS

Fig. 5.11b

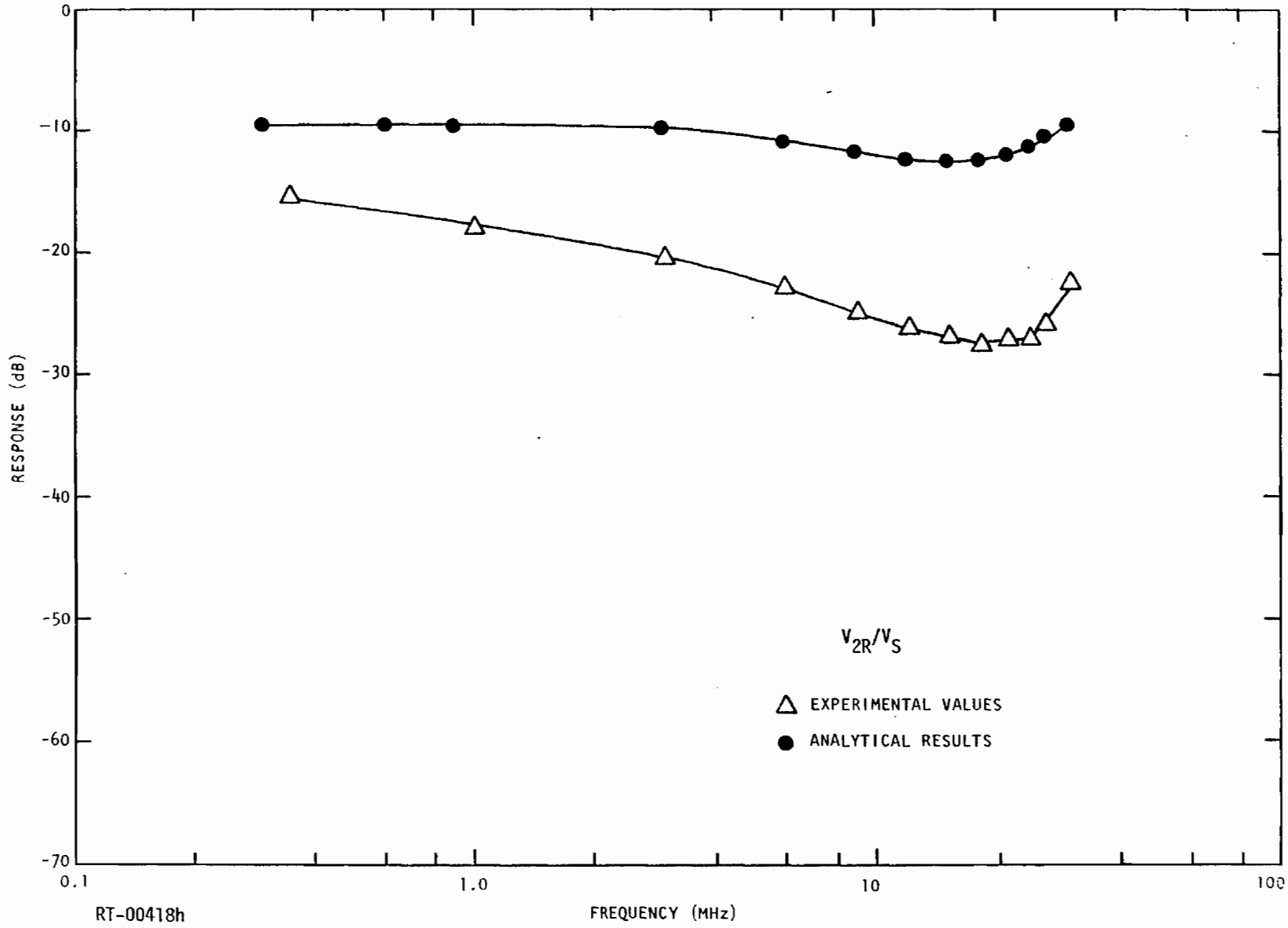
0
-10
-20
-30
-40
-50
-60
-70
RESPONSE (dB)
0.1
1.0
10
100
FREQUENCY (MHz)
V_{2R}/V_S
EXPERIMENTAL VALUES
ANALYTICAL RESULTS
RT-00418h

Fig. 5.11c

Two drive schemes were used, with conductor 20, the center conductor, driven against the shield at the sending end for both. The difference was in the termination of conductor 20 at the receiving end, being open-circuited for one case and shorted to the shield for the other.

Before proceeding to presentation of the results, a discussion of the parameter value determination is in order. Only the capacitance method was applied to this cable, and sign problems of the sort encountered with the shorted-Z method on the shielded trio were observed in this application. The capacitance measurements were made in the same manner and using the same equipment as before. A 20 x 20 $\underline{C^m}$ matrix resulted, which, due to its size, will not be presented here. However, the measured capacitances were in the following ranges for the indicated conductor pairings.

C_{ii}^m = 529 to 611 pF ,

C_{ij}^m = 813 to 998 pF , i and j adjacent conductors ,

C_{ij}^m = 1027 to 1216 pF , i and j separated by one or more conductors .

The diagonal elements of $\underline{K}$ are, of course, simply the C_{ii}^m, but the off-diagonal terms must be calculated from

$$K_{ij} = \frac{1}{2}(C_{ij}^m - C_{ii}^m - C_{jj}^m) ,$$

and are supposed to be always negative. However, it is clear from the ranges of C_{ii}^m and C_{ij}^m noted above that it is entirely possible for some K_{ij} to come out positive, and this in fact occurred in 43 of 190 K_{ij} calculations. These positive values were all in the range 0.5 to 7.5 pF and are associated with the very small partial capacitances between conductors that are shielded from each other by intermediate conductors.

The source of this problem is error in the capacitance measurements resulting from basic equipment inaccuracy, unavoidable stray capacitance, operator bias, etc. Considering equipment error alone, if the bridge accuracy is ±0.5%, then the errors in C_{ii}^{m} could be ~2.5 to 3.0 pF, and in C_{ij}^{m} they could be ~4 to 6 pF. If these errors are cumulative, they can easily account for the appearance of positive K_{ij} terms of the small size encountered in this application. Thus, even small measurement errors become significant for those K_{ij} which are inherently small.

These errors in K_{ij} will have an effect on the $\underline{C^{p}}$ calculations also. In particular, the C_{ii}^{p} calculations will be very sensitive to K_{ij} error since these require the summation of a large number of K_{ij} terms, each of which contributes error. If the errors are cumulative, they can even result in the appearance of negative C_{ii}^{p} terms, which should always be positive, of course, Again, this effect was observed in this application. In fact, five of eight C_{ii}^{p} calculations for conductors 13 through 20 resulted in negative values. These particular C_{ii}^{p} are inherently small due to the shielding effect of the layer of conductors 1 through 12, and the errors were large enough compared to C_{ii}^{p} to cause the negative values.

The errors in K_{ij} also appear to have affected even the larger C_{ii}^{p} of conductors 1 through 12. Because these conductors are in the outer layer and in very close proximity to the shield, it would be expected that their partial capacitances to the shield would be relatively large and reasonably uniform. In fact, however, the range of C_{ii}^{p} for this outer layer was from 53 to 214 pF, a variation of ±60% from the mean value of 133 pF. This lack of uniformity apparently resulted from the errors in K_{ij}.

For this and subsequent cables with such sign problems, the problems were handled in the following manner. All K_{ij} were forced to be negative by simply taking the absolute value of each calculated value and changing the sign to minus. These K_{ij} were then used for all $\underline{C^{p}}$

calculations. Where negative C_{ii}^{p} values occurred, the C_{ii}^{p} were set to zero for purposes of modeling, since they were inherently small to begin with.*

The parameters derived by this method were used to create a model consisting of five "π" sections, each of 0.62 m length. For the 2.015×10^{8} m/sec mean phase velocity, these sections are less than 0.1 λ up to 32.5 MHz. (Phase velocity was still relatively uniform for this cable, the 3σ limits being 8.5%.) The results for the case of the driven wire terminated in an open circuit are presented in Figs. 5.12a through 5.12g. By the criteria defined in Section 5.2, the results for the seven transfer functions taken are five "Fair" and two "Good." (The notation used to designate the transfer functions are the same as used before; i.e., V_{1R} means voltage from wire 1 to reference at the receiving end, and V_{20S} means the drive voltage applied between wire 20 and reference at the sending end.) The results for the case of the driven wire shorted to the shield at the receiving end are presented in Figs. 5.13a through 5.13g. The results for all seven transfer functions taken are "Fair."

Considering the problems encountered in deriving the parameters for this cable and its relative complexity, these results are very encouraging indeed. In particular, the results show very clearly that the modeling technique adequately accounts for the shielding effect of intermediate wire layers as evidenced by the ~20-dB shift in both analytical and experimental results between wires 13 and 14 which are adjacent to the driven wire, and wires 1, 2, and 3 which are two layers away.

*Since the positive K_{ij} terms are also inherently small, the question could well be raised as to why they were not set to zero also. In retrospect, this is probably a better approach, but early in the modeling effort, this was not recognized.

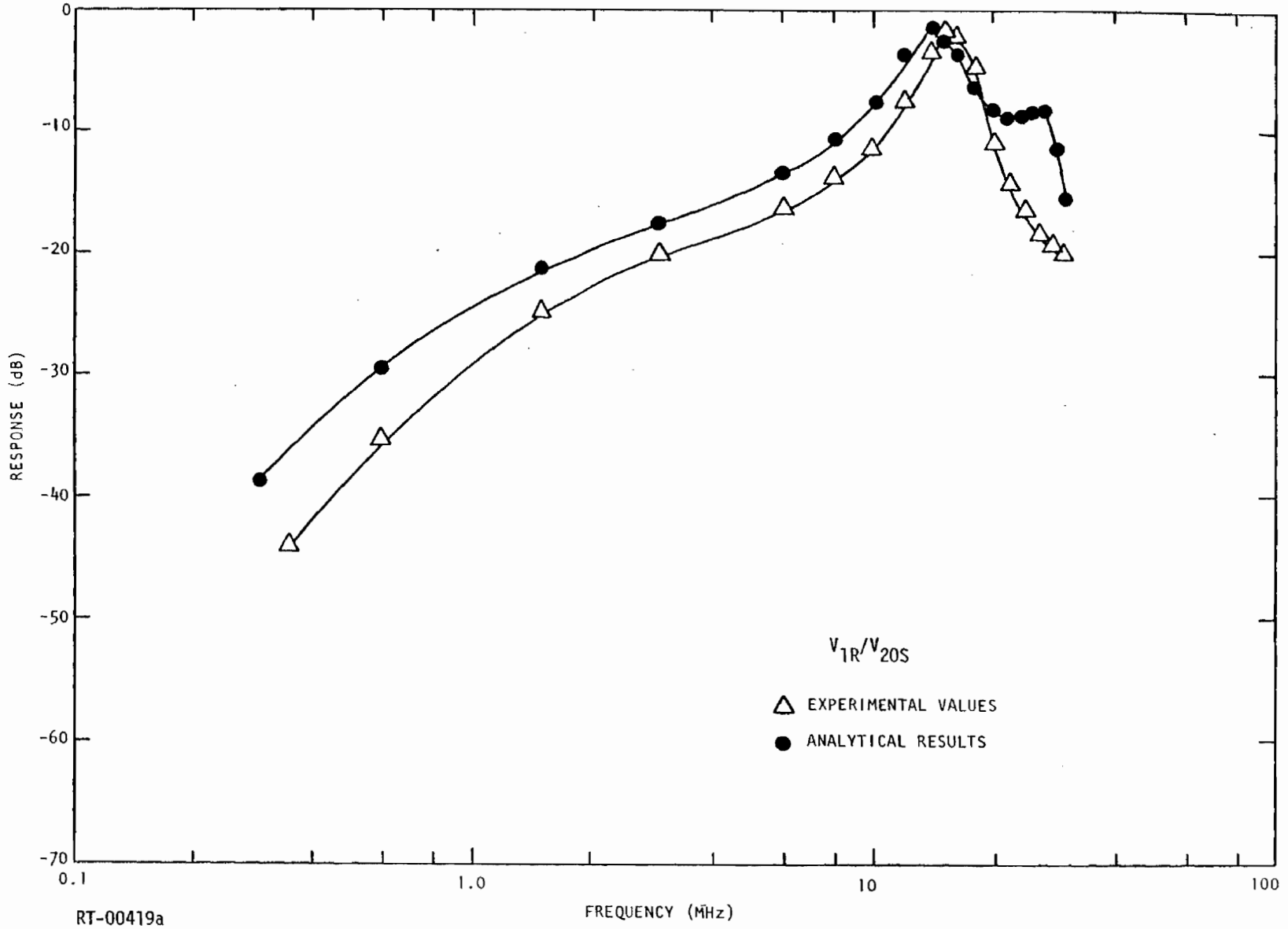

Fig. 5.12a. Transfer functions for 20-conductor controlled cable with driven wire terminated in an open circuit, capacitance method parameters

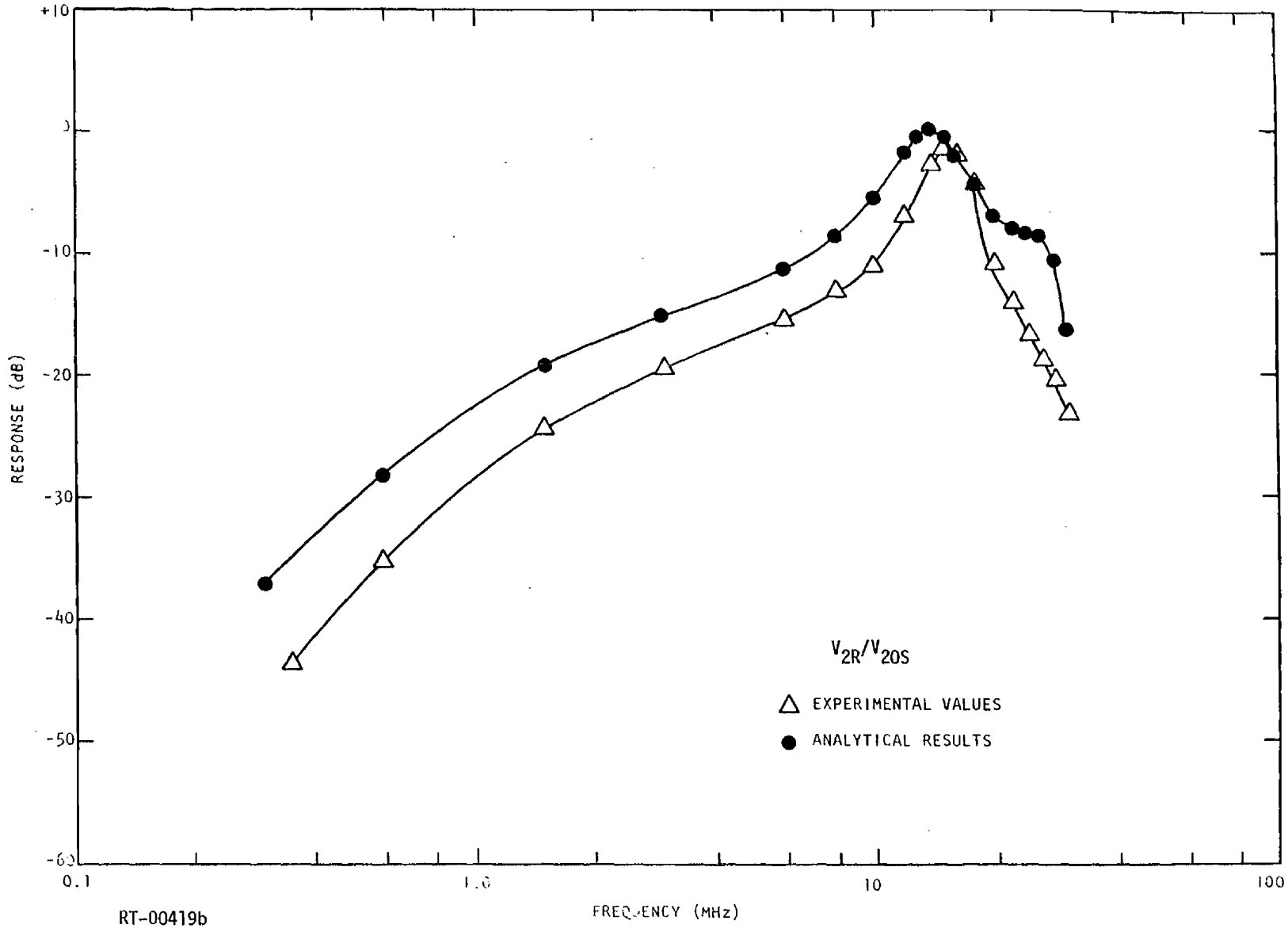
+10
0
-10
-20
-30
-40
-50
-60
RESPONSE (dB)
0.1
1.0
10
100
FREQUENCY (MHz)
V_{2R}/V_{20S}
EXPERIMENTAL VALUES
ANALYTICAL RESULTS
RT-00419b

Fig. 5.12b

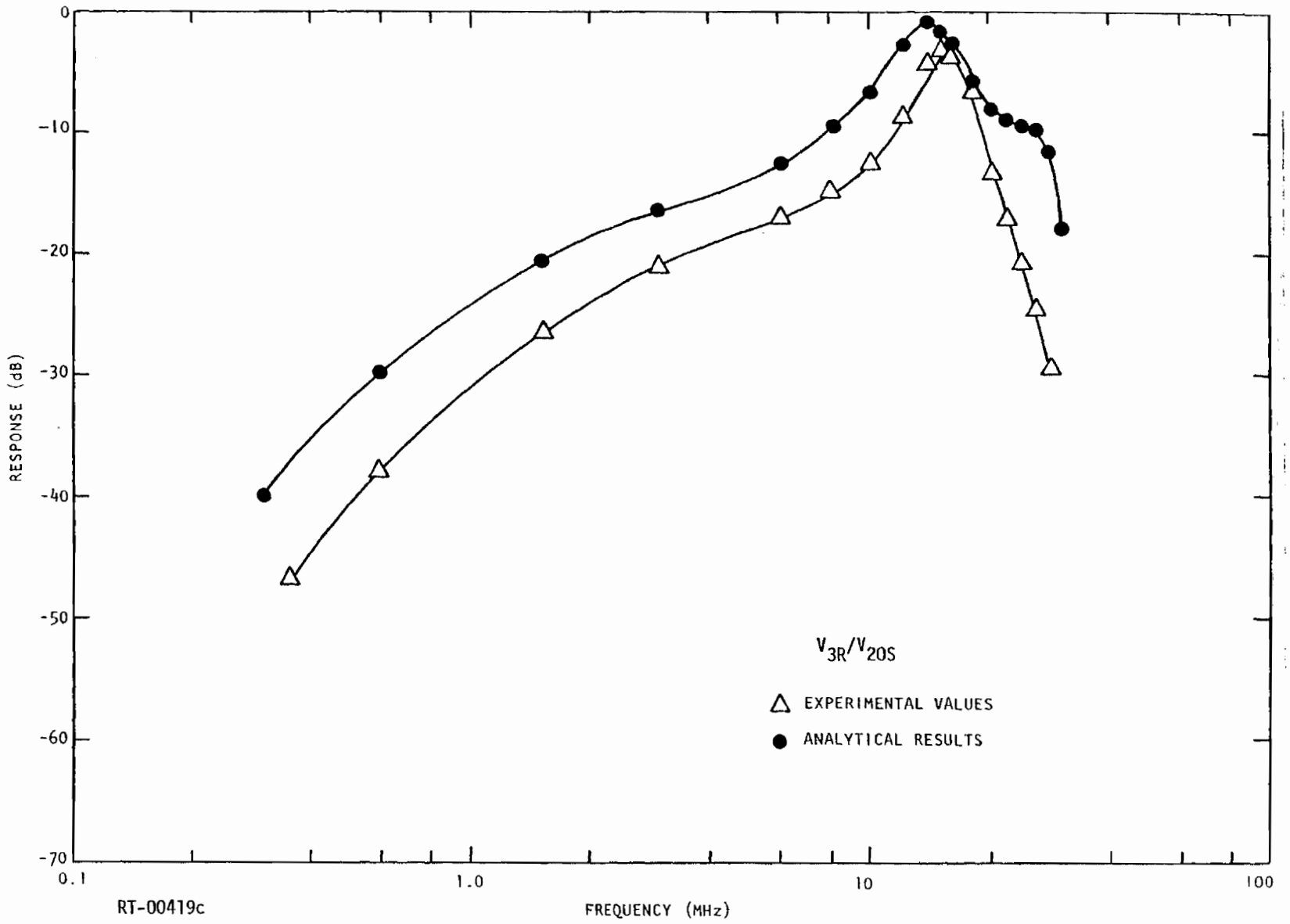
0
-10
-20
-30
-40
-50
-60
-70
RESPONSE (dB)
0.1
1.0
10
100
FREQUENCY (MHz)
RT-00419c
V_{3R}/V_{20S}
EXPERIMENTAL VALUES
ANALYTICAL RESULTS

Fig. 5.12c

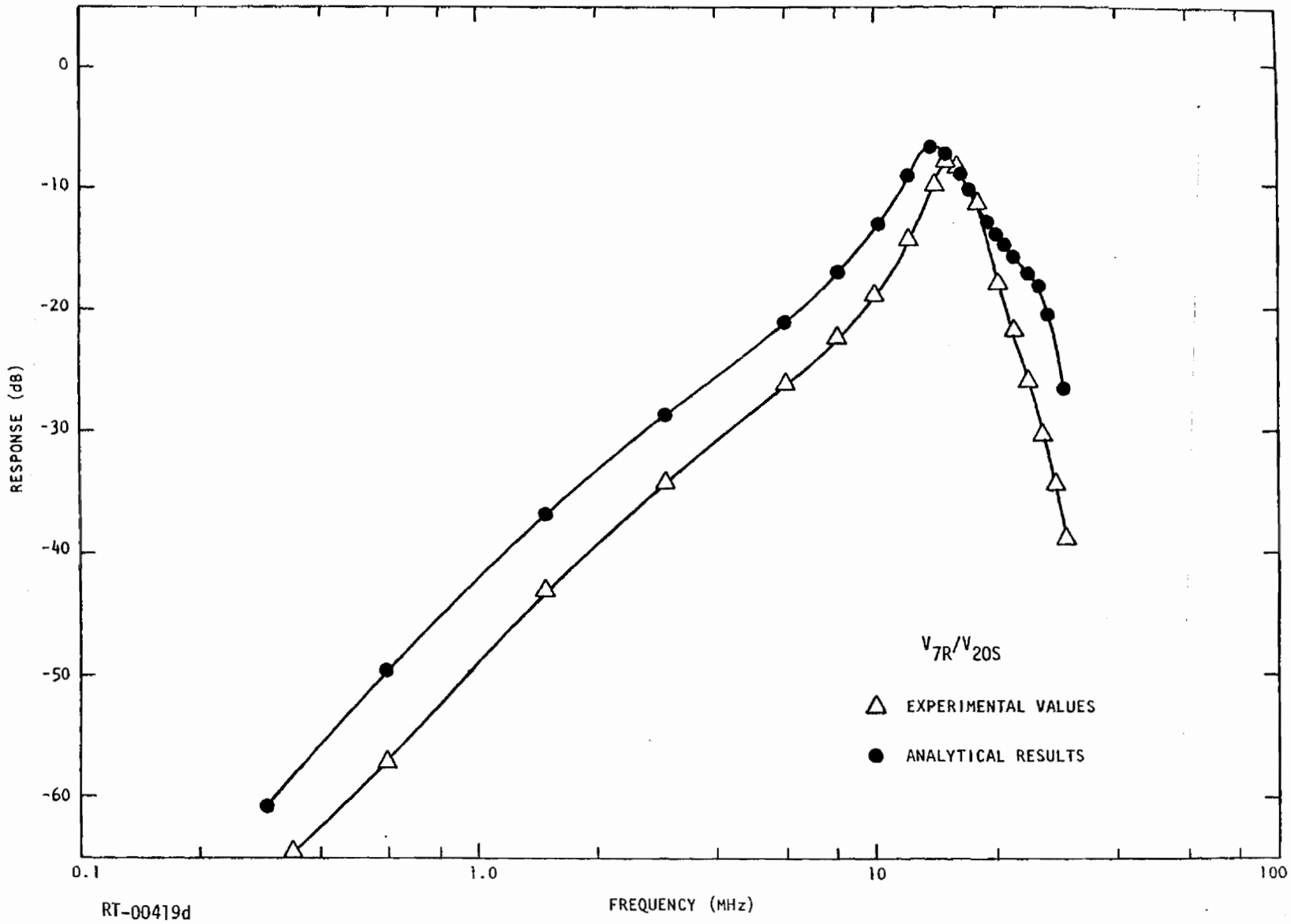
0
-10
-20
-30
-40
-50
-60
RESPONSE (dB)
0.1
1.0
10
100
FREQUENCY (MHz)
V_{7R}/V_{20S}
EXPERIMENTAL VALUES
ANALYTICAL RESULTS
RT-00419d

Fig. 5.12d

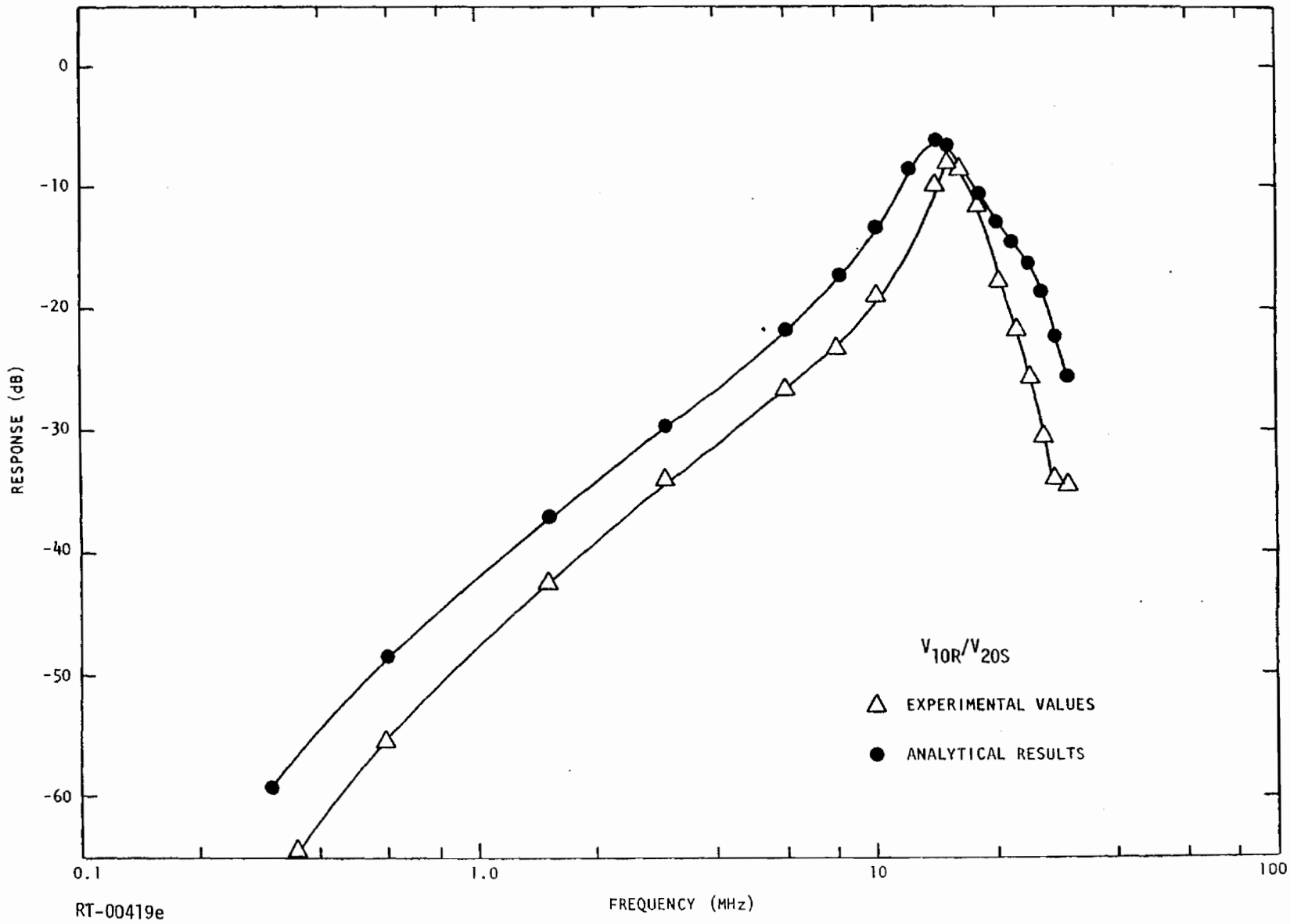
0
-10
-20
-30
-40
-50
-60
RESPONSE (dB)
0.1
1.0
10
100
FREQUENCY (MHz)
V_{10R}/V_{20S}
EXPERIMENTAL VALUES
ANALYTICAL RESULTS
RT-00419e

Fig. 5.12e

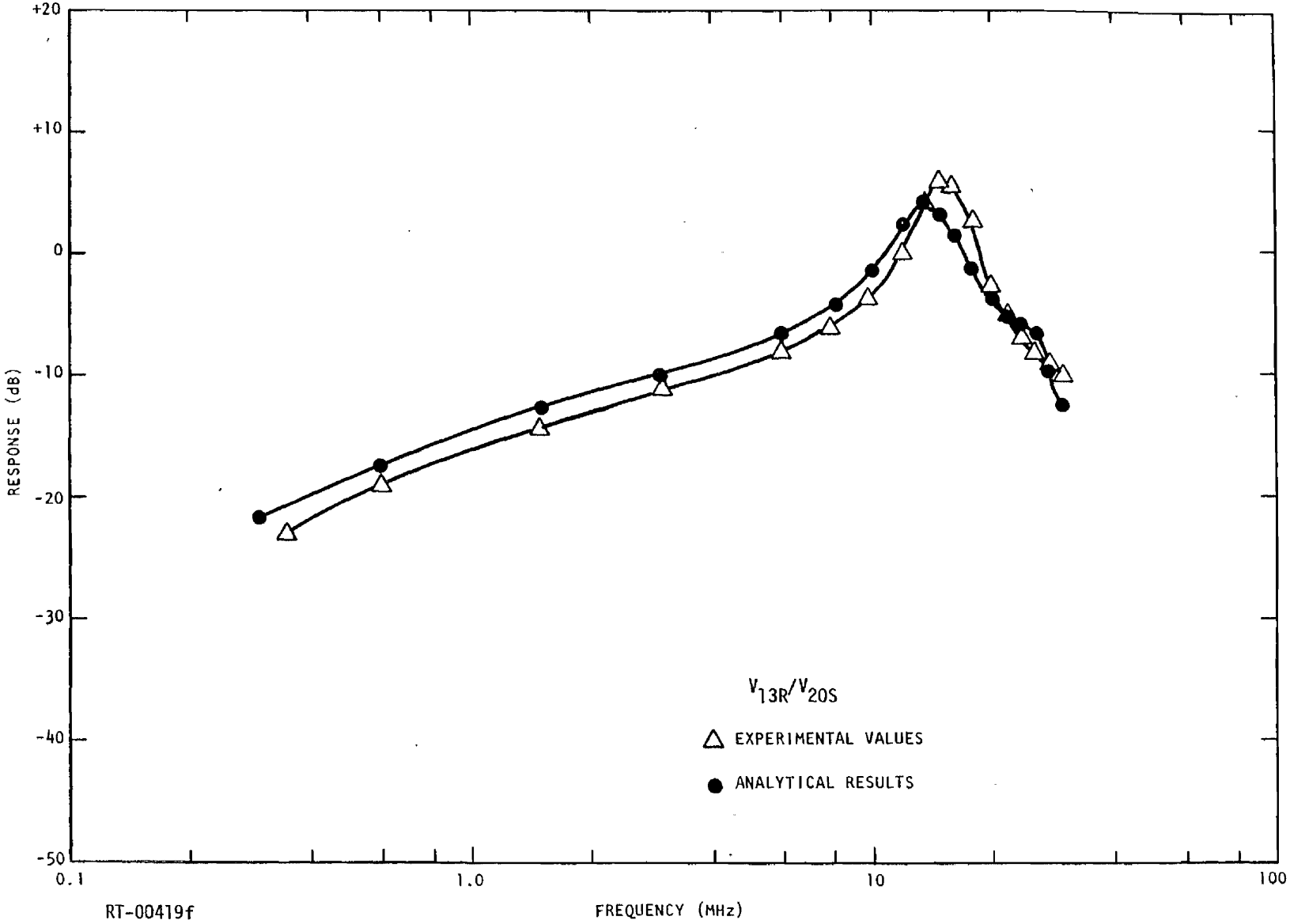
+20
+10
0
-10
-20
-30
-40
-50
RESPONSE (dB)
0.1
1.0
10
100
FREQUENCY (MHz)
V_{13R}/V_{20S}
EXPERIMENTAL VALUES
ANALYTICAL RESULTS
RT-00419f

Fig. 5.12f

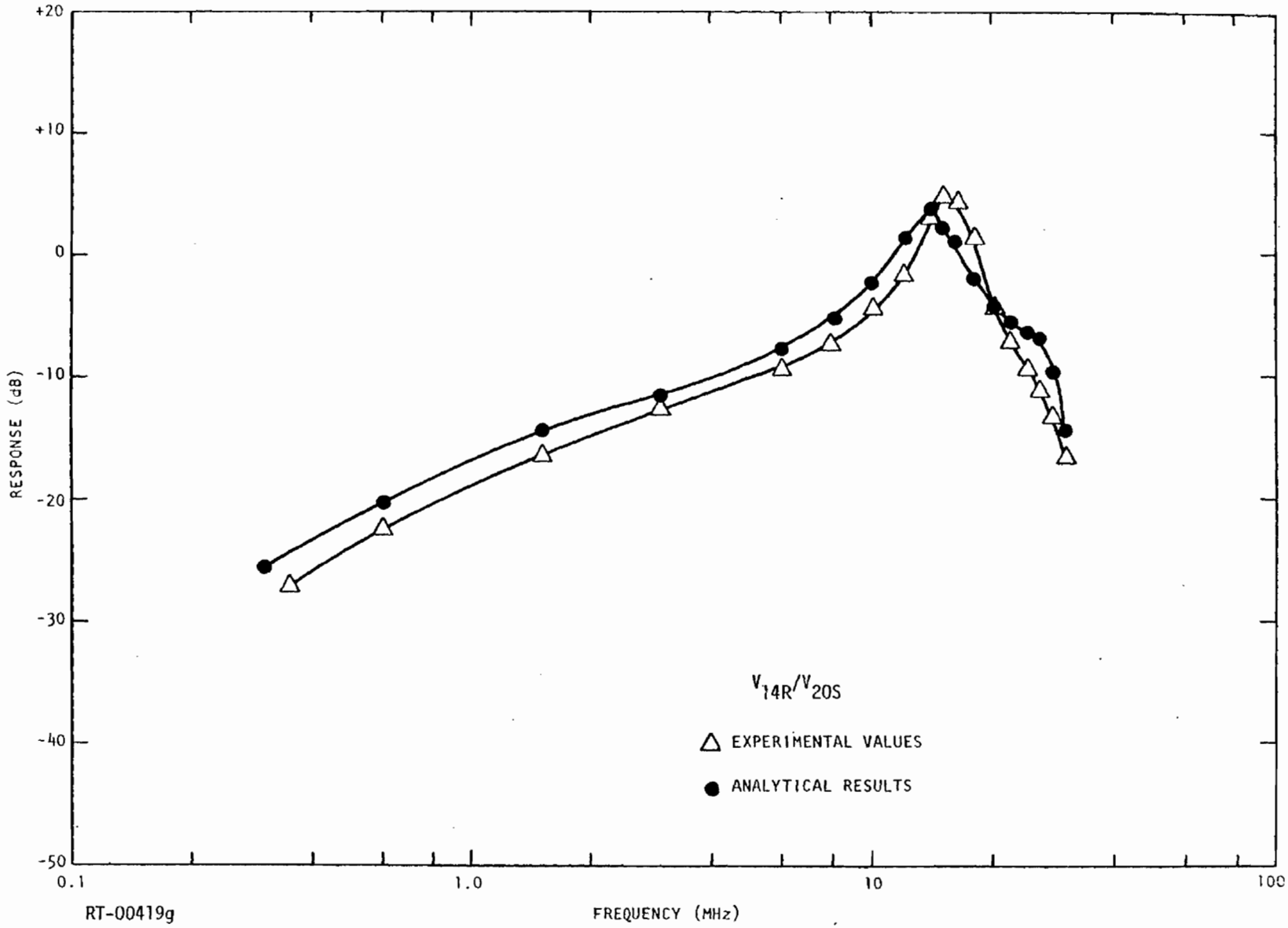
+20
+10
0
-10
-20
-30
-40
-50
RESPONSE (dB)
0.1
1.0
10
100
FREQUENCY (MHz)
V_{14R}/V_{20S}
EXPERIMENTAL VALUES
ANALYTICAL RESULTS
RT-00419g

Fig. 5.12g

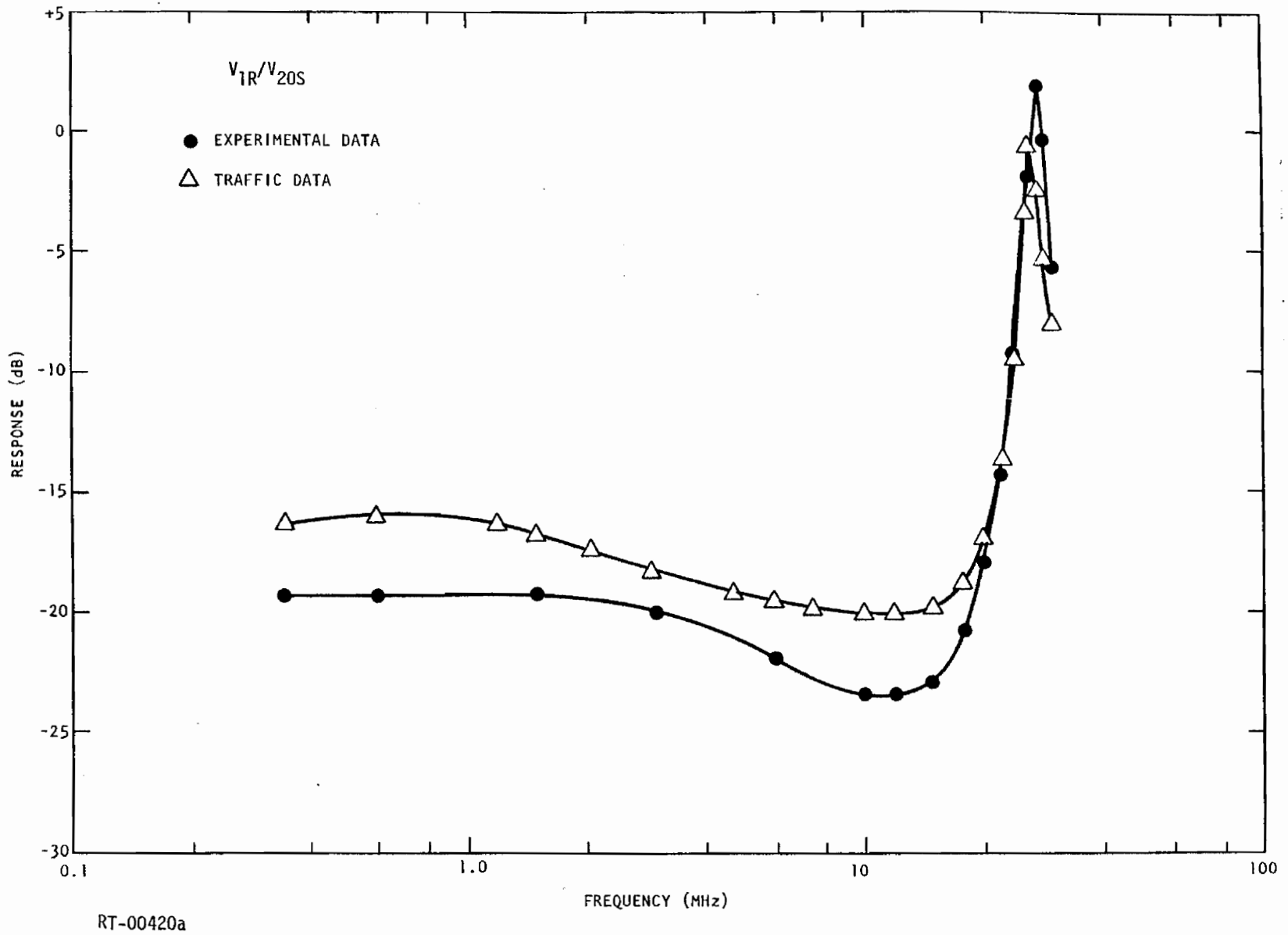

Fig. 5.13a. Transfer functions for 20-conductor controlled cable with driven wire terminated in a short circuit, capacitance method parameters

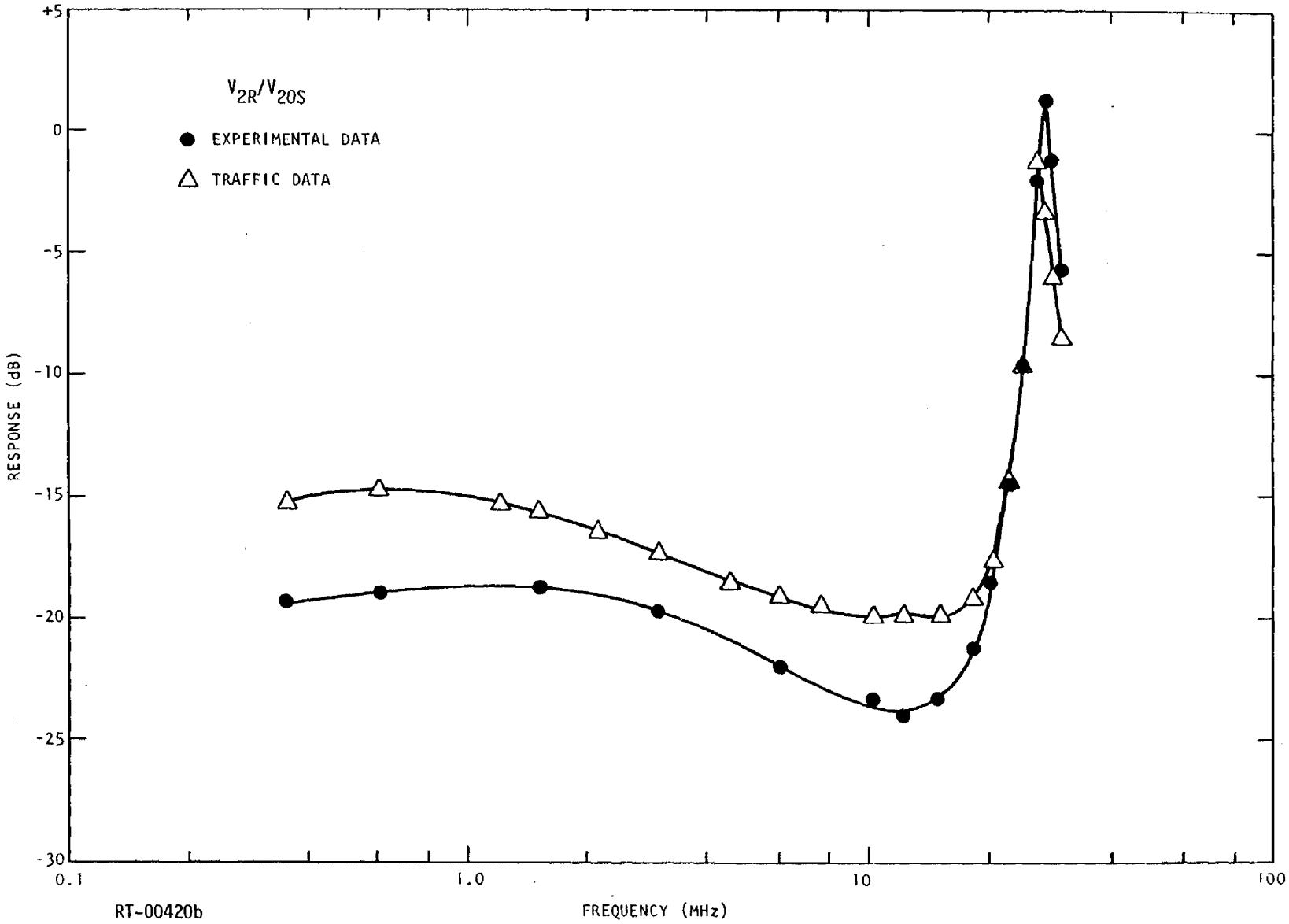
V_{2R}/V_{20S}
EXPERIMENTAL DATA
TRAFFIC DATA
RESPONSE (dB)
+5
0
-5
-10
-15
-20
-25
-30
0.1
1.0
10
100
FREQUENCY (MHz)
RT-00420b

Fig. 5.13b

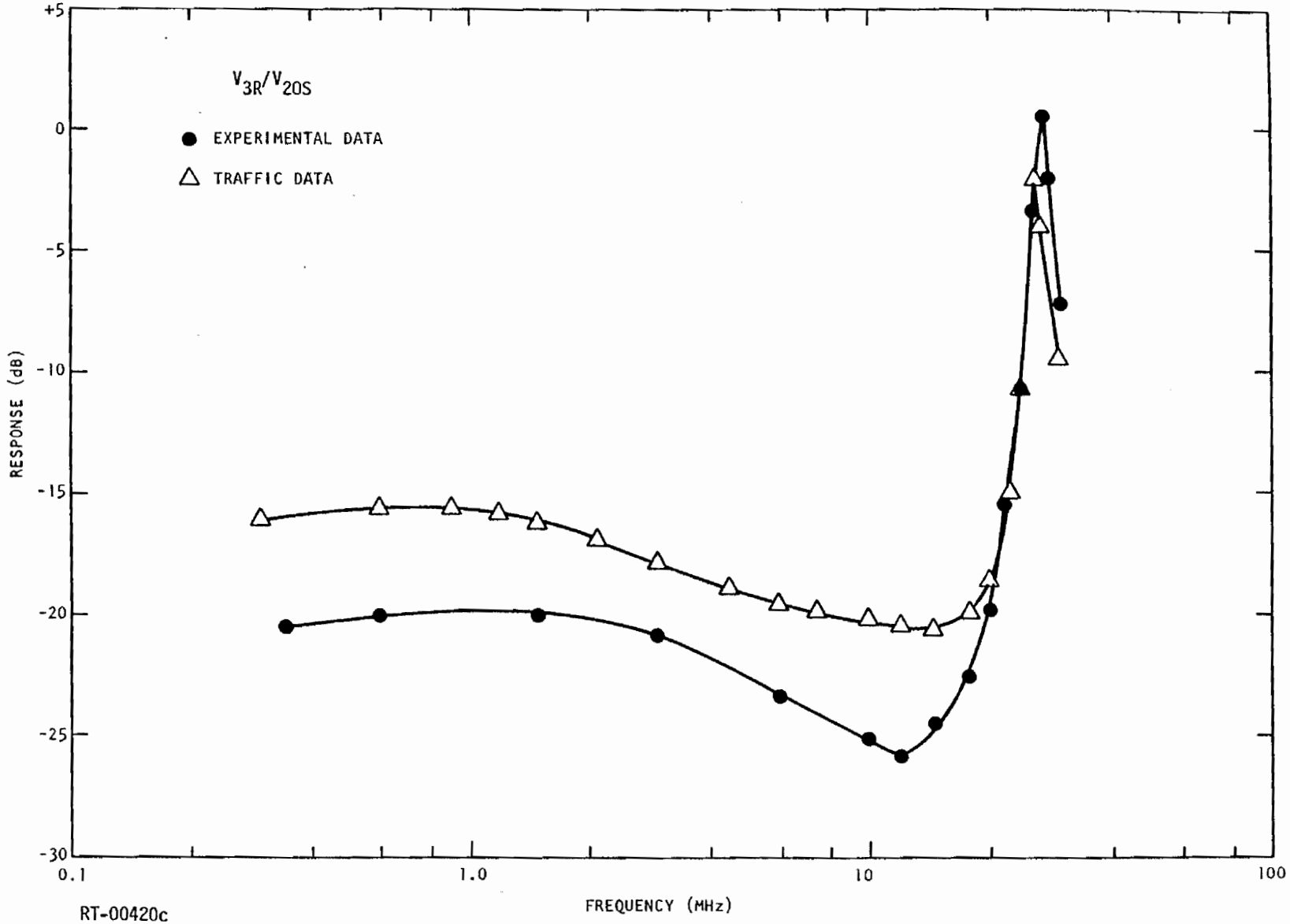
V_{3R}/V_{20S}
EXPERIMENTAL DATA
TRAFFIC DATA
RESPONSE (dB)
+5
0
-5
-10
-15
-20
-25
-30
0.1
1.0
10
100
FREQUENCY (MHz)
RT-00420c

Fig. 5.13c

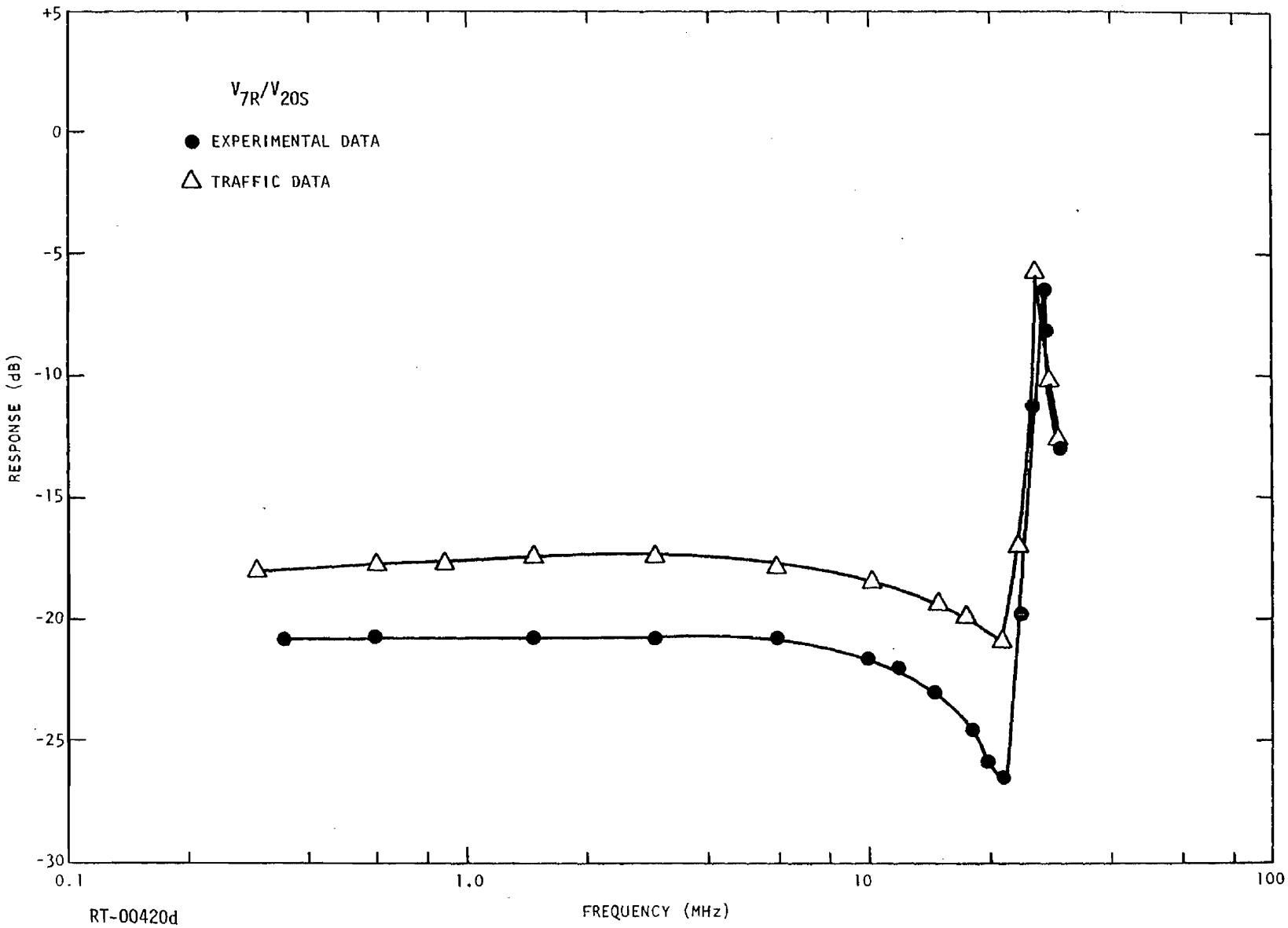
V_{7R}/V_{20S}
EXPERIMENTAL DATA
TRAFFIC DATA
+5
0
-5
-10
-15
-20
-25
-30
RESPONSE (dB)
0.1
1.0
10
100
FREQUENCY (MHz)
RT-00420d

Fig. 5.13d

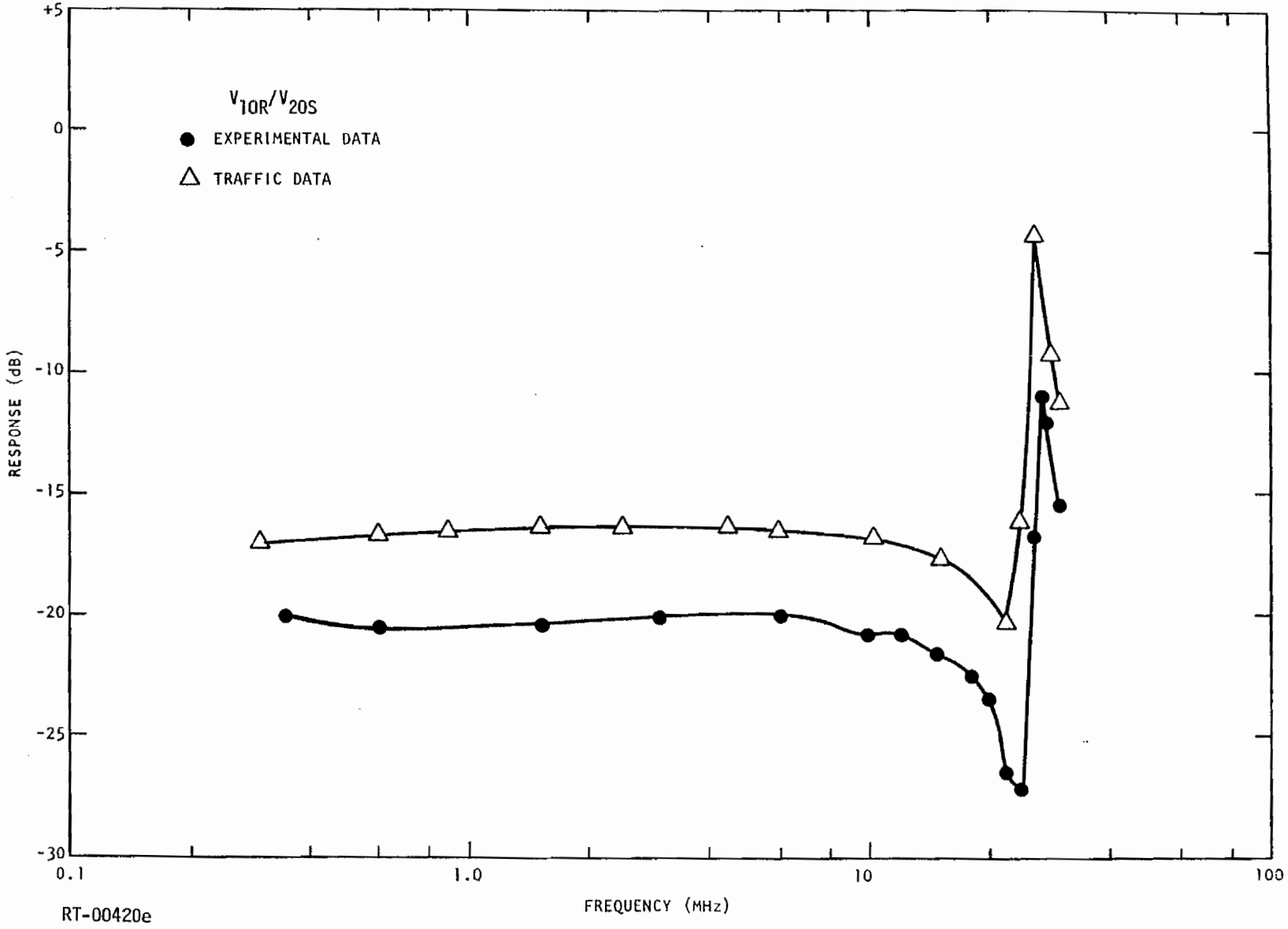
V_{10R}/V_{20S}
EXPERIMENTAL DATA
TRAFFIC DATA
RESPONSE (dB)
+5
0
-5
-10
-15
-20
-25
-30
0.1
1.0
10
100
FREQUENCY (MHz)
RT-00420e

Fig. 5.13e

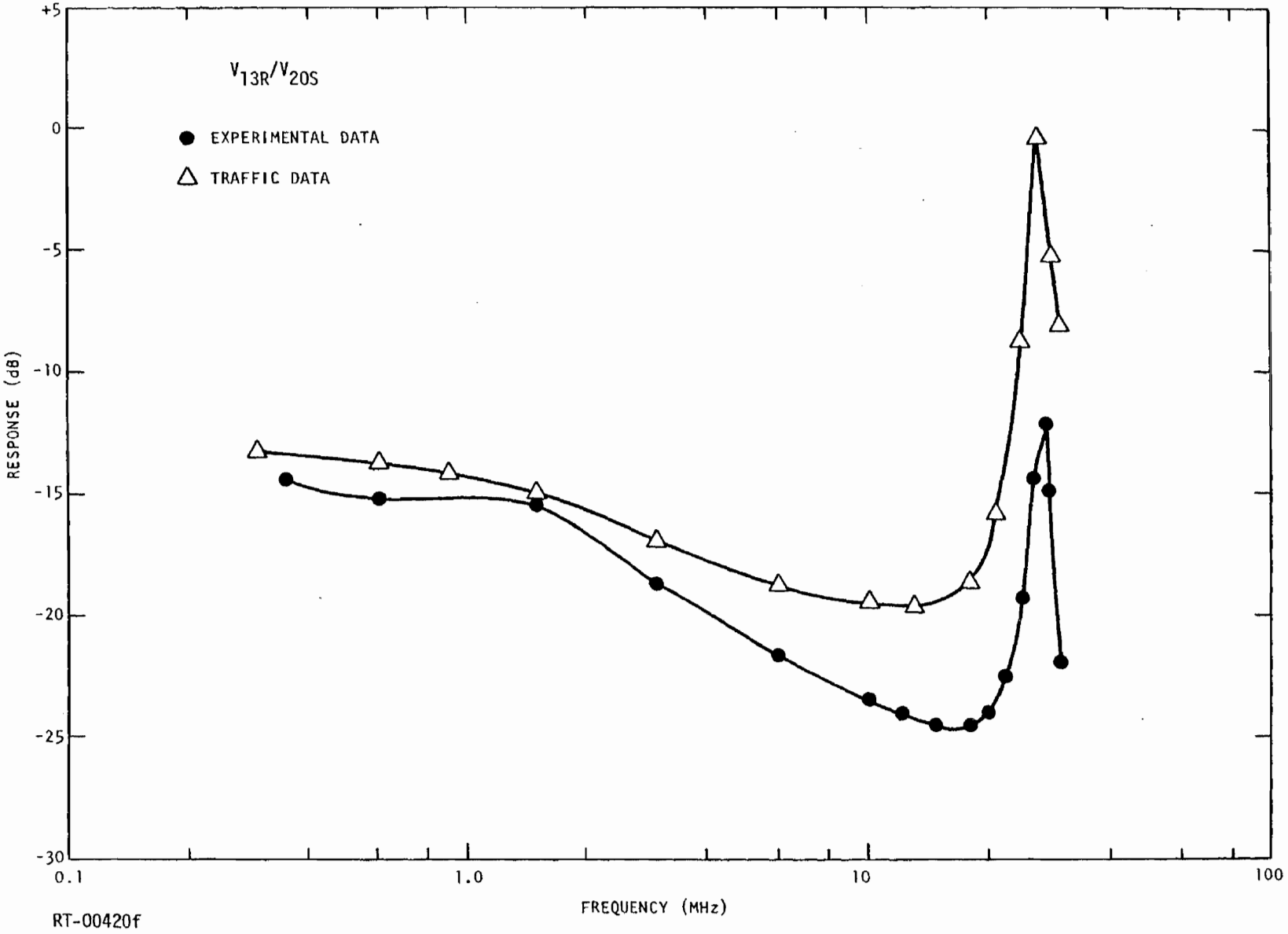
V_{13R}/V_{20S}
EXPERIMENTAL DATA
TRAFFIC DATA
+5
0
-5
-10
-15
-20
-25
-30
RESPONSE (dB)
0.1
1.0
10
100
FREQUENCY (MHz)
RT-00420f

Fig. 5.13f

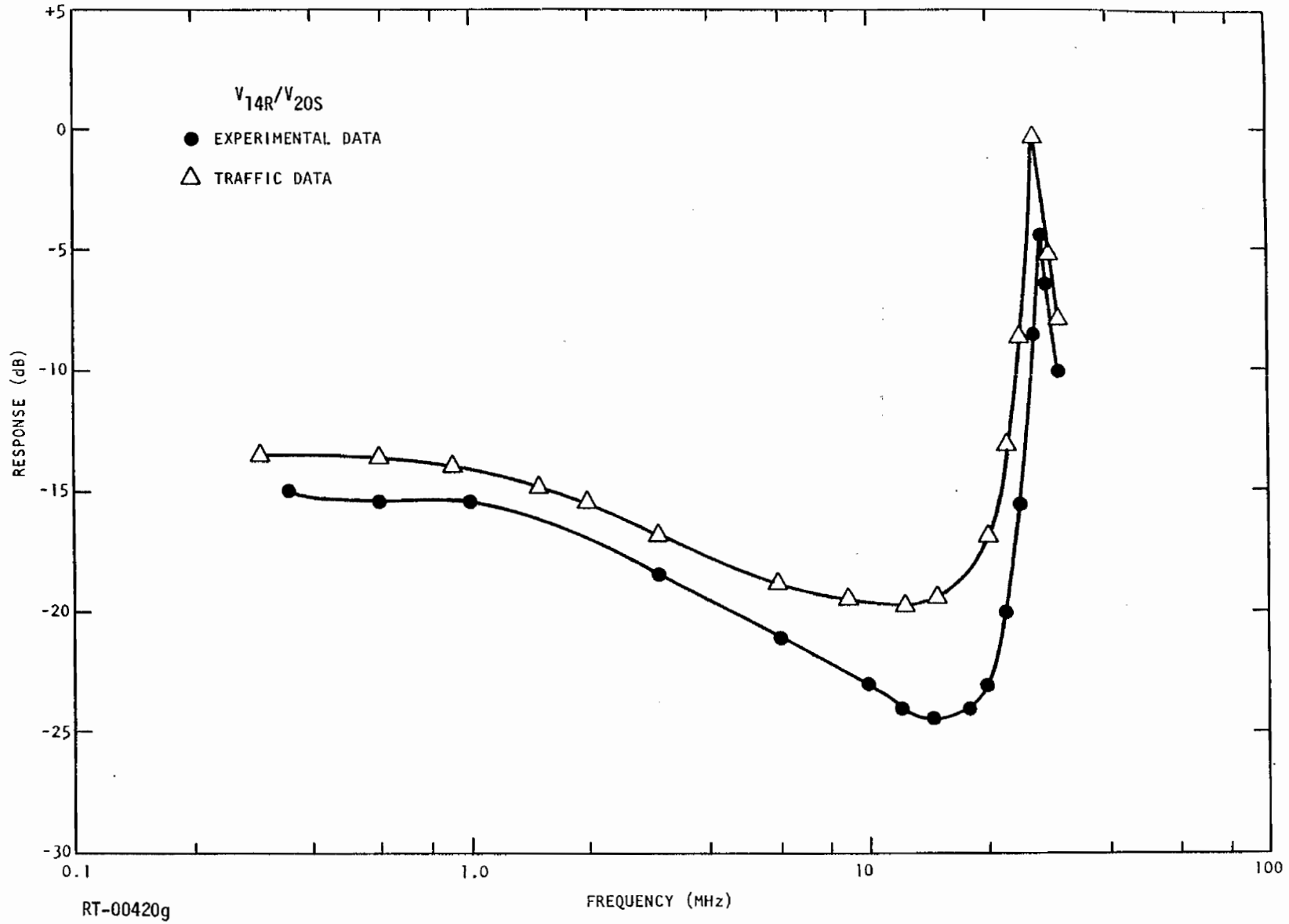
V_{14R}/V_{20S}
EXPERIMENTAL DATA
TRAFFIC DATA
RESPONSE (dB)
+5
0
-5
-10
-15
-20
-25
-30
0.1
1.0
10
100
FREQUENCY (MHz)
RT-00420g

Fig. 5.13g

Cable 3, 20-Conductor, Random-Lay Cable

This is the most complex cable, in terms of conductor configuration, that was modeled during this effort. Only the capacitance method was used for the determination of parameter values, and the calculations proceeded without difficulty using a computer program to be discussed in an appendix.

The termination scheme used for this cable is shown in Fig. 5.14. This scheme is quite complex also, and was carefully chosen to be representative of a typical termination scheme which might occur in real system cables. For example, the shield grounding scheme is one which is known to be used in a particular missile. The use of a signal ground wire for common-mode signals is standard practice, as is the use of ungrounded differential-mode circuits. The 100- and 1000-ohm resistances were selected to be representative of typical driver and receiver circuit impedances, respectively.

Two different models of this cable were analyzed, one having five sections of 0.62 m length and the other having 15 sections of 0.207 m length. The same set of distributed parameter values and the same termination scheme were used for both, with only the section length changed. The mean phase velocity for this cable was 1.711×10^8 m/sec with 3σ limits of 28%. For this value of v_p, the 5-section model has sections of less than 0.1 λ up to 27.6 MHz and the 15-section model up to 82.8 MHz. However, the upper frequency limits for which the lumped approximation produces at worst 1-dB error are 16.4 and 28.9 MHz, respectively, based on the error analysis of Section 3.

The results for the 5-section model are presented in Figs. 5.15a through 5.15e. The designations are as before; i.e., V_{2R} means the voltage from wire 2 to reference (wire 16, in this case) at the receiving end, and V_{8S} means the drive voltage applied between wire 8 and reference (wire 16) at the sending end. By the previously defined criteria,

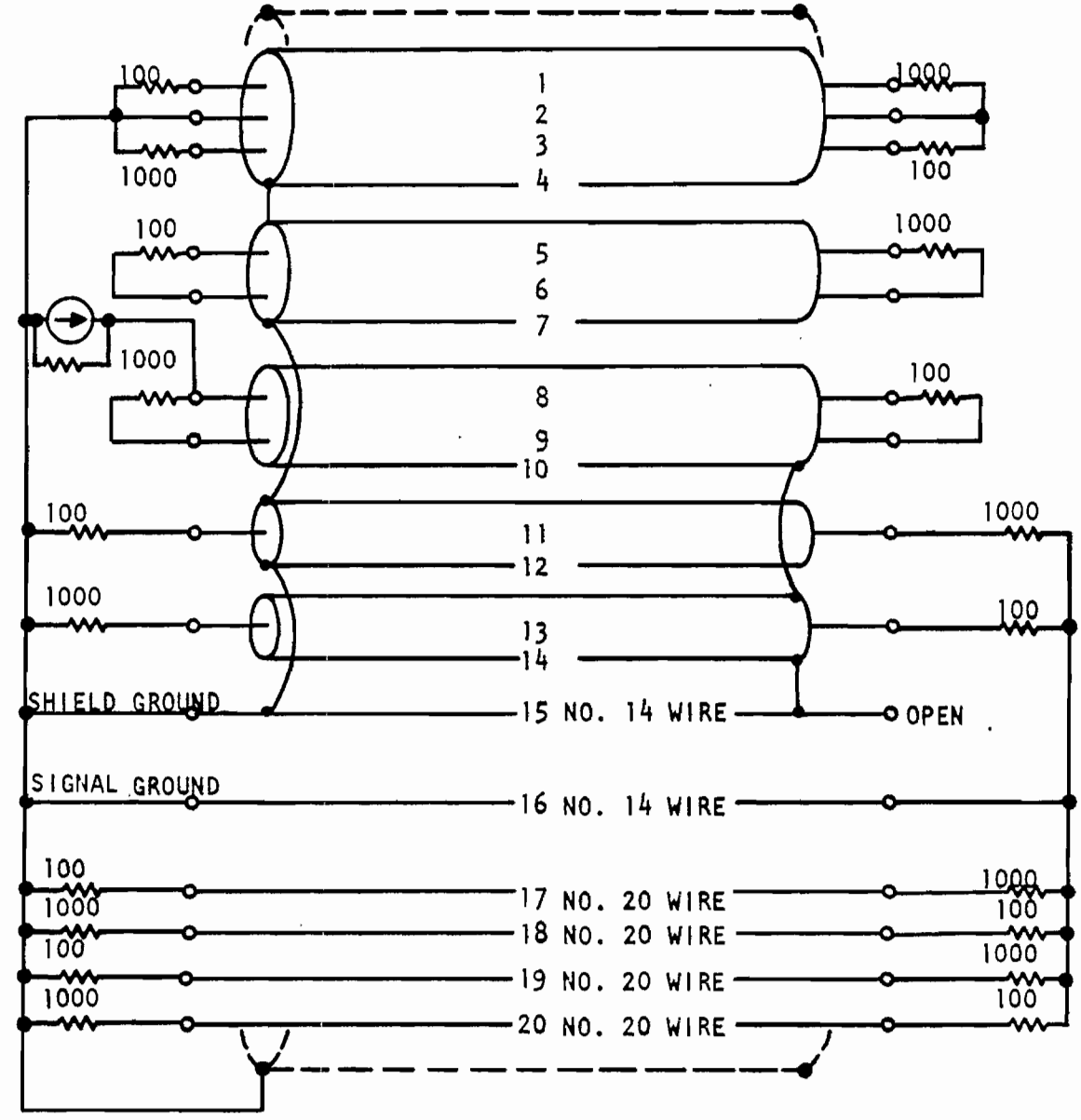

Fig. 5.14. Termination and drive scheme, 20-conductor random cable

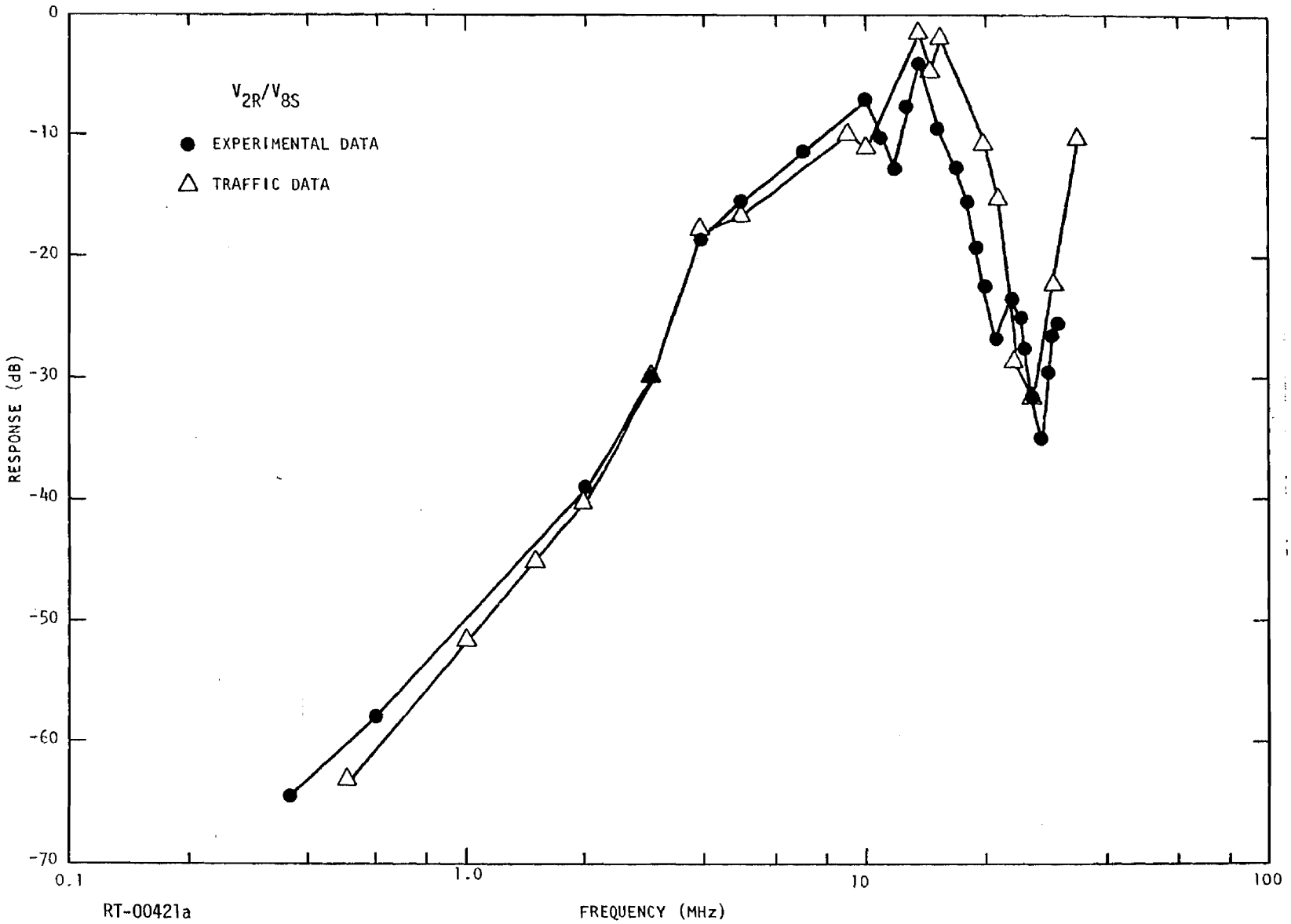

Fig. 5.15a. Transfer functions for 20-conductor random cable, 5-section model

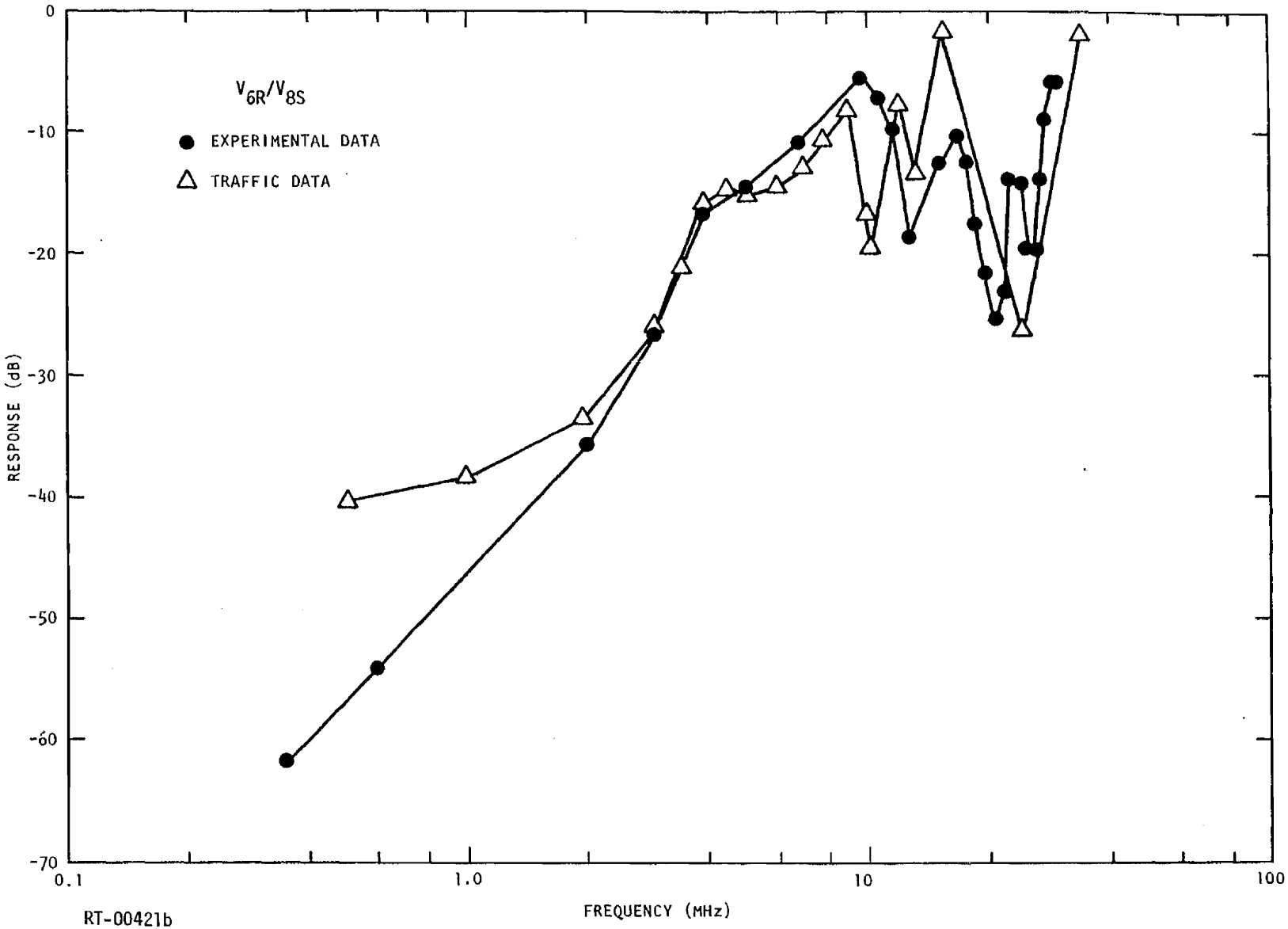
V_{6R}/V_{8S}
EXPERIMENTAL DATA
TRAFFIC DATA
RESPONSE (dB)
0
-10
-20
-30
-40
-50
-60
-70
0.1
1.0
10
100
FREQUENCY (MHz)
RT-00421b

Fig. 5.15b

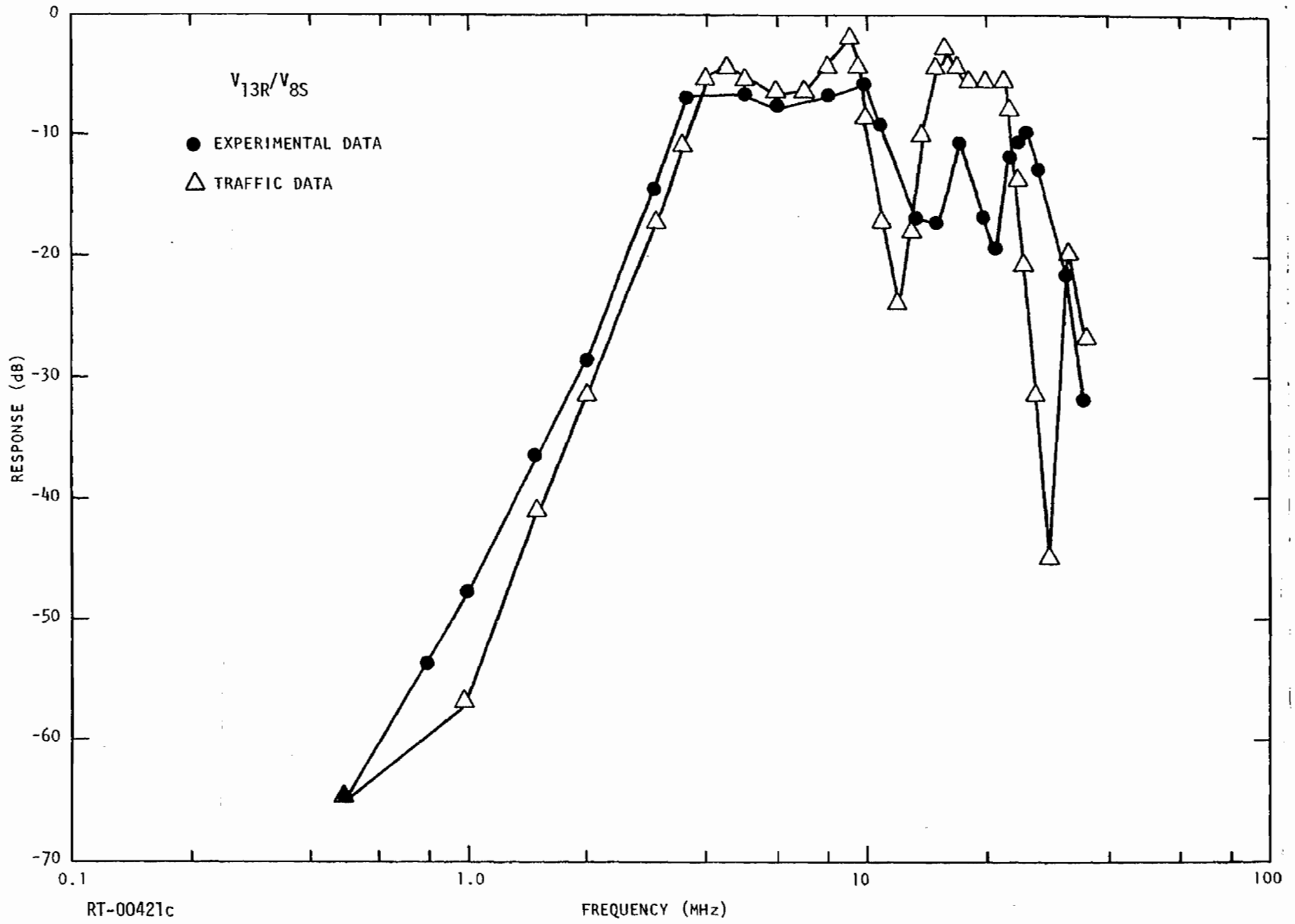
V_{13R}/V_{8S}
EXPERIMENTAL DATA
TRAFFIC DATA
RESPONSE (dB)
0
-10
-20
-30
-40
-50
-60
-70
0.1
1.0
10
100
FREQUENCY (MHz)
RT-00421c

Fig. 5.15c

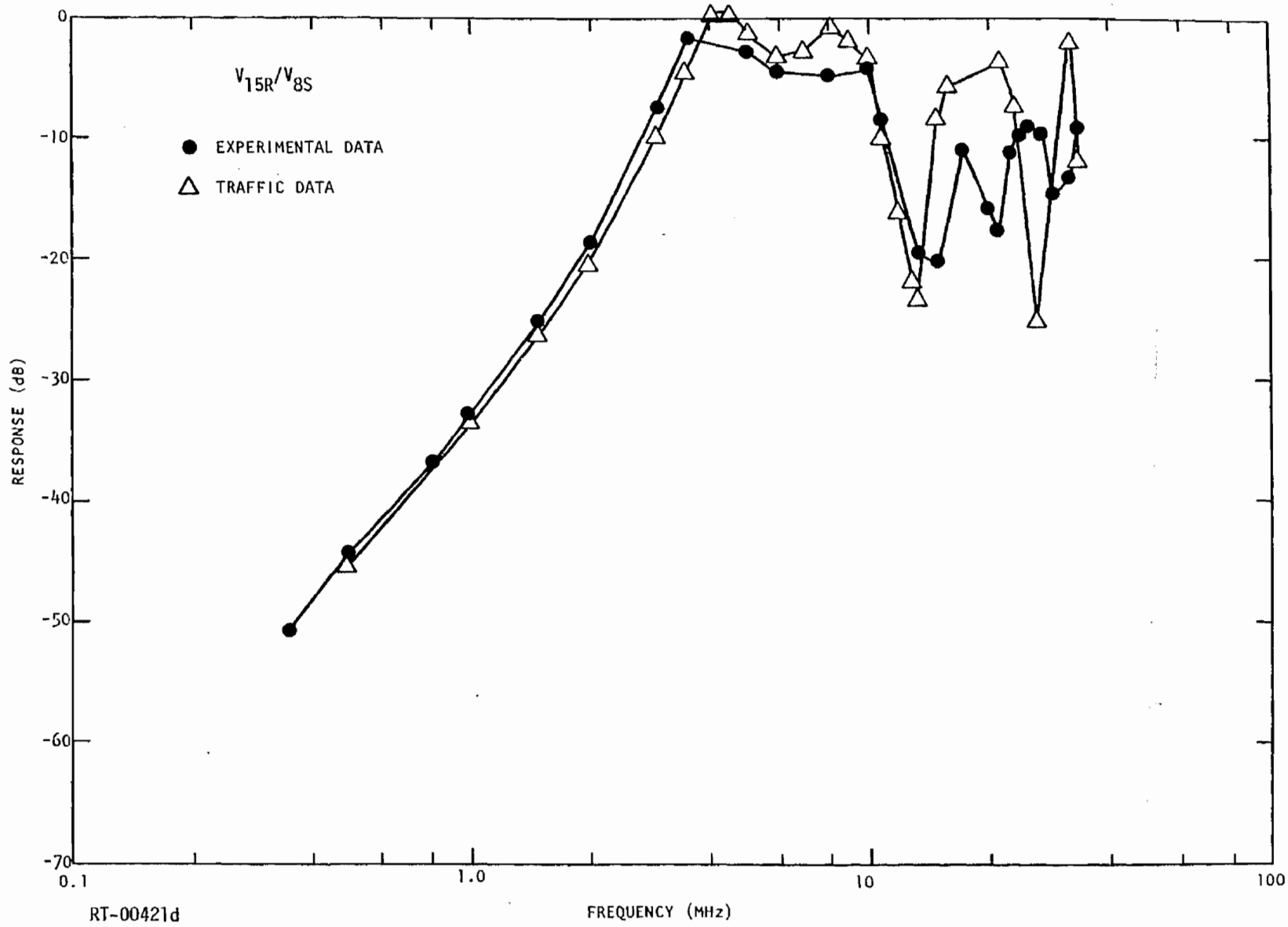
V_{15R}/V_{8S}
EXPERIMENTAL DATA
TRAFFIC DATA
RESPONSE (dB)
0
-10
-20
-30
-40
-50
-60
-70
0.1
1.0
10
100
FREQUENCY (MHz)
RT-00421d

Fig. 5.15d

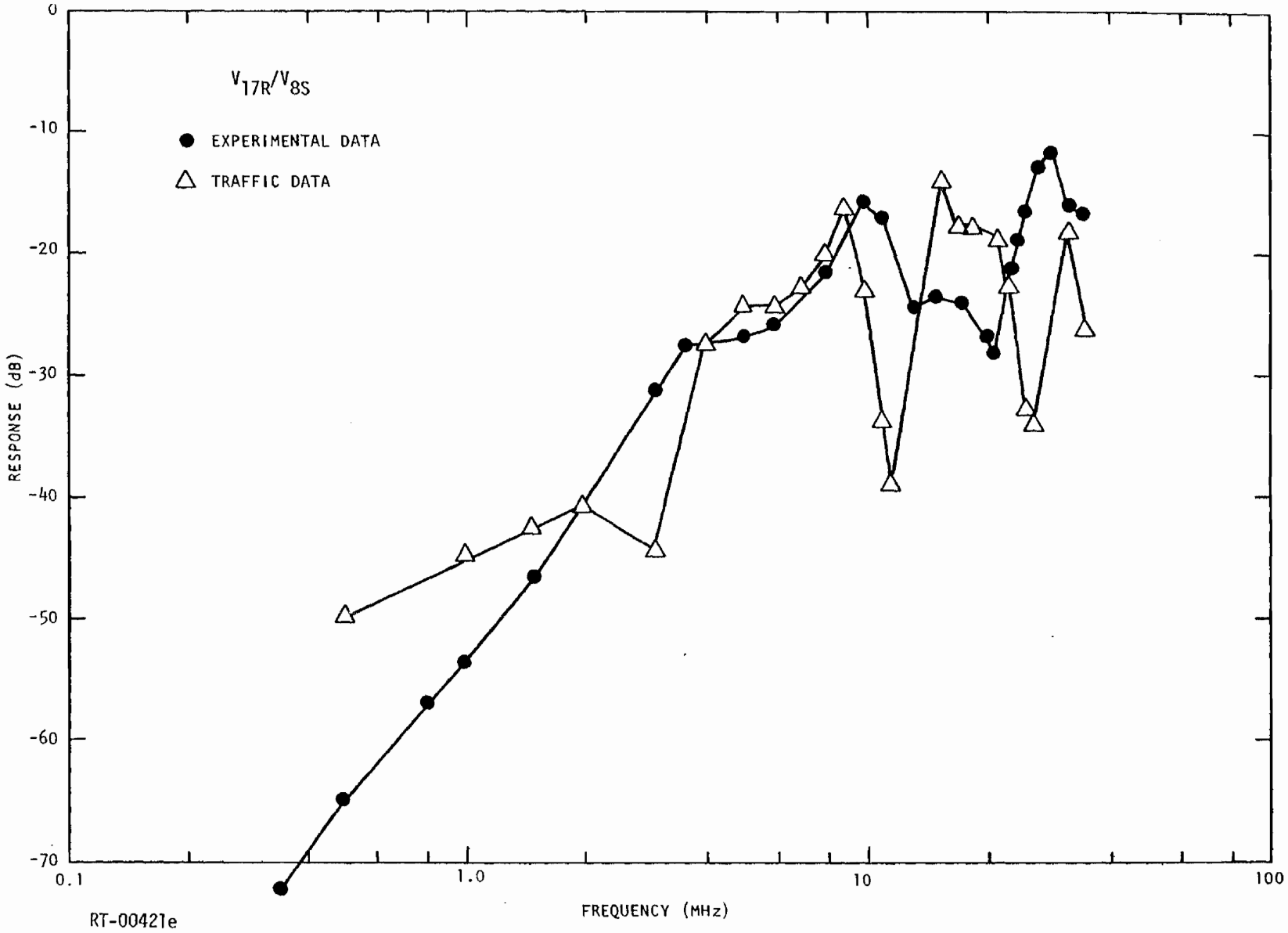
V_{17R}/V_{8S}
EXPERIMENTAL DATA
TRAFFIC DATA
RESPONSE (dB)
0
-10
-20
-30
-40
-50
-60
-70
0.1
1.0
10
100
FREQUENCY (MHz)
RT-00421e

Fig. 5.15e

the results for three of the transfer functions are "Good" and the other two are "Fair." The results for the 15-section model are presented in Figs. 5.16a through 5.16e. The results are not significantly different since most of the disagreement between analysis and experiment occurred in the low-frequency end of the two "Fair" results, and these will not be affected by the use of smaller section lengths. Even at the high end, however, the results are not greatly improved.

The results of this modeling effort are again very encouraging. The technique seems quite capable of modeling cables of the complexity to be found in real system cables, which it must do if it is to be generally useful.

Cable 4, 11-Conductor Controlled Cable

This cable is a simplified version of cable 3, but at 7 m in length is more than two times as long as any other cable tested. The increased length requires more sections, of course, and even though the section length was maintained short enough to still be less than 0.1 λ up to 30 MHz, the frequency at which the maximum error due to lumping is 1 dB dropped to just 12 MHz. In order to maintain the same 20-MHz 1-dB error frequency that was used for the other cables would require 32 sections to model this 7-m cable. This very clearly points out the problem of obtaining adequate high-frequency models for cables of even moderate length, and that caution must be exercized when applying the frequently used rule-of-thumb that 0.1-λ sections will give good accuracy.

All three methods for determining L and C parameters were applied to this cable, and some discussion of the problems encountered is in order, since they are very typical.

The capacitance method calculations resulted in three positive K_{ij} values out of 55 calculated. These positive K_{ij}, of course, resulted in the corresponding three C^p_{ij} being negative and, in addition, three C^p_{ii}

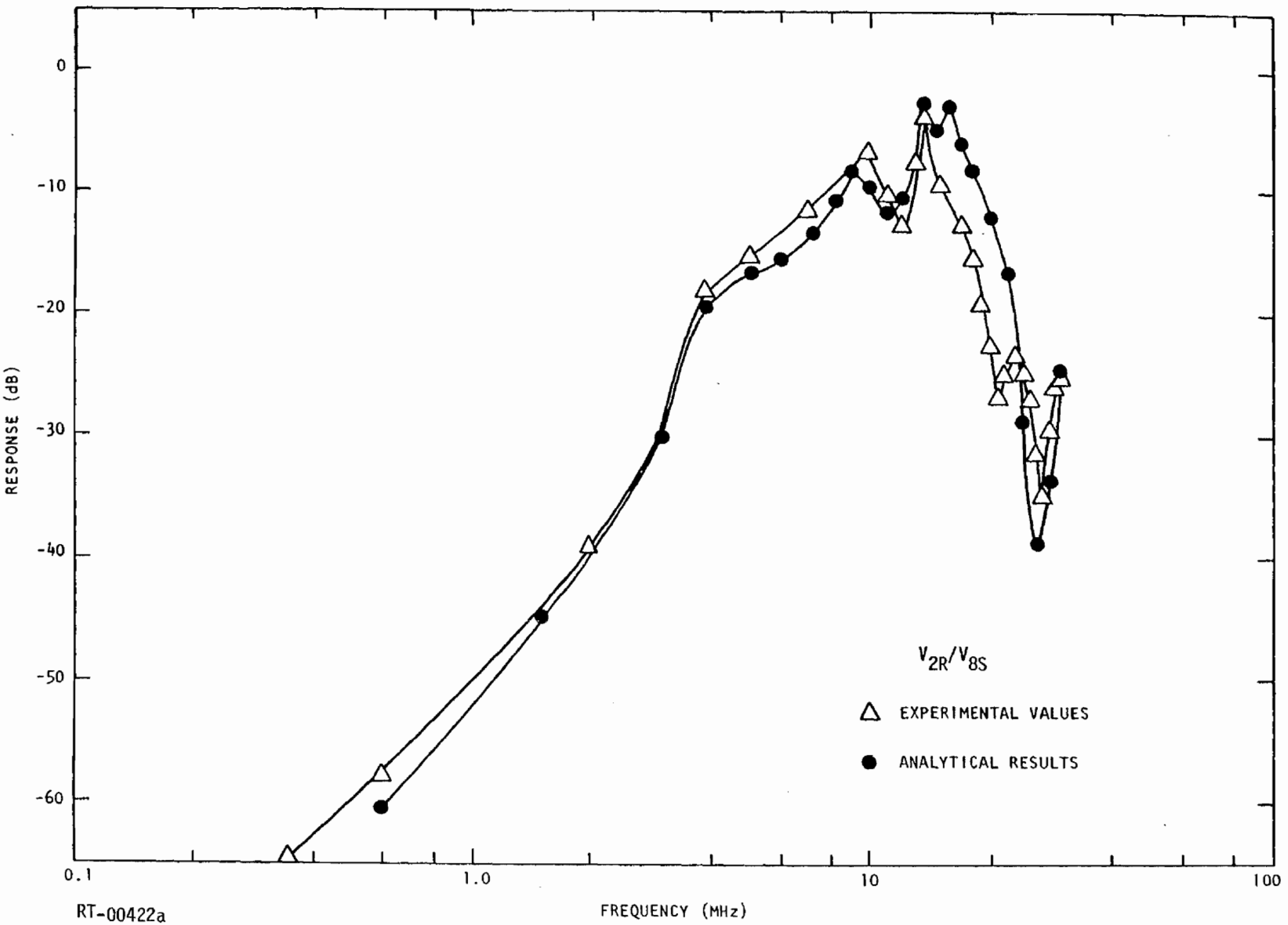

Fig. 5.16a. Transfer functions for 20-conductor random cable, 15-section model

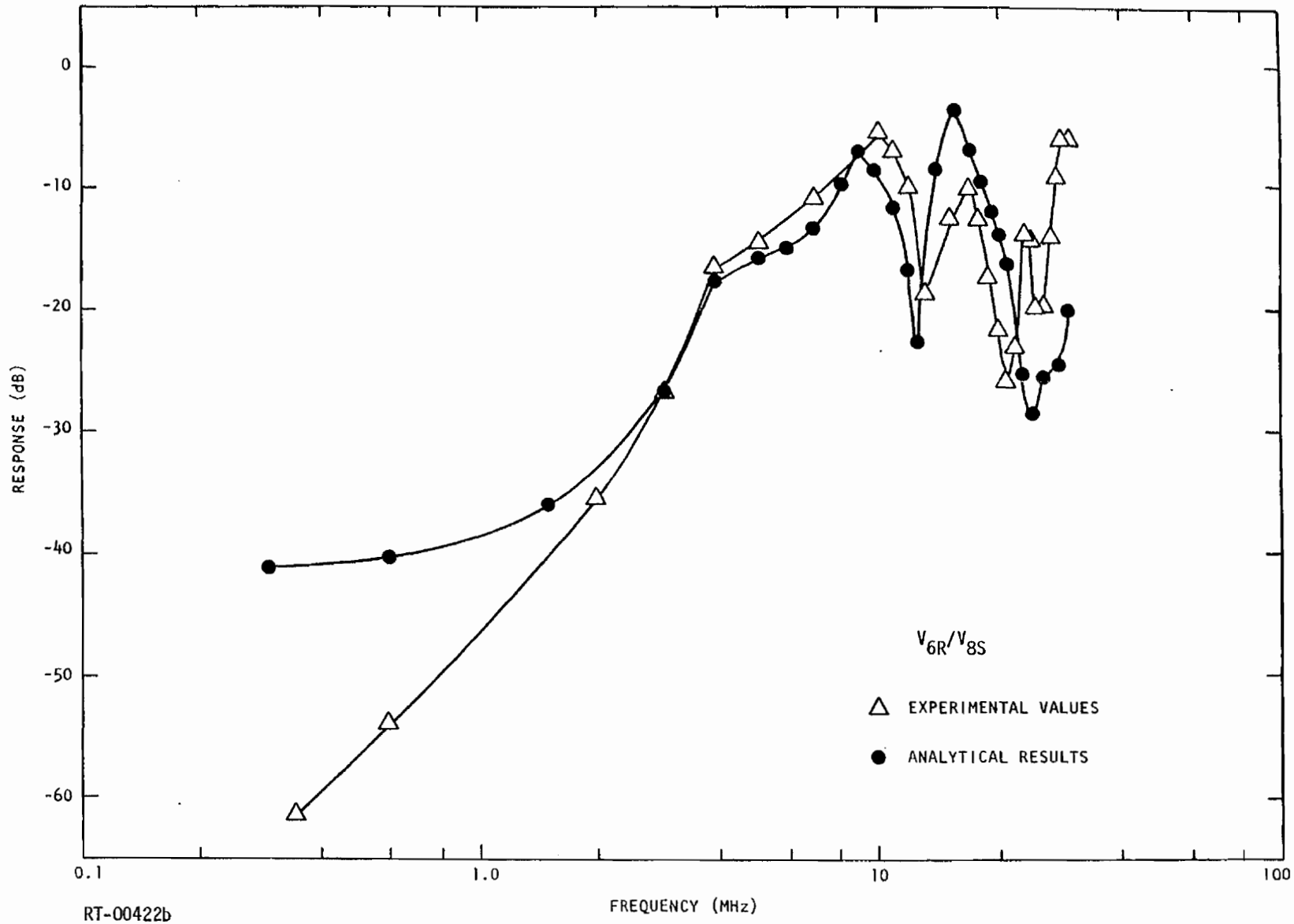
0
-10
-20
-30
-40
-50
-60
RESPONSE (dB)
0.1
1.0
10
100
FREQUENCY (MHz)
V_{6R}/V_{8S}
EXPERIMENTAL VALUES
ANALYTICAL RESULTS
RT-00422b

Fig. 5.16b

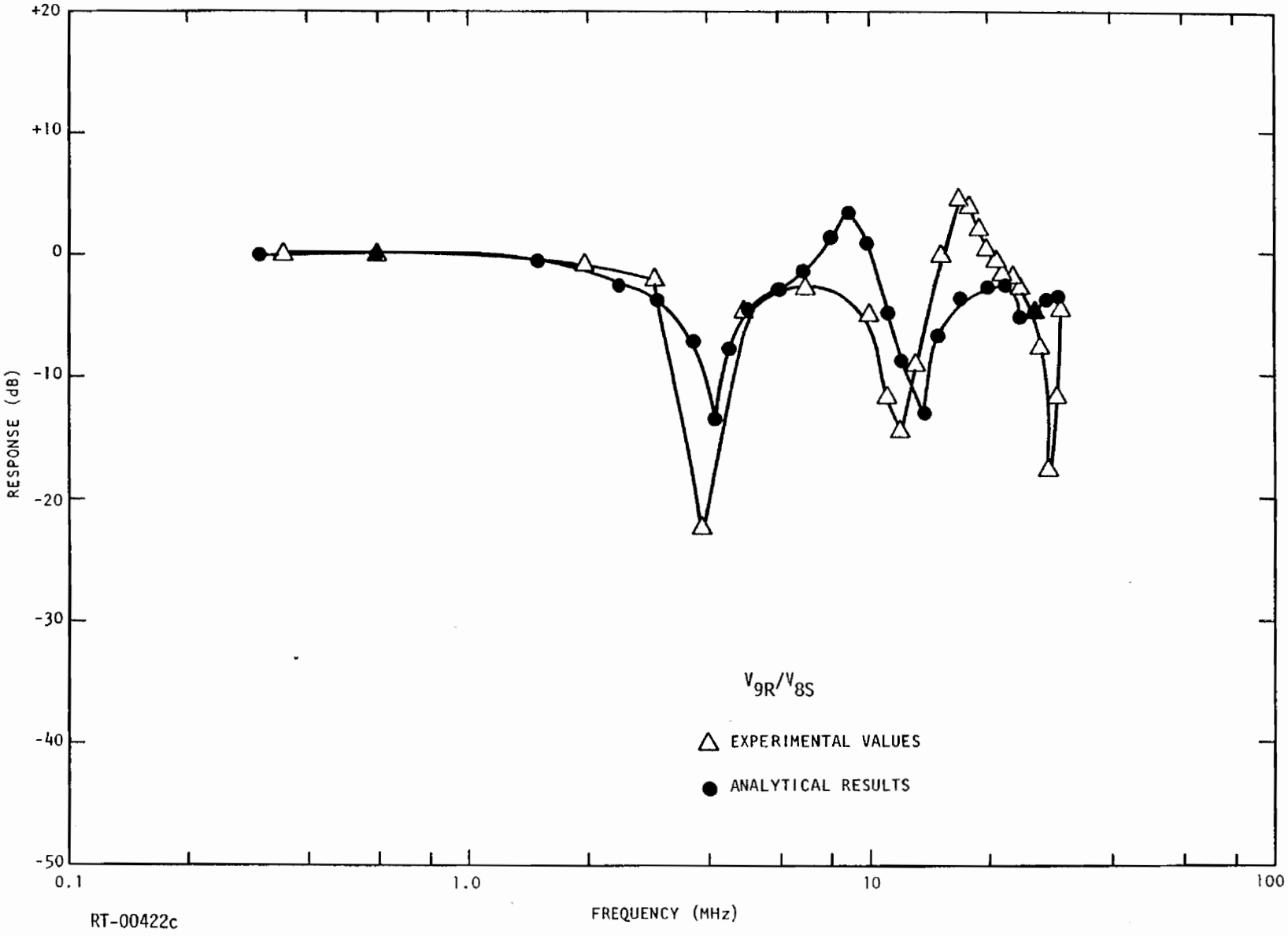
+20
+10
0
-10
-20
-30
-40
-50
RESPONSE (dB)
0.1
1.0
10
100
FREQUENCY (MHz)
V_{9R}/V_{8S}
EXPERIMENTAL VALUES
ANALYTICAL RESULTS
RT-00422c

Fig. 5.16c

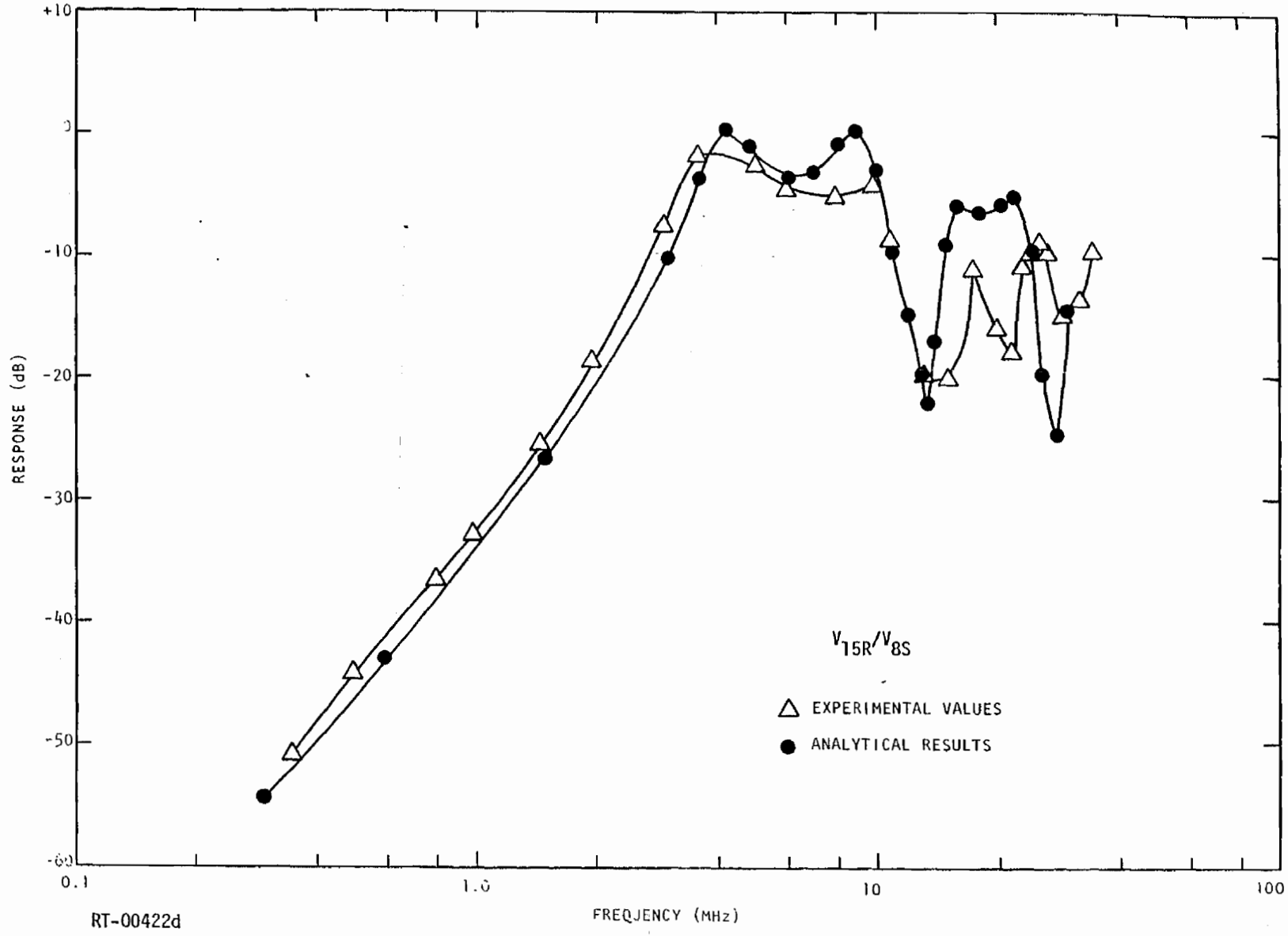
+10
0
-10
-20
-30
-40
-50
-60
RESPONSE (dB)
0.1
1.0
10
100
FREQUENCY (MHz)
V_{15R}/V_{8S}
EXPERIMENTAL VALUES
ANALYTICAL RESULTS
RT-00422d

Fig. 5.16d

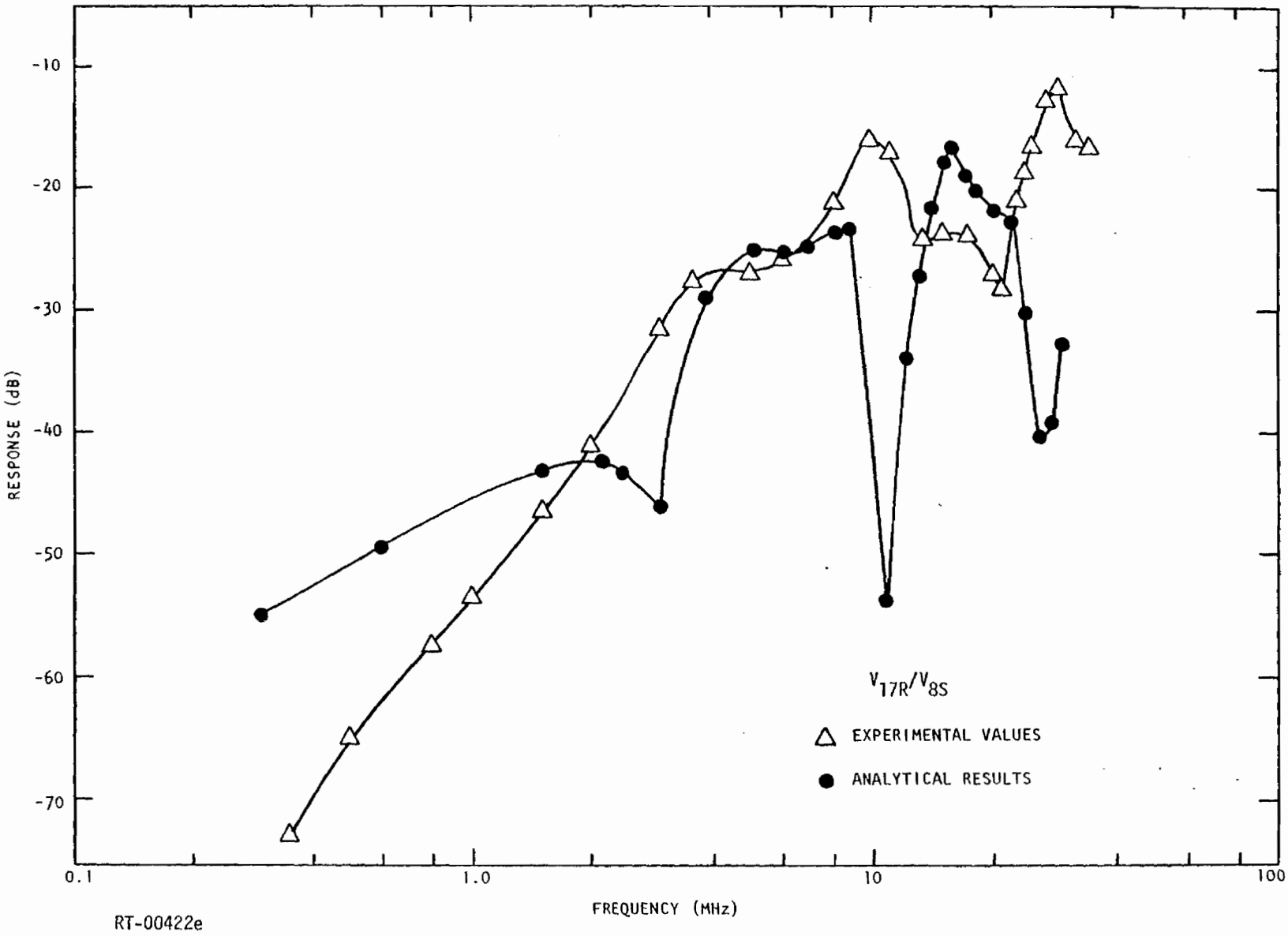
-10
-20
-30
-40
-50
-60
-70
RESPONSE (dB)
0.1
1.0
10
100
FREQUENCY (MHz)
V_{17R}/V_{8S}
EXPERIMENTAL VALUES
ANALYTICAL RESULTS
RT-00422e

Fig. 5.16e

values came out negative as well. These are indicated in Table 5.3. The open-Z method calculations resulted in 15 positive K_{ij} out of 55 calculated and two negative C^p_{ii}, as noted in Table 5.3. Finally, the shorted-Z method calculations resulted in nine positive K_{ij} out of 55 calculated and six negative C^p_{ii}, as noted in Table 5.3.

Table 5.3

BREAKDOWN, BY METHOD, OF ERRONEOUS SIGNS OBSERVED IN PARAMETER CALCULATIONS FOR THE 11-CONDUCTOR CABLE

Category of i-j Conductor Pair	Negative C^p_{ij} by Method		
	C	Open-Z	Shorted-Z
1. Shielded wire to another internal shield		1-7, 1-9, 2-7, 2-9, 3-7, 3-9, 4-5, 4-6, 4-8, 5-9, 6-9, 7-8	4-5, 4-6, 4-8
2. Shielded wire to another shielded wire	2-5, 5-8, 6-8		
3. Shielded wire to an unshielded wire		8-11	1-10, 1-11, 8-10, 8-11
4. Shielded wire to overall shield reference	2-2, 3-3, 8-8	2-2, 3-3	
5. Internal shield to an unshielded wire		7-10, 4-11	
6. Internal shield to another internal shield			4-7
7. Unshielded wire to another unshielded wire			10-11

Table 5.3 was created to show as clearly as possible just where the sign problems occurred and why. Observe that 28 of the 32 C^p_{ij} and C^p_{ii} calculations which resulted in negative values fall in categories 1 through 4, where conductors i and j are separated by at least one internal shield. Since these internal shields are usually very effective, the C^p_{ij} are expected to be quite small and then tolerance buildup on the measurements simply overwhelms the small C^p_{ij} and results in negative values. The important point is that by recognizing the problem, judgment can be used to correct it; i.e., realizing that these small C^p_{ij} will not seriously affect the analytical results, we can arbitrarily set small positive values for these C^p_{ij}, and this was done on the final model of this cable.

The four remaining negative partial capacitances are somewhat more difficult to explain, since there are no shields completely enclosing any of the conductors involved. However, unintentional shielding may be occurring. Consider, for example, conductors 4 and 11 as shown in Fig. 5.1d. Note that the two shields designated 7 and 9 are physically between 11 and 4, thus providing a shielding effect which results in a small $C^p_{4\text{-}11}$ value and the subsequent sign reversal. The same argument applies to pairs 7-10 and 10-11, and the corrections previously mentioned can be applied to all three of these pairs; i.e., small positive values are arbitrarily set.

The negative partial $C^p_{4\text{-}7}$ is the only one which cannot be explained by shielding. These two conductors are adjacent to one another and of large size; therefore, the capacitance between them is expected to be large. The problem is still one of measurement accuracy, however. The impedances measured in the shorted-Z method are inherently lower than those measured in the open-Z method, being less than 10 ohms in some cases. Unfortunately, using a 50-ohm TDR system, the resolution for impedances that small is only about an ohm at best, and a reading of

10 ±1 ohm is only 10% accurate. Thus, when measuring very low impedances, tolerance buildup can be significant enough to cause even larger C^p_{ij} values to be erroneous. For the case of conductors 4 and 7 in this cable, Z^m_{44} = 10.5 ohms, Z_{77} = 17 ohms, and Z_{47} = 6.5 ohms. These values are all small enough to be subject to considerable error. Recognizing, then, that the calculated C^p_{47} value is not reasonable, judgment can be used to adjust the value. The other shield-to-shield capacitances are C^p_{7-9} = 41.6 pF/m and C^p_{4-9} = 52.7 pF/m; since conductor 7 is larger in diameter than conductor 9, C^p_{4-7} should be larger than C^p_{49}, and we arbitrarily set C^p_{4-7} = 60 pF/m. This is the value used to determine the model parameters.

The sets of distributed parameters, calculated and adjusted as discussed above, were used to create models consisting of 12 sections of 0.583 m length each. Analytical transfer functions were obtained for the termination scheme shown in Fig. 5.17. These are compared to the experimentally determined transfer functions in Figs. 5.18a through 5.20e. The results for the capacitance method are considered "Fair" by the established criteria up to the 12-MHz 1-dB frequency. The results for the open-Z method are "Fair" with one exception, which is considered "Poor." The results for the shorted-Z method are "Fair" with two exceptions, which are considered "Poor."

The poorer quality of agreement obtained for this particular cable may be explained at least in part by experimental difficulties which make the experimental results somewhat suspect. Note from Fig. 5.17 that the cable was driven through a 1000-ohm resistor. This resulted in very low signal levels at the receiving end of the cable, especially at the higher frequencies. For the other cables tested, the resonant point generally produced levels in the range of -15 to 0 dB. For this cable, the maximum levels were -43 dB, and these very low levels resulted in extreme sensitivity to hand and other stray capacitance effects. Thus, the confidence in the experimental results for this cable are lower than for any other cable tested.

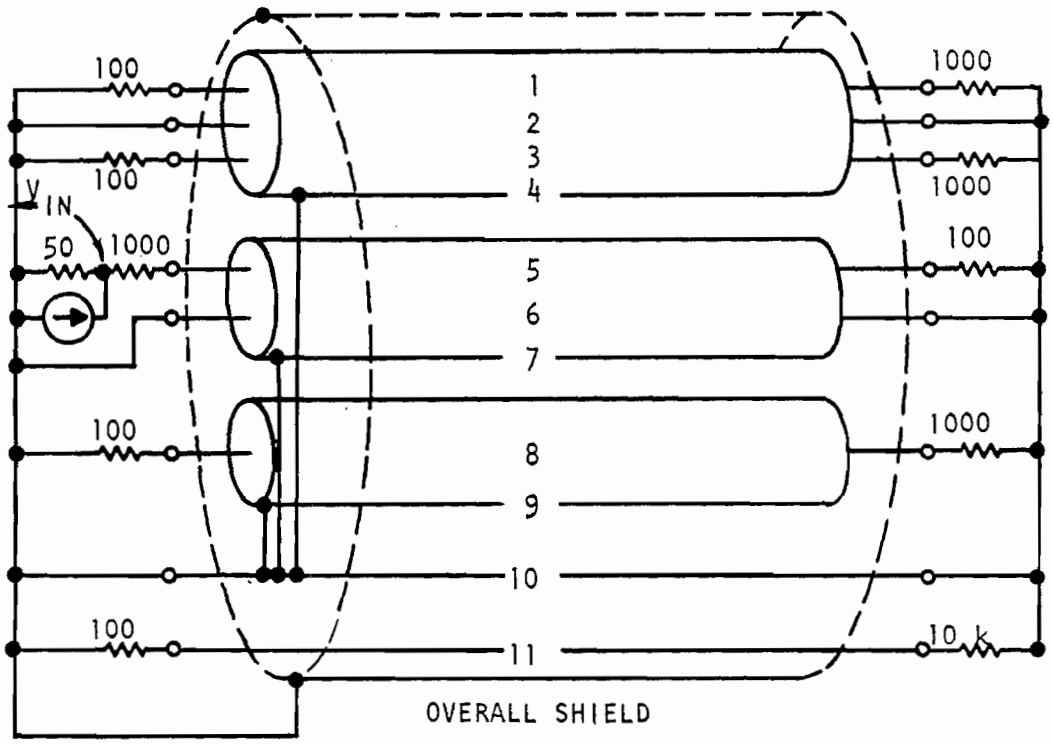

Fig. 5.17. Drive and termination scheme for 11-conductor cable

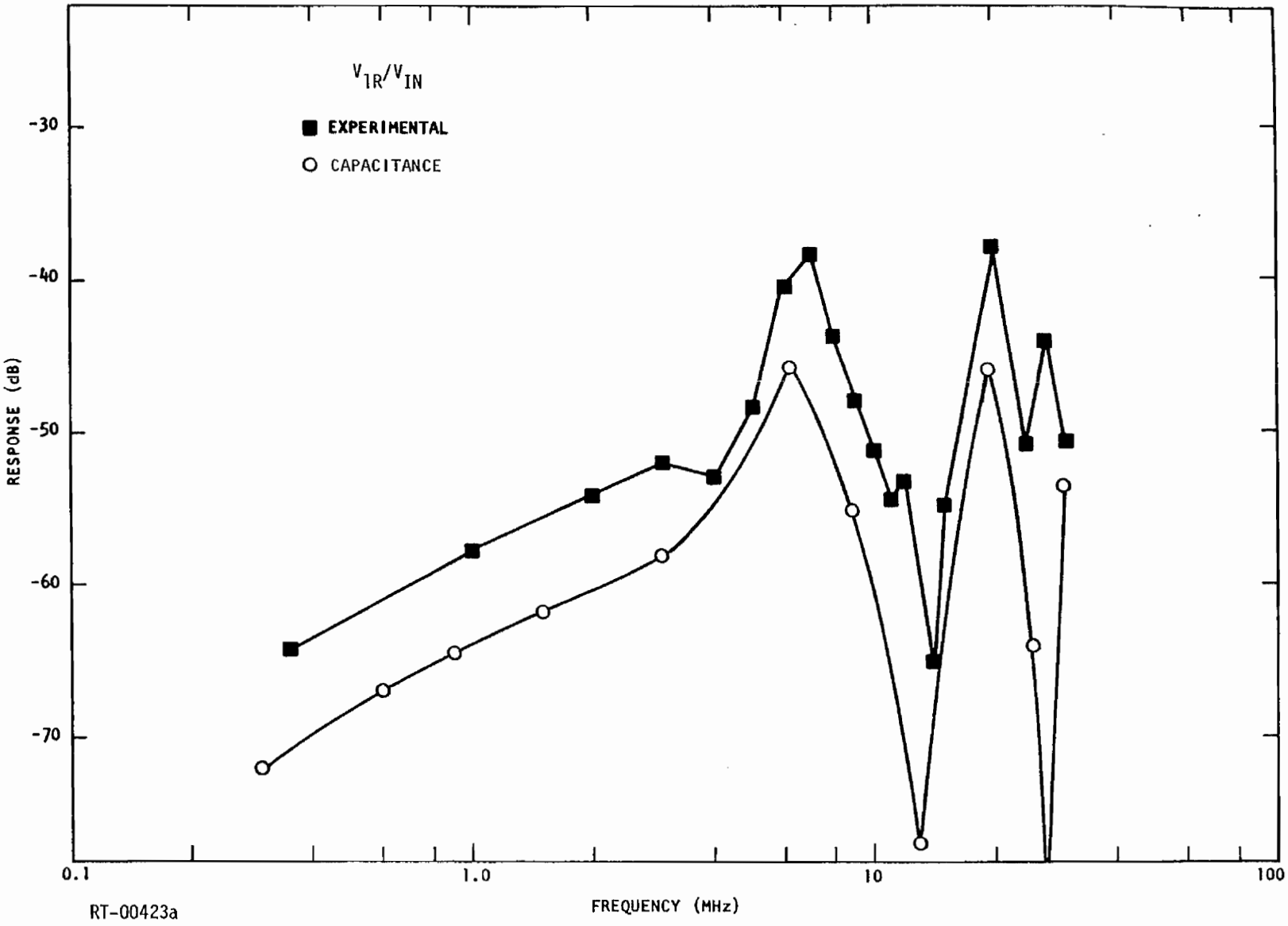

Fig. 5.18a. Transfer functions for 11-conductor cable, capacitance method

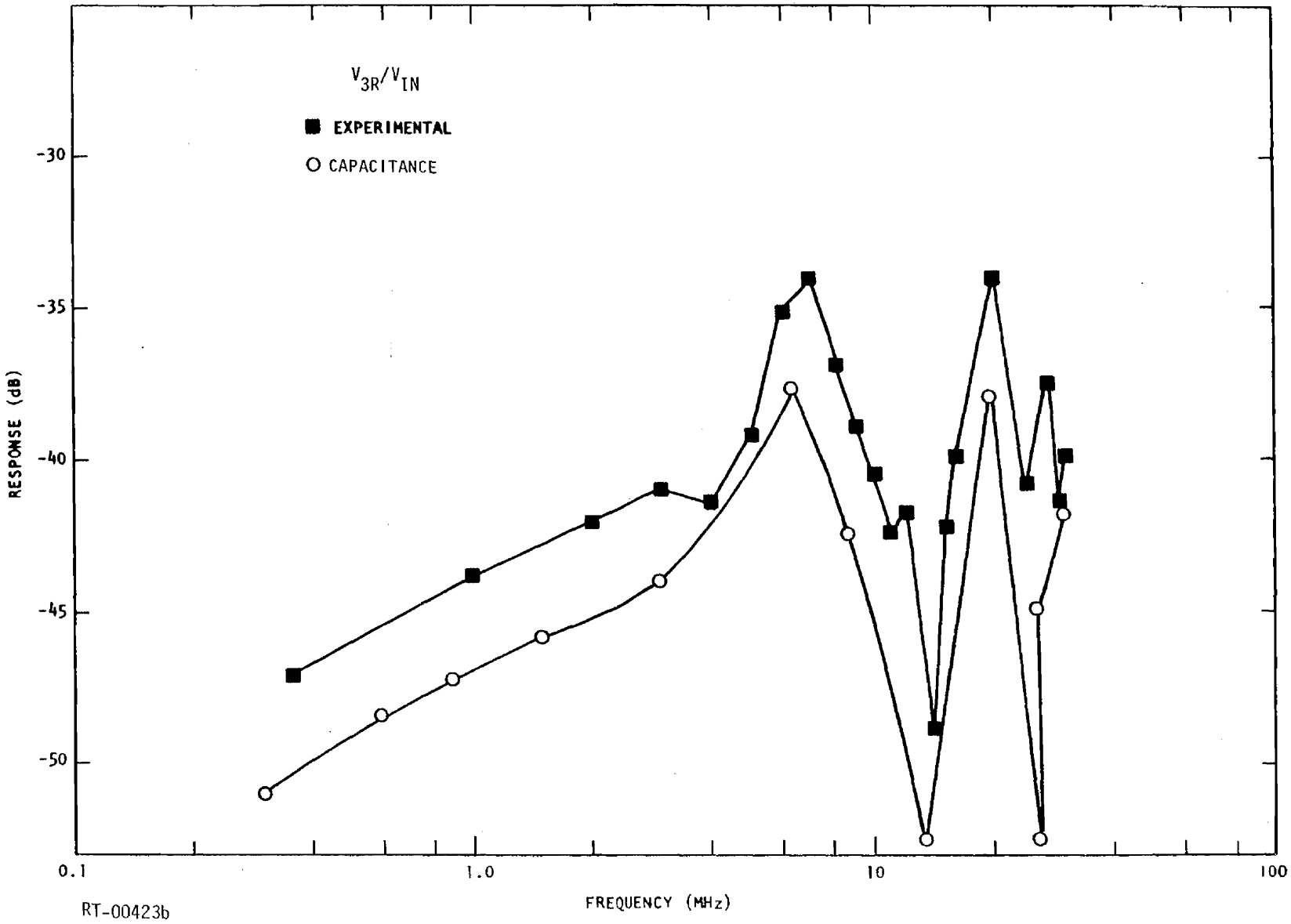
V_{3R}/V_{IN}
EXPERIMENTAL
CAPACITANCE
-30
-35
-40
-45
-50
RESPONSE (dB)
0.1
1.0
10
100
FREQUENCY (MHz)
RT-00423b

Fig. 5.18b

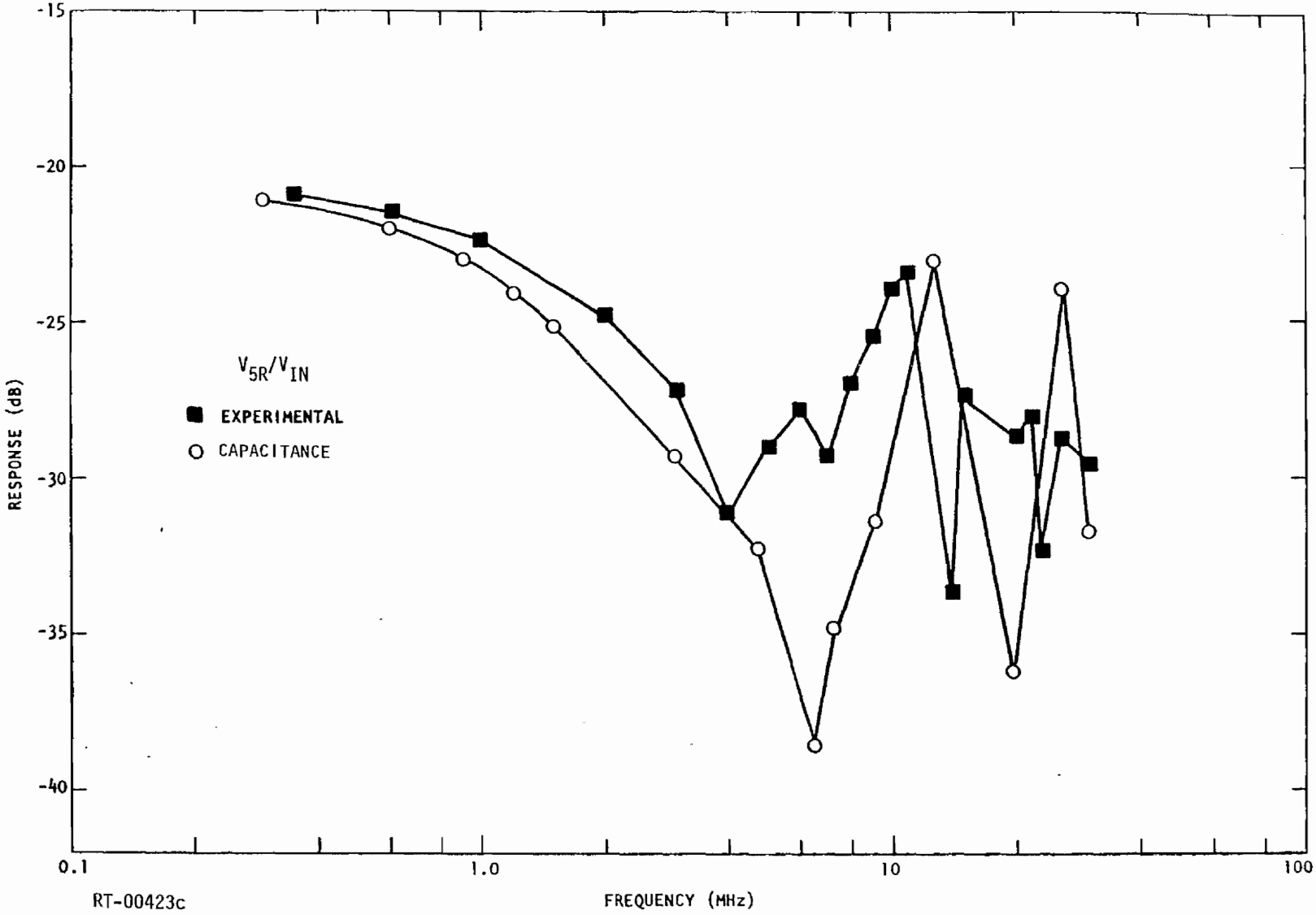
-15
-20
-25
-30
-35
-40
RESPONSE (dB)
V_{5R}/V_{IN}
EXPERIMENTAL
CAPACITANCE
0.1
1.0
10
100
FREQUENCY (MHz)
RT-00423c

Fig. 5.18c

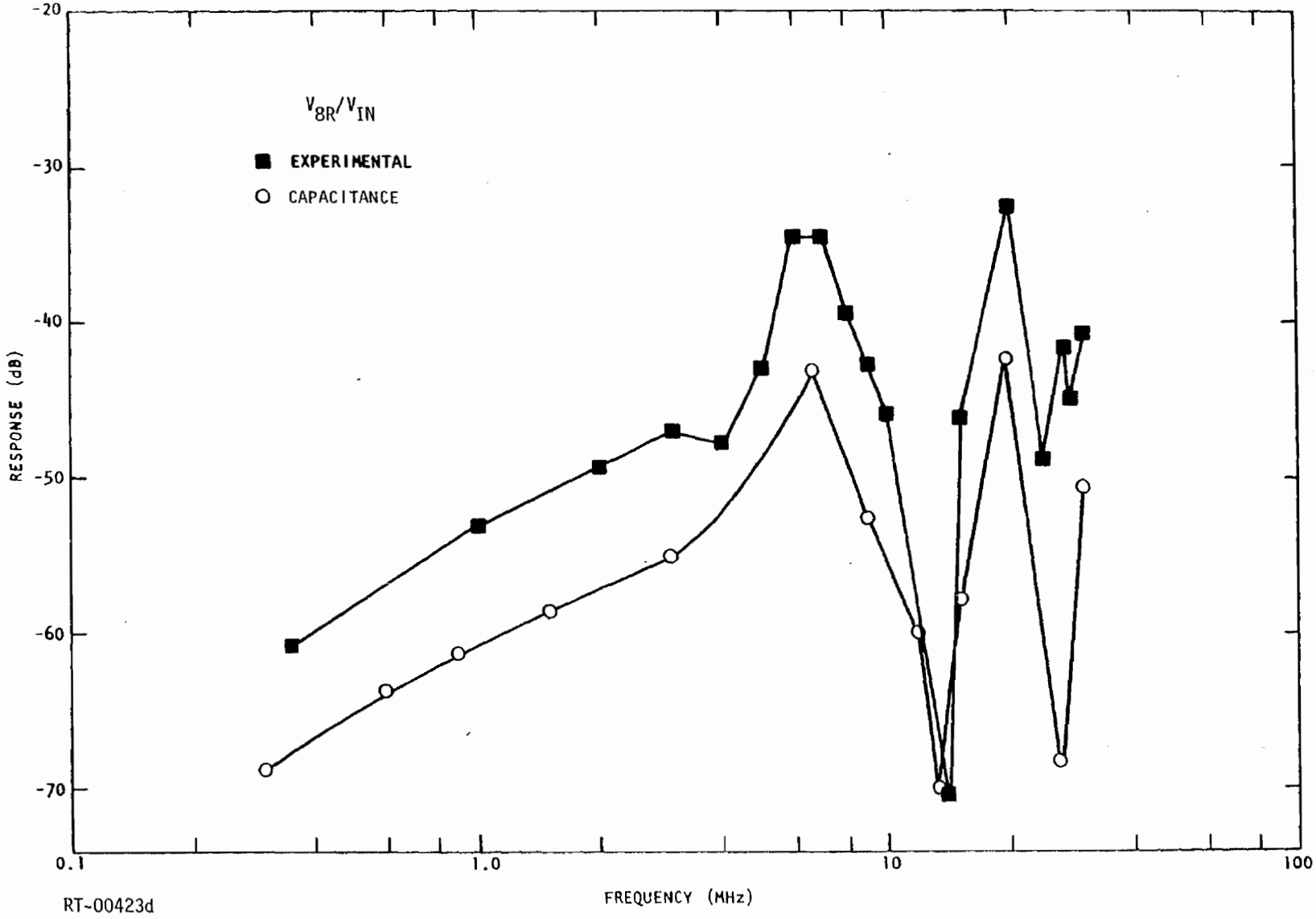
V_{8R}/V_{IN}
EXPERIMENTAL
CAPACITANCE
RESPONSE (dB)
-20
-30
-40
-50
-60
-70
0.1
1.0
10
100
FREQUENCY (MHz)
RT-00423d

Fig. 5.18d

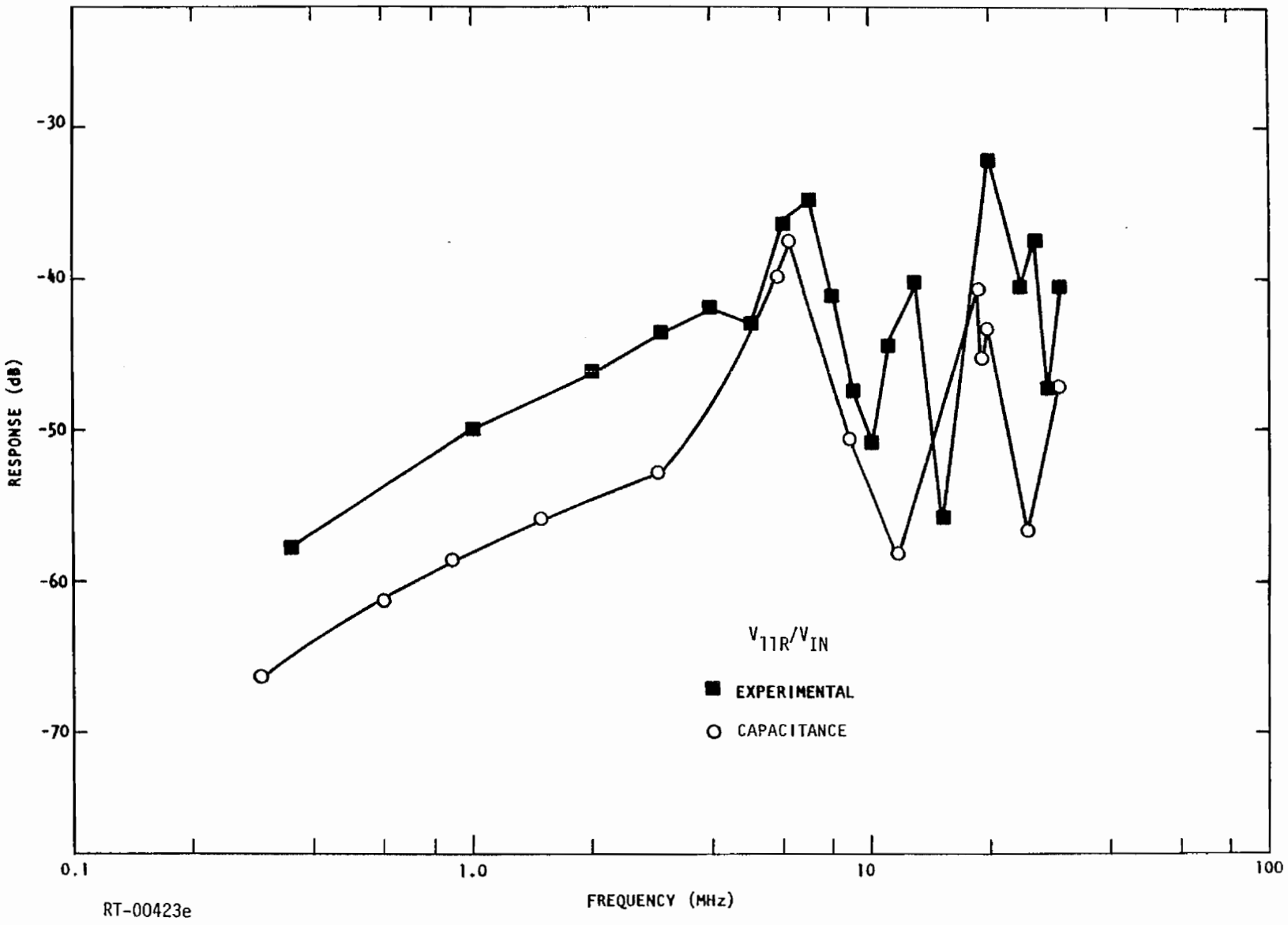
-30
-40
-50
-60
-70
RESPONSE (dB)
0.1
1.0
10
100
FREQUENCY (MHz)
V_{11R}/V_{IN}
EXPERIMENTAL
CAPACITANCE
RT-00423e

Fig. 5.18e

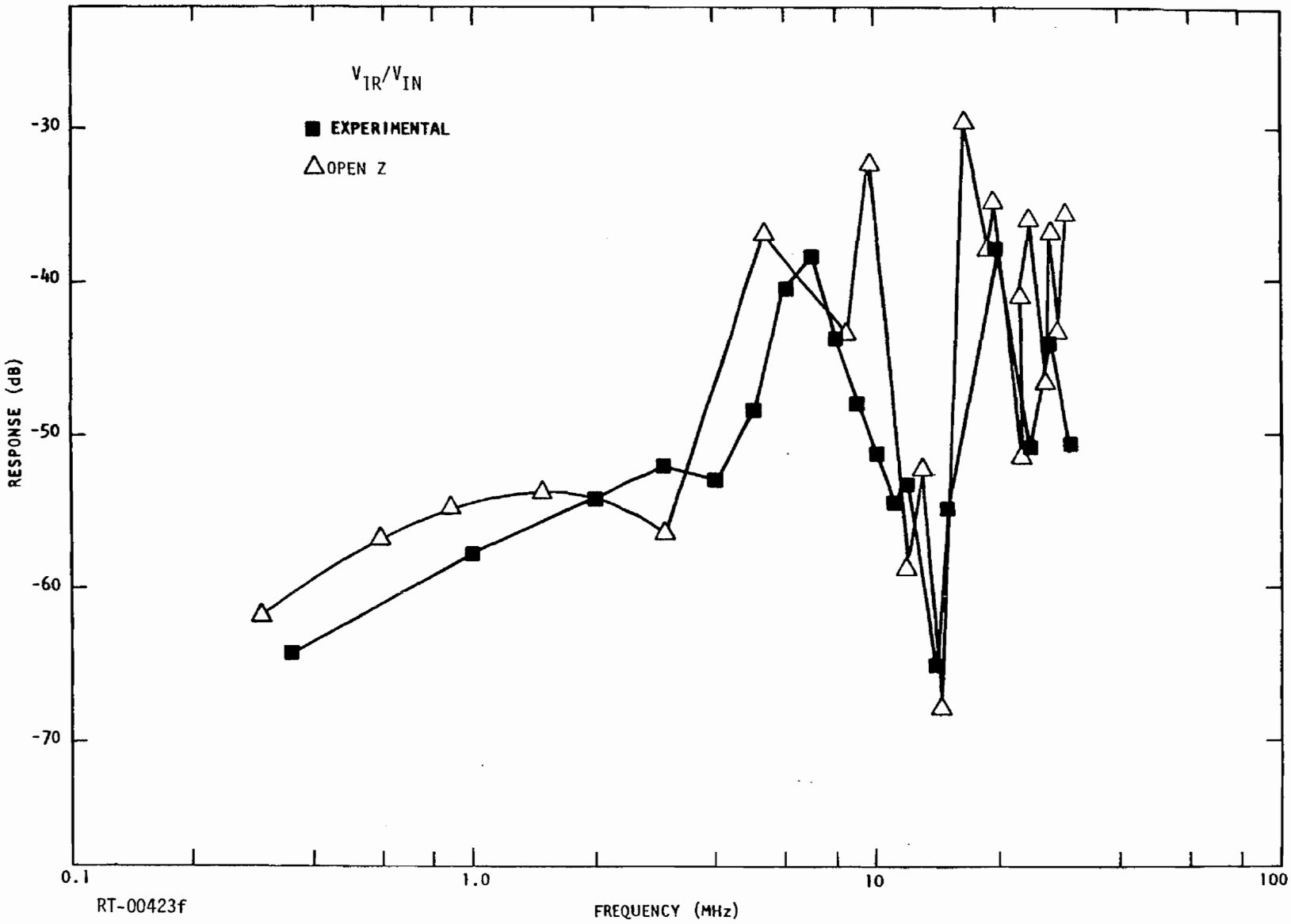

Fig. 5.19a. Transfer functions for 11-conductor cable, open-Z method

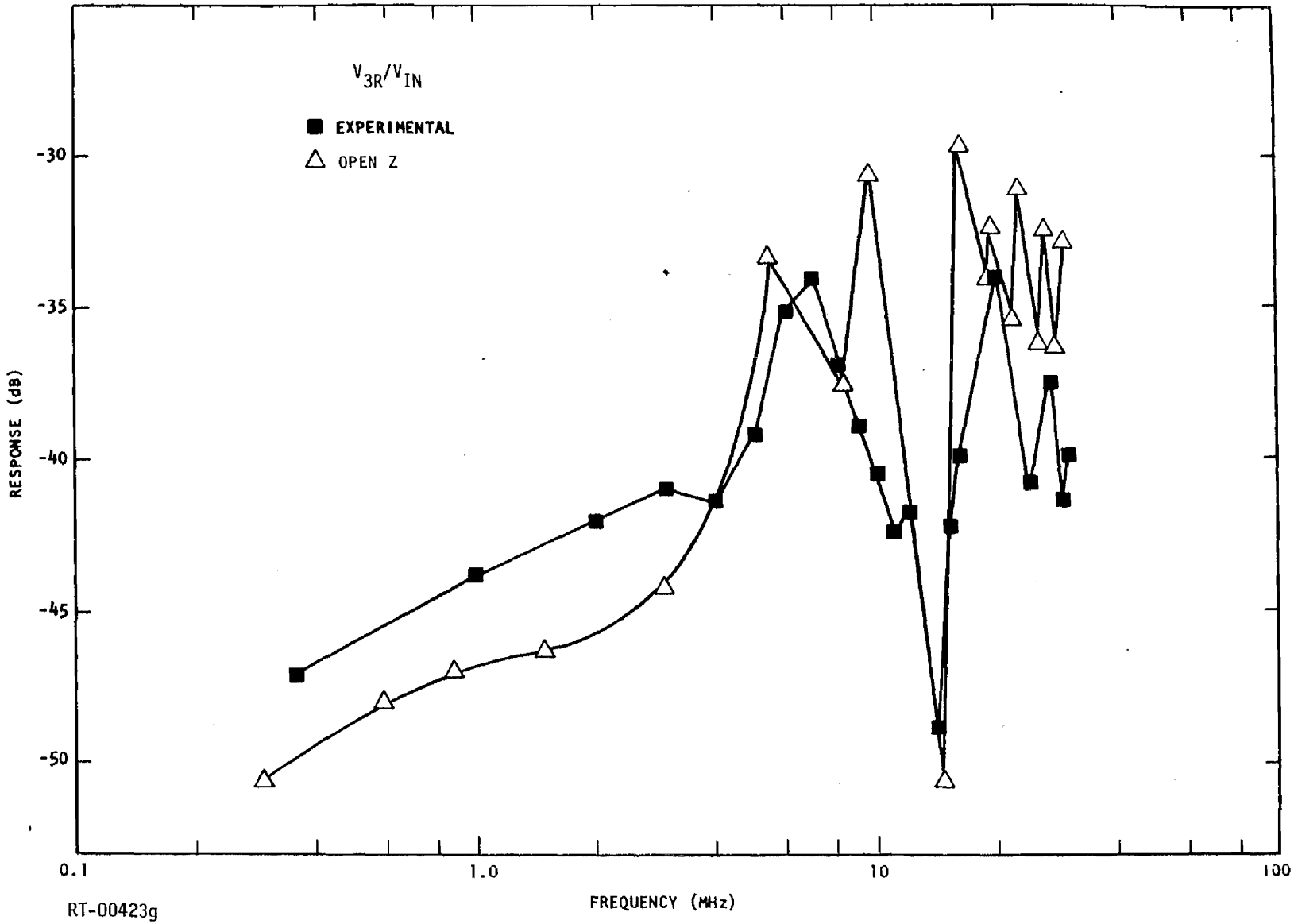
V_{3R}/V_{IN}
EXPERIMENTAL
OPEN Z
-30
-35
-40
-45
-50
RESPONSE (dB)
0.1
1.0
10
100
FREQUENCY (MHz)
RT-00423g

Fig. 5.19b

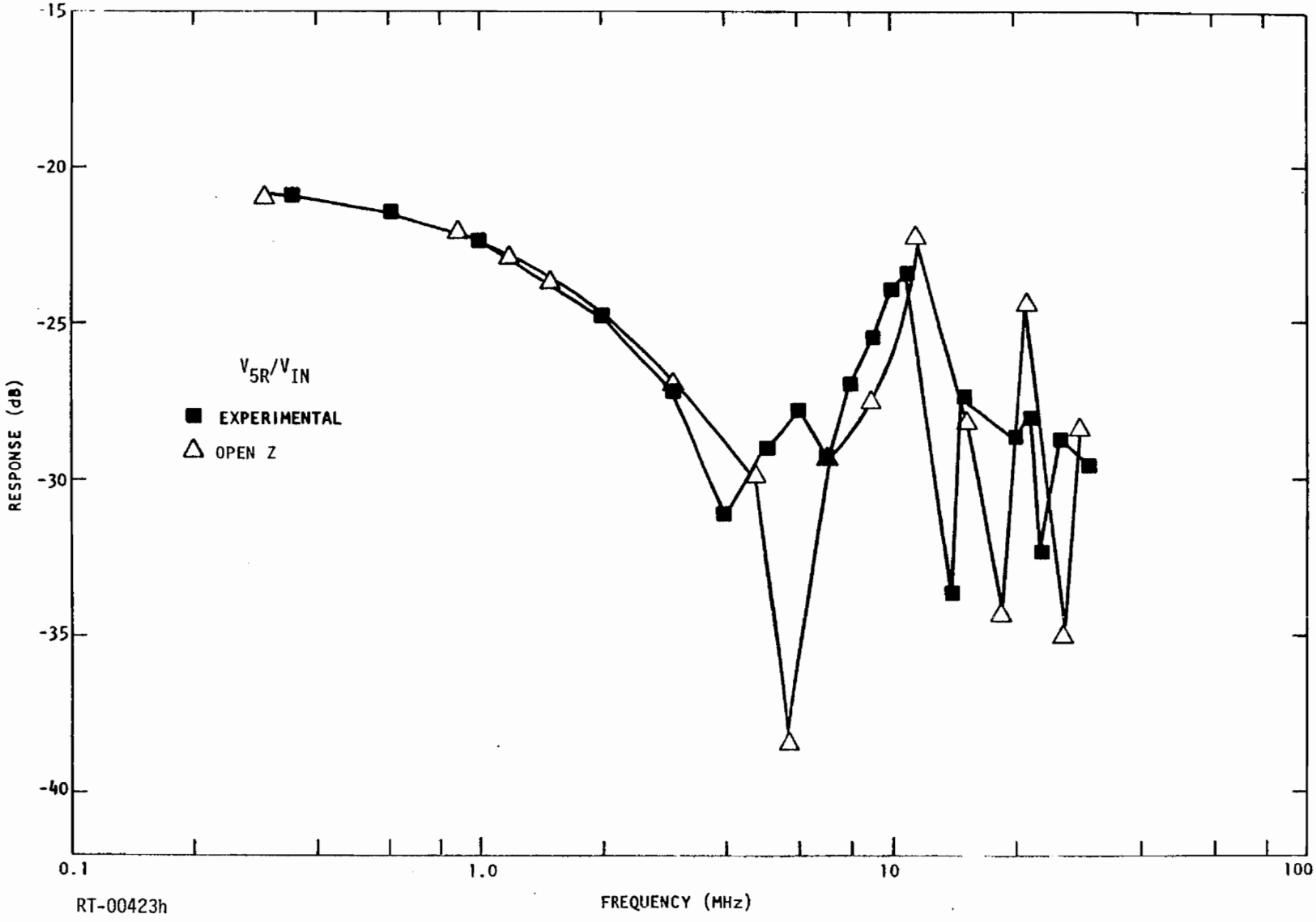
-15
-20
-25
-30
-35
-40
RESPONSE (dB)
V_{5R}/V_{IN}
EXPERIMENTAL
OPEN Z
0.1
1.0
10
100
FREQUENCY (MHz)
RT-00423h

Fig. 5.19c

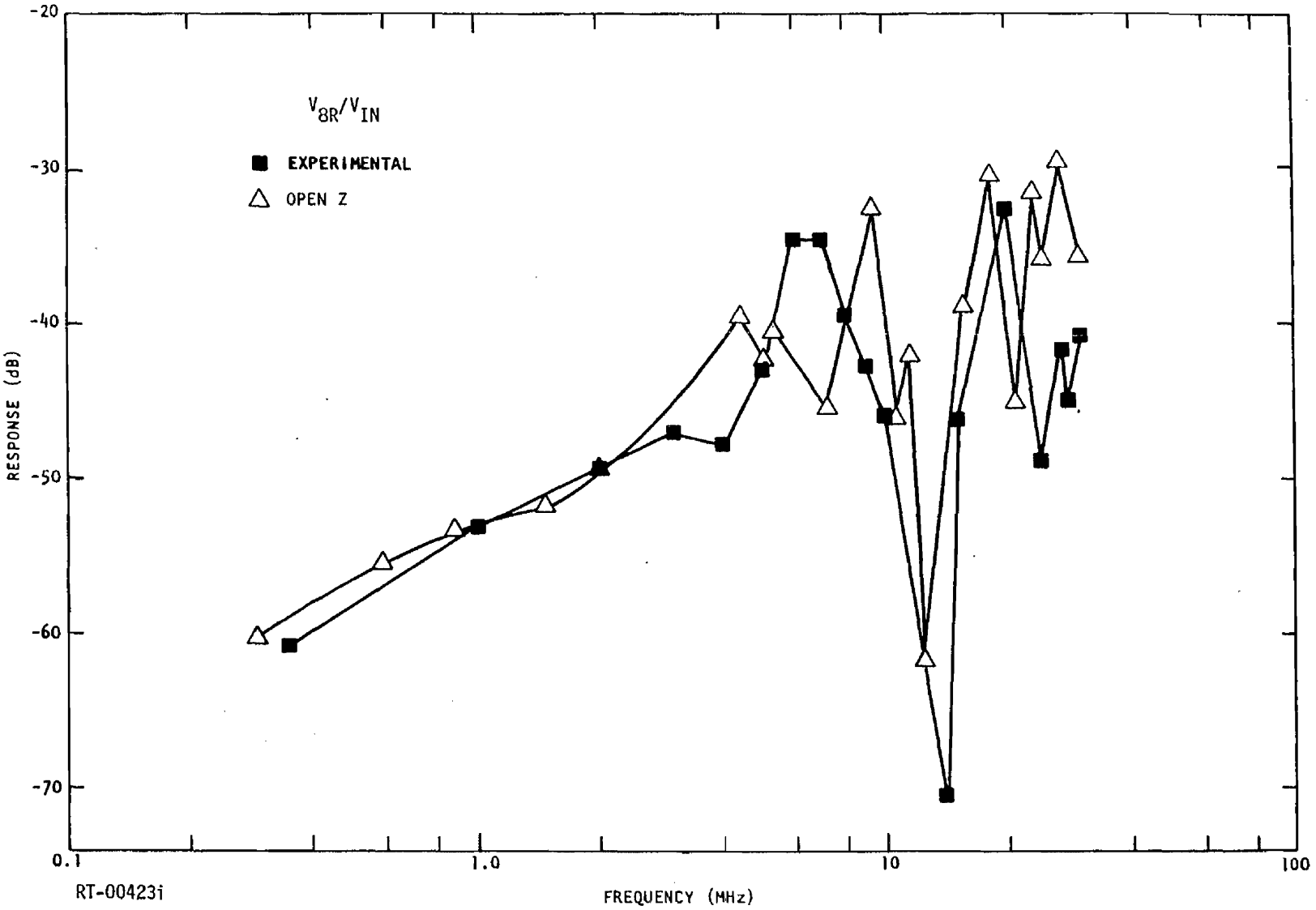
V_{8R}/V_{IN}
EXPERIMENTAL
OPEN Z
RESPONSE (dB)
-20
-30
-40
-50
-60
-70
0.1
1.0
10
100
FREQUENCY (MHz)
RT-00423i

Fig. 5.19d

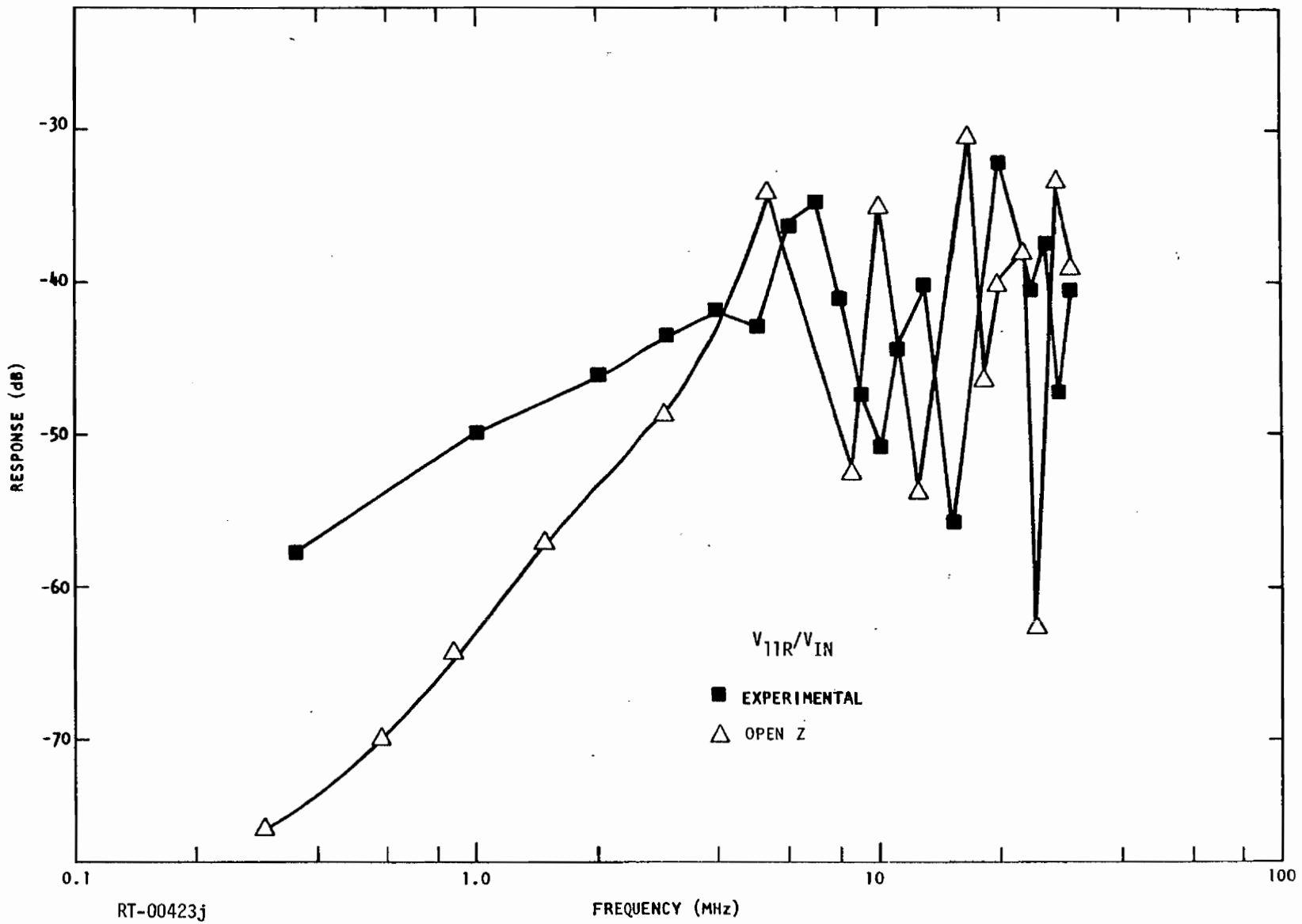
-30
-40
-50
-60
-70
RESPONSE (dB)
0.1
1.0
10
100
FREQUENCY (MHz)
V_{11R}/V_{IN}
EXPERIMENTAL
OPEN Z
RT-00423j

Fig. 5.19e

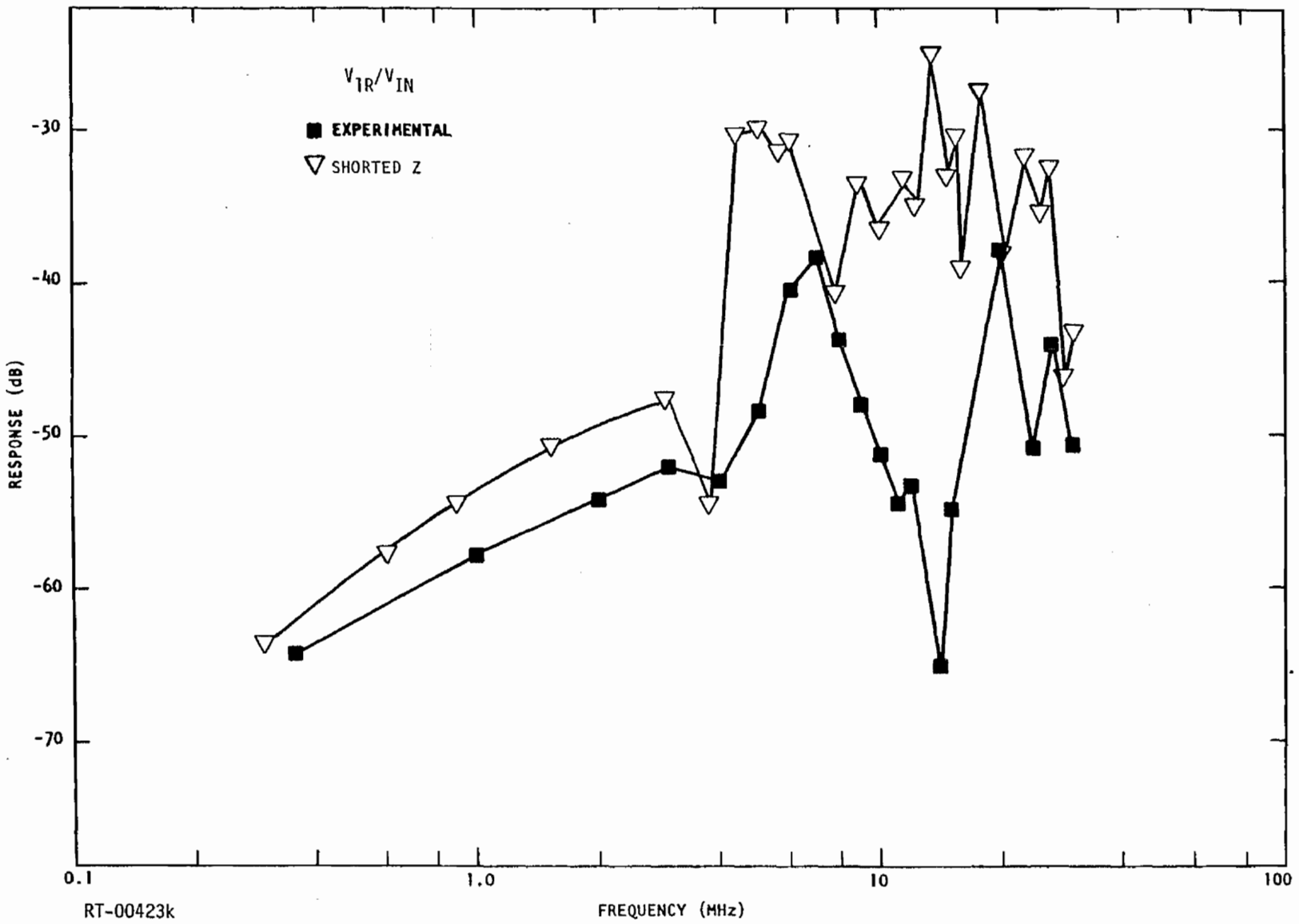

Fig. 5.20a. Transfer functions for 11-conductor cable, shorted-Z method

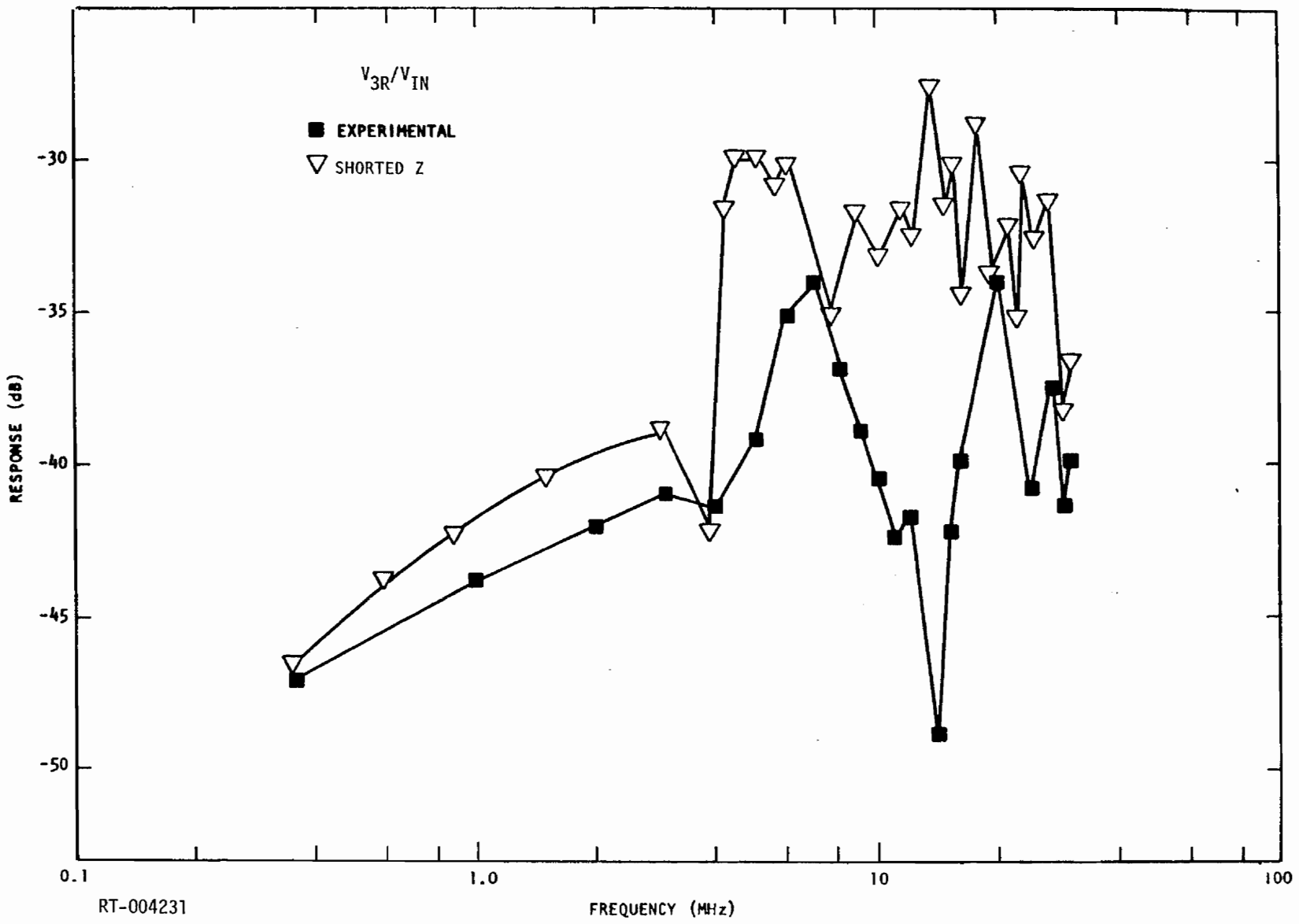
V_{3R}/V_{IN}
EXPERIMENTAL
SHORTED Z
RESPONSE (dB)
-30
-35
-40
-45
-50
0.1
1.0
10
100
FREQUENCY (MHz)
RT-004231

Fig. 5.20b

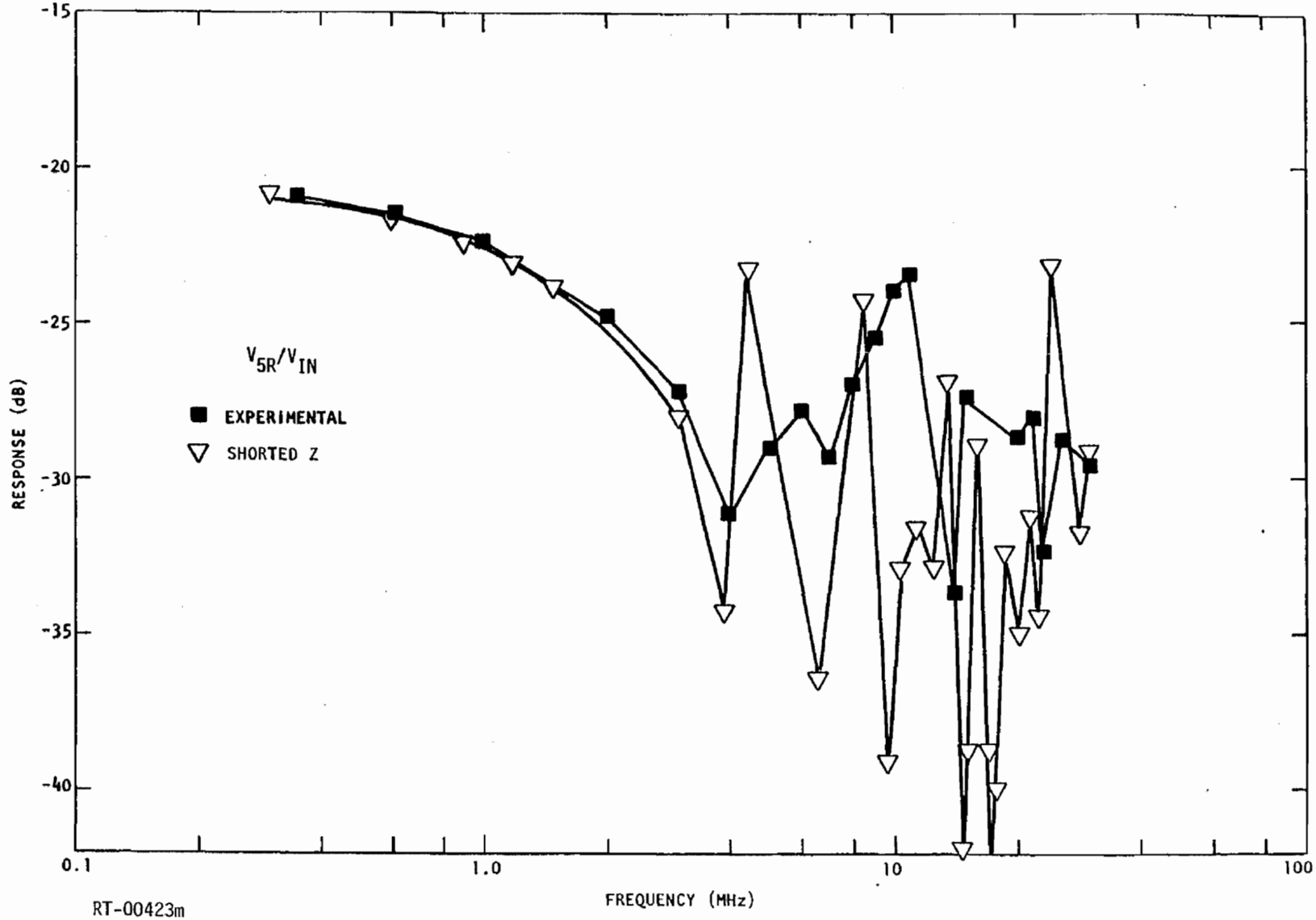
-15
-20
-25
-30
-35
-40
RESPONSE (dB)
V_{5R}/V_{IN}
EXPERIMENTAL
SHORTED Z
0.1
1.0
10
100
FREQUENCY (MHz)
RT-00423m

Fig. 5.20c

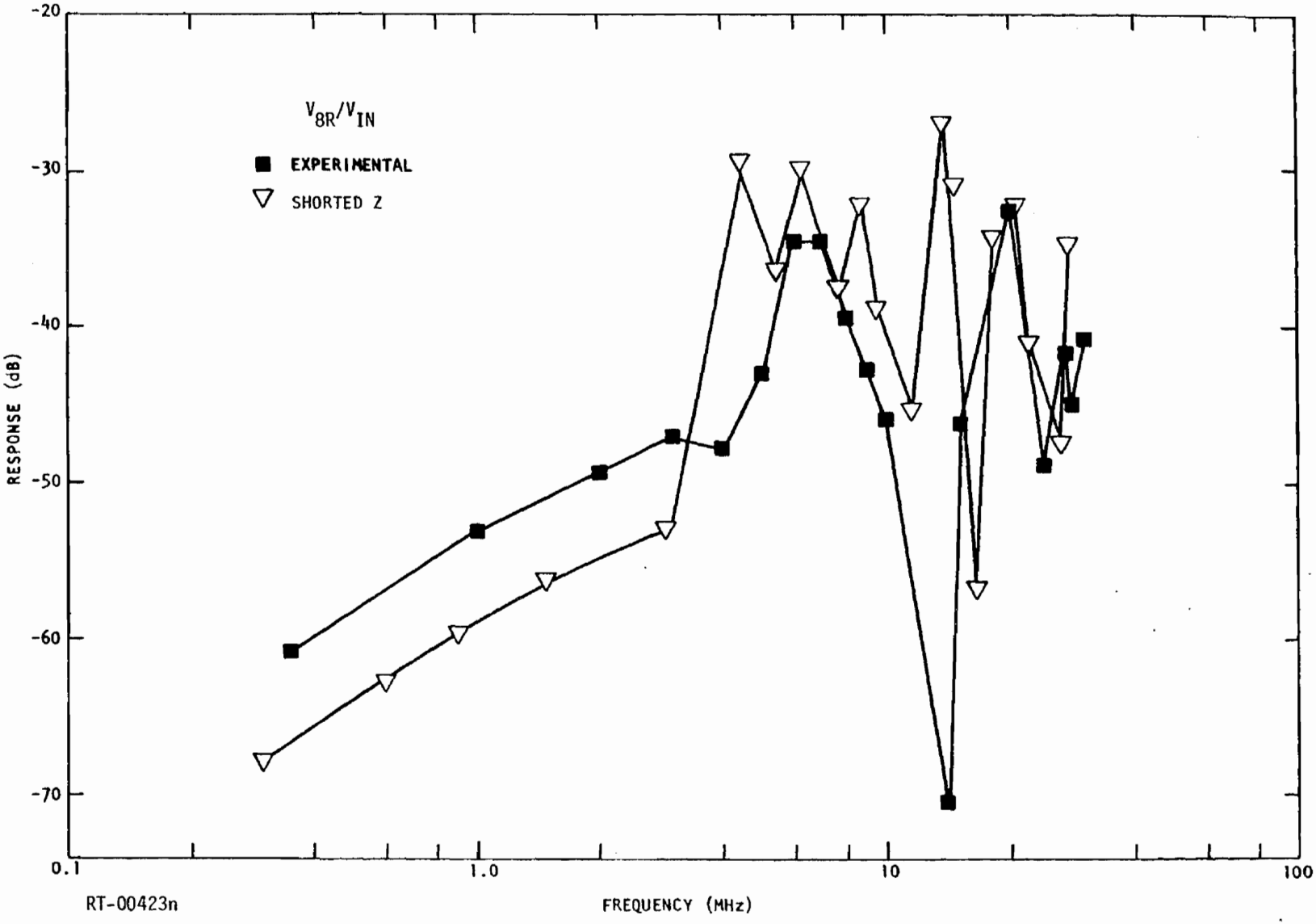
V_{8R}/V_{IN}
EXPERIMENTAL
SHORTED Z
-20
-30
-40
-50
-60
-70
RESPONSE (dB)
0.1
1.0
10
100
FREQUENCY (MHz)
RT-00423n

Fig. 5.20d

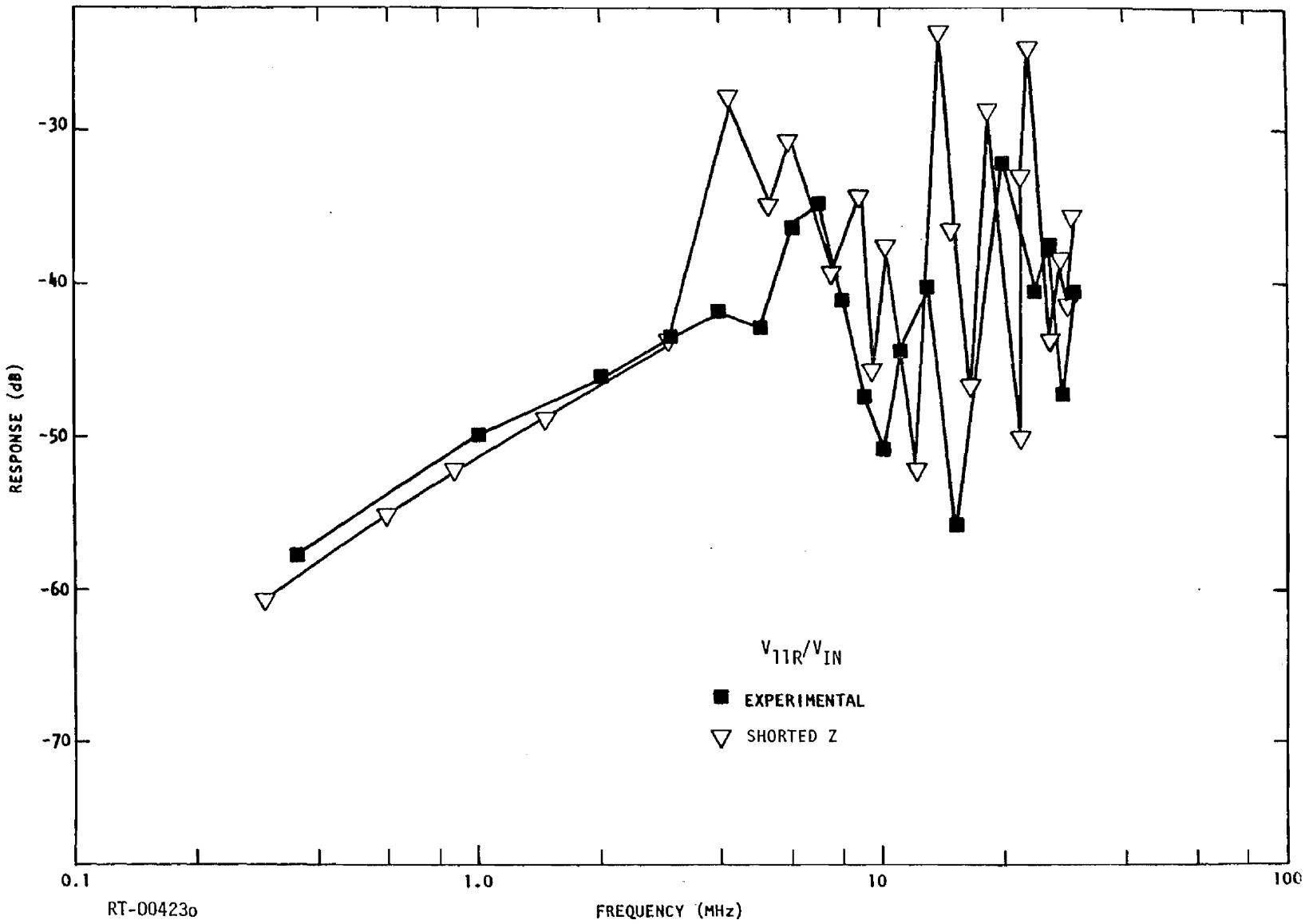
-30
-40
-50
-60
-70
RESPONSE (dB)
V_{11R}/V_{IN}
EXPERIMENTAL
SHORTED Z
0.1
1.0
10
100
RT-00423o
FREQUENCY (MHz)

Fig. 5.20e

Cable 5, 3-Branch Cable

The impetus for developing the two impedance methods for determining L and C parameters was to model branched cables where the capacitance method is not applicable. It is anticipated that the time and distance resolution of the TDR used for making impedance measurements will allow the operator to distinguish between branches, something he could not do with a capacitance bridge. The impedance methods have already been verified as valid. The modeling of this cable is intended to verify that the necessary resolution is possible.

The cable is rather simple in terms of internal makeup, consisting of only 6, 4, and 2 unshielded wires in branches A, B, and C, respectively. as shown in Fig. 5.21. The overall shield is a copper braid joined at the junction by very careful soldering. The branches are not uniform with respect to distance; i. e., the conductor lay varies with distance.

The determination of model parameters by both open-Z and shorted-Z methods proceeded without difficulty. The measured impedances were in the following ranges.

Shorted-Z	Z_{ii}^{m} = 37 to 40 ohms
	Z_{ij}^{m} = 19 to 25 ohms
Open-Z	Z_{ii}^{m} = 40 to 45 ohms
	Z_{ij}^{m} = 61 to 68 ohms

The open-Z method measured values are very close to the 50-ohm TDR standard, where good resolution is possible. The shorted-Z measured values are somewhat further from the 50-ohm standard, with resulting poorer resolution, but are still in an acceptable range. As a result, the distributed parameters were calculated with no negative signs or unreasonable values appearing in any case.

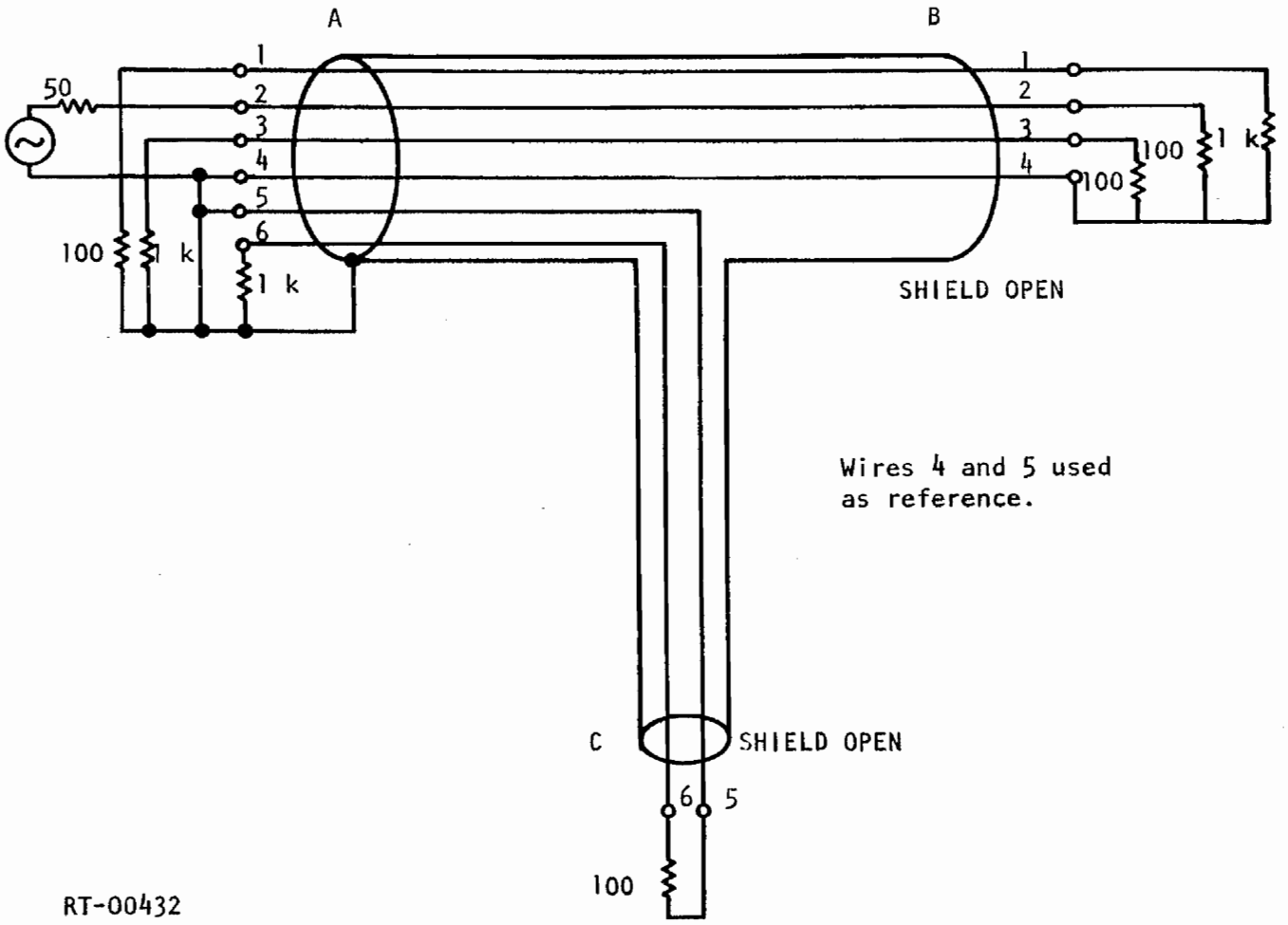

Fig. 5.21. Drive and termination scheme for 6-conductor, 3-branch cable

The distributed parameters were used to create a model consisting of three 0.508-m-long sections for each branch of the cable. The termination and drive scheme shown in Fig. 5.21 was used for analysis and experiment. The results for all possible transfer functions are shown in Figs. 5.22a through 5.22f for the open-Z method parameters and in Figs. 5.23a through 5.23f for the shorted-Z method parameters. Wire 4 or 5 was used, as appropriate, for the reference in branches B and C, and wires 4 and 5 together as the reference in branch A.

Examination of these results shows that they are very good for both methods, with the open-Z results having a slight edge over the shorted-Z results. Thus, the methods are clearly capable of modeling cables with multiple branches of at least this complexity.

Cable 2, Special 9-Conductor Grouped Configuration

The 20-conductor controlled cable was modeled a second time, but with 14 of the 20 conductors divided into three groups of 5, 5, and 4 conductors. These groups were then treated as three single conductors and, with the remaining six ungrouped conductors, the result is a 9-conductor cable. The purpose of this effort was to determine if the analytical results for the five ungrouped and undriven conductors would remain correct with the altered modeling of the other 14 conductors, i.e., to determine if grouping is a potentially valid technique for simplifying a cable model.

The termination scheme used for the analysis is shown in Fig. 5.24. The termination resistors on the ungrouped conductors (1, 2, 3, 13, 14) are the same as were used for the previous analysis. The values of the termination resistors on groups A, B, and C were determined by simply taking the parallel values of the previously used termination resistors. This was done in order to maintain the same impedance levels on the groups.

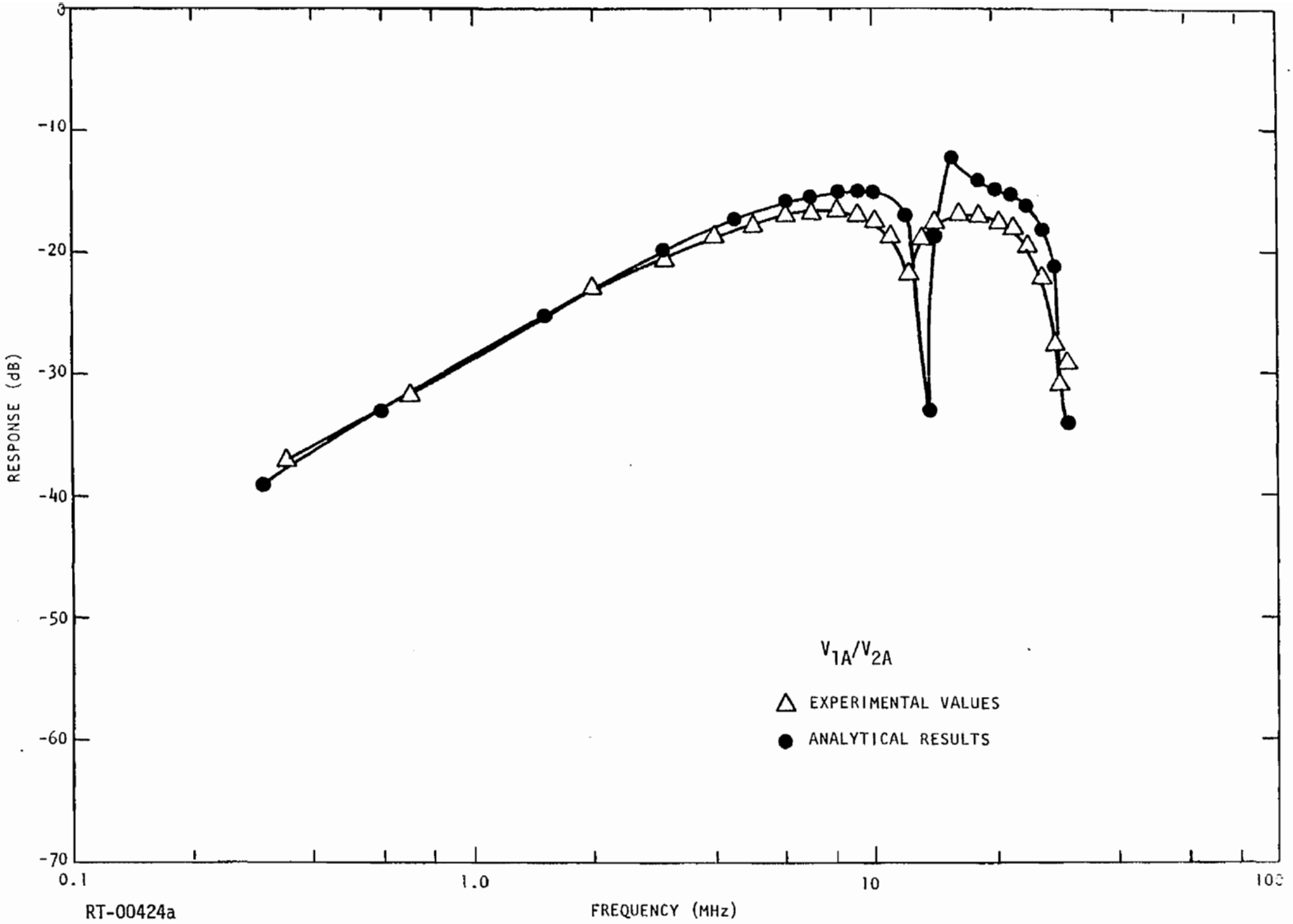

Fig. 5.22a. Transfer functions for 3-branch cable, open-Z method parameters

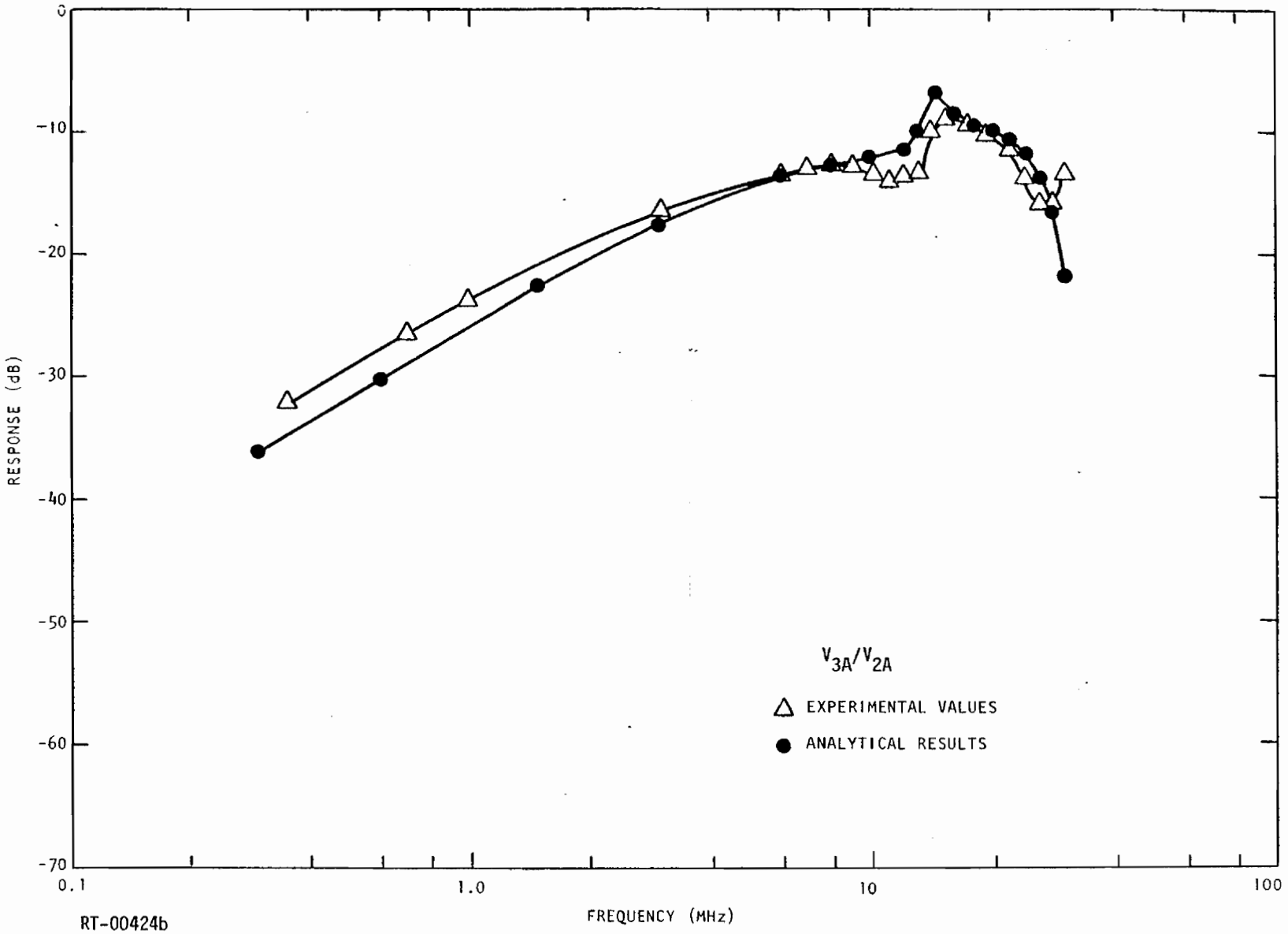
0
-10
-20
-30
-40
-50
-60
-70
RESPONSE (dB)
0.1
1.0
10
100
FREQUENCY (MHz)
V_{3A}/V_{2A}
EXPERIMENTAL VALUES
ANALYTICAL RESULTS
RT-00424b

Fig. 5.22b

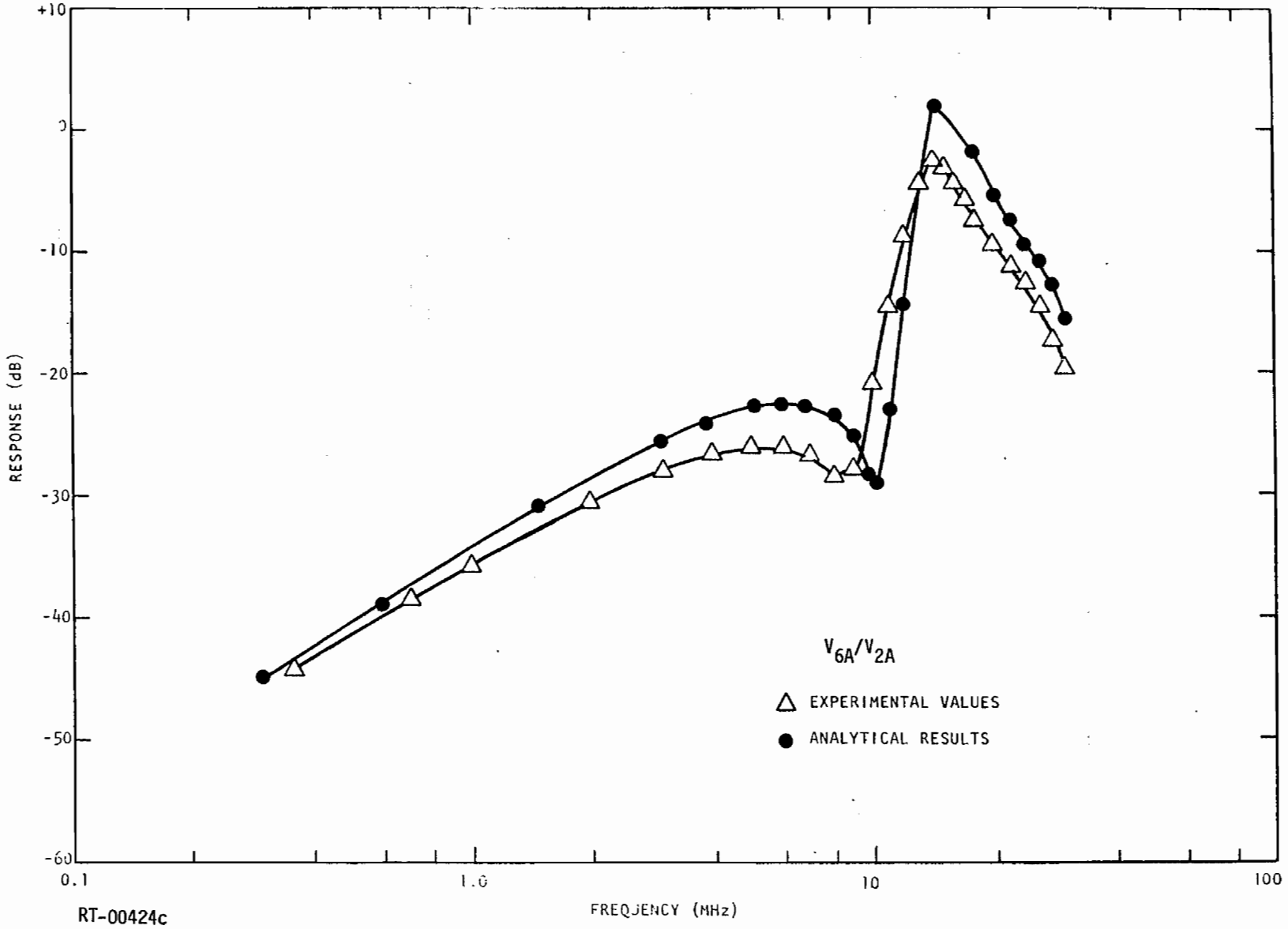
+10
0
-10
-20
-30
-40
-50
-60
RESPONSE (dB)
0.1
1.0
10
100
FREQUENCY (MHz)
V_{6A}/V_{2A}
EXPERIMENTAL VALUES
ANALYTICAL RESULTS
RT-00424c

Fig. 5.22c

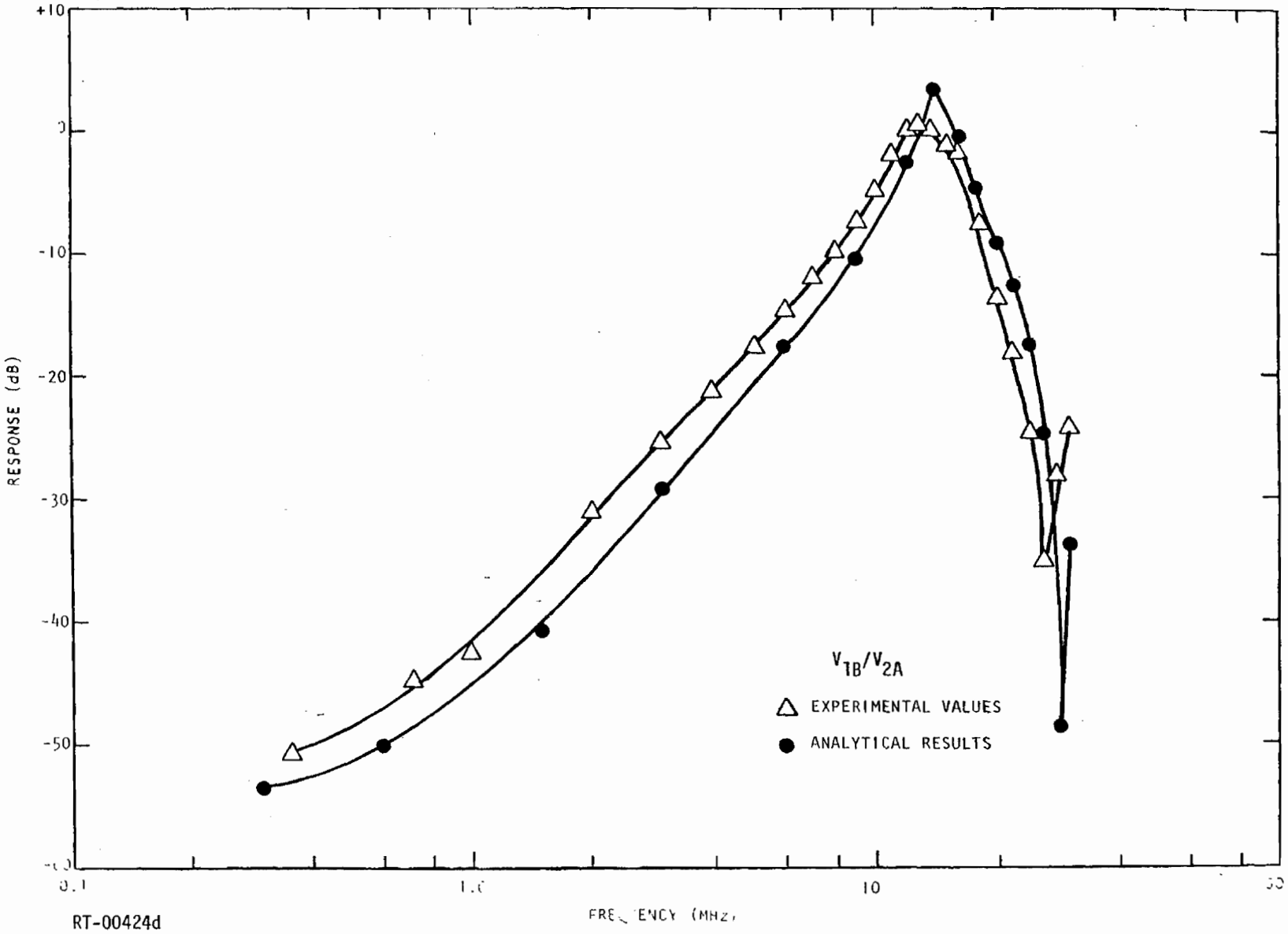
+10
0
-10
-20
-30
-40
-50
RESPONSE (dB)
0.1
1.0
10
FREQUENCY (MHz)
V_{1B}/V_{2A}
EXPERIMENTAL VALUES
ANALYTICAL RESULTS
RT-00424d

Fig. 5.22d

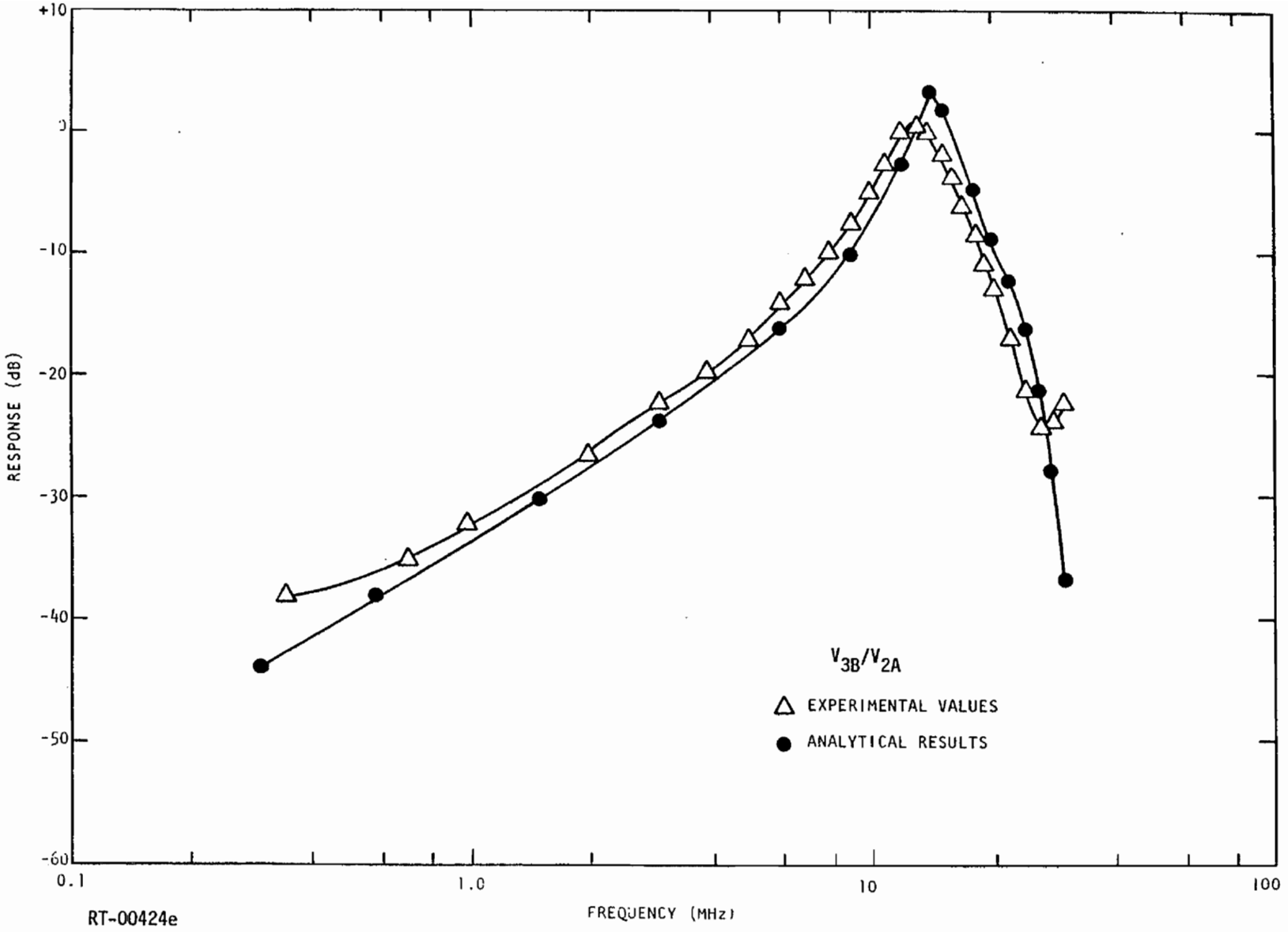
+10
0
-10
-20
-30
-40
-50
-60
RESPONSE (dB)
0.1
1.0
10
100
FREQUENCY (MHz)
V_{3B}/V_{2A}
EXPERIMENTAL VALUES
ANALYTICAL RESULTS
RT-00424e

Fig. 5.22e

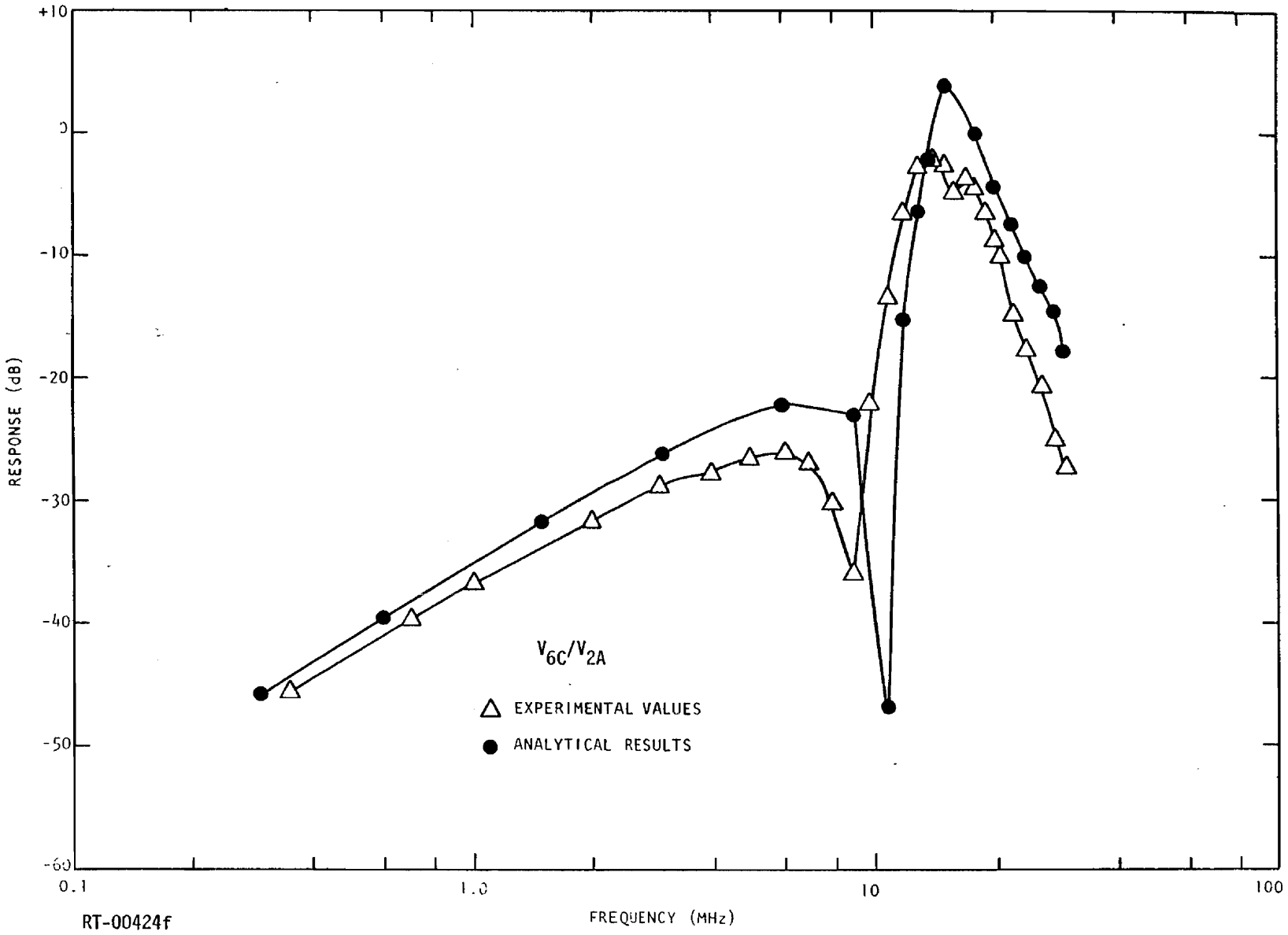
+10
0
-10
-20
-30
-40
-50
-60
RESPONSE (dB)
0.1
1.0
10
100
FREQUENCY (MHz)
V_{6C}/V_{2A}
EXPERIMENTAL VALUES
ANALYTICAL RESULTS
RT-00424f

Fig. 5.22f

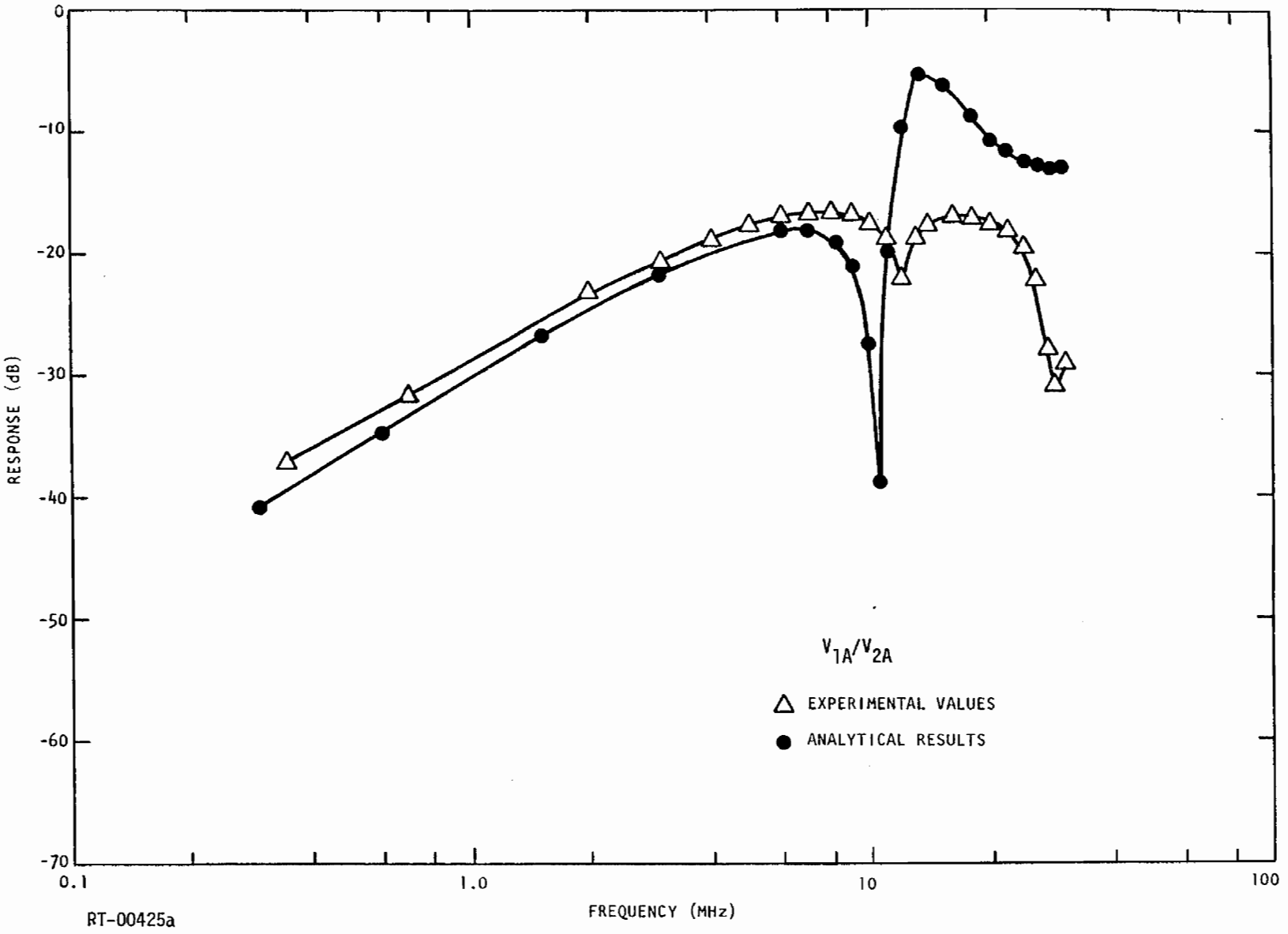

Fig. 5.23a. Transfer functions for 3-branch cable, shorted-Z method parameters

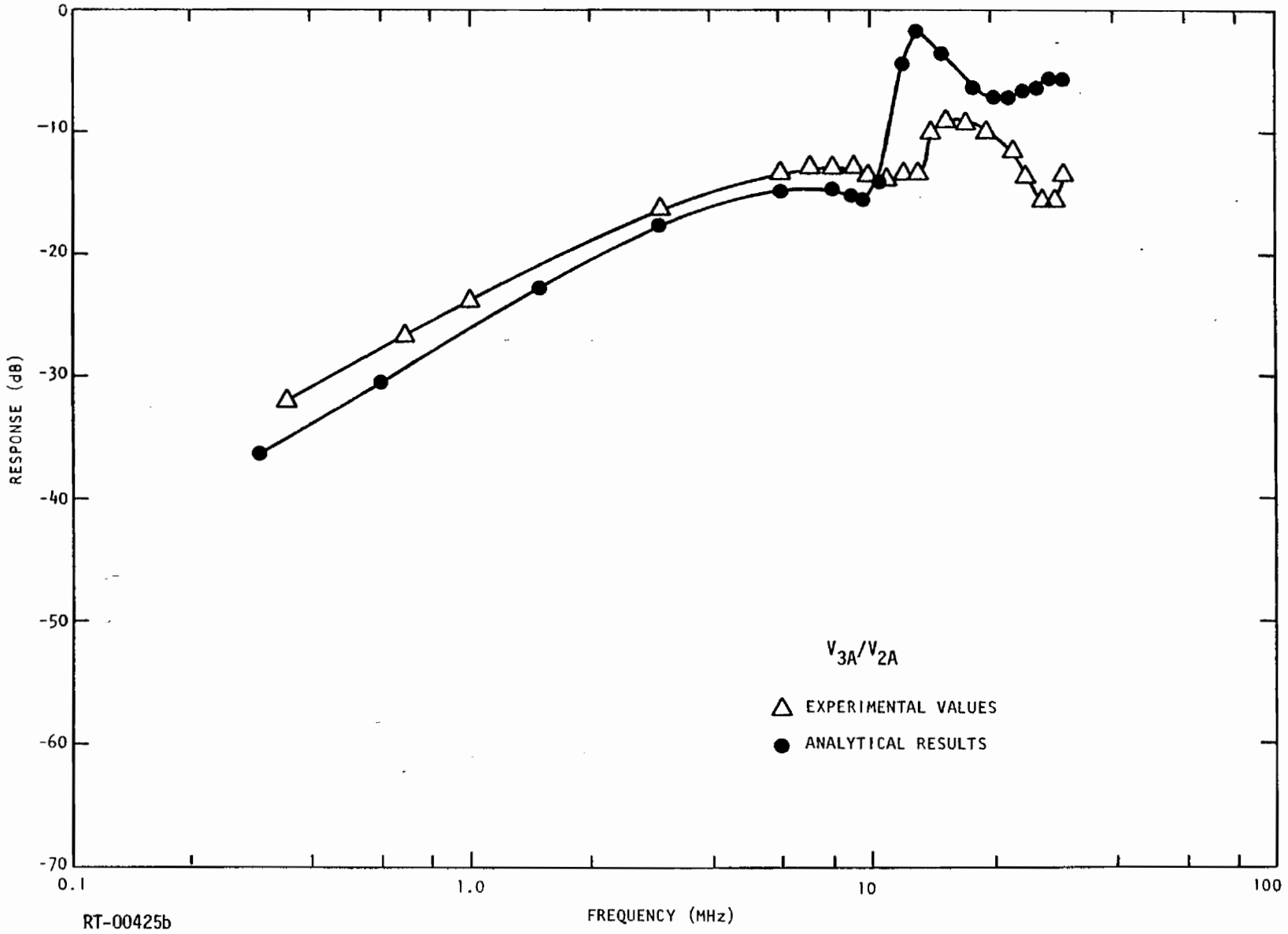
0
-10
-20
-30
-40
-50
-60
-70
RESPONSE (dB)
0.1
1.0
10
100
FREQUENCY (MHz)
V_{3A}/V_{2A}
EXPERIMENTAL VALUES
ANALYTICAL RESULTS
RT-00425b

Fig. 5.23b

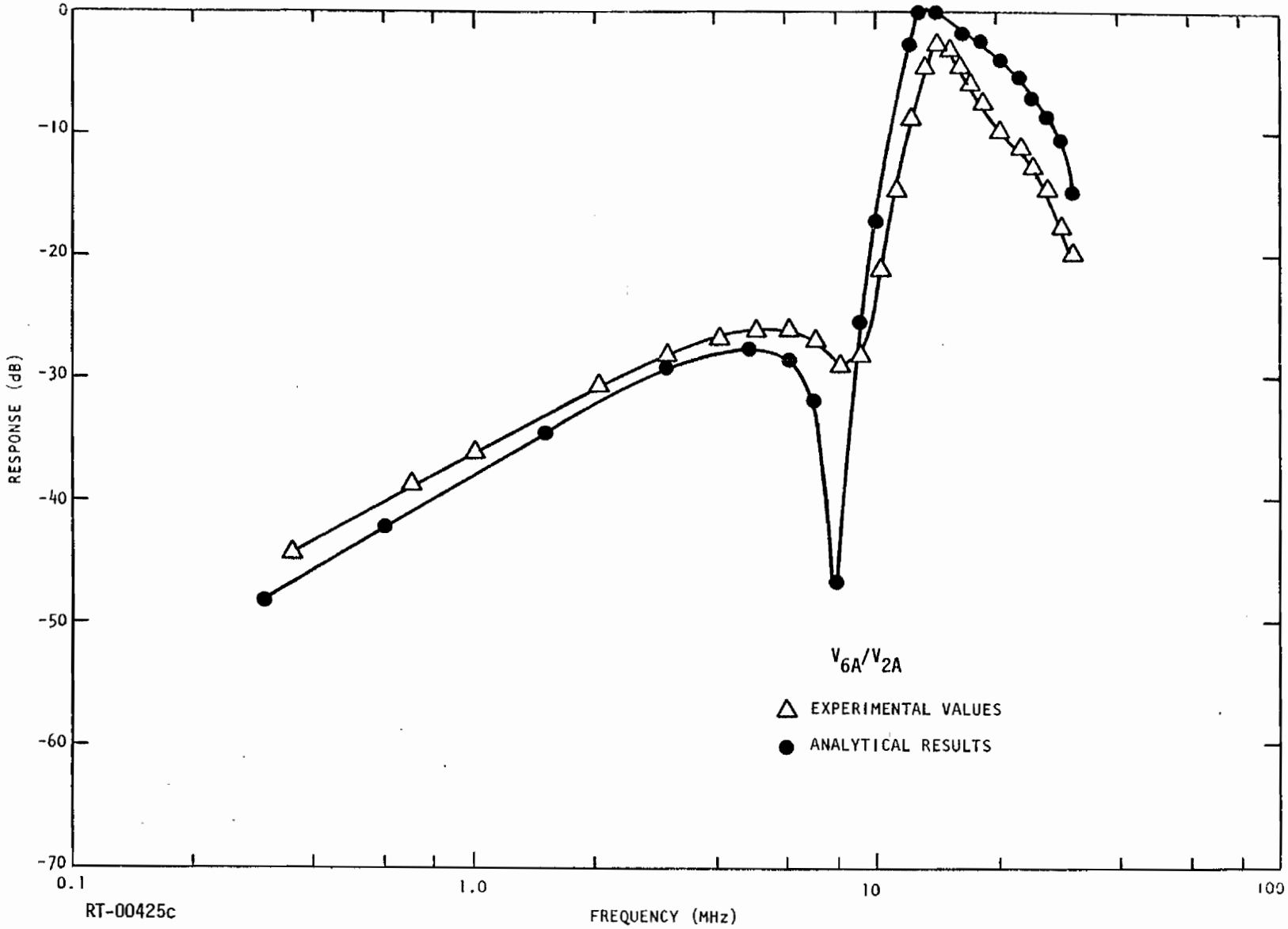
0
-10
-20
-30
-40
-50
-60
-70
RESPONSE (dB)
0.1
1.0
10
100
FREQUENCY (MHz)
RT-00425c
V_{6A}/V_{2A}
EXPERIMENTAL VALUES
ANALYTICAL RESULTS

Fig. 5.23c

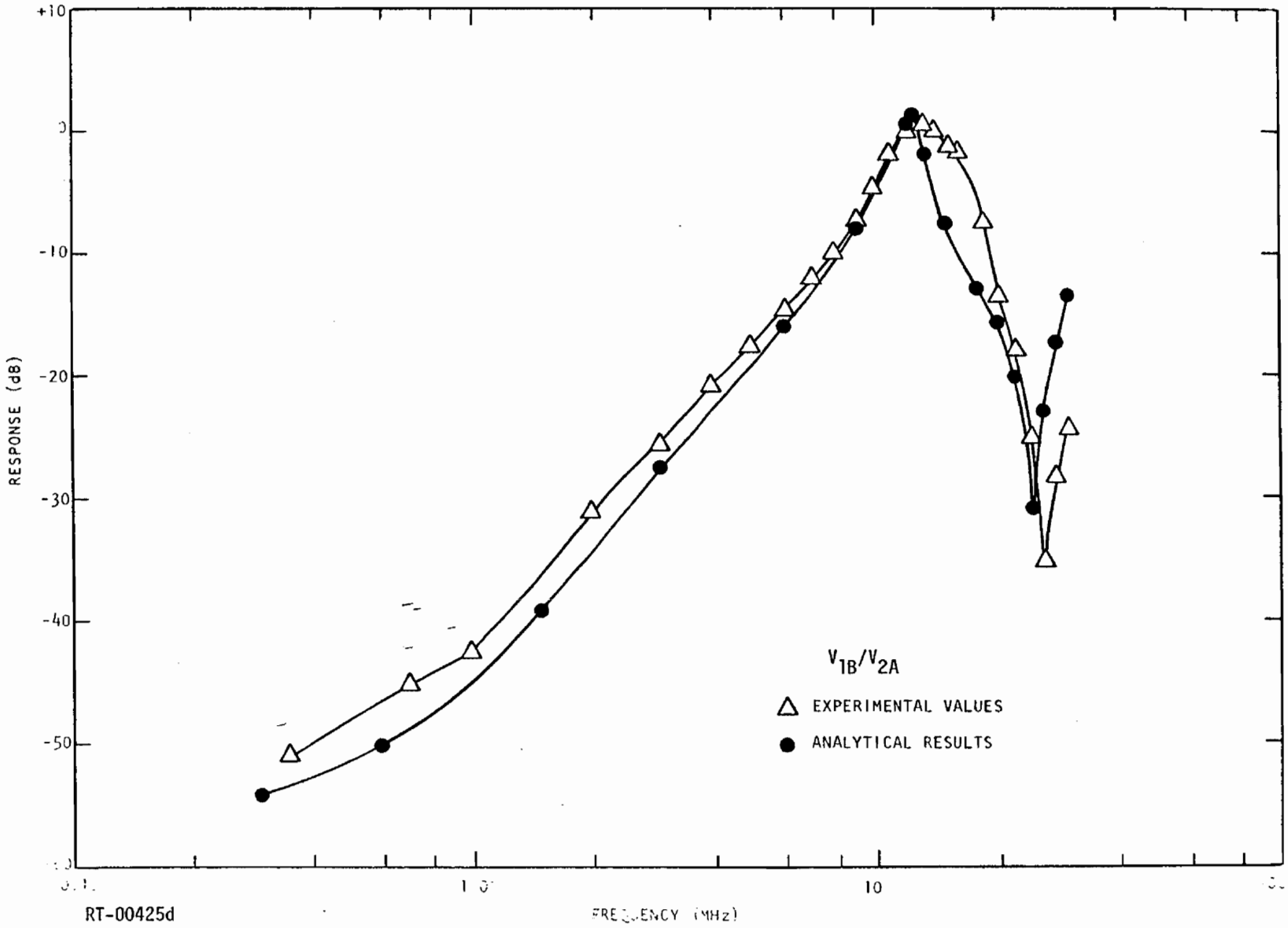
+10
0
-10
-20
-30
-40
-50
RESPONSE (dB)
10
FREQUENCY (MHz)
V_{1B}/V_{2A}
EXPERIMENTAL VALUES
ANALYTICAL RESULTS
RT-00425d

Fig. 5.23d

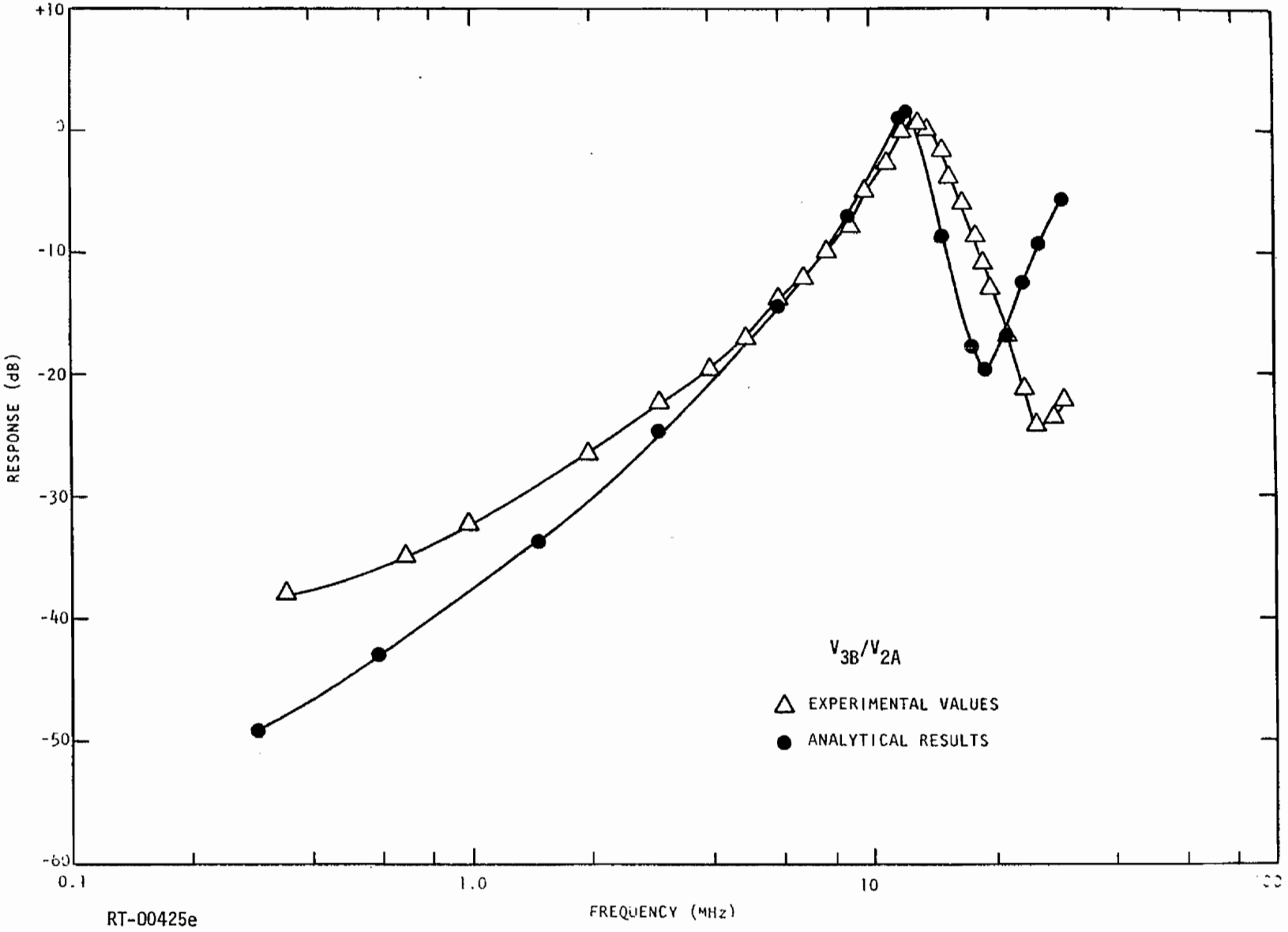
+10
0
-10
-20
-30
-40
-50
-60
RESPONSE (dB)
0.1
1.0
10
FREQUENCY (MHz)
V_{3B}/V_{2A}
EXPERIMENTAL VALUES
ANALYTICAL RESULTS
RT-00425e

Fig. 5.23e

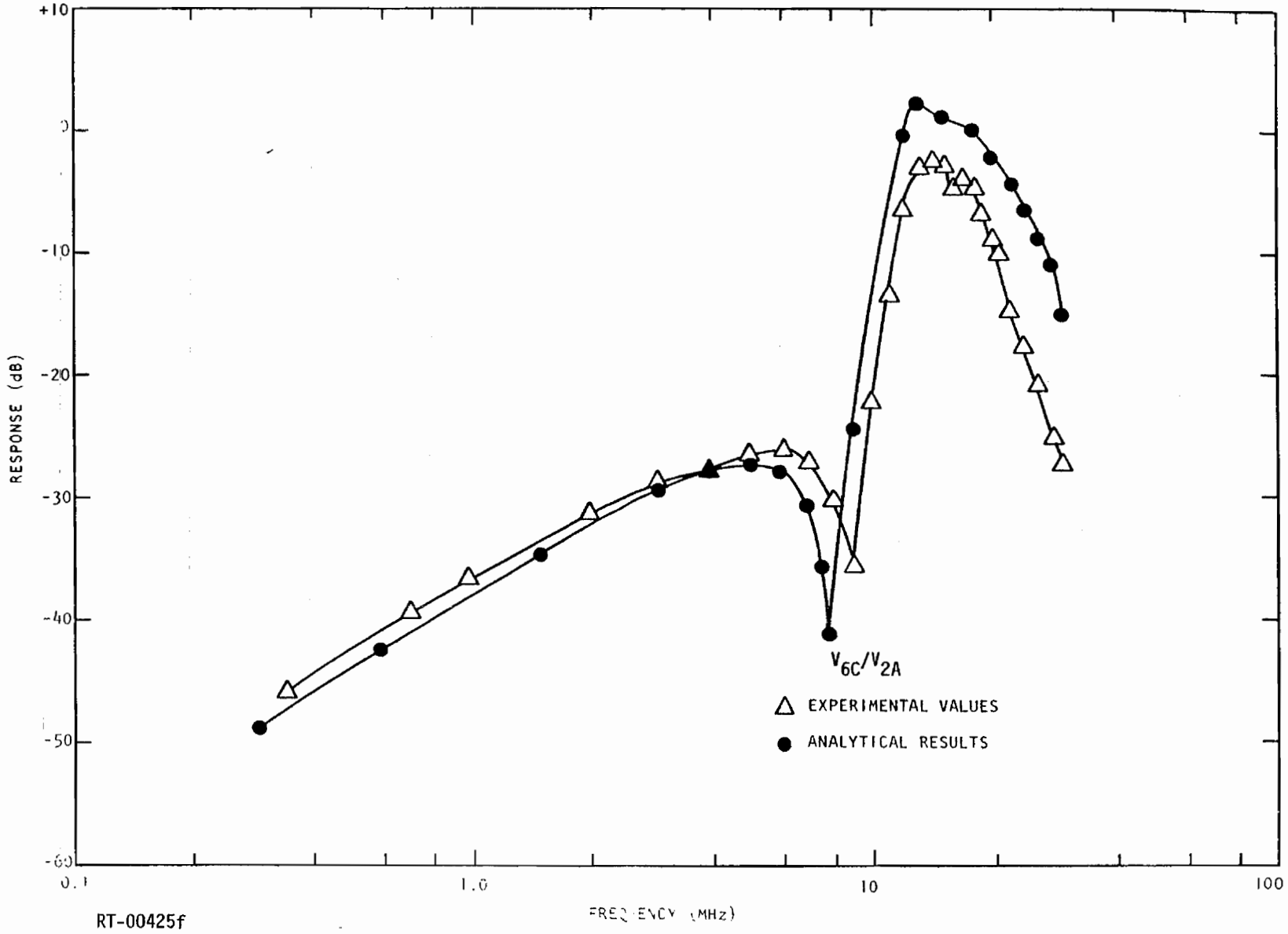
+10
0
-10
-20
-30
-40
-50
-60
RESPONSE (dB)
0.1
1.0
10
100
FREQUENCY (MHz)
V_{6C}/V_{2A}
EXPERIMENTAL VALUES
ANALYTICAL RESULTS
RT-00425f

Fig. 5.23f

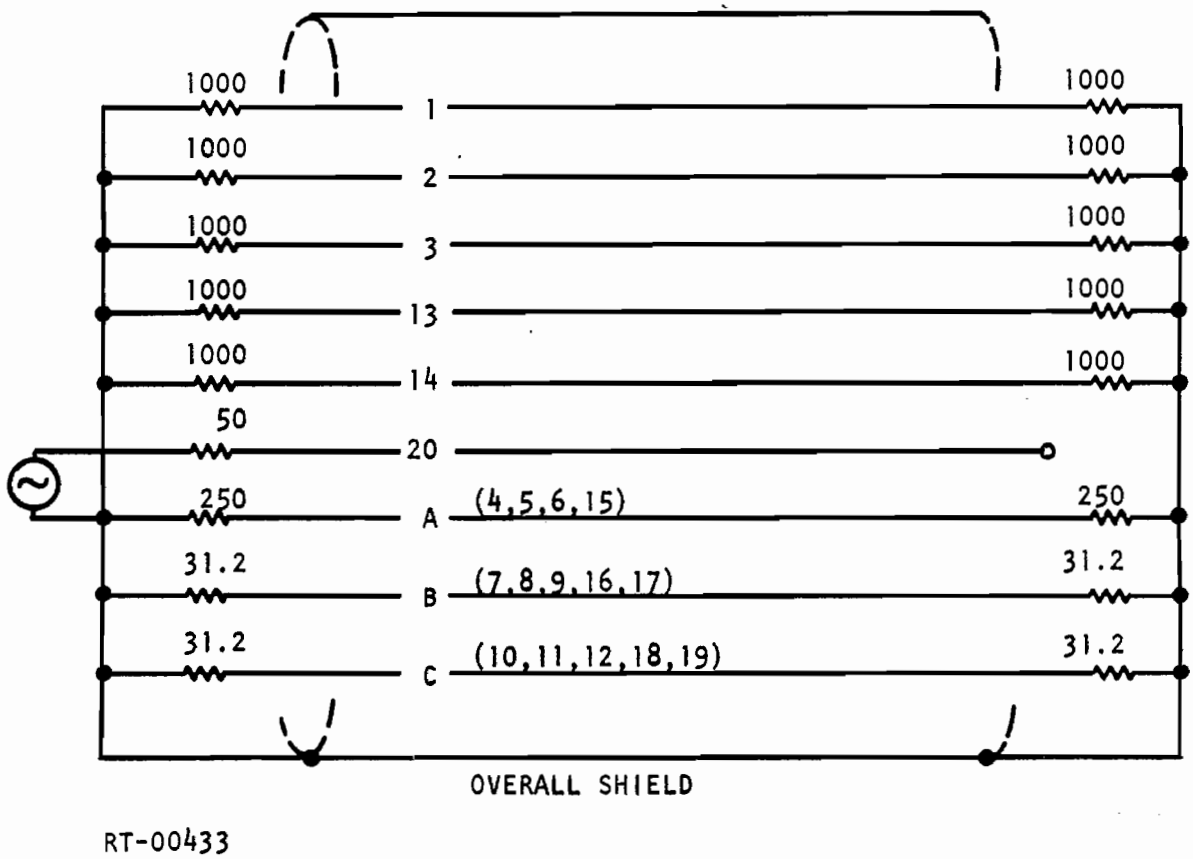

Fig. 5.24. Drive and termination scheme for 9-conductor cable

Two methods of determining parameter values were applied to this cable. In both, the conductors in each group were shorted together at both ends of the cable. These shorted groups were then simply treated as another conductor for all required measurements and calculations, including new R_{ac} values. The model which was created from the calculated parameters consisted of the same number and length of sections as was used for the 20-conductor model.

The results for the capacitance method parameters are shown in Figs. 5.25a through 5.25e and for the open-Z method parameters in Figs. 5.26a through 5.26e. The results for both methods are quite good and, in fact, are actually better than the results obtained using the full 20-conductor model. This better agreement is probably a result of summing over fewer elements, combined with the increased experience of the personnel in making measurements.

It is very important to note that the experimental results to which the 9-conductor analytical results are compared were not taken on a grouped configuration. These results are the same ones taken previously on the full 20-conductor cable. Thus, the 9-conductor grouped model is an accurate representation of the six ungrouped conductors of the full 20-conductor cable. The quality of the results obtained for this modeling effort shows clearly that the technique of grouping is a potentially useful one.

5.4 CONCLUSIONS FROM MODELING PROGRAM

The modeling and experimental program on actual cables has produced a total of 85 transfer functions taken on six cable configurations, using three different methods of determining the L and C^p parameters. A breakdown of the resulting agreement by method is shown in Table 5.4.

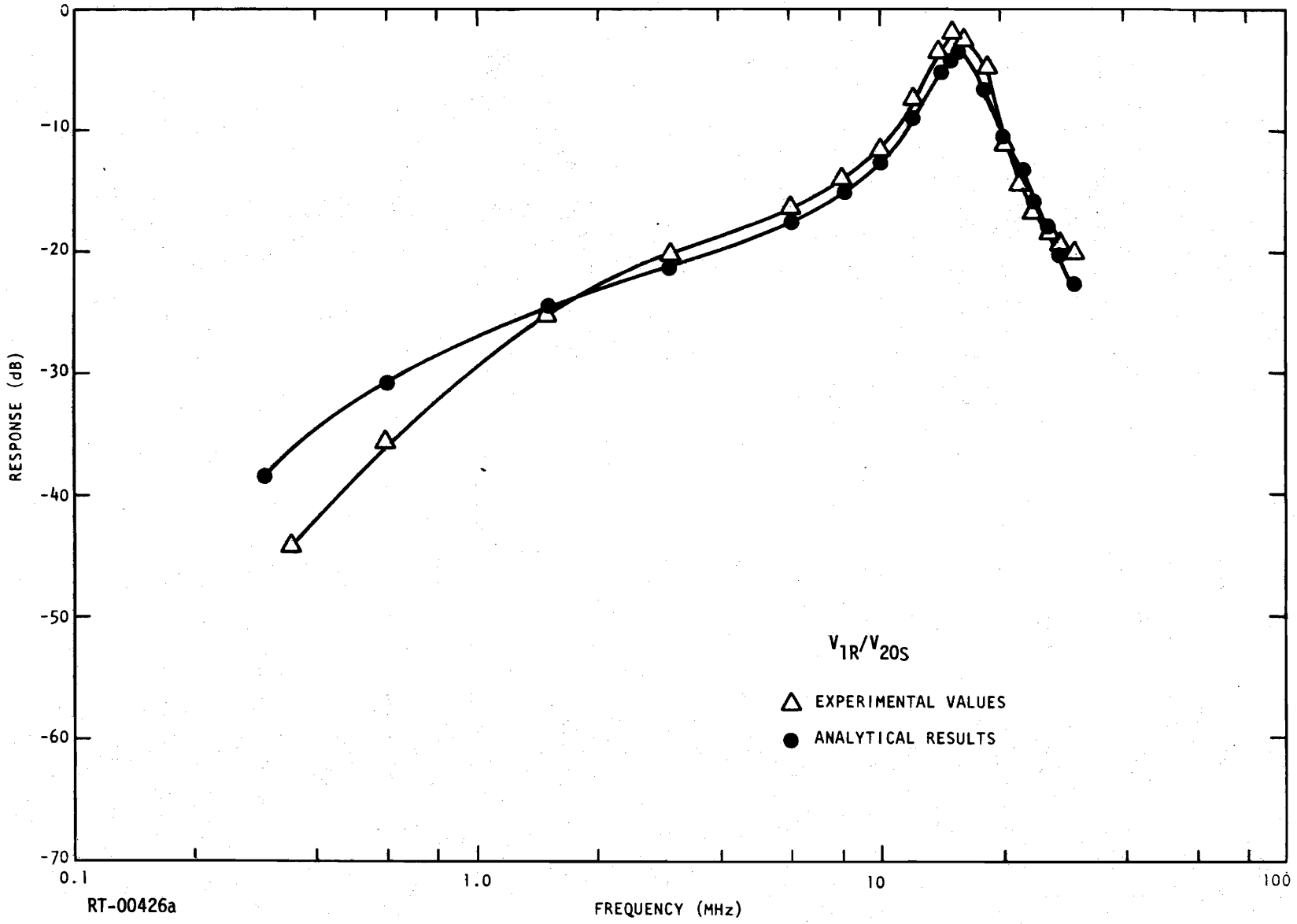

Fig. 5.25a. Transfer functions for 9-conductor grouped cable, capacitor method parameters

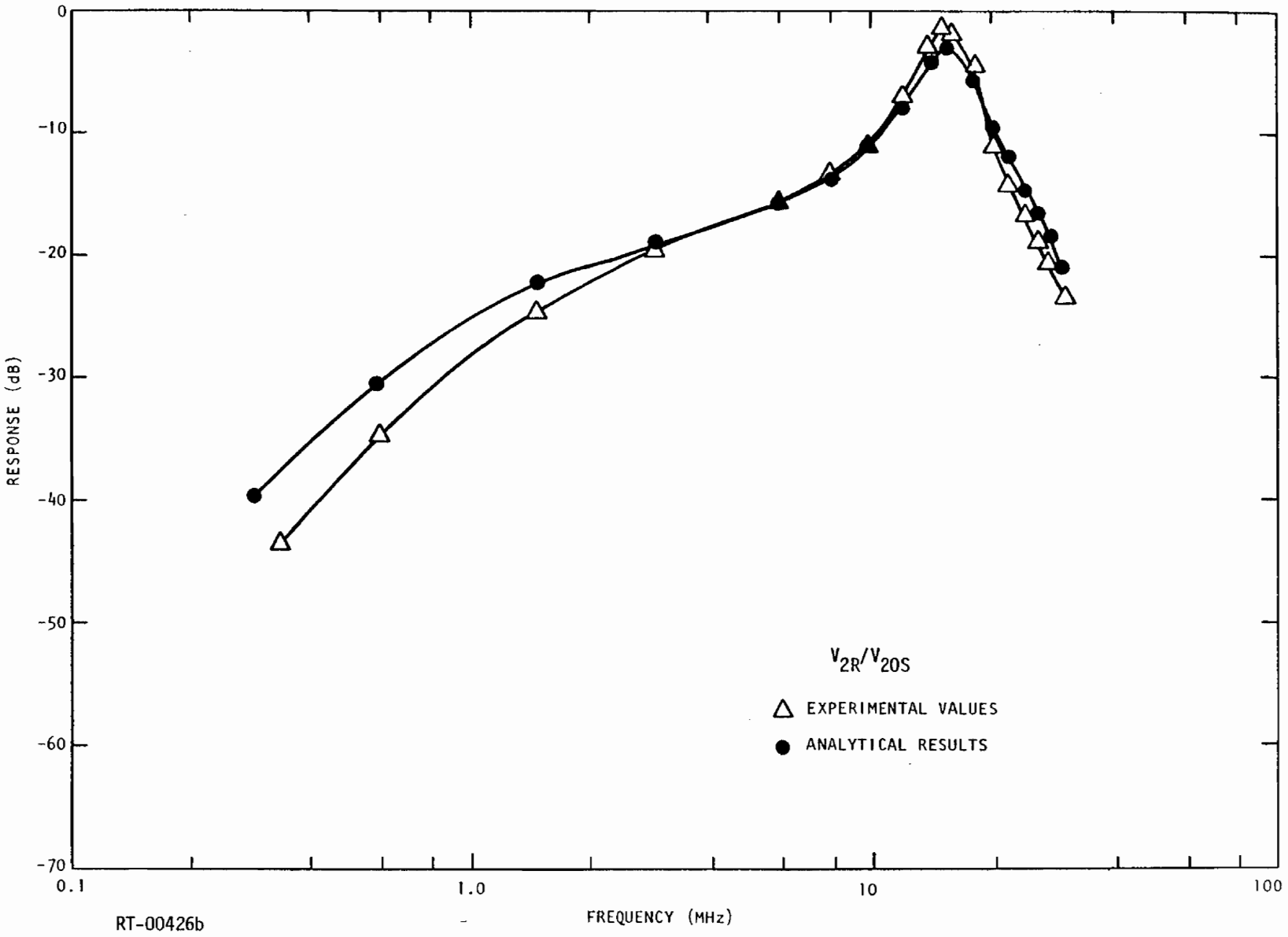
0
-10
-20
-30
-40
-50
-60
-70
RESPONSE (dB)
0.1
1.0
10
100
FREQUENCY (MHz)
V_{2R}/V_{20S}
EXPERIMENTAL VALUES
ANALYTICAL RESULTS
RT-00426b

Fig. 5.25b

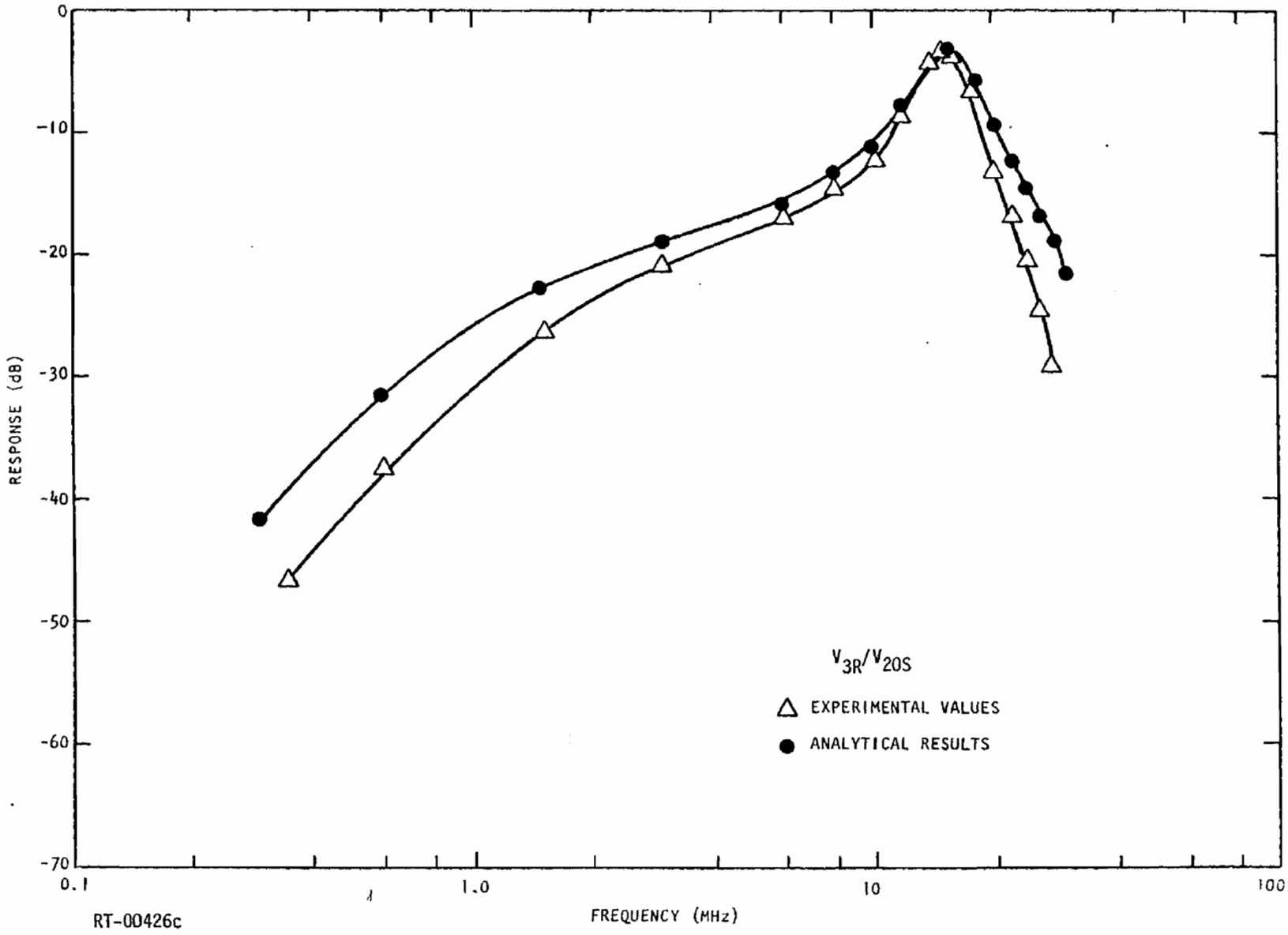
0
-10
-20
-30
-40
-50
-60
-70
RESPONSE (dB)
0.1
1.0
10
100
FREQUENCY (MHz)
V_{3R}/V_{20S}
EXPERIMENTAL VALUES
ANALYTICAL RESULTS
RT-00426c

Fig. 5.25c

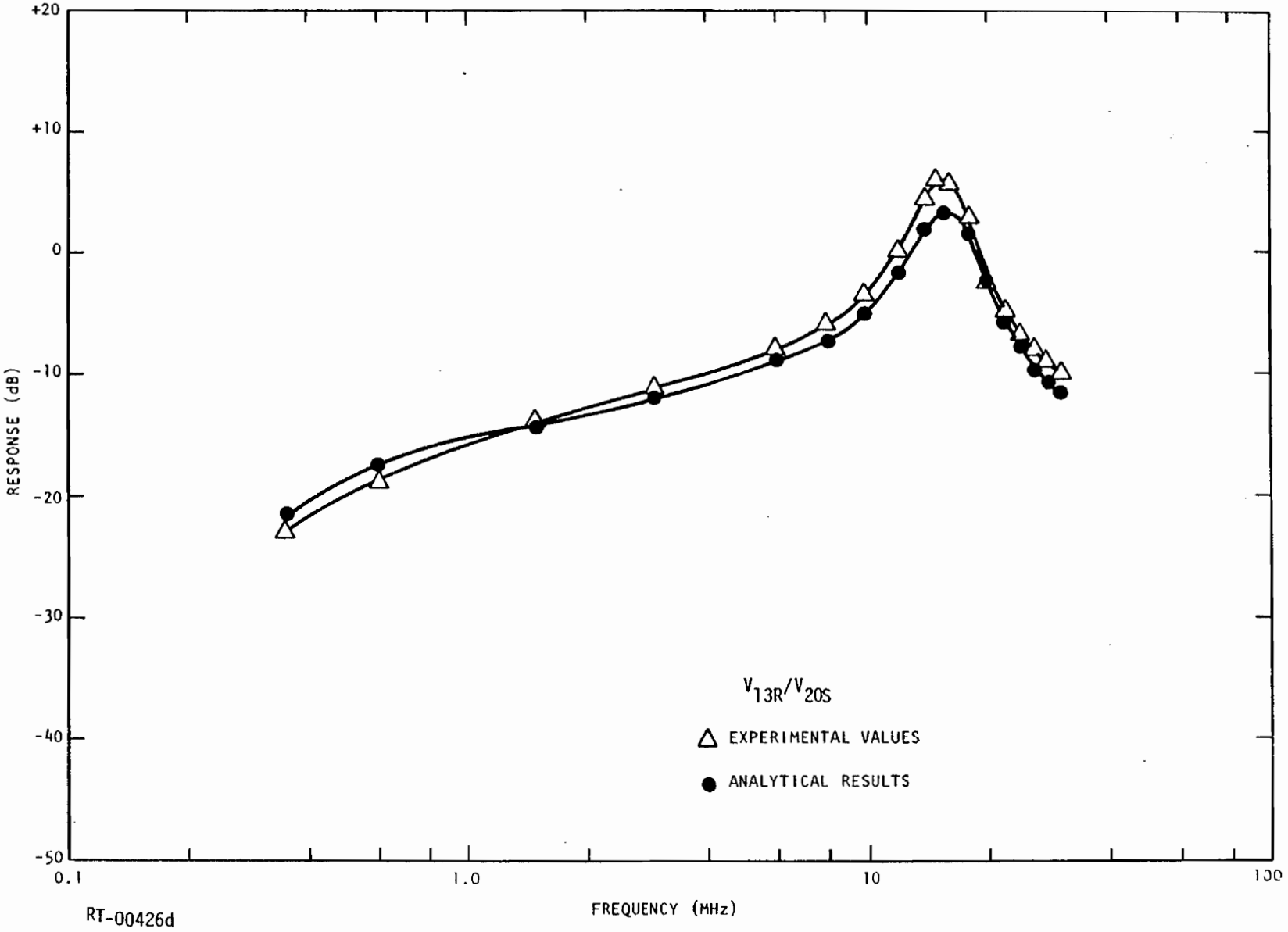
+20
+10
0
-10
-20
-30
-40
-50
RESPONSE (dB)
0.1
1.0
10
100
FREQUENCY (MHz)
V_{13R}/V_{20S}
EXPERIMENTAL VALUES
ANALYTICAL RESULTS
RT-00426d

Fig. 5.25d

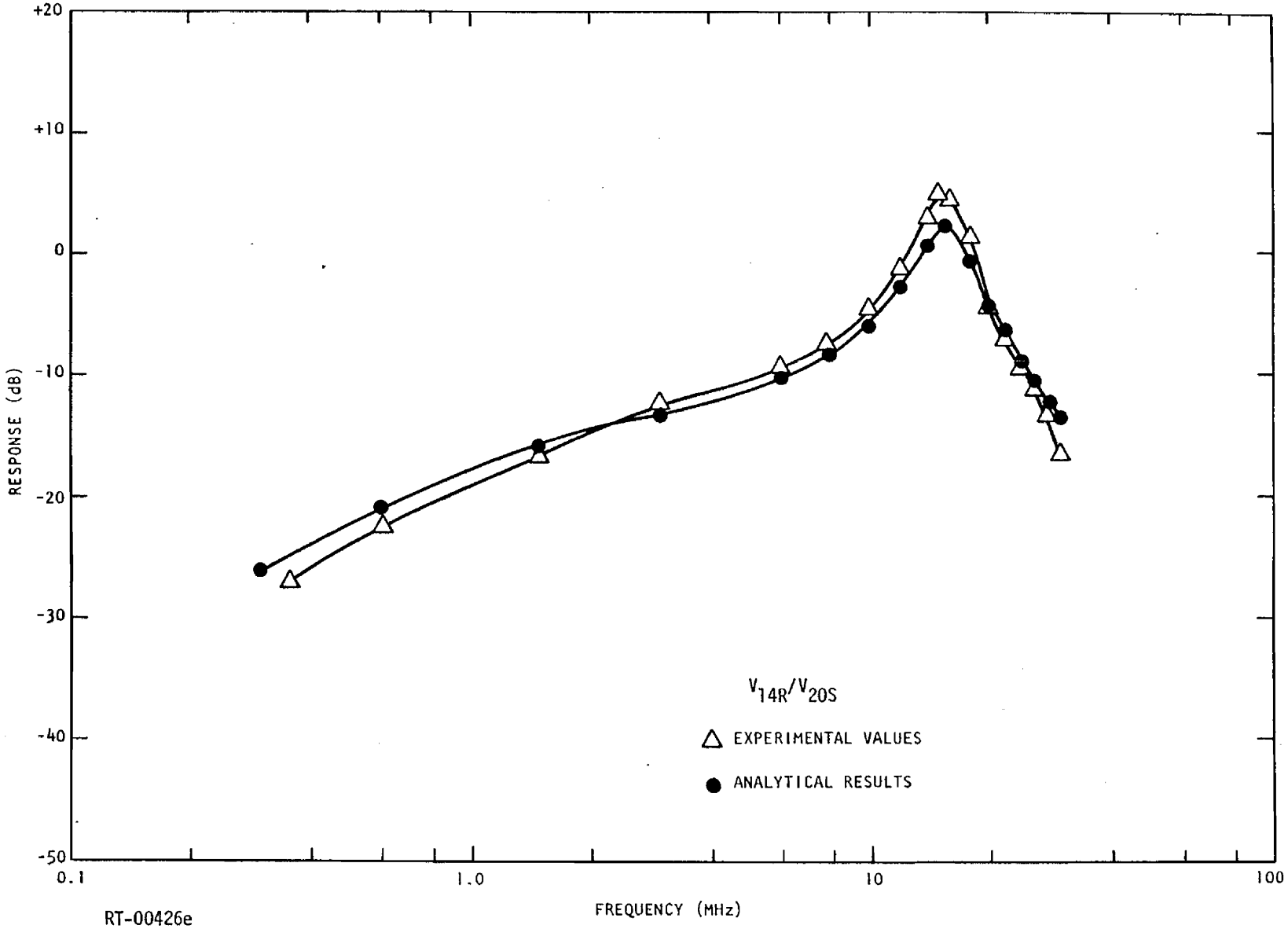
+20
+10
0
-10
-20
-30
-40
-50
RESPONSE (dB)
0.1
1.0
10
100
FREQUENCY (MHz)
V_{14R}/V_{20S}
EXPERIMENTAL VALUES
ANALYTICAL RESULTS
RT-00426e

Fig. 5.25e

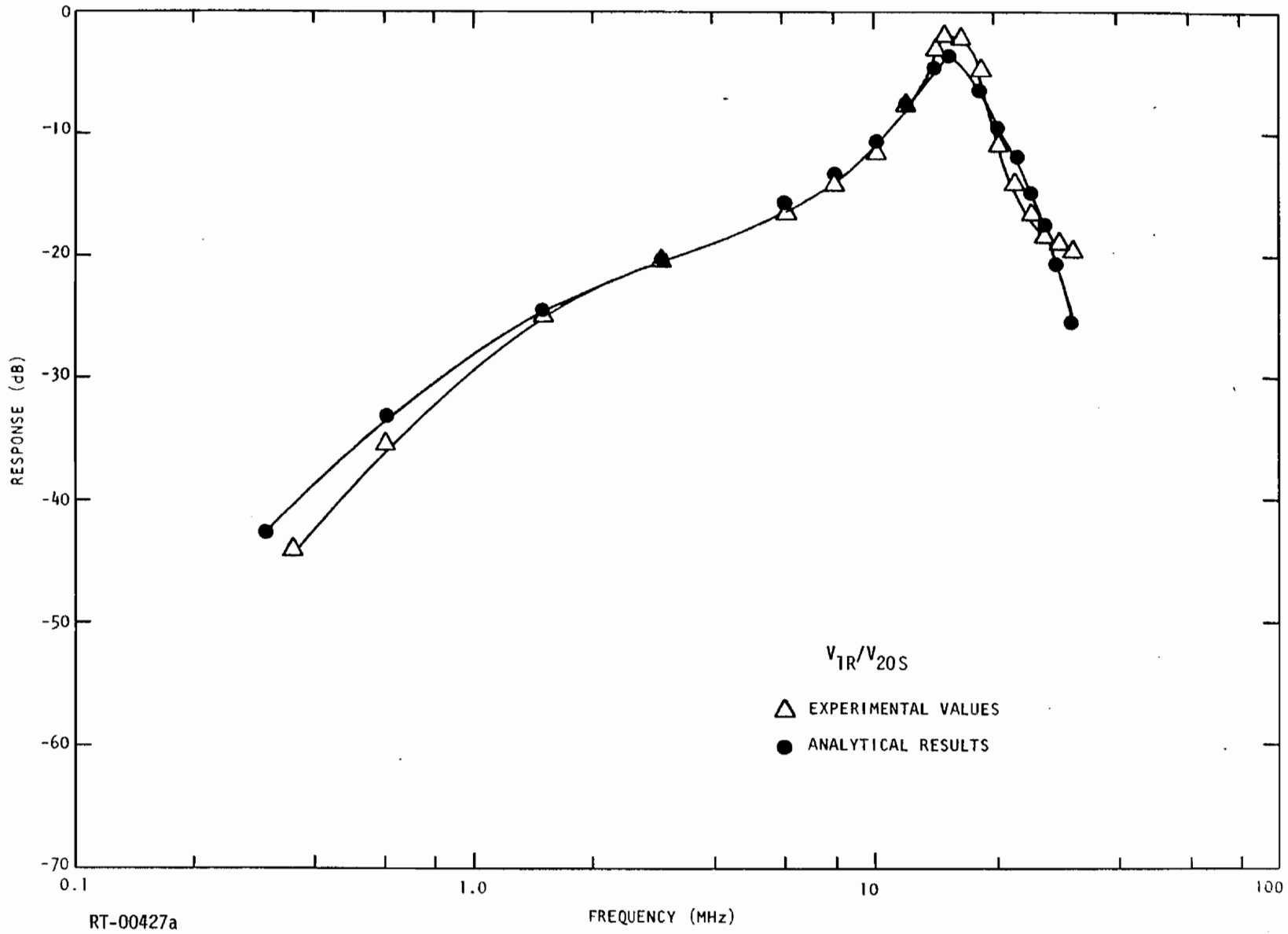

Fig. 5.26a. Transfer functions for 9-conductor grouped cable, open-Z method parameters

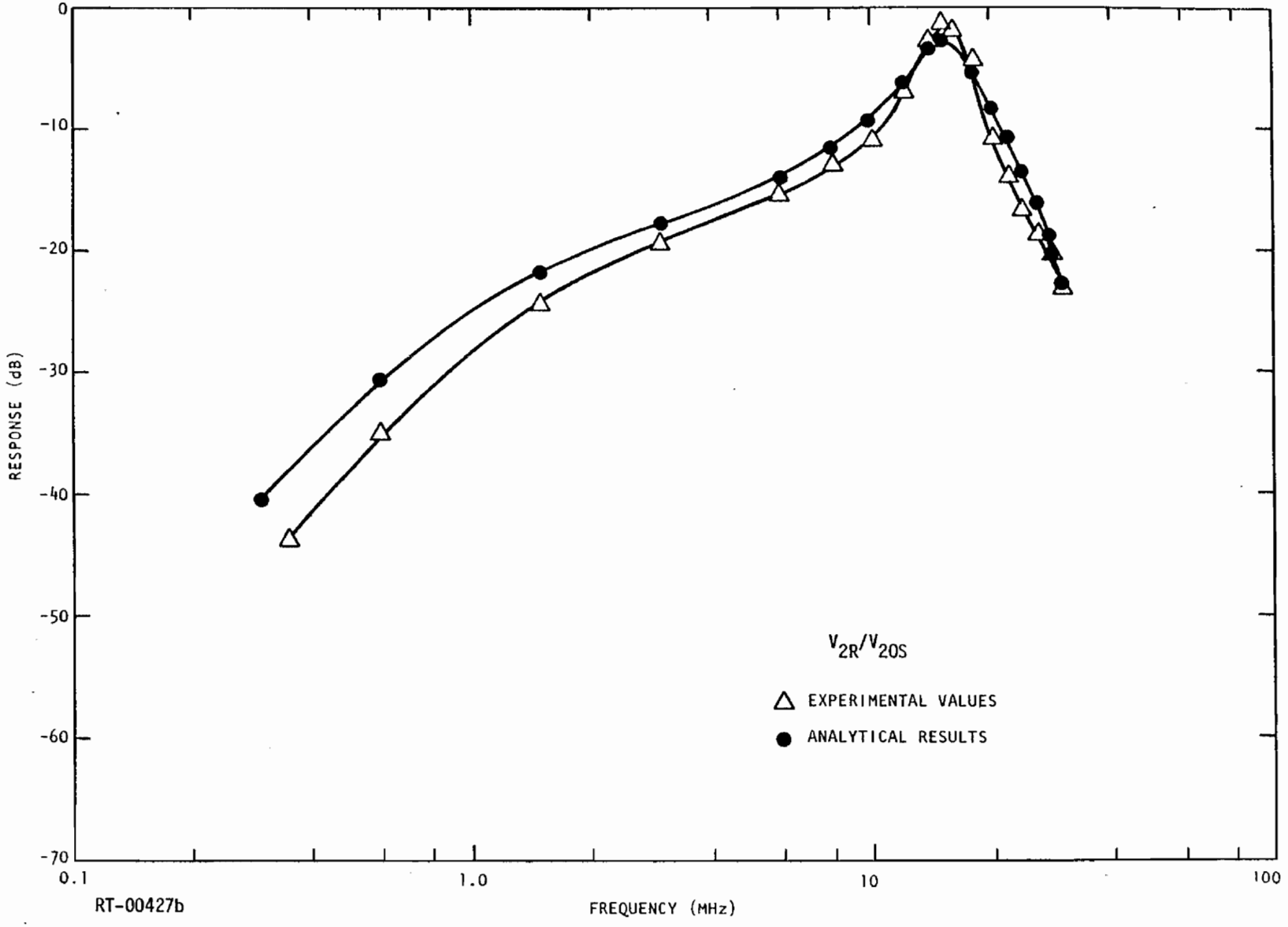
0
-10
-20
-30
-40
-50
-60
-70
RESPONSE (dB)
0.1
1.0
10
100
FREQUENCY (MHz)
RT-00427b
V_{2R}/V_{20S}
EXPERIMENTAL VALUES
ANALYTICAL RESULTS

Fig. 5.26b

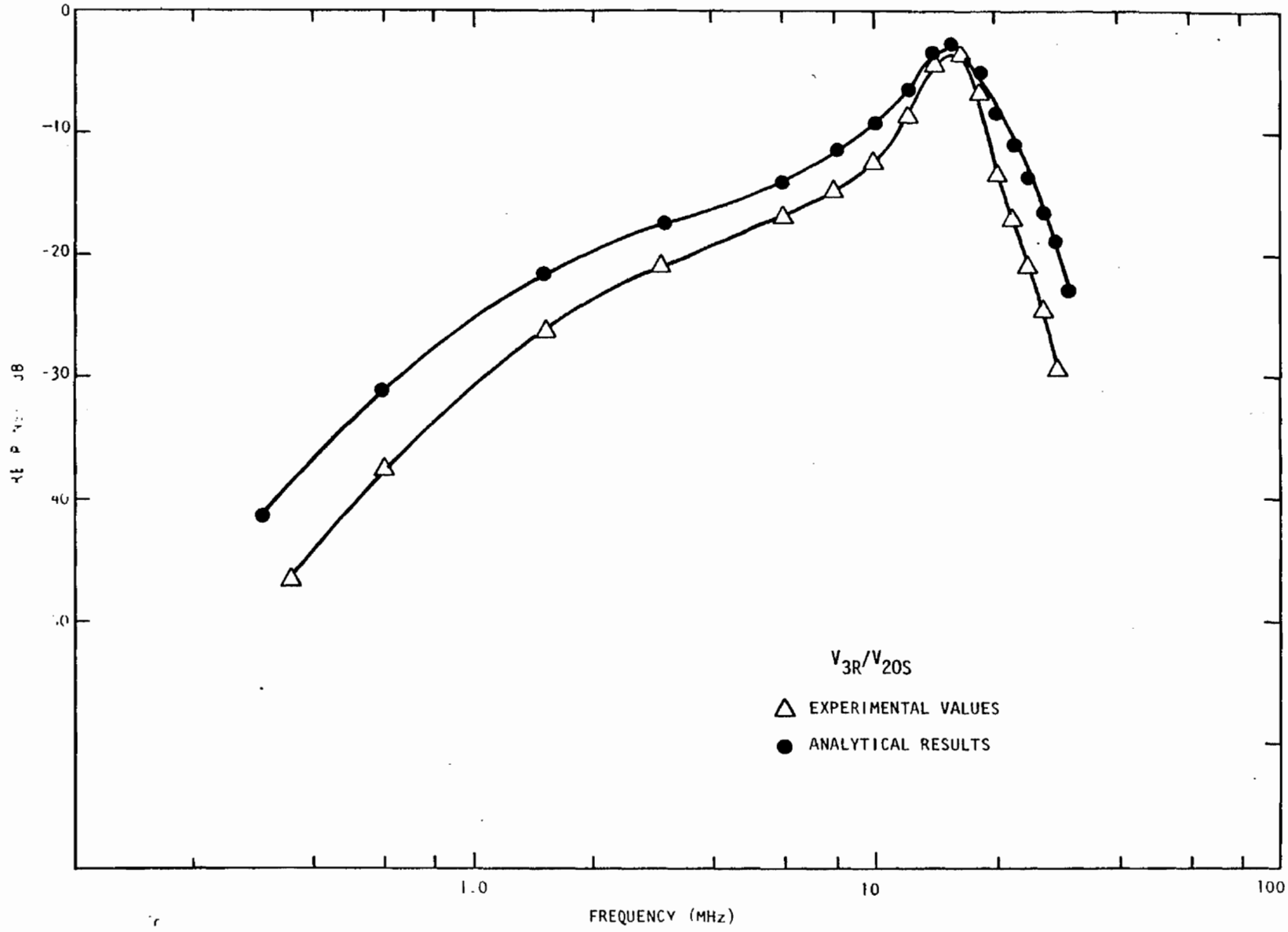
0
-10
-20
-30
1.0
10
100
FREQUENCY (MHz)
V_{3R}/V_{20S}
EXPERIMENTAL VALUES
ANALYTICAL RESULTS

Fig. 5.26c

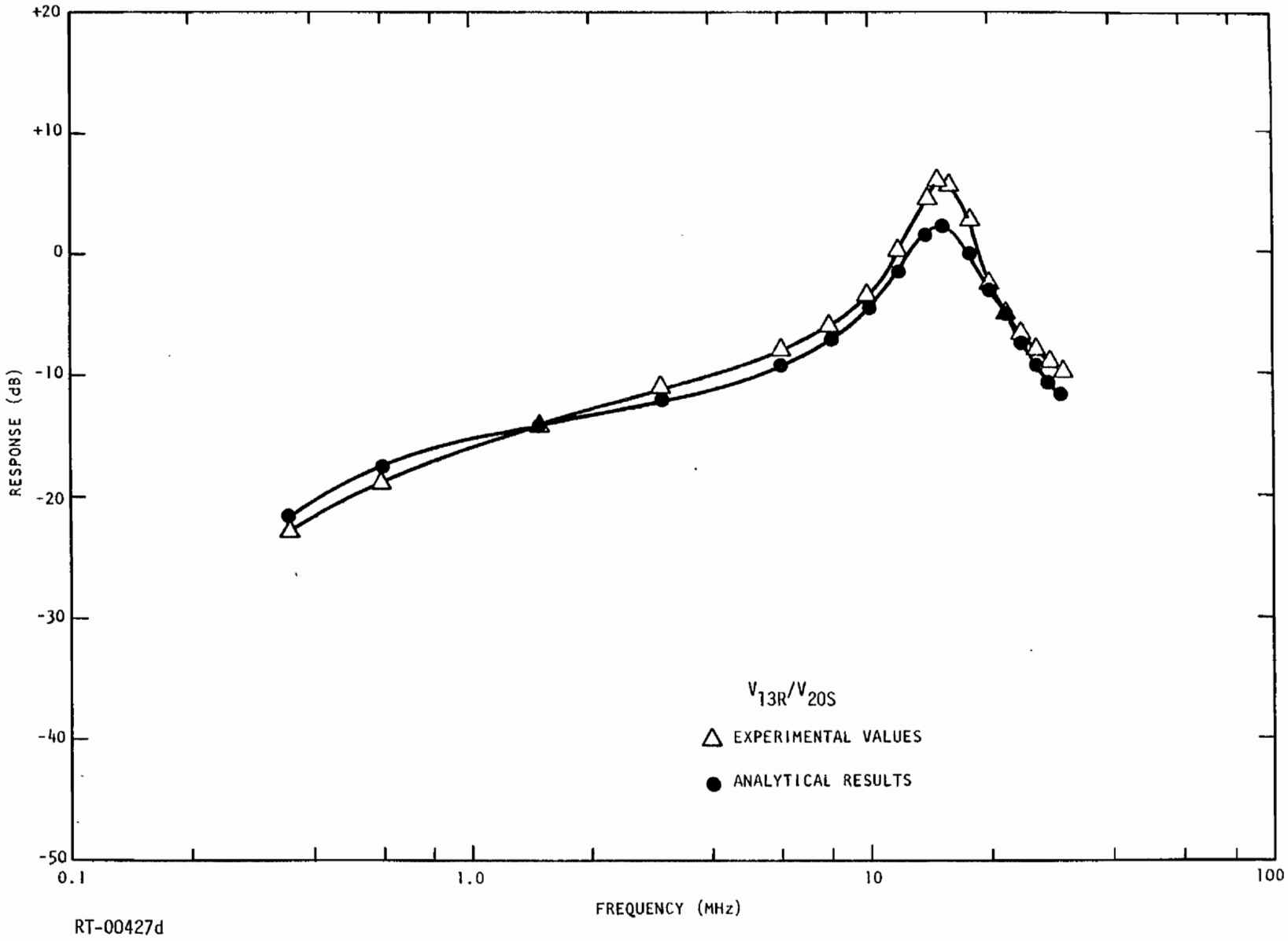
+20
+10
0
-10
-20
-30
-40
-50
RESPONSE (dB)
0.1
1.0
10
100
FREQUENCY (MHz)
V_{13R}/V_{20S}
EXPERIMENTAL VALUES
ANALYTICAL RESULTS
RT-00427d

Fig. 5.26d

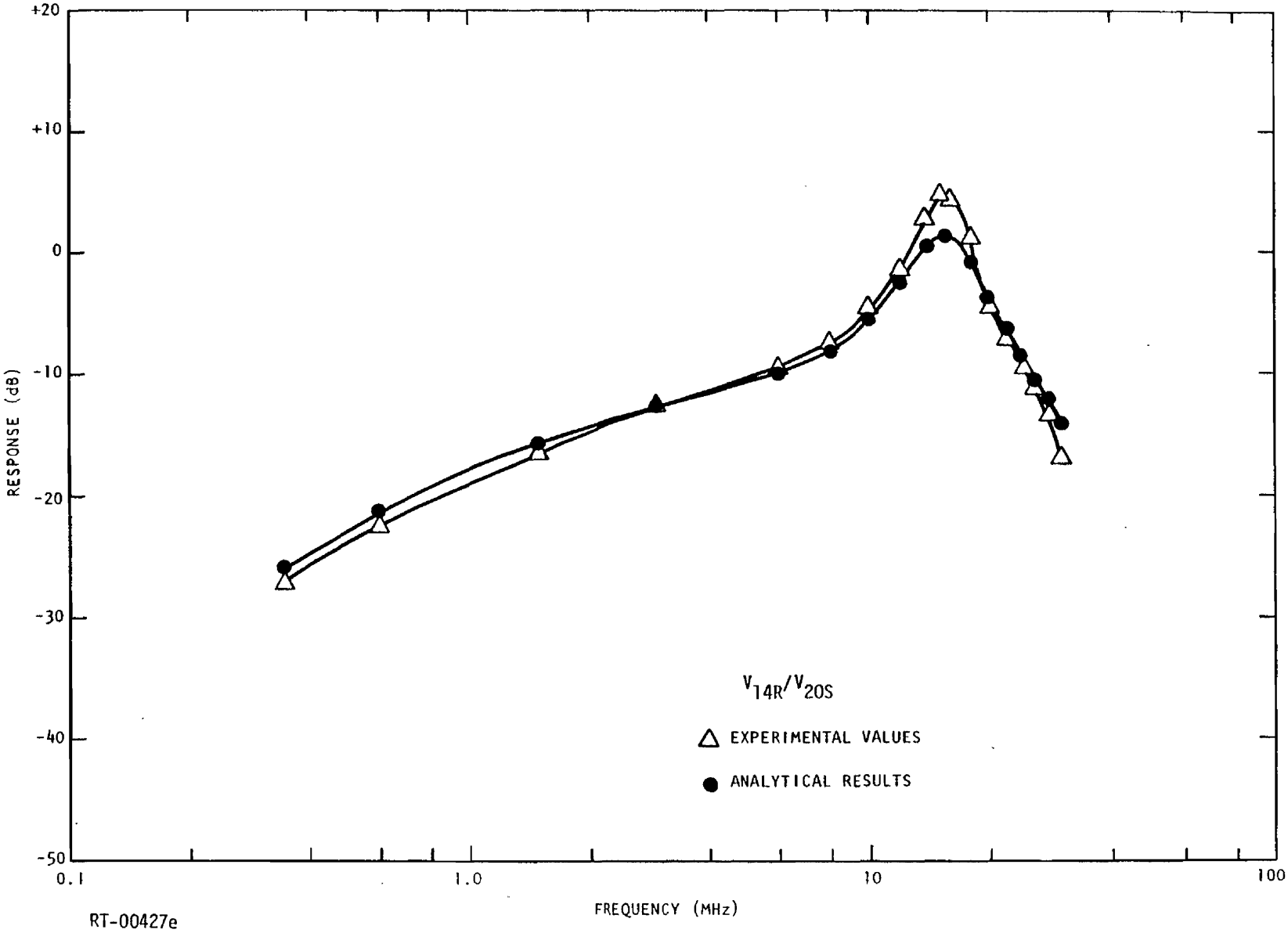
+20
+10
0
-10
-20
-30
-40
-50
RESPONSE (dB)
0.1
1.0
10
100
FREQUENCY (MHz)
V_{14R}/V_{20S}
EXPERIMENTAL VALUES
ANALYTICAL RESULTS
RT-00427e

Fig. 5.26e

Table 5.4

BREAKDOWN OF RESULTS BY METHOD

Method	Results			
	Good	Fair	Poor	Total
Capacitance	20 (48%)	22 (52%)	0	42
Open-Z	10 (42%)	13 (54%)	1 (4%)	24
Shorted-Z	6 (32%)	11 (58%)	2 (10%)	19
Total	36 (42%)	46 (54%)	3 (4%)	85

Table 5.4 shows that the results were "Good" for >40% of the sample, "Fair" for >50%, and that "Poor" results occurred for a very small (only 4%) part of the sample. It should also be noted that, of the "Fair" results, about half were very near the 6-dB limit, so that overall, ~70% of the results were within ~6-dB agreement between analysis and experiment. Thus, the methods which have been presented in this report are clearly useful for modeling of complex cables.

A point which must be emphasized again is that these results were obtained with absolutely no attempt made to alter the calculated parameters to obtain better agreement between analysis and experiment. The originally calculated parameters, altered only as necessary to eliminate obviously unreasonable values, were used for all analytical calculations.

Table 5.4 also shows rather clearly that no one method stands out as being the best from the standpoint of results obtained. Thus, there is not a "method of choice" based on results. There is, however, a subjective order of preference based on difficulties encountered while measuring parameters on the cables and calculating the model parameters.

This order of preference is (1) capacitance method, (2) open-Z method, and (3) shorted-Z method.

The capacitance method is preferred for the following principal reasons: (1) the measurements require the least operator interpretation and are, therefore, less subjective; (2) accuracy is essentially uniform over the range of values to be measured; and (3) connection problems are minimized.

Considering reason (1), with the impedance methods, the impedance mismatch at the transition between the known standard and the unknown pair being measured, combined with nonuniformity of the actual unknown impedance, makes the waveforms very difficult to interpret. This is not the case with the capacitance method, where all that is required is to obtain a null on the capacitance bridge and make direct readings of the dial.

Considering reason (2), we have noted previously that, as the measured impedances range further from the value of the standard, resolution and accuracy are severely affected. This is not the case with capacitance bridges, as they have nearly equal accuracy over all their ranges.

Considering reason (3), the impedance mismatch problem mentioned above greatly complicates the problem of having a convenient method of connecting to the unknown, and convenience is required when so many measurements are necessary. Again, the capacitance bridge does not suffer from this problem.

The open-Z method is preferred over the shorted-Z method due to the fact that the Z_{ij}^{m} values are much closer to the 50-ohm standard with the open-Z method, resulting in better accuracy. The use of standards nearer the unknown impedance has the potential to solve this problem, but such standards are not generally available.

The conclusions from this effort are, then, that (1) the modeling techniques are useful for complex cables, yielding results within ~6 dB in ~70% of the cases and (2) the capacitance method of determining L and C parameters is the preferred one where applicable.

6. MISCELLANEOUS TOPICS

During the course of the analytical and experimental investigations, a number of somewhat unrelated but very important observations were made. These are discussed in this section.

6.1 VERIFICATION OF PARAMETER VALUES

The ultimate use of the measured cable parameters is, of course, in an analytical model of that cable. In order to verify that the analytical model accurately represents the real cable, results of analytical solutions for the model can be compared to cable experimental results for similar excitation and termination schemes. But it is important to note that the termination scheme will have a strong effect on whether the coupling between wires is predominantly electric field or magnetic field, or some combination of both. This effect will, in turn, determine whether or not the accuracy of both mutual L and C parameters are being tested, or whether only one of them is tested by a given configuration.

Analysis of the analytical and experimental results for the shielded twisted trio demonstrates the problem very nicely. The model parameters for the cable, as determined by three different methods, are presented in Table 6.1. A summary comparison of the analytical and experimental results over the frequency range 0.3 to 10 MHz is presented in Table 6.2. Examination of Table 6.2 and the actual transfer function plots in Section 5.3 shows that by far the best agreement between analysis and experiment occurred for the model using parameters determined by the capacitance method. Therefore, using these capacitance method

Table 6.1

MODEL PARAMETERS FOR SHIELDED TRIO

$\underline{C^P}$ or $\underline{L^P}$ Element	Capacitance		Open-Z		Shorted-Z	
	C^P (pF/m)	L^P (μH/m)	C^P (pF/m)	L^P (μH/m)	C^P (pF/m)	L^P (μH/m)
11	111	0.189	94	0.194	112	0.458
12	12.7	0.018	22.3	0.036	7.0	0.137
13	13.1	0.020	23.5	0.038	17.6	0.134
22	118	0.183	100	0.187	139	0.468
23	10.5	0.016	21.9	0.035	9.2	0.144
33	113	0.189	94	0.194	125	0.469

Table 6.2

COMPARISON OF EXPERIMENTAL AND ANALYTICAL RESULTS FOR SHIELDED TRIO FOR FREQUENCIES FROM 0.3 TO 10 MHz

(Driven Wire Terminated in 1000 ohms)

Transfer Function	Analytical Amplitude Error in dB		
	Capacitance	Open-Z	Shorted-Z
V_{3S}/V_S	-0.3 to +2	+5 to +7	+3 to +5
V_{2S}/V_S	0 to +3	+5 to +7.5	-4 to -6
V_{1R}/V_S	0 to +2*	0 to +2*	0 to +2*
V_{2R}/V_S	+0.3 to +2	+5 to +7	0 to -6
V_{3R}/V_S	+0.5 to +1.5	+5.5 to +7	+3 to +4.5
$f\lambda/4$**	24 MHz	24 MHz	21.5 MHz

*This figure applies up to 8 MHz only. At 10 MHz, the error increased to +5 dB due to the shift in frequency between experiment and analysis of the sharp resonant peak at one-quarter wavelength. This is the receiving end of the driven wire.

**The experimental value is 17 MHz.

parameters as the reference, the shift in mutual L and C parameters determined by the other two methods were expressed in dB. These parameter shifts in dB are then compared to the crosstalk response curve shifts in dB in Table 6.3.

Table 6.3

COMPARISON OF CROSSTALK SHIFT TO MUTUAL PARAMETER SHIFT

(Driven Wire Terminated in 1000 ohms)

	Open-Z vs Capacitance			Shorted-Z vs Capacitance		
Wire Pair	Crosstalk Shift (dB)	Mutual C^P Shift (dB)	Mutual L Shift (dB)	Crosstalk Shift (dB)	Mutual C^P Shift (dB)	Mutual L Shift (dB)
1-2	4.5 to 5	+4.9	+6.0	-0.3 to 9	-5.2	+17.6
1-3	5 to 5.5	+5.1	+5.6	2.5 to 3	+2.6	+16.5

Table 6.3 shows very clearly that the shift in crosstalk response agrees very well with the shift in mutual capacitance parameters, but very poorly with the shift in mutual inductance parameters. Thus, for this case, the mutual capacitance parameters only have been verified, due directly to the fact that the driven wire was terminated in a high impedance, 1000 ohms. That is, for this high-impedance termination, very little current flows on the driven wire and the mutual inductance has little, if any, effect on the resulting crosstalk response curve. Thus, the mutual L parameters could well be in considerable error, even though the analytical and experimental response curves agree quite well.

In order to verify the mutual L parameters, then, it is necessary to terminate the driven wire so that these parameters will dominate the crosstalk response. A short-circuit termination on the driven wire will

accomplish this. A summary comparison of experimental and analytical results for such a configuration is shown in Table 6.4. Again, from examination of this table and the data plots in Section 5, the capacitance-based parameters still give the best agreement. In Table 6.5, the crosstalk shift for the short-circuited drive wire is compared to the mutual parameter shift previously calculated. Although the agreement between the crosstalk shift and mutual L shift is not as good as noted before when mutual C dominated the coupling, the results are still indicative that the coupling is, in fact, being dominated by the mutual L parameters.

In summary, if it is necessary to verify the model parameters, care must be exercised in the technique used. It will not be generally valid to use just any terminating impedance on the driven line. The verification will require two sets of comparisons, one for a high-impedance termination so that capacitance will dominate crosstalk, and one for a low-impedance termination so that inductance will dominate. By this method, the accuracy of each set of parameters can be verified.

6.2 ERRORS RESULTING FROM ASSUMPTION OF UNIFORM PHASE VELOCITY

In Section 2.2, we developed the equation relating the $\underline{L}$ and $\underline{K}$ matrices for a cable with nonuniform phase velocities for the individual conductors; i.e.,

$$\underline{L}\,\underline{K} = (\underline{v}_p^{\,2})^{-1}$$

where

$$\underline{v}_p = \begin{bmatrix} v_{p_{ii}} = \text{phase velocity of } i^{th} \text{ wire to return} \\ v_{p_{ij}} = 0 \qquad i \neq j \end{bmatrix} .$$

Table 6.4

COMPARISON OF EXPERIMENTAL AND ANALYTICAL RESULTS FOR SHIELDED TRIO FOR FREQUENCIES FROM 0.3 TO 10 MHz

(Driven Wire Terminated in a Short Circuit)

Transfer Function	Analytical Amplitude Error in dB		
	Capacitance	Open-Z	Shorted-Z
V_{3S}/V_S	-8 to +1.5	-2.5 to +6.5	+2.5 to +9.5
V_{2S}/V_S	-4 to +1	+1.5 to +6.5	+4 to +7
V_{2R}/V_S	-6 to +1.5	0 to +6.5	+6 to +13.5

Table 6.5

COMPARISON OF CROSSTALK SHIFT TO MUTUAL PARAMETER SHIFT

(Driven Wire Terminated in a Short Circuit)

Wire Pair	Open-Z vs Capacitance			Shorted-Z vs Capacitance		
	Crosstalk Shift (dB)	Mutual C^p Shift (dB)	Mutual L Shift (dB)	Crosstalk Shift (dB)	Mutual C^p Shift (dB)	Mutual L Shift (dB)
1-2	+5 to +7.5	+4.9	+6.0	+6 to +12	-5.2	+17.6
1-3*	+5 to +5.5	+5.1	+5.6	+8 to +10.5	+2.6	+16.5

*Sending-end data only.

As noted, then, if the phase velocities are uniform or are assumed to be uniform, this reduces to

$$\underline{L}\,\underline{K} = \frac{\underline{I}}{v_p^2}$$

where v_p is the uniform phase velocity. This latter form of the equation is the one which was used throughout the subsequent modeling work on actual cables, even though two of them exhibited quite nonuniform phase velocities. The expected errors in parameters due to the assumption of uniform v_p will be discussed here.

The mean phase velocities and the variation of phase velocity for the five cables are shown in Table 6.6. The 20-conductor random cable exhibited the widest percentage range of variation of the cables modeled.

Table 6.6

MEAN PHASE VELOCITY AND VARIATION FOR MODELED CABLES

Cable	Mean v_p x 10^8 m/sec	Variation (%)
20-Conductor, Controlled	2.02	+4.6/-3.1
20-Conductor, Random	1.71	+9.4/-21.0
11-Conductor	1.85	+4.9/-17.8
Shielded Trio	1.98	~0
3-Branch Cable	1.91	~0

Only the $\underline{L}$ parameters, as determined by the capacitance method applied to the 20-conductor random cable, will be in error due to errors in v_p since the $\underline{K}$ parameters were determined directly from capacitance

measurements. The L_{ii} can each be expressed in terms of the $\underline{K}$ parameters and $1/v_{p_i}^2$; e.g., for N = 2,

$$L_{11} = \frac{1}{v_{p_1}^2 (K_{11} - K_{12}^2/K_{22})}$$

and

$$L_{22} = \frac{1}{v_{p_2}^2 (K_{22} - K_{12}^2/K_{11})} .$$

Now, if we have assumed a uniform phase velocity $\overline{v_p}$ and $v_{p1} \neq v_{p2} \neq \overline{v_p}$, L_{11} and L_{22} will be in error by

$$\Delta L_{ii} = \frac{1}{k} \Delta \frac{1}{v_{p_i}^2} = \frac{1}{k} \left(\frac{1}{v_{p_i}^2} - \frac{1}{\overline{v}_p^2} \right)$$

where k is a constant of proportionality determined by v_{p_i} and the appropriate K_{ij}. For an error as large as the -21% shown in Table 6.6,

$$\Delta \frac{1}{v_{p_i}^2} = \frac{1}{[\overline{v_p} (1 - 0.21)]^2} - \frac{1}{\overline{v_p}^2}$$

$$= \frac{1}{0.62\, \overline{v_p}^2} - \frac{1}{\overline{v_p}^2} = 60\% ,$$

and then the error in the corresponding L_{ii} will be 60%. Since the L_{ij} can be expressed in terms of L_{ii}, the L_{ij} may be erroneous by as much as 60% also. This same analysis can be applied to the more complex case (i.e., N > 2).

This analysis shows very clearly that the assumption of uniform phase velocity can produce significant errors, and these may well account for the only fair results obtained for cables 3 and 4. It should be noted, however, that the spread in v_{p_i} will probably never be very much greater

than that shown in Table 6.6 for the 20-conductor random cable, and if only approximate results are required, the assumption of uniform v_p may be adequate.

6.3 SEPARATE MODELING OF CABLE AND STRUCTURE

Section 6.2 discussed the errors which result from the assumption of uniform v_p when in fact v_p is not uniform. One conductor pairing where the difference in v_p is frequently very large is between a wire in a cable and a piece of structure over which the cable is located. This is a problem only if the structure is treated as a part of the multiconductor transmission line for the actual parameter measurements.

The reason for this difference in v_p is that cables are usually supported at some distance, (on the order of a cable diameter or more) from the structure. Thus, for the pairing mentioned above, the dielectric medium is predominantly air, and v_p then approaches the velocity of waves in a vacuum, c. The velocity between pairs within the cable will be only on the order of 0.5c of 0.7c, however, based on measurements on the example cables.

The easy way to get around this problem for shielded cables is simply to use a two-step approach; i.e., first, model the cable with the shield as the reference, using the techniques of Section 4, and second, model the structure to the shield pair, using either the same methods or else from conductor geometry. The result is a complete model with the shield as the reference.

If it is desired to have the structure as the reference, some manipulation of the parameters is required. The necessary modifications, presented here without proof, are:

1. To each L_{ii} of the cable, add an inductance equal to the inductance of the shield-structure circuit, L_{ss}.

2. Add to the shield an inductor of value L_{ss}.

3. Add between each L_{ii} and L_{ss} a mutual L_{is} equal to L_{ss}.

A simple example will illustrate the approach.

An RG58A coaxial cable has a capacitance of 101 pF/m and a phase velocity of 0.66 c, as specified in a catalog. This is a cable of N = 1, and the value of L_{11} is

$$L_{11c} = \frac{1}{v_p^2 C_{11}} = 0.253 \ \mu H/m \ .$$

There are no mutuals, of course. It is desired to model this cable for the case of the cable suspended 1.0 inch (to cable center) above a ground plane. The shield-to-ground plane parameters, as determined from simple geometry, are

$$C_{ss} = 16.8 \text{ pF/m}$$

and

$$L_{ss} = 0.663 \ \mu H/m \ .$$

The models for the cable alone and for the shield-ground plane pair above are shown in Figs. 6.1a and b, respectively, for 1-m-long π sections. To combine these models into a single model, the shield inductance shown in Fig. 6.1b must be added to the shield conductor of Fig. 6.1a, which does not have an inductor. Then L_{11} must be increased to

$$L_{11} = L_{11c} + L_{ss}$$

$$= 0.253 + 0.663 = 0.916 \ \mu H/m \ ,$$

and a mutual L_{1s} equal to L_{ss} must be added between L_{11} and L_{ss}. The final model is as shown in Fig. 6.2. This model has been tested using both time-domain and frequency-domain techniques, and has been shown to be accurate.

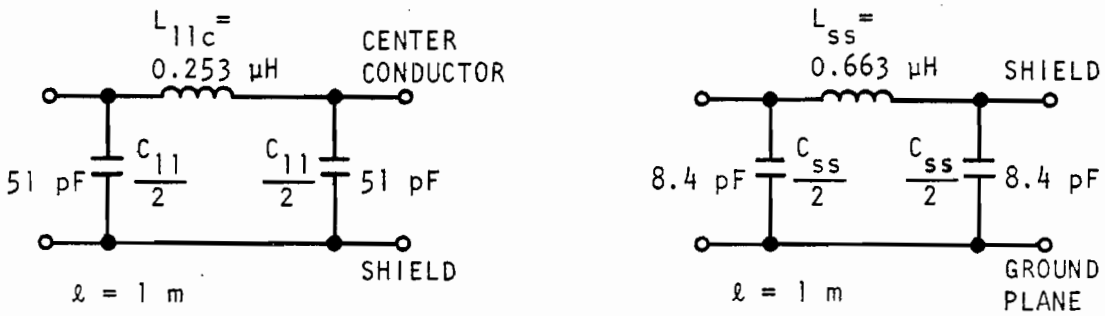

a. Coax cable alone

b. Shield-to-ground plane alone

RT-00434

Fig. 6.1. Two components of the model of a coaxial cable over a ground plane

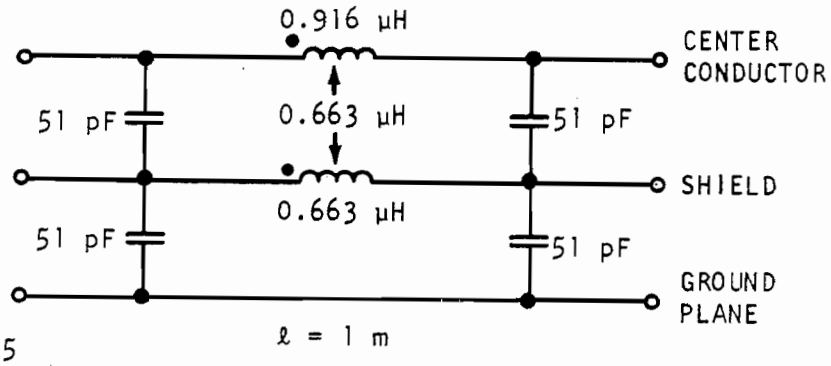

RT-00435

Fig. 6.2. Combined model of a coaxial cable over a ground plane

It is interesting to compare these parameters to two other sets of parameters derived by (1) direct calculation from geometry only and (2) the capacitance method of Table 4.1, using a uniform v_p. The three sets of L parameters are summarized in Table 6.7. The capacitances are, of course, unaffected by the method used.

Table 6.7

PARAMETERS FOR COAX OVER GROUND PLANE AS DETERMINED BY THREE METHODS

Parameter	Method 1 Direct Calculation	Method 2 Capacitance*	Method 3 Separate Modeling
L_{11}	0.954	1.065	0.919
L_{ss}	0.662	0.915	0.661
L_{1s}	0.678	0.915	0.661

*Assuming a uniform v_p equal to the average of the cable velocity (0.66 c) and shield-structure velocity (~c); i.e., $\overline{v_p} = 0.83$ c.

The direct calculation method treated the center conductor-ground plane and shield-ground plane pairs separately to obtain L_{11} and L_{ss}. L_{1s} was determined from circuit theory to be

$$L_{1s} = \frac{L_{11} + L_{ss} - L_{11c}}{2}$$

$$= \frac{0.954 + 0.662 - 0.253}{2} = 0.678 \ .$$

As may be seen, good correlation is achieved between methods 1 and 3. This good correlation results from the fact that, in both of these methods, the actual velocity of propagation for each pair of conductors was used. In method 2, however, an average value between v_p for pair

1-s (0.66 c) and v_p for pair s-g (~1.0 c) was used, i.e., v_p = 0.83 c. That value is ~15% low for the s-g pair and, when squared and inverted, results in an error of

$$\Delta\frac{1}{v_p^2} = \left(\frac{1}{(0.83\ c)^2} - \frac{1}{c^2}\right)\ 100\%$$

$$= \left(\frac{1.39}{c^2} - \frac{1}{c^2}\right)\ 100\% \ = \ 39\% \ .$$

Multiplying the L_{ss}, as determined by methods 1 and 3, by 1.39 results in

$$L_{ss(0.85\ c)} = 1.39\ (0.66\ \mu H) = 0.915\ \mu H \ ,$$

which is the value determined by method 2, as expected. In this case, the use of an average v_p resulted in an error of ~40%. Similarly, the difference between L_{11} and L_{ss}, which is the inductance of the coaxial pair 1-s, is ~60% low for method 2 because the average v_p used was too high (v_p in RG58A is 0.66 c rather than 0.83 c).

The use of separate modeling of cable and shield to structure is the recommended method, based on the results. Another big advantage of this method is that it allows the cables to be brought into the laboratory for the necessary measurements rather than having to do them in the field, as would be required in many cases.

6.4 VERIFICATION OF THE R_{ac} MEASUREMENT TECHNIQUE

The R_{ac} measurement technique described in Section 4.4 was applied to four different coaxial cables. Since such cables have specified attenuation factors, the corresponding R_{ac} values can be calculated from these and can serve as a check on the laboratory method. The measurements and calculations were made as follows.

A Tektronix 191 constant-amplitude generator (V_{oc} = 10 V_{p-p}, R_o = 50 Ω) loaded with a 50-ohm termination was used to excite the sending end of the cable and the sending end voltage (V_{IN}) was measured using a Tektronix 454 scope with a P6047 X10 probe. The open-circuit voltage at the receiving end (V_{OUT}) was measured with a Hewlett-Packard 410B vacuum tube voltmeter. The generator was swept from the lowest frequency obtainable (0.35 MHz) to the frequency of the first V_{OUT} peak and V_{IN} null. Because the V_{OUT} peak tends to be broad and the V_{IN} null very sharp, the null was used as the $\lambda/4$ resonance indicator. The frequency, V_{IN}, and V_{OUT} were then recorded.

From the experimental results on the four cables, the values of K and of R_{ac} at 10^8 Hz have been calculated. They are shown in Table 6.8 along with values of R_{ac} as determined from the Belden catalog specified attenuation factors at 10^8 Hz using the approximate relation

$$R = 2 \alpha Z_0 ,$$

where α is in nepers/unit length. In each case, the specified value of Z_0 was used for the calculations rather than measuring the actual Z_0. The agreement between experimental and specified values of R_{ac} is quite good, especially considering that the "specified" value is only a nominal one, and probably subject to some variation.

It is interesting to note the variation of α with frequency as specified in the catalog for these four cables. Assuming that Z_0 remains constant, then α will vary only due to variation of R_{ac}. Table 6.9 shows the actual variation of nominal α versus the variation predicted by $R_{ac} = \sqrt{f}$, using 10^8 Hz as the baseline value of α for both cases, for the four cables. Comparing these, it appears that R_{ac} is not varying exactly as $\sqrt{f}$ even at these high frequencies.

6.5 EFFECT OF R_{ac} VARIATION ON ANALYTICAL RESULTS

The discussions of L and C parameter value determination for actual cables and the comparisons of analytical and experimental results for these cables has given insight into the effects of L and C variation on the analytical results. In order to gain the same insight into the effects of R_{ac} variation, two sets of runs were made on the 20-conductor random cable, using the calculated values of R_{ac} and twice the calculated values.

The results for two typical transfer functions are shown in Figs. 6.3a and b. As can be seen in these two plots, the effect of a 2:1 variation in R_{ac} is not very great, being on the order of 2 dB except in resonant dips, where the effect is as great as 6 to 10 dB. For these transfer functions, the calculated values give the best results, indicating that they are correct.

This lack of sensitivity to R_{ac} and the relative ease and accuracy with which R_{ac} can be determined indicates that no problems are to be expected.

It should be noted that, in these two transfer functions and all of those shown in Section 5.3, R_{ac} has been treated as having a $\sqrt{f}$ variation, i.e.,

$$R_{ac} \text{ at } f = K\sqrt{f} .$$

6.6 MODELING OF CABLES WITH FOUR OR MORE BRANCHES

When the two impedance methods of determining L and C were first developed, it was hoped that they would have sufficient resolution to be able to determine parameters in "trunk" sections of very complex cables such as shown in Fig. 6.4. Applying the methods to very simple coaxial cable versions of the cable shown in Fig. 6.4 did, in fact, produce good results. That is, the impedance of each segment of the cable could be determined, even though they were quite different.

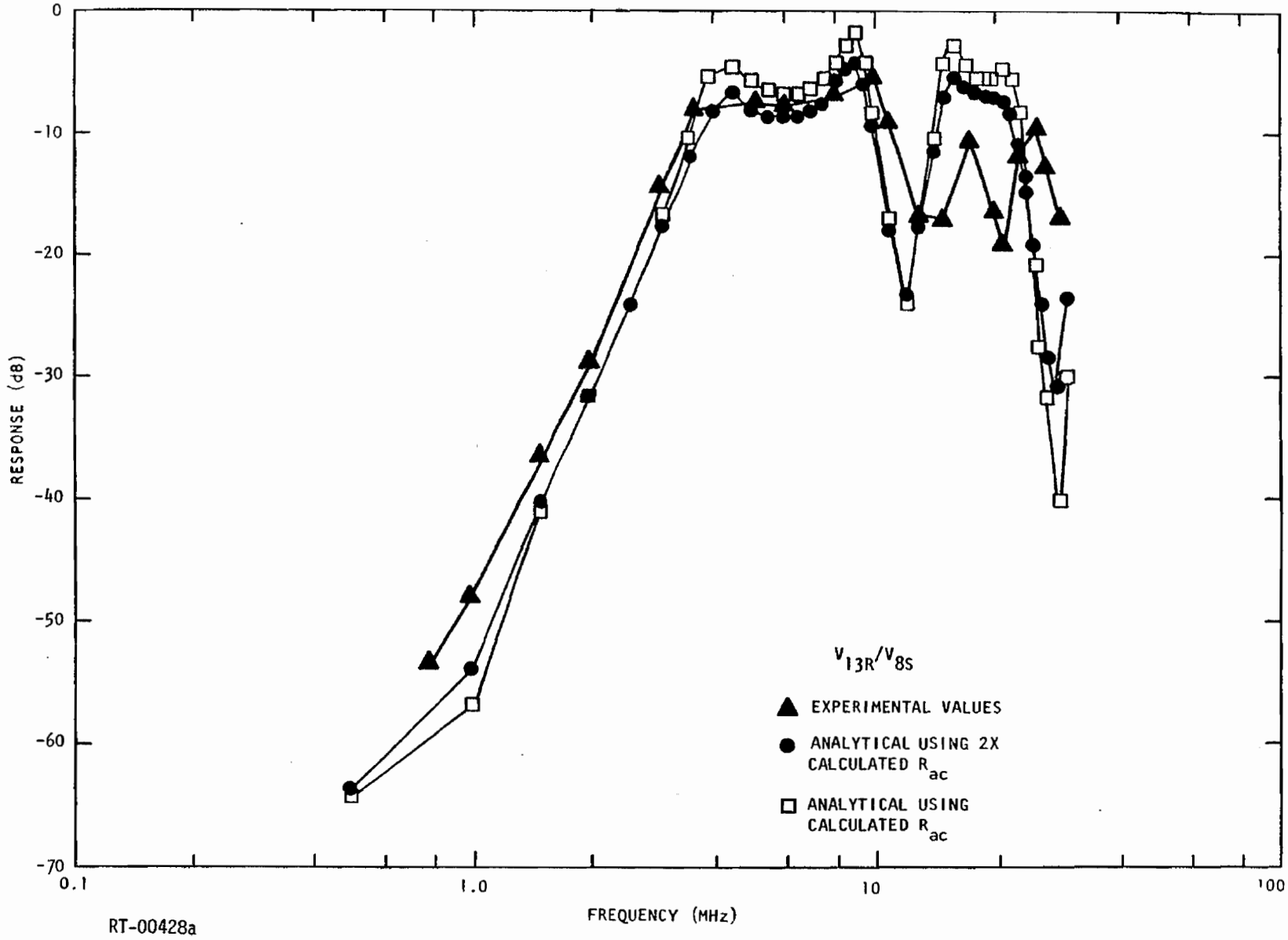

Fig. 6.3a. Transfer functions for 20-conductor random cable, two R_{ac} values

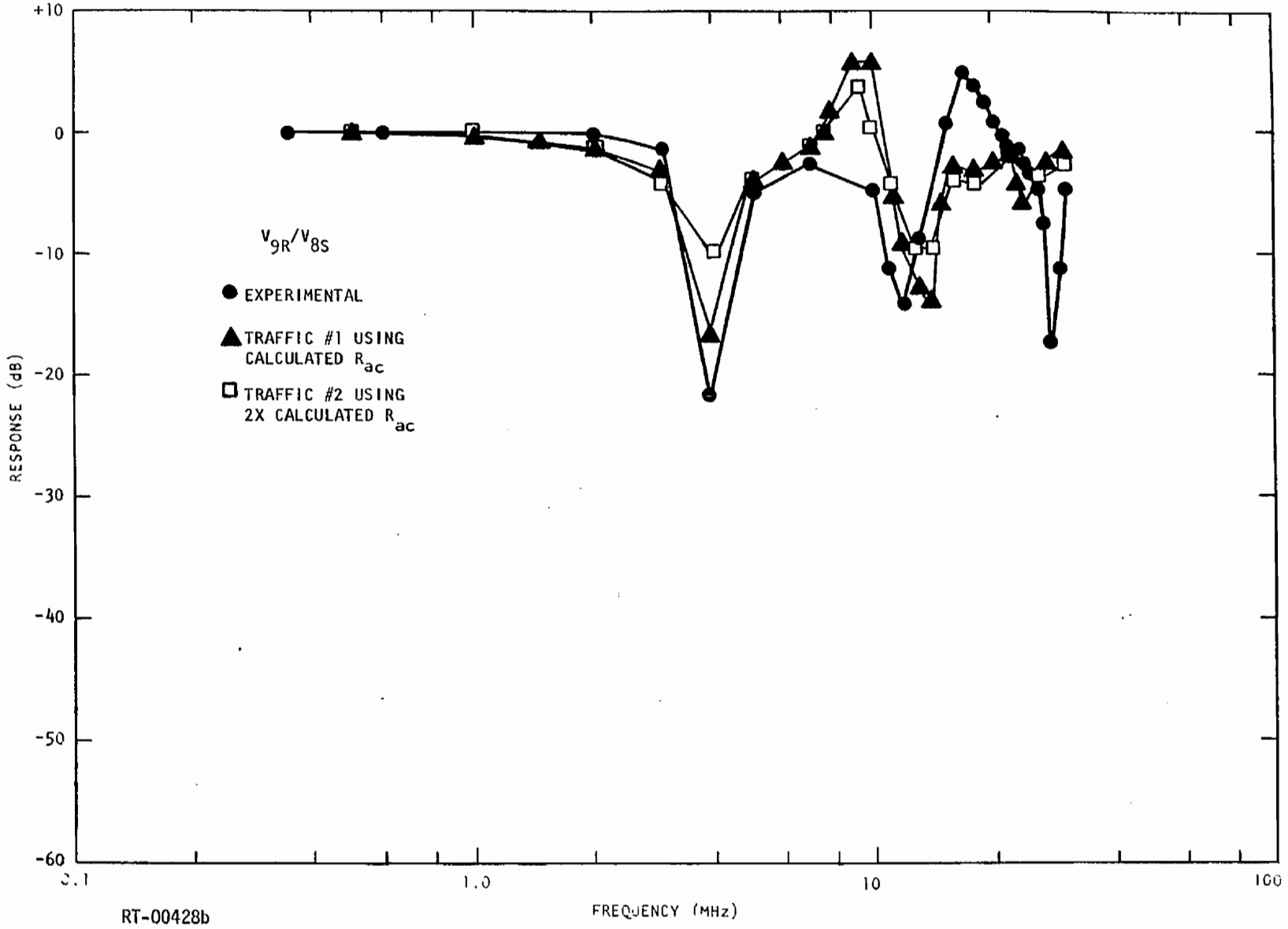
+10
0
-10
-20
-30
-40
-50
-60
RESPONSE (dB)
V_{9R}/V_{8S}
EXPERIMENTAL
TRAFFIC #1 USING CALCULATED R_{ac}
TRAFFIC #2 USING 2X CALCULATED R_{ac}
0.1
1.0
10
100
FREQUENCY (MHz)
RT-00428b

Fig. 6.3b

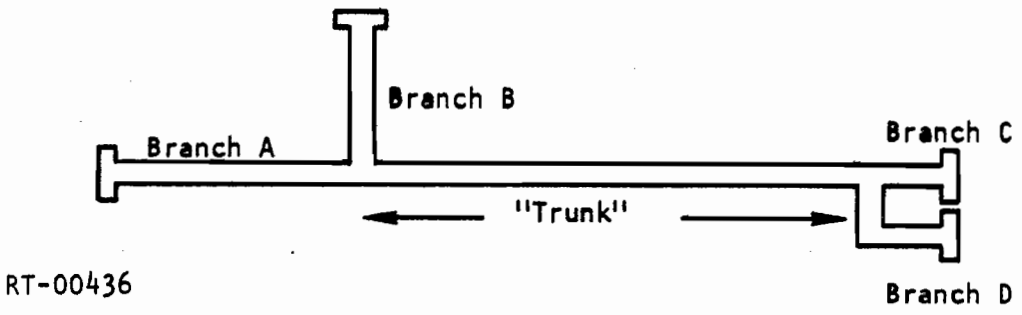

Fig. 6.4. Cable with four branches and "trunk"

Unfortunately, real multiconductor cables are simply not as well behaved as are coaxial cables. For cables of any complexity at all, it was not possible to distinguish between segments with all the myriad reflections that were occurring from the various junctions and ends. Thus, whenever a cable contains such a "trunk" section which cannot be reached directly, the only approach possible will be to dissect the cable so that each segment becomes available. This will undoubtedly render the cable useless, and that being the case, the process of dissection can be carried to the point of separating every segment. Then the preferred capacitance method can be applied.

6.7 TDR IMPEDANCE MEASUREMENT ACCURACY AS A FUNCTION OF STANDARD IMPEDANCE

The problem of measuring, with a TDR, impedances which are significantly different from the standard value (50 ohms) of the TDR have been mentioned repeatedly. A more detailed discussion of the problem will be presented here.

A typical TDR calculator scale is shown in Fig. 6.5. The instructions for use of this calculator are as follows.

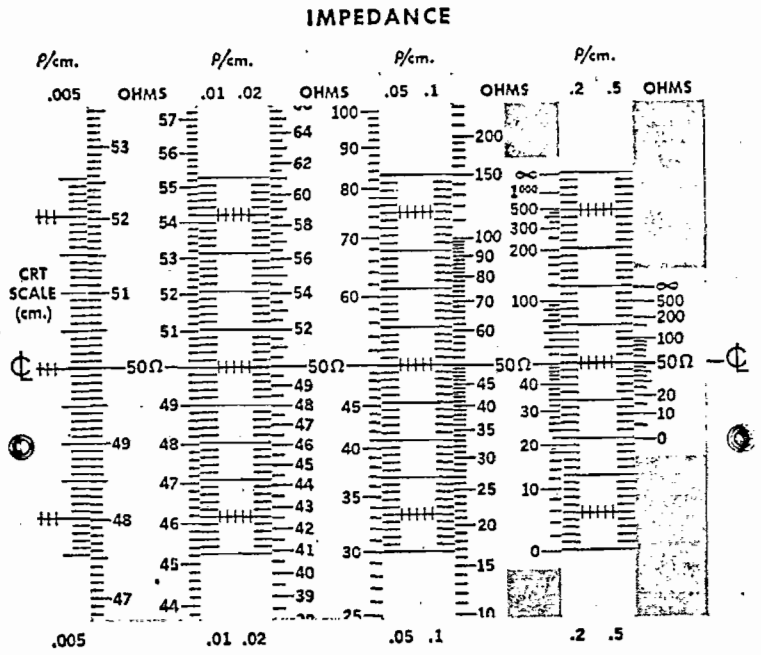

Fig. 6.5. Typical TDR calculator scale, 50-ohm standard

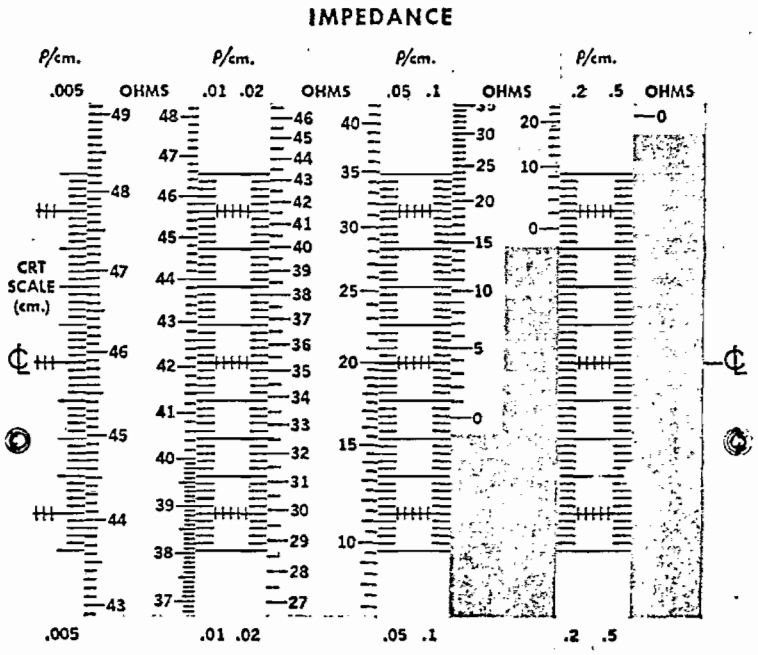

Fig. 6.6. Typical TDR calculator scale, 20-ohm standard on ρ/cm = 0.05 scale

1. On oscilloscope, set the reflection from a known impedance even with the center horizontal graticule line. Note setting of Reflection Coefficient (ρ/cm) control.
2. On the appropriate ρ/cm scale of the slide rule, set the known impedance at the center line (℄).
3. Replace known impedance with the unknown, and note the deflection from the center line.
4. Read impedance at appropriate CRT scale marking on slide rule.

The problem in applying these instructions is that only a limited deflection, usually ±5 cm, is available on the oscilloscope. If the unknown impedance is very much different from the 50-ohm standard, then lower-resolution ρ/cm scales must be used to keep the deflection within the range of the scope. The ρ/cm = 0.1 scale, for example, can only measure impedance in the range 16 to 150 ohms. Outside this range, the ρ/cm = 0.2 scale must be used, which covers the full range 0 to ∞. These larger ρ/cm scales, unfortunately, suffer from very poor resolution, being on the order of only ±1 ohm for the ρ/cm = 0.2 scale.

The TDR calculator shown in Fig. 6.5 is for a known standard of 50 ohms. Figure 6.6 shows a view of the calculator set up for a 20-ohm known standard on the ρ/cm = 0.05 scale. From this, impedances in the range 9 to 35 ohms can be read with very high resolution. This points out clearly the gains to be achieved from the use of lower impedance standards. The two impedance methods for determining L and C, and in particular the shorted-Z method, will not be fully tested until such lower impedance standards are used.

Ideally, a range of standards (e.g., 10, 20, 35, 50, 75, and 100 ohms) should be available so that the optimum one — i.e., the one which allows use of the smallest ρ/cm scale — can be used for each measurement.

7. SUMMARY AND CONCLUSIONS

This report has presented in considerable detail the theoretical background and practical problems of a technique for modeling of multiconductor cables. The important results will be summarized here for convenience, and appropriate conclusions drawn from these results.

7.1 THEORETICAL BACKGROUND

The theoretical foundation for the technique requires the assumption of pure TEM-mode signal propagation between conductor pairs. This is not a significant limitation so long as:

1. Frequencies of interest are below $\sim 10^8$ Hz,
2. Conductor size and spacings are less than ~1 cm, and
3. Attenuation is less than ~20 dB/m.

Conditions 2 and 3 are met for nearly all practical cable bundles, and condition 1 is an acceptable limit for most applications.

With the assumption of pure TEM propagation, the transmission line differential equations for an N+1 conductor line with uniformly distributed parameters and sinusoidal excitation are

$$\frac{d^2}{dx^2}\vec{E} = \underline{Z}\,\underline{Y}\,\vec{E}$$

and

$$\frac{d^2}{dx^2}\vec{I} = \underline{Y}\,\underline{Z}\,\vec{I},$$

where $\underline{Z}$ and $\underline{Y}$ are NxN matrices and $\vec{E}$ and $\vec{I}$ are Nx1 column vectors. The elements of $\underline{Z}$ and $\underline{Y}$ are defined by

$$Z_{ii} = R_{ii} + j\omega L_{ii} \qquad i = 1, 2 \ldots N$$

$$Z_{ij} = j\omega L_{ij} \qquad i \neq j$$

and

$$Y_{ii} = \sum_{j=1}^{N} (G_{ij} + j\omega C_{ij}) \qquad i = 1, 2 \ldots N$$

$$Y_{ij} = -(G_{ij} + j\omega C_{ij}) \qquad i \neq j \ .$$

The solutions to these differential equations are

$$\vec{E} = \exp(\underline{\gamma} x)\ \vec{E}_{+} + \exp(-\underline{\gamma} x)\ \vec{E}_{-}$$

and

$$\vec{I} = \exp(\underline{\gamma}' x)\ \vec{I}_{+} + \exp(-\underline{\gamma}' x)\ \vec{I}_{-} \ .$$

The Nx1 column vectors $\vec{E}_{+}$, $\vec{E}_{-}$, $\vec{I}_{+}$, and $\vec{I}_{-}$ are constants determined by the boundary conditions. The matrices $\underline{\gamma}$ and $\underline{\gamma}'$ are the propagation constants for voltage and current waves, respectively, and they will, in general, be NxN matrices. Two special cases were examined and produced the results that (1) for uniform propagation constants on all conductor pairs, $\underline{\gamma} = \underline{\gamma}' = \gamma \bar{I}$ where γ is a scalar; and (2) if wire interaction is neglected, $\underline{\gamma} = \underline{\gamma}'$ where $\underline{\gamma}$ is formed by placing the N individual propagation constants γ_i on the diagonal with all off-diagonal terms equal to zero.

If the line is assumed lossless, the real terms in $\underline{Z}$ and $\underline{Y}$ disappear, and the attenuation constants α_{ii} in $\underline{\gamma}$ also go to zero. Then

$$\underline{L}\underline{K} = (\underline{v_p}^2)^{-1} \qquad \text{(nonuniform } v_p\text{)}$$

or

$$\underline{L}\underline{K} = \frac{\vec{I}}{v_p^2} \qquad \text{(uniform } v_p\text{)}$$

where

$$\underline{v}_p = \begin{bmatrix} v_{p_{ii}} = \text{phase velocity of wire i to return} \\ v_{p_{ij}} = 0 \end{bmatrix}$$

and

$$v_p = \text{uniform or average phase velocity .}$$

The characteristic impedance matrix $\underline{Z_0}$ is defined in the same manner as for the two-conductor case; i. e.,

$$\underline{Z_0} = \frac{\underline{L}}{\underline{K}} = \frac{1}{v_p} K^{-1} = v_p \underline{L} .$$

These equations relating $\underline{K}$, $\underline{L}$, $\underline{Z_0}$, and $\underline{v}_p$ form the basis for three methods of determining the distributed L and C parameters for cables from certain measured parameters.

7.2 MODEL DEVELOPMENT TECHNIQUE

The interrelation of the transmission line parameters shows that if any two sets of parameters can be determined, then all four sets are known. The phase velocity matrix is the easiest to determine, since it requires only the measurement of N phase velocities which then form the $\underline{v}_p$ matrix or are used to find the average v_p. Of the remaining three parameter sets, $\underline{L}$ is the most difficult to determine, and so attention is directed toward determining $\underline{K}$ and/or $\underline{Z_0}$.

The definitions of the elements of $\underline{K}$ are inherent in the definition of $\underline{Y}$, since $\underline{Y} \rightarrow \underline{K}$ for the lossless case; i. e., all $G_{ij} = 0$. Then,

$$K_{ii} = \sum_{j=1}^{N} C_{ij} ,$$

and

$$K_{ij} = -C_{ij} .$$

The C_{ij} is the actual partial capacitances which exist between wires, and these cannot be measured directly with a bridge due to interaction with other wires. However, by making capacitance measurements on a cable in a specified manner (see Table 4.1), the K_{ii} and K_{ij} terms can be calculated. These can then be manipulated to obtain the partial capacitances directly, and the inductance matrix can be obtained using the phase velocity matrix.

The capacitance method cannot be used for cables with three or more branches because the various branches cannot be distinguished using a capacitance bridge. However, impedances can be measured with time-domain reflectometry (TDR) techniques, and the time and distance resolution of this technique allows the branches to be distinguished from one another. As with $\underline{K}$, the $\underline{Z_0}$ matrix cannot be measured directly, but by making impedance measurements in a specified manner (see Table 4.2), the elements of $\underline{Z_0}$ can be calculated. Then, using the phase velocity matrix, $\underline{L}$ and $\underline{K}$ can be determined, and the partial capacitances can be calculated from $\underline{K}$.

A third method was also developed, one which requires a different set of impedance measurements but which is based on the same theoretical foundation. This method is shown in Table 4.3.

In addition to these L and C parameters, real terms are required in the model to account for losses. The real terms are series resistance R and shunt conductance G. It was shown in Section 4 that R dominates losses for practical cable dimensions and materials, and G was consequently neglected. A method for calculating R_{ac} for wire pairs was then developed, based on measuring

$$\left.\begin{matrix} E_{OUT} \\ E_{IN} \end{matrix}\right\} \text{ at the quarter-wavelength resonant frequency, } f_{\lambda/4} ,$$

ℓ in meters ,

Z_0 in ohms ,

and calculating R_{ac} from

$$R_{ac} \text{ at } f_{\lambda/4} = \frac{2\ Z_0}{\ell} \left(\frac{E_{IN}}{E_{OUT}\Big|_{f_{\lambda/4}}} \right) .$$

The assumptions used in developing the method require that (1) input impedance of the instrument used for measuring E_{OUT} be high (1.5 to 15 kΩ) at the measurement frequency ($f_{\lambda/4}$), and (2) that the total cable loss ($\alpha \ell$) be small ($\leq$0.8 neper). For the worst-case parameters observed during the modeling effort, this latter requirement is met for cables up to ~100 m in length, but to allow a margin of safety, the actual length used should be limited to about 10 m. It should be emphasized that this low total loss requirement applies only to the cable on which the measurements are made; it in no way limits losses on the overall cable model.

In the actual cable model, the ac resistances calculated by this method are assumed to vary as $\sqrt{f}$ over all frequencies, and then

$$R_{ac} \text{ at } f = K \sqrt{f}$$

where

$$K = \frac{R_{ac} \text{ at } f_{\lambda/4}}{\sqrt{f}_{\lambda/4}} .$$

The $\sqrt{f}$ variation is valid for practical cable conductors only for frequencies above ~1 MHz, and if a model is to be used below this frequency, some additional error must be expected. The resistance factor K determined for wire pairs can be apportioned to the individual wires by (1) measuring a number of pairs and solving simultaneous equations, (2) by having one conductor of each pair be a known K, or (3) by judgment for many simple cases.

With the necessary distributed inductance, capacitance, and series resistance parameters available, a lumped-parameter equivalent circuit

model can be created. This model can then be analyzed using any available computer code capable of handling the resulting network size. The maximum errors resulting from the use of the lumped approximation, as a function of the section length in wavelengths, were calculated in Section 3 and are summarized in Fig. 7.1. These results allow the creation of models no more complex, in terms of model sections, than required to meet the desired accuracy limits or, conversely, allow the prediction of error bounds where computational ability limits total network size. An example will illustrate the significance of this ability. Consider a typical missile cable of 20-m length and a phase velocity of 2×10^8 for which a model good to 30 MHz is desired. Applying the frequently used rule of thumb that section lengths of 0.1λ at the highest frequency of interest will yield "good" results, the cable model requires only 30 sections, but the resulting error bounds are ±16.8 dB. To meet an arbitrarily set accuracy limit of ±6 dB, the model requires 85 sections. This example shows clearly that to obtain reasonable accuracy (e.g., factor of 2) for cables of even moderate length at relatively high frequency requires the use of a great many model sections. Thus, in preparing to model multiconductor cables, the required accuracy and upper-frequency limits should not be set arbitrarily, but rather, careful consideration must be given to establishing reasonable limits.

7.3 RESULTS OBTAINED FOR REAL CABLES

The modeling technique described was applied to a number of actual cables of varying complexity. The modeling and experimental program on actual cables produced a total of 85 transfer functions taken on six cable configurations, using the three different methods for determining the L and C parameters. A breakdown of the resulting agreement between analysis and experiment, by method, is shown in Table 5.4, page 189. The results were "Good" (±3 dB agreement over most of the frequency range) for >40% of the sample, "Fair" (6 to 14 dB) for >50%, and "Poor" (>14 dB) results

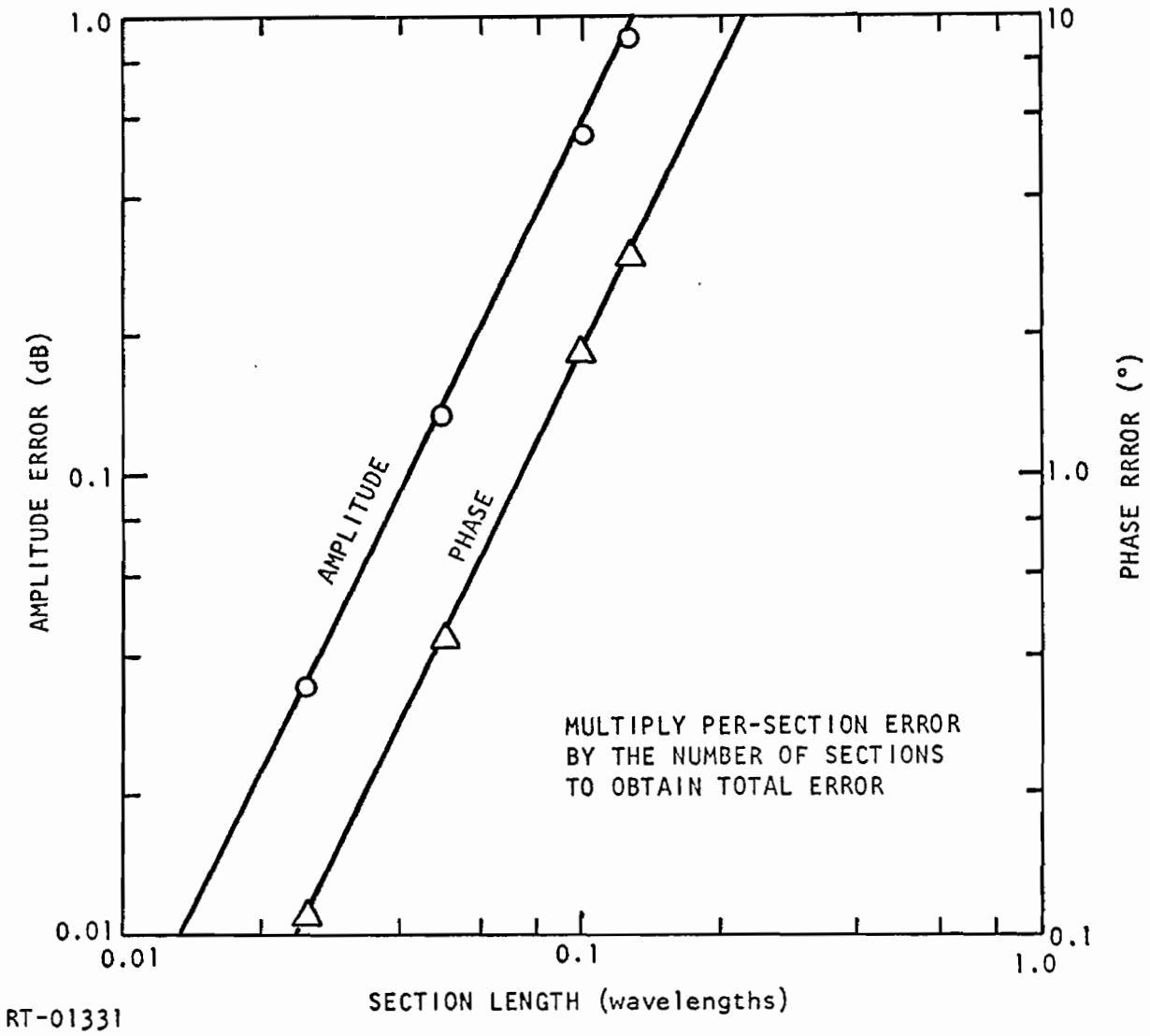

Fig. 7.1 Worst-case amplitude and phase errors per section versus section length

occurred for a very small (only 4%) part of the sample. It should also be noted that, of the "Fair" results, about half were very near the 6-dB limit, so that, overall, ~70% of the results were within ~6 dB agreement between analysis and experiment. These results were obtained with absolutely no attempt made to alter the calculated parameters to improve agreement between analysis and experiment. The originally calculated parameters, altered only as necessary to eliminate obviously unreasonable values, were used for all analytical calculations.

The modeling effort also showed that, while based on sound theoretical foundations, all three of the methods for determining inductance and capacitance parameters suffered problems in practical applications. The problems resulted from errors and uncertainties in the required measurements which, at times, produced obviously unreasonable capacitance parameters. However, it was also shown that judgment could be used to correct these unreasonable values.

No one method stands out as being the best from the standpoint of results obtained; thus, there is not a "method of choice" based on results. There is, however, a subjective order of preference based on the difficulties encountered while measuring parameters on the cables and calculating the model parameters. This order of preference is (1) capacitance method, (2) open-Z method, and (3) shorted-Z method.

The two impedance-based methods which were developed specifically to handle multibranch cables yielded good results on a cable with three branches. A sample cable with four branches and a "trunk" section, which could not be reached directly, was also examined. This examination showed rather conclusively that impedances within this trunk cannot be measured from the branch ends due to the presence of numerous reflections. Thus, such cables must be dissected to make the required measurements.

The modeling effort also revealed a very important consideration regarding experimental verification of cable model parameters. A generally

valid cable model must have accurate L and C parameters. If it is desired to test the accuracy of the model by experimental verification, termination schemes which adequately test both L and C parameters will be required. To verify the L parameters, low-impedance ($<\sim$10 ohms) termination of the driven wire is required to maximize magnetic coupling. Conversely, to test the C parameters, high-impedance ($>\sim$ 1 kΩ) termination of the driven wire is required to maximize electric-field coupling. If the real-life cable terminations are known to always be high or low, this may not be necessary. But then the simplifications suggested by Greenstein and Tobin[12] may be useful, obviating the need for a distributed model.

The complexity of the models required for even a 20-wire cable prompted a very brief investigation into grouping of some wires for purposes of modeling. This concept is based on the realization that, in many cases, not every wire will be of interest from the standpoint of detailed signal distribution. The results of this investigation were encouraging and indicate that the concept merits further investigation.

One final point which should be made is that, even though the methods for determining L and C were based on the assumption of a lossless line, they have been shown to be applicable to lossy cables.

7.4 CONCLUSIONS

A number of important conclusions can be drawn from the results of this modeling program.

1. Accuracy of Results: All three methods for determining L and C parameters are capable of good results, within ±6 dB for most cases.
2. Preferred Method: The capacitance method is preferred because it is least subject to measurement error and ambiguity.

3. Multibranch Cables: Using the impedance methods, branches can be modeled without dissecting the cable, but "trunk" sections cannot.
4. Model Simplification: Grouping, for purposes of modeling, of uninteresting wires within a cable appears to have merit.
5. Lumped-Element Approximation: Arbitrary accuracy can be obtained, but accuracy and upper-frequency limit must be traded off against model simplicity for even moderately long (~20 m) cables.

The only limitations resulting from the various assumptions made during the theoretical development are as follows.

Cable Physical Characteristics

1. The technique is intended to be used with "tightly packed" cable bundles; i. e., conductor spacings should be small ($<\sim 1$ cm).
2. Conductor sizes are limited to those found in practical cables; i. e., No. 22 AWG or greater, but less than ~1-cm maximum diameter of largest internal shield or conductor.
3. The techniques require uniformity with respect to distance on the cable. For practical cables, this implies no abrupt transposition of internal conductors, but twisting and gradual weaving in and out are acceptable.
4. Internal shielding of wires is permissible.

Cable Electrical Characteristics

1. Attenuation must be less than 20 dB per meter. Practical cables have, at most, a few dB/m attenuation up to 100 MHz.
2. Total loss on the cable on which R_{ac} measurements are made must be ≤ 0.8 neper. The maximum length used should, therefore, not exceed ~10 m.

Frequency Range

The assumptions generally require operation in the range 1 to 100 MHz. However, based on the results obtained, the lower-frequency limit can be extended to at least 100 kHz. The upper-frequency limit can be extended to at least 300 MHz, so long as the conductor size and spacing limitations are not exceeded and the loss remains below 20 dB/m.

REFERENCES

1. J. J. Karakash, "Transmission Lines and Filter Networks," Macmillan Publishing Company, 1950.
2. R. K. Moore, "Traveling-Wave Engineering," McGraw-Hill Publishing Company, 1960.
3. S. A. Schelkunoff, "Electromagnetic Waves," van Nostrand Publishing Company, 1943.
4. W. B. Boast, "Principals of Electric and Magnetic Fields," Harper and Rowe, 1948.
5. D. Kajfez, "Scattering Matrix Approach to the Multiconductor Transmission Lines," National Technical Information Service PB 197-578, December 1970.
6. "Reference Data for Radio Engineers," 5th Ed., Howard W. Sams & Company, p. 22-13.
7. H. Kogo, "A Study of Multielement Transmission Lines," IEEE Trans. Microwave Theory and Techniques, March 1960.
8. R. A. Chipman, "Theory and Problems of Transmission Lines," Shawn Outline Series
9. H. Kaden, "Wirbelstrome und Shirmung in der Nachrichtentechnik," Springer-Verlag.
10. G. A. and T. M. Korn, "Mathematical Handbook for Scientists and Engineers," McGraw-Hill Book Company, 1961.
11. Ramo, Whinnery and Van Duzer, "Fields and Waves in Communication Electronics," Wiley & Sons, 1965.
12. Greenstein and Tobin, "Analysis of Cable-Coupled Interference," IEEE Trans. Radio Frequency Interference, March 1963.

UNCLASSIFIED
Security Classification

DOCUMENT CONTROL DATA - R & D

(Security classification of title, body of abstract and indexing annotation must be entered when the overall report is classified)

1. ORIGINATING ACTIVITY (Corporate author)	2a. REPORT SECURITY CLASSIFICATION
Gulf Radiation Technology P. O. Box 608 San Diego, California 92112	Unclassified
	2b. GROUP

3. REPORT TITLE

MODELING TECHNIQUES FOR MULTICONDUCTOR CABLES: THEORY AND PRACTICE

4. DESCRIPTIVE NOTES (Type of report and inclusive dates)

1 June 1971 through 30 June 1972

5. AUTHOR(S) (First name, middle initial, last name)

Robert C. Keyser

6. REPORT DATE	7a. TOTAL NO. OF PAGES	7b. NO. OF REFS
March 1973	230	12

8a. CONTRACT OR GRANT NO.	9a. ORIGINATOR'S REPORT NUMBER(S)
F29601-70-C-0029	AFWL-TR-72-89
b. PROJECT NO. 133B	
c.	9b. OTHER REPORT NO(S) (Any other numbers that may be assigned this report)
d.	Contractor Rpt No. GULF-RT-A12024

10. DISTRIBUTION STATEMENT

Distribution limited to US Government agencies only because of test and evaluation (March 1973). Other requests for this document must be referred to AFWL (ELE), Kirtland AFB, NM 87117.

11. SUPPLEMENTARY NOTES	12. SPONSORING MILITARY ACTIVITY
	AFWL (ELE) Kirtland AFB, NM 87117

13. ABSTRACT

(Distribution Limitation Statement B)

An approach to modeling of complex multiconductor cables is developed, based on measuring a set of parameters for the cable to be modeled, and then manipulating these to obtain the required model parameters. The theoretical foundation for the approach is based on the assumption of pure TEM-mode propagation on the cable, and this is shown not to impose any significant limitation for practical cables. The approach is then applied to a series of actual cables of varying complexity up to 15 wires and five internal shields within an overall shield. The results for 85 transfer functions taken on these cables show that ~70% of them exhibit agreement of ~6 dB between analysis and experiment. Also included is an analysis of the errors to be expected from the use of a lumped approximation as a function of the section length.

DD FORM 1 NOV 65 1473

UNCLASSIFIED
Security Classification

14. KEY WORDS	LINK A		LINK B		LINK C	
	ROLE	WT	ROLE	WT	ROLE	WT
Cable modeling Electromagnetic compatibility EMP susceptibility prediction Multiconductor transmission lines						